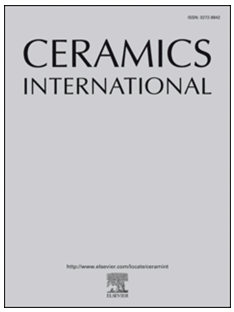

Ceramic pigments and dyes beyond the inkjet revolution: From technological requirements to constraints in colorant design

C. Molinari, S. Conte, C. Zanelli, M. Ardit, G. Cruciani, M. Dondi

PII: S0272-8842(20)31622-9

DOI: https://doi.org/10.1016/j.ceramint.2020.05.302

Reference: CERI 25403

To appear in: *Ceramics International*

Received Date: 3 May 2020

Revised Date: 28 May 2020

Accepted Date: 28 May 2020

Please cite this article as: C. Molinari, S. Conte, C. Zanelli, M. Ardit, G. Cruciani, M. Dondi, Ceramic pigments and dyes beyond the inkjet revolution: From technological requirements to constraints in colorant design, *Ceramics International* (2020), doi: https://doi.org/10.1016/j.ceramint.2020.05.302.

Ceramic Pigments and Dyes beyond the Inkjet Revolution: from Technological Requirements to Constraints in Colorant Design

Molinari C.[1,*], Conte S.[1,*], Zanelli C.[1], Ardit M.[2], Cruciani G.[2], Dondi M.[1,§]

[1] CNR-ISTEC, Institute of Science and Technology for Ceramics, Via Granarolo 64, 48018 Faenza, Italy
[2] Physics and Earth Sciences Department, University of Ferrara, Via Saragat 1, 44122 Ferrara, Italy

Abstract

The advent of digital decoration has changed the technological requirements of colorants and the way they are applied onto ceramic substrates. This technological revolution has introduced additional steps in colorant production (ink micronization) and new constraints in application (ink-jet printing) that cannot be reproduced in a standard ceramic laboratory, so stretching the distance between academic and industrial research. The goal of this work is to provide an up-to-date picture of ceramic pigments, dyes and effects, with emphasis on their behavior in the current decoration technologies, which are shortly reviewed. Technological performance expected for ceramic colorants and new requirements imposed by digital decoration are discussed in detail. An extensive overview of both industrially used and candidate pigments, dyes and effects is focused on the suitability to different ceramic applications and firing conditions. Finally, lines of future research are outlined and commented.

Key-words: ceramics, colorant, dye, effect, glaze, pigment.

CONTENTS

* Both authors equally contributed to the study.
§ Corresponding author.

1. Introduction

Coloration of ceramic materials implies the use of technologies that are different from many other applications, mainly because of the high temperature treatment that imposes specific requirements to colorants. This peculiarity makes it advisable to reappraise the conventional definitions and classification of *colorants* (hereafter used as a comprehensive term for pigments and dyes) in order to explain the terminology commonly utilized in the ceramic industry (Table 1).

The industry of ceramic colorants is apparently a mature sector: almost all pigments, currently on the market, entered in use since the 19th century to 1960 [1,2]. Ceramic pigments and dyes are utilized to bestow color on wall and floor tiles, tableware, sanitaryware, art wares, roof tiles, and enamels (for metallic wares). However, the quantity of colorants globally used in ceramic tile production is much larger (and it grew faster in the last decades) than in all the other sectors and at present represents over 80% of the global demand for ceramic pigments and dyes. For this reason, trends in colorant manufacturing have been essentially driven by the ceramic tile industry.

The strong technological innovation in tile-making that occurred in the 1980s (introduction of fast single firing) and the 1990s (development of porcelain stoneware) had limited effects on the range of pigments and dyes actually used in the industrial practice. This occurred despite the complete change in chemical composition of bodies, frits and glazes [3-5] which now need much higher firing temperatures (from ~900-1000°C of traditional fire to 1100-1160°C for porous tiles and 1180-1240°C for vitrified tiles). Also, the way by which pigments and dyes are applied on ceramic tiles has evolved over time [4-6].

Such a steady picture was revolutionized by the advent of digital decoration of ceramic tiles that took place on a large scale since 2009 [7-9]. The introduction of inkjet printing (IJP) has completely changed both the way colorants are applied onto the ceramic tiles and the technological requirements for pigments and dyes [9-11]. By this way, pigment manufacturers had to face a paradigm shift: the finished product is no longer a powdered colorant (to be admixed with vehicles in the customer's factory) but turned into an ink (encompassing colorant, carrier and additives) with a proper technological behavior certified for each type of inkjet print head and printer. Nowadays, digital decoration is spreading through other ceramic sectors (tableware, decals, etc) and allied industries (glass, artificial stone).

This new situation has important repercussions on the R&D of ceramic colorants. As a matter of fact, the requirements that pigment must fulfil have changed in the last decade: old issues have been readdressed (*e.g.*, reaction kinetics during firing) and new targets appeared (*e.g.*, behavior during micronization). The goal of the present overview is to provide an up-to-date picture of ceramic pigments, dyes and effects, with special attention to technological requirements and suitability of different colorants for the current decoration technologies, in order to shorten the distance between academic research and industry needs.

The paper is structured as follows: technologies used in ceramic decoration are briefly described (section 2) to introduce the technological performance required to ceramic colorants (section 3) with emphasis on the new requirements of digital decoration (section 4). The suitability of both industrially used and candidate pigments and dyes to different ceramic applications is discussed in detail (section 5). Finally, open questions and lines of future research are addressed in section 6.

2. Technological evolution in the ceramic tile industry

A continuous technological upgrading occurred in ceramic tile manufacturing and deeply influenced the way colorants are applied by different decoration techniques and the conditions they undergo during firing [3,5,6].

Basically, five technologies have been utilized to decorate ceramic tiles of different kinds: they are distinguished by application techniques, firing schedules, ceramic matrices, and pigment features, particularly particle size (Fig. 1).

In this framework, the decoration department underwent an evolution over the last decades regarding the application techniques (Fig. 2). In particular, the digital decoration caused two disruptive innovations [9-10]:

i) IJP replaced almost totally the preceding means of decoration, as only the technological solutions for unglazed bodies survived (at variance of previous advancements that always saw the coexistence for long time of various techniques).
ii) IJP requires a further step of micronization to get particle size in the submicronic range, while the other techniques make use of standard ceramic pigments, that have the particle size in the micrometer range (Fig. 1). This implies a considerable change in specific surface area of colorants, which in turn affects the color saturation and reaction kinetics during firing.

Figure 3 illustrates how ceramic technologies evolved along the last sixty years, starting from low temperature treatments: slow double-firing, now disappeared, and present day third fire applications (LT). Next step was the fast single-firing at intermediate temperature to produce porous and semi-vitrified tiles (IT). The follow-up was at high temperature for unglazed porcelain stoneware (BO) and then glazed porcelain stoneware (HT). Both the IT and HT decoration technologies are going to be completely replaced by the novel solutions developed to implement IJP and further digital techniques on ceramic tiles (DD).

Further factors have been playing a crucial role, beyond the technological aspects, in the design of ceramic colorants. They are connected with the growing concern on health and safety issues all along the colorant value chain, entailing effluents, gaseous emissions, hazardous substances and, in general, the reduction of chemical risk. Current regulations – like REACH in the EU [12] or TSCA in the USA [13] – may determine the fate or a given colorant. For instance, the occurrence of a carcinogenic ingredient among precursors may turn the manufacture too costly, because of all the preventive measures and controls imposed to the pigment industry [14,15].

3. Technological requirements for ceramic colorants

Pigments and dyes must fulfil a set of technical requirements to be applied in ceramic manufacturing [2,16]. These specifications concerned – in the pre-IJP technologies – essentially refractoriness, color saturation, optical properties, resistance to chemical attack, and particle size distribution. Such requirements will be henceforward discussed in some detail for industrial pigments, which basic crystallographic and physical features are summarized in Table 2, and for industrial dyes and effects as well, which general features are described in Table 3.

3.1. Refractoriness

Ceramic pigments must have a high melting point, consistently above the firing temperature they have to withstand in the industrial kiln. Indeed, the melting point reasonably matches the colorant behavior usually recognized in the industrial practice. Significantly, all the pigment structures widely used in large-scale ceramic production melt above 1600°C (Table 2), with the single exception of malayaite, that means at least 400°C above the highest temperature of industrial kilns for ceramic tiles (~1240°C). In particular, melting temperatures above 2000°C correspond to highly stable structures – like baddeleyite, zircon, spinel, or corundum – that are known to withstand high firing temperatures in a wide range of ceramic matrices [2,16]. On the other hand, a melting point in the 1800-2000°C range characterizes reliable host structures – such as

periclase-bunsenite, perovskite or rutile – which, however, denote some instability either at the highest firing temperatures or in touch with aggressive glazes [16-18]. Certain stability problems are recognized when the melting occurs below 1800°C – as for garnet, hematite, willemite and wurtzite – which are generally used in low temperature applications or once encapsulated by protective layers [18-19]. Thus, melting point should be considered as a basic prerequisite in the pigment design.

Completely different is the case of dyes, since a low melting point is needed to ensure an easy and complete dissolution into the ceramic matrix. Particulate dyes exhibit melting temperatures usually in the 900-1100°C range (Table 3), thus well below the firing temperatures of the IT and HT technologies (Fig. 1). A separate case is that of silicate dyes (Cobalt olivine and liebenbergite) that melt over 1400°C, though are readily dissolved in most glazes. Low melting temperatures (600 to 900°C) are typical of the sink effect, which is obtained by drastically boosting the fusibility in order to locally drop the viscosity of glazes or glassy coatings. On the other hand, glitter and luster effects imply crystallization that may occur either during sintering or cooling. Therefore, the melting points of crystallizing phases vary in a wide range: from 900 to 1650°C.

3.2. Color saturation

The typical color palette obtainable with standard ceramic colorants can be plotted in the a*-b* equatorial plane of CIE-L*a*b* coordinates (Fig. 4) where +a* is red, –a* is green, +b* is yellow and –b* is blue [2,16,19-20]. The sector between the +a* and +b* axes is rather crowded by several pigments of warm color, going from red to orange and yellow. Less numerous are the industrial colorants in the yellow to green quarter (+b* to –a*) and some plot in the green to blue (–a* to –b*) and blue to purple (–b* to +a*) quarters. It deserves to be noticed there are “pure colors” (i.e., those approaching the highest value of chroma) and “pastel colors” (plotting somehow midway to the origin of axes).

However, it must be emphasized that the concept of color intensity for ceramic applications involves both color saturation and brightness [1,19-20], so it should not be merely expressed by the chromatic coordinates of Figure 4. In order to overcome this limit, the *tinctorial strength* index is proposed for the first time:

$$T^* = (100 - L^*) + C^* = (100 - L^*) + (a^{*2} + b^{*2})^{1/2}$$

where L* is lightness (0=white, 100=black) and C* is chroma. It should not be confused with the *tinting strength* (used in paints), the *color strength* (applied in the textile sector) or the *tinctorial power* (utilized in the food industry) all based on the Kubelka-Munk equation.

From this standpoint, the industrial pigments and dyes exhibit tinctorial strength that, in most cases, is in between T*~70 and T*~100 (Fig. 5). These values can be devised as another basic requirement for ceramic pigments and dyes to enter in the industrial practice. Significantly, most of the pigment candidates proposed in the literature – that did not find an industrial application yet – exhibit a tinctorial strength that is lower than the industrial colorant of similar hue. A detailed discussion on the colorant suitability for present day applications is in section 5.

Even more important are the chromatic coordinates of pigments once applied in the various types of ceramic bodies and glazes. Indeed, the performance of ceramic colorants depends to a large extent on the matrix and decreases moving from transparent glazes/glasses to opaque glazes to bodies [19-20]. On the other hand, it is well known that the color yield varies upon the amount of colorant added. Examples for the main ceramic pigments are given in Figure 6. Any direct comparison of the tinctorial strength of different colors, nonetheless, is not fully reliable, because the colorimetric system in use in the ceramic sector, i.e. CIE L*a*b* [21], does not reproduce the intensity of all the colors in the same way [22].

Color has a strong dependence on optical properties and particle size distribution of pigments, which role will be discussed in detail in the next sections. However, the behavior of ceramic dyes is different, since it entails the efficiency by which the metal ions are incorporated – with the desired oxygen coordination number – into the vitreous phase of bodies and glazes.

3.3. Optical properties

Besides the knowledge of the origin of color in ceramics is fundamental for pigment design, a detailed discussion of optical spectra goes beyond the scope of the present overview. Here, *chromophores* (metal ions responsible for coloration once coordinated by a given number of oxygens) are summarized in Table 4. Reference is done to mechanisms behind color development that encompass the crystal field, ligand, and band theories, for which the Reader is addressed to specific treatises [24-27]. These formalisms may be associated to cooperative phenomena, like intervalence charge transfer or paired spin exchange transitions.

The chromatic coordinates, by which the tinctorial strength is calculated, are affected by both the refractive indexes and the main absorption bands in the visible spectrum. The difference in refractive indexes between pigments (see Table 2) and the vitreous phase in which they are incorporated determines the degree of light scattering that is often seen as the ability to “cover” the substrate [28-29]. It consequently affects the brightness of color. The refractive index of ceramic glazes and glasses is usually in the 1.50-1.55 range [29]. The difference in refractive indexes between pigment and matrix should be at least 0.2 to ensure an adequate light scattering and therefore a satisfactory covering effect. This requirement implies a threshold for effective pigments as high as 1.75 or so. Indeed, industrial pigments always exhibit refractive indexes over 1.7 and the best performance is found for values over 1.9.

Looking at the optical spectra of the main ceramic pigments and dyes (Fig. 7) it can be appreciated that absorbance bands shift leftwards when colorants are considered in the order: white, yellow, orange, and red.

White pigments (so called *opacifiers*) have indeed a negligible absorbance in the visible range – as for zircon, baddeleyite and cassiterite – or may induce a yellowish shade, due to a slight absorption of violet wavelengths, as usually occurs with cerianite and rutile.

Yellow pigments absorb intensely all wavelengths above the ~20,000 cm^{-1}, so leaving a wide transmittance window (250-500 nm) that ensures bright colors. Two distinct kinds of optical band occur: steep in zircon-Pr and bindheimite pigments and less abrupt in baddeleyite-V, rutile-NiSb, and cassiterite-V pigments. The color shade depends on the wavelength of minimum absorbance, which can shift from the yellow region (where it gives rise to “cold” colors, like zircon-Pr and rutile-NiSb) towards the orange one, determining “warm” yellows, as those of bindheimite, baddeleyite-V, or cassiterite-V pigments.

Red pigments are featured by sharp bands absorbing most of the orange to violet wavelengths, *i.e.* above the ~16,000 cm^{-1} (below ~600 nm) as shown by cadmium sulfoselenide and Cr-doped yttrium aluminate perovskite. By this way, the transmitted light is limited to the red-orange region, resulting in rather dark colors. Magenta to burgundy shades, as those of malayaite-Cr and the so called Cassius’ purple (gold nanoparticles), are originated by an additional transmittance in the blue-violet region, while purple colors require a second minimum of absorbance in the violet region, like that at ~24,000 cm^{-1} (~420 nm) of the cassiterite-Cr pigment. On the other hand, pink colors have an absorbance band that occurs at the same wavenumber of red pigments (onset at ~16,000 cm^{-1}) but with a distinctly weaker intensity, as the case of hematite encapsulated in zircon. The spectrum of Cr-doped corundum reveals, in addition, the transmission of some blue and violet wavelengths, justifying the typical ruby shade.

Orange pigments exhibit optical features intermediate between yellow and red colorants. Cr-doped rutile pigments, for instance, are characterized by a slope not so steep and a rather wide transmittance window, by which light is increasingly absorbed moving from orange (minimum around 15,500 cm^{-1}) to green regions of the visible spectrum.

Optical features different from the shutter-like bands observed in red to yellow pigments are necessary in order to get the remaining colors. For instance, a selective wavelength absorption that allows the transmission of either the green or the blue light only. On the other hand, dark colors are obtained through a non-selective light absorption over the whole visible spectrum, but with different intensity for brown, gray and black shades.

Green pigments require a light absorption at both the red-orange and blue-violet extremes of the visible spectrum. The resulting transmission window has a minimal absorption at ~19,000 cm^{-1} that is more accentuated for green pigments (e.g., eskolaite, uvarovite) than for bluish-green ones (cochromite) which exhibit a plateau over the green and blue regions.

Blue colorants must absorb selectively the orange to green wavelengths (15,000 to 20,000 cm^{-1}, 500-650 nm) to achieve the desired blue hue, as in the case of the cobalt aluminate spinel pigment. Instead, cobalt dyes (olivine, but also phosphates and borate, see Table 4) are filters less selective, because they absorb also some blue and violet light, giving rise to a deep, ultramarine blue tint. Turquoise shades occur in case of a narrower absorption band – like that of zircon-V pigments, usually extended over the 14,000 to 17,500 cm^{-1} range (580-700 nm) – which let some green light to be transmitted, so the overall hue is between green and blue.

Brown pigments are a variegated family of compounds, exhibiting broad optical spectra, not easily attributable to single bands. A more or less accentuated light absorption is observed growing from red to violet wavelengths. It is the intensity of such an optical hump to discriminate between light brown (e.g., spinel Zn-Cr-Fe) and dark brown shades (e.g., spinel Mn-Cr-Fe and rutile Mn-Sb). The window transmitting in the low energy region of the visible spectrum accounts for brown colors with reddish to yellowish tints.

Black pigments should in principle absorb all the visible spectrum, as it practically occurs in the best cases (like complex Co-Ni-Fe-Cr-Mn spinels). In comparison, eskolaite-hematite pigments have a weak transmission in the red region that is enough to justify some brownish shade. Gray colors are expected to differ from black just for the lower absorbance over the whole visible spectrum (e.g., bunsenite-Co). In reality, some selective absorption can lead to bluish, greenish or yellowish overprints.

3.4. Interaction of pigments and dyes with ceramic matrices

Ceramic pigments must be stable in contact with the melt formed during the firing of glazes and bodies. Therefore, the resistance to chemical attack is a relative concept, depending on the substrate composition (glaze or body) that varies upon the technology used in ceramic manufacturing. In practice, there are different arrays of 'chemical composition x firing schedule', which define a variable degree of aggressiveness of the liquid phase towards the pigment.

The differences in chemical composition among glazes and bodies used by the ceramic industry are illustrated in Figure 8 with reference to the decoration technologies of Figure 1. The main fluxes are arranged in Figure 8A according to their technological role and chemical action against the ceramic pigments [4,28,29]. Account must be taken since there are three basic mechanisms by which a ceramic pigment can be chemically attacked with permanent color deterioration [10]:

a) pigment dissolution in the liquid phase;

b) pigment transformation into another crystalline phase;

c) change in the crystal chemical composition of the pigment, which keeps its structure.

Alkaline fluxes, i.e. Na_2O, K_2O and Li_2O, enhance fusibility, so reducing the maturing temperature, and increase the brightness of glazes (but in the case of lithium a devitrification may occur). Alkali do not enter the crystal structure of pigments and usually do not promote the crystallization of phases hosting transition metal ions [28-29]. Thus, their action is principally to foster pigment dissolution by lowering viscosity and increasing surface tension of melt.

Alkaline-earth fluxes, i.e. MgO, CaO, SrO and BaO, play different roles, depending on concentration and firing conditions, with some variation from one element to another [19,28,30]. At high concentration, they promote devitrification, leading to opaque glazes, but at low percentages tend to improve brightness (useful for glassy coatings). On the other hand, they enhance fusibility at higher firing temperatures, whilst boost viscosity at lower temperatures. Therefore, alkaline-earth fluxes can take part into the chemical attack by various reactions, depending on the colorant. For instance, magnesium can affect spinel pigments, since Mg^{2+} ions compete with divalent transition metal ions (Co^{2+}, Mn^{2+}, Ni^{2+}) mainly to access the tetrahedral site [31]. Similarly, in bunsenite pigments Mg can replace both Ni and Co at the octahedral site [32]. On the other hand, calcium may have opposite functions: it stabilizes Ca-bearing pigments, like garnet and malayaite, but heavily attacks rutile, hematite, and eskolaite, as $CaTiO_3$, $CaFe_2O_4$ and $CaCr_2O_4$ phases turn to be thermodynamically favored with respect to simple oxides [33]. Eventually, all colorants are attained to some extent by dissolution into the melt, which is more effective at lower viscosity, thus with higher temperature and BaO content.

Strong fluxes, i.e. B_2O_3, PbO and Bi_2O_3, reduce viscosity and surface tension of the melt, thus promoting the diffusion in the liquid phase of other glaze components [30]. Account must be taken that present-day glazes are nominally leadless, while bismuth is utilized only in some third fire applications. Boron does not enter the crystal structure of ceramic pigments; thus, its role is essentially to enhance the fluxing effect of alkali.

Zinc oxide has a wide range of effects in glazes, including a fusibility enhancement through the reduction of viscosity and surface tension of the melt or, at high concentration, the tendency to crystallize Zn-phases (gahnite, willemite, hardystonite). Zinc can interfere with the coloration of glazes because it may be incorporated in the crystal structure of many pigments. In fact, it can replace transition metal ions at tetrahedrally- and octahedrally-coordinated sites, e.g. in spinel, periclase, malayaite. In addition, zinc easily reacts with TiO_2, Cr_2O_3, Al_2O_3, Fe_2O_3, and SnO_2 pigments, giving rise to Zn-rich phases [29].

The *silica-to-alumina ratio* governs many chemical and physical properties of glazes and glassy coatings [29,30]. Indeed, the amounts of silica and alumina determine the appearance (transparency and gloss) of glazes, which can be described as matt, semi matt, and bright (Fig. 8B).

Pigment dissolution in bodies and glazes always occurs to some extent, depending on both the phase refractoriness and its solubility in the melt. This phenomenon has commonly a twin effect: loss of the desired color (due to pigment breakdown) and onset of undesired shades due to element “leaching” (transition metal ions incorporated into the glassy phase). No data exist on pigment solubility into ceramic liquid phases, but information is available about some minerals in granitic melts, which can be somehow approximated to those present in porcelain stoneware bodies. The saturation concentration at 1200°C is below 1%wt for cassiterite [34], approximately 1.2%wt for zircon [35], and around 2%wt for rutile [36]. However, the solubility in ceramic melts is difficult to predict from phase diagrams, because of the remarkable complexity of glaze compositions. To overcome this problem, a common practice is to “saturate” the glaze with the major

components of the pigment, in order to improve the chemical stability of colorants. This was typically an additional role of opacifiers, which are usually selected also to ensure the color yield, e.g. tin oxide for cassiterite pigments or zirconium silicate for zircon pigments [2,16]. This solution is no longer feasible with IJP, but it was revitalized in digital decoration by using “primers” and “protective” layers (i.e., glassy coatings with a very low amount of the most aggressive components, like ZnO and alkaline-earth oxides).

Pigment phase transformation is apparently a phenomenon restricted to specific circumstances, as in the classic example of the eskolaite green pigment, once applied on a zinc-bearing glaze: the reaction Cr_2O_3 + ZnO leads to the formation of the brown $ZnCr_2O_3$ spinel [16]. In reality, such reactions are easily overlooked, because the resulting chromatic change can be erroneously attributed to a pigment dissolution. These transformations typically occur when a thermodynamically favored crystalline phase exists in the relevant chemical system, which is usually hard to represent in a phase diagram due to the conspicuous complexity of glaze compositions.

A *change in the pigment crystal chemistry* can affect the chromatic coordinates, since factors that are fundamental in color development are usually modified. Such factors encompass the transition metal ion valence and oxygen coordination, as well as the metal-oxygen distances and distortion of the polyhedron where the cation is accommodated. These phenomena are governed by the partition equilibria, for each ion, between melt and pigment. In addition, the diffusion kinetics through the pigment crystal structure turns crucial. As a rule of thumb, structures with more than one crystallographic site, where transition metal ions can be allocated, are more prone to variation of crystal chemistry. A classic example is spinel: the Ni-free black spinel, once in touch with zinc-rich glazes, changes color by shifting towards a brown shade. This occurs because Zn^{2+} replaces Co^{2+} at the tetrahedral site; as a consequence, light absorption in the red-orange region no longer occurs and the outcome is a brown spinel.

Dye dissolution into the melt formed during firing is required and depends on the composition of ceramic matrices. The different compositional fields of glazes and bodies utilized in the various technologies are illustrated in Figure 8. They imply a spectrum of chemical environments and thermal treatments, hence conditions where dye melting (and the three causes of pigment deterioration) can play with a changing relative weight. This aspect must be considered when the chemical compatibility of a dye/pigment with single components of glazes and bodies is evaluated, as known from the industrial practice (Table 5). Some crystal structures suffer from the attack of alkaline fluxes and particularly strong fluxes (e.g., garnet, pyrochlore, bunsenite, baddeleyite, and cassiterite). It is not a case that the relevant pigments have a relatively low stability, as witnessed by the maximum temperatures allowed in the firing schedules that are among the lowest in industrial colorants. In contrast, pigments based on corundum and spinel structures are more exposed to phase transformations and/or change in their crystal chemistry, especially under the effect of element that can easily accommodated in the crystal sites (i.e., Zn, Mg, Sn).

Transition elements can be released to the liquid phase, present at high temperature in glazes and bodies, as a consequence of dye dissolution or pigment breakdown or even ion exchange between melt and pigment [2,16]. In case of pigments, such a leaching process determines the dissolution of transition metal ions into the glassy matrix with undesired repercussions on color purity [37]. Each transition metal ion will absorb in the visible light spectrum, depending on its valence and oxygen coordination in the silicate glass, giving rise to specific color shades, which is the mechanism exploited with dyes (Table 6). These more or less accentuated nuances, depending on the transition metal concentration, may significantly alter the original coloration due to the pigment.

Ceramic effects behave either as a dye or a pigment. Sink effects (SE) and bright/matt glasses (BE) must dissolve in the glassy phase, as some speckle effects do. In contrast, glittering (GE) or phosphorescence require crystals dispersed in the glaze. Lusters (LE) are obtained by controlled crystallization during firing.

4. New technological requirements of ceramic colorants for digital decoration

The advent of IJP imposed to move from conventional pigments and dyes delivered as powders towards micronized colorants dispersed in a carrier (ink). This paradigm shift made some technical solutions no longer practicable and, at the same time, introduced new requirements (or emphasized some technological aspects).

For instance, the control on the pigment color saturation, which was commonly achieved through a careful addition of a filler [37], is unappropriated in inks. As a consequence, nowadays pigments must be even more constant in their color performance, because only the colorants (not diluted by filler) are used in inks [10]. On the other hand, no easy adjustment of color saturation by increasing the pigment concentration is possible in IJP, since it has immediate repercussions on the density, shear viscosity and surface tension of the suspension, hence on ink printability [9-11].

New requisites concern the behavior of ceramic pigments during micronization and their interactions with ink carriers and print head components. Particle size distribution assumed a crucial role in IJP, involving the micronization process adopted to make inks. Therefore, pigment grindability is now a key issue for both ink productivity and color saturation, and consequently the relevant parameters, such as the mechanical properties and the resistance to amorphization of the crystal structures of ceramic pigments. Further factors are the interactions between colorant and carrier, as electro-magnetic properties of pigments and dyes.

4.1. Particle size distribution

Most colorants are utilized as powders, directly or as feed in ink making. Therefore, pigments, effects and particulate dyes always undergo, after synthesis, a comminution or disaggregation stage to obtain the desired particle size distribution [37]. Such a process can be performed either by the dry route (typically through jet milling) or by the wet route (ball milling followed by spray-drying) depending on specific needs (e.g., washing any mineralizer residue out).

Particle size is the most important feature to keep under control in the industrial practice, because it affects both the optical properties and reaction kinetics during firing [38,39]. Thus, granulometry ultimately influences tinctorial strength in the various decoration technologies. For this reason, pigment-making companies spend considerable efforts to find out the best particle size distribution for every product to be applied as powder or entering the micronization process for ink-making [37,40].

Different requirements exist in the various applications, as exemplified in Figure 9A. The pigments utilized in conventional technologies (i.e., from LT to VHT and BO) are commonly milled to a median particle diameter in between 3 and 7 µm, irrespective of being allochromatic (AP) or idiochromatic (IP). The same pigments, once addressed to digital inks, undergo a more intensive comminution, down to approximately 1-2 µm or even less, in order to damp the cost of the high-energy micronization process. In contrast, encapsulated pigments are kept to a coarser particle size, in order to preserve the protective coating on the heat-liable pigment, so that the median particle diameter can span from 10 to 20 µm.

The micronization process, carried out in high-energy mills with Y-stabilized zirconia microspheres, leads to a narrow particle size distribution of the colorant dispersed in the ink medium. The median particle diameter for pigments is usually in the 0.3-0.6 µm range, with the d_{90} always below 1 µm [9-11], while micronized

effects are slightly coarser, with a median particle diameter ordinarily from 0.6 to 1 μm. Such a drastic reduction of particle size brings about two different effects: a proportional increase of the specific surface area and a physical deterioration of pigments (see section 4.2 for a further discussion on pigment behavior during milling). Both have relevant repercussions on the colorant performance of inks by two mechanisms: less intense light absorption (due to a loss of pigment) combined with undesired shades (due to transition metals migrating to the glaze or glassy coating, Table 6).

The specific surface area grows from conventional pigments, having normally values close to 1 $m^2 \cdot g^{-1}$, to 15-35 $m^2 \cdot g^{-1}$ in the resulting inks (Fig. 9B). Such an increased specific surface area implies an enhanced reactivity of pigments in touch with glazes and glassy coatings [40-41]. Thus, a much lower resistance to chemical attack is generally observed during firing. This fact reflects on color saturation, which is notoriously weaker in digital inks with respect to conventional pigments [10,41].

4.2. Pigment grindability

As introduced in the previous paragraph, DOD-IJP entails some strict requirements, among which ensuring that >99% of the pigment particles are less than 1 μm in diameter [8,9,11]. Being mainly dependent on the specific energy input (i.e., on the energy supplied to the grinding chamber in relation to the mass of product), pigments micronization down to the requested particles size proves to be the most energy-consuming comminution process per unit weight of product [42]. It derives that comminution of ceramic pigments is a key issue for ink production, which has strong repercussions on tinctorial strength, mechanical properties and resistance to amorphization of the pigment crystal structure.

In an ideal case, when a particle undergoes brittle fracture, a crack propagates through the particle creating new surface area. On the other hand, in the real cases, most of the energy supplied during comminution processes is dissipated into effects other than the new surface itself, *e.g.*, elastic deformations, friction between particles and/or between particles and apparatus walls, heat, vibrations, and so on [43]. Despite the effort in finding the best relationship that can rationalize the energy-dependent particle size variation during a comminution process and, at the same time, to account for all the above-mentioned secondary effects, the main relationship commonly used to describe a comminution processes of a brittle solid originates from a single differential equation of the general form [44]:

$$dE = -K\frac{dx}{x^{f(x)}} \quad (1)$$

where *dE* is the infinitesimal energy change per unit weight required during comminution, *dx* is the infinitesimal size change, *x* is the particle size, *K* and *f*(*x*) are a constant and a variable dependent on the particle size *x*, respectively, related with the material (*e.g.*, initial particles size, and particles physical properties) and with the size reduction method [44-47]. When particles fall at the boundary of the micrometric-submicrometric range, $f(x) \rightarrow 2$, and the Rittinger's law is considered the most suitable in describing the energy change in a comminution process [44,46,47]. Rittinger postulated that the energy per unit mass is proportional to the new surface area produced, and the Rittinger's relationship can be easily derived through the integration of equation 1 [44,46,47], such as:

$$E = K\left(\frac{1}{x_2} - \frac{1}{x_1}\right) \quad (2)$$

where *E* is the net energy (expressed in $J \cdot kg^{-1}$) required to micronize a particle from the initial (x_1) to the final (x_2) particle size (defined as the integrated mean particle size, in m [44,46]) in a given grinding cycle (*i.e.*, time × milling rounds), and *K* is expressed in the units of $J \cdot m \cdot kg^{-1}$ [43]. Once eqn. (1) and its derived form (2)

have to be applied in fitting experimental data, a tough limitation occurs in finding the best fit values for K and $f(x)$. In particular, the Rittinger's equation, eqn. (2), requires the values of K and $f(x)$ to be known a priori [46].

In the case of ceramic pigments, the literature on their micronization is limited to few experimental investigations [40,48-51]. From these works, it emerges that the energy required to downsize a particle from x_1 to x_2 (*i.e.*, expressed as the variation of the median particle diameter, d_{50} in μm) is proportional to the total number of milling rounds, r_T [*e.g.*, 40], which is an experimental inference to what postulated by Hukki [44]. In figure 10, the variation of the reciprocal of the particles size (*i.e.*, $(\frac{1}{x_2} - \frac{1}{x_1}) \propto \frac{E}{K}$) for pigments micronized in a pilot plant is plotted as a function of the total milling rounds.

Data in Figure 10 clearly show the strong dependence of particles size reduction on grinding cycles (by definition, proportional to the energy supplied during the comminution process). Along with this observation, a detailed inspection of data in Figure 10 reveals that the particles size reduction strongly depends on the structural features (*i.e.*, crystal structure and chemical composition) of the micronized ceramic pigments. Consistently to what reported by Güngör et al. [40], it appears that ceramic pigments with spinel structure are less grindable than those with rutile and zircon structure, respectively. In addition, while the particle size variation of both zircon and rutile pigments scales almost linearly with the milling rounds, the particle size variation for spinel pigments undergoes a constant but gradual decreasing. In particular, above 2×10^5 and 2.5×10^5 milling rounds for Co-aluminate and CoFe-chromite, respectively, no appreciable particle size variation is observed.

The particles size variation for spinel and zircon ceramic pigments during micronization is highlighted in two distinct plots (A and B, respectively) in Figure 11. Beyond the general remarks of above, the comminution of spinel ceramic pigments returns different micronization trends depending on their crystal chemistry, with Co-aluminate pigments more grindable than Co-ferrite and CoFe-chromite spinel ceramic pigments, which in turn have a common particle downsizing (Fig. 11A).

This behavior apparently contrasts with that highlighted during the comminution of zircon ceramic pigments (Fig. 11B). Although purchased from different manufacturers and investigated at different laboratories [40, 48,50], data in Figure 11B unequivocally show that the zircon structure undergoes the same particles downsizing irrespective of the dopant cation nature. This fact can be readily explained because of the small substitution (or incorporation) of dopant cation within the zircon lattice. Pigment manufacturers produce yellow and turquoise zircon pigments by a doping of about 3% to 5% of Pr^{4+} and V^{4+}, respectively [49,51,52]. It derives that the presence of dopants in small amounts does not influence the grindability of zircon ceramic pigments.

The comparison of the selected data, at the micrometric scale, suggests that the energy supplied during a comminution process is used/dissipated by two main mechanisms related to two different energetic contributions. In the first mechanism, the energy supplied during the comminution process will be mainly devoted to the creation of new surface area, as in the ideal case entailed by the general comminution laws [43-47]. This energy is preserved as long as a particle undergoes brittle fractures: "energy conservation process". The second mechanism implicates a process for which the crystal structure of a particle loses long-range order by means of interatomic bonds breaking and lattice disorder, *i.e.*, the structure undergoes amorphization [53]. Hence, in terms of particle comminution, this process has a "dissipative/non-conservative" energetic contribution. Both mechanisms, and by consequence both energetic contributions, mainly depend on the resistance of a crystal structure to an external compression, which is defined by its isothermal bulk modulus (K_{T0}, in GPa) [54,55].

The isothermal bulk modulus (or incompressibility) for the crystal structures of the ceramic pigments under comparison is listed in Table 7. The listed K_{T0}, is the average value among several from literature. For sake of clarity the range of variation of K_{T0} is also reported in Table 7.

Incompressibility data in Table 7 perfectly match with the grindability ranking derived from the particle size variation of micronized ceramic pigments (see Fig. 10), where the stiffest structure of zircon pigments has the highest rate of micronization, while the more compressible structures of Co-ferrite and CoFe-chromite spinel pigments show a little aptitude at micronizing.

Although the concept of resistance at the compression could be misleading, it results evident, when a crystal structure is stiffer than another, that the process of micronization can be prolonged at higher milling rounds. This means that a particle with a high bulk isothermal modulus undergoes brittle fracture when micronized, and the energy supplied during the comminution process will be largely devoted to the creation new surface area. Conversely, when the energy supplied to micronize a particle dissipates into other effects, the comminution efficiency will drastically decrease. Indeed, data on the phase composition for micronized ceramic pigments achieved by means of X-ray diffraction experiments highlighted a higher tendency to amorphization for spinel pigments than for zircon ceramic pigments [41]. In addition, the different trends for spinel and zircon ceramic pigments in Figure 11 are consistent, although qualitatively, with two different kinds of energy change. Indeed, the ball milling mechanical energy transforms into an energy process which is predominantly conservative in the case of zircon pigments, where the particle downsizing scales linearly with grinding cycles, while it changes into a largely dissipative energy process (*e.g.*, amorphization) in the case of spinel pigments, where the particle downsizing turns to be curvilinear.

Other bulk properties, such as density, which in turns is related with the pressure of amorphization [55], brittleness, hardness, etc. can play important roles during the comminution of ceramic pigments, but the driving force which governs the micronization of ceramic pigments is their resistance at the compression (i.e. the isothermal bulk modulus or incompressibility).

The high-energy micronization is able to progressively damage the crystal structure of colorants, leading eventually to a pigment loss due to amorphization [41]. This phenomenon brings about a lower yield at the end of the micronizing stage, which can vary widely from a few percent to 60% of the initial amount of pigment. The average loss in commercial inks, estimated by X-ray powder diffraction through Rietveld refinement with internal standard, is around 30% (Fig. 12). The differences amongst crystal structures – zircon, rutile, malayaite, and various spinel types – are just indicative, because data are not fully representative of ceramic inks, since the number of samples varies upon the different pigments.

This picture lets the micronization of ceramic pigments to be a crucial stage to define quality, performance, yield and cost of digital inks. Key points for a better comprehension of this process are the dependence of results on the pigment crystal structure, and the chance of a direct estimation of the energy required for pigments comminution. On the other hand, the need of a direct measurement of the Rittinger's constant K and exponent $f(x)$ still represents a challenging issue. Further relevant parameters to be considered during comminution of ceramic pigments encompass the feed size (starting particle diameter) and the evolution of particle size and shape, for increasing milling time, that can reveal the onset of agglomeration phenomena (which mechanism is not fully understood). In addition, type and amounts of additives (dispersant, block copolymers, etc.), grinding media, chamber mill dimension and rotation speed introduce variables that influence the comminution process. These aspects are only partially known and need to be furtherly investigated.

4.3. Colorant interaction with ink carriers

Colorants interact with the carrier and the additives in the various stages of the ink life: micronization, storage, inkjet application on the tile surface, drying and firing. Although, in principle, chemical reactions between the colorant and the organic components should be negligible, there are evidences of some interactions occurring mainly during long time storage and fast firing.

A prolonged contact of some effects (glazes and glassy coatings) with the carrier may turn into a partial solubilization, depending on the type (water, polar and non-polar organic media), pH, etc. Available data for the $CoAl_2O_4$ pigment point to high ion concentration (>800 $mg \cdot dm^{-3}$) in diethylene glycol, while the dissolution was less significant in aqueous medium [89].

The organic components of the ink deposited on the tile surface undergo a rapid thermal decomposition once entering the first module of roller kiln, where temperatures can be as high as 300 to 500°C. In these shocking conditions, organic compounds can be stripped by the water vapor stream coming out from tiles. Otherwise, they can undergo pyrolysis or combustion under the effect of the hot flue gases flowing from the heating zone of the roller kiln [90,91]. There are clues that the formation of the different organic by-products during combustion, pyrolysis or stripping are affected also by a sort of catalytic action attributable to the pigment present in the ink.

5. Suitability of colorants in the different ceramic technologies

In this section, the suitability of colorants in the various decoration technologies used in ceramic tile-making is overviewed by taking into account different issues: technological behavior, cost, and possible health hazards. The technological performance is considered under various viewpoints: chemical stability during firing, color saturation and purity, and behavior during micronization.

Along with pigments, dyes, and effects currently utilized by the ceramic tile industry, this analysis is extended to colorants under development that were proposed for ceramic applications in the literature. Reference to the Colour Index (C.I., by the Society of Dyers and Colourists) is given, when available. The list of candidate pigments and dyes is not exhaustive: only those with enough pieces of information on technological performance were included in the discussion.

For every colorant, the outcome is given for each decoration technology (as listed in Fig. 1): low temperature (LT), intermediate temperature (IT), high temperature (HT), unglazed body (BO), very high temperature (VHT), and digital decoration (DD). The verdict can be ‘suitable’ or ‘unsuitable’. If suitable, additional information is provided, as: currently in industrial use; no longer in use; never entered in use. If unsuitable, the main motive is indicated: technological reasons; insufficient tinctorial strength or color purity; possible environmental impact or health hazards; economic reasons (high cost of precursors).

Pigments and dyes are hereafter illustrated color by color. In few cases, the color definition is ambiguous (for instance, greenish yellow or yellowish green). As far as possible, it was followed the color attribution given in the literature, but sometimes the technological behavior (coloration in glaze) was in contrast. In this circumstance, technological data were plotted in the most appropriate color graph.

5.1. Red and purple colorants

There are no “universal” colorants able to impart red (or purple) shades with all the ceramic technologies. The rather wide array of colorants utilizable with the LT application turns to be progressively restricted with IT, HT-VHT and BO applications (Fig. 13). The situation is critical in DD, where no frankly red colors can be achieved and burgundy to magenta and purple pigments are employed.

Malayaite doped with Cr is widely used, despite it suffers from some chemical instability in glazes that limits the maximum temperature attainable [92,93]. Control on burgundy color during synthesis is difficult, because different shades develop from relative abundance of multiple chromophores: octahedrally-coordinated Cr^{3+}, tetrahedrally-coordinated Cr^{4+}, and even some Cr^{5+} [94-96]. Color shades are also in accord with co-doping with La, Zn, Fe or Ti [37]. In addition, there is a strong influence of firing conditions and mineralizers on synthesis yield [97-99]. Overall, this pigment behaves best in glazes (typically T*~85 at 1100°C, T*~75 at 1200°C) – with several constraints (Table 5) – and is not suitable in bodies.

Purple of Cassius has a high potential as red pigment, due to an intense plasmonic band of gold nanoparticles (T*~80 at 1150°C). These are rather stable in most applications, even if the highest temperatures the magenta-red color turns into brown [100-102]. There are various synthesis procedures, including soluble salts [103] and ceramic inks [104,105]. The main hindrance is the very high cost, even if the red color can be achieved with diluted concentrations, connected with the growing price of gold. To overcome this limitation, Ag-Au alloys were industrially developed, but never used because the color has a strong yellowish shade [106,107].

Cassiterite doped with Cr was a pigment with a marginal importance in the conventional technologies that has been revitalized by the advent of digital decoration, even though handicapped by the high cost of tin oxide. It bestows a peculiar violet color on glazes (T*~60 at 1200°C) likely originated by a unique combination of different chromophores [95,96]. Color shades are achieved with further dopants (Co, Ce). For as concerns the synthesis, since the traditional ceramic one can cause serious environmental and health problems due to the formation of carcinogenic Cr^{6+} during the process, a wet method can be preferred. This low temperature synthesis limits the Cr oxidation [108-111]. It has a fair stability in glazes [37] and rather good performance in DD.

Cadmoselite-greenockite solid solution, encapsulated in zircon, provides an unrivalled red color that is the reference colorant for all applications in glazes (90<T*<100 at 1200°C). Its stability is satisfactory, if encapsulation is complete, in all matrices but low viscosity glazes [37,112]. The synthesis is complex: the sulfo-selenide seeds must be incorporated in the silicate mass and preserved during formation of zircon [113]. Its utilization in DD is problematic, because micronization can break the encapsulation, leading to chemical attack of the pigment by glaze. However, some application was recently attempted by reducing the particle size prior micronization. A major issue is the high toxicity of cadmium and selenium that imposes a standard control on Cd release from finished ceramic products [114].

Hematite encapsulated in zircon can be used in all technologies but DD, because micronization causes the rupture of the protective envelope made of zircon. Nevertheless, it is mainly addressed to mass-stone and is the reference red pigment in BO application [115]. It has a characteristic pink coral hue (Fig. 14) that turns redder in Zn-bearing matrices (80<T*<90 at 1200°C). Encapsulation is a complex process depending on several variables, not straightforward to control, that was investigated in depth [116-121].

Hematite encapsulated in silica presents analogies with the previous pigment: it has a pink color as well, but less performing in glazes (80<T*<88 at 1100°C) to the point it is used essentially in BO applications (60<T*<78 at 1200°C). A natural analogue is the *Grès de Thiviers* [122-123]. Its synthesis appears to be easier that the hematite-zircon encapsulation and seems possible by various routes [124-130]. It cannot be used in DD.

Yttrium-aluminium perovskite doped with Cr is the most recent ceramic pigment added to the industrial palette [131,132]. It exhibits a red color stemming from Cr^{3+}-Ca^{2+} pairs, where calcium can be substituted by

other impurities coming from mineralizers, like Mg [17,132,133]. Its synthesis is not straightforward, because of the crucial role played by mineralizers [131,134-136]. It is stable particularly in HT glazes (80<T*<90 at 1200°C) where it takes advantage by the high content of Ca and Al in these matrices [37,137]. No information exists about its performance in DD, where the high cost of yttrium represents a notable hindrance. Reddish perovskites have been synthesized also with lanthanides (e.g., La, Nd) and with mixed chromophores (Cr+Fe) but coloration is worse [138-140].

Corundum doped with Cr and/or Mn is the basis of two classic rose pigments, rather stable in most applications [141]. Now $(Al,Cr)_2O_3$ is utilized essentially for LT-IT (52<T*<62 at 1140°C) while $(Al,Mn)_2O_3$ for BO (60<T*<70 at 1200°C). Color stems from transitions due to the high crystal field of Cr^{3+} or Mn^{3+} in the Al site [142,143]. Color variants are obtained by co-doping Mn with Ca or P [37]. Not used in DD, both not suitable for quadrichromy and cost of micronization (due to its hardness). Easy synthesis by solid state, possible also in absence of mineralizers [144], and by mechanosynthesis [145].

Gahnite doped with Cr is another classic rose pigment [2,146]. $ZnAl_2O_4$ is a common phase in zinc-rich glazes, and the pigment is rather stable in all applications. Its synthesis is quite easy, in presence of borate mineralizers [37]. This spinel has been developed in many variants, with Mg, Fe, Ni, Cr, as co-dopants [147-149]. It is still used in LT (50<T*<60 at 1050°C) since its incompatibility with B, Ca, Mg and Ba precludes applications at higher temperatures. Peculiar colors – peach to salmon pink (Fig. 14) – are obtained and tend to exhibit some degree of metamerism [37].

There is a set of red and purple pigments not entered in the industrial practice, along with colorants used in the past but now completely abandoned. Modern production does not employ crocoite ($PbCrO_4$) or further chromate pigments. **Pyrochlore** $Y_2Sn_2O_7$ doped with Cr was developed as a burgundy to brown pigment [150,151]. Its color (60<T*<70 at 1080°C) is similar to the less intense shades of malayaite-Cr (Fig. 14) and similarly stems from multiple chromophores (Cr^{3+} and Cr^{4+} in octahedral coordination). Synthesis is complicated by an uneasy control on accessory phases [150,152]. Although stable in the main applications, it is handicapped by a higher cost and worse color with respect to industrial colorants. Other pyrochlores were investigated, as reddish brown $Y_2Ti_2O_7$ doped with Cr [152] and pink $Er_2(Zr,Ti)_2O_7$ doped with Cr [153,154] or $Y_2Zr_2O_7$ co-doped with Cr and Pr [155]. They all suffer from an insufficient tinctorial strength, most of all for as concerns pink $Er_2Ti_2O_7$ doped with Cr, which if prepared by solid-state synthesis presents a very pale pink shade whatever the temperature; otherwise, if prepared by sol-gel method shows an intense pink coloration when calcinated at 700°C [153]. The color stability significantly diminishes above this temperature, unless the sample contains zirconium, which stabilizes the fluorite structure and ensures a color intensity also at higher calcination temperature [154].

Further proposals include **$CaYAlO_4$ doped with Cr** that exhibits pink shades (55<T*<60 at 1050°C) comparable to the weakest achieved with encapsulated hematite (Fig. 14). Color stems from Cr^{3+} and Cr^{4+} in a distorted octahedral site [156] and its stability was tested at 1050°C in transparent frit (Ca-Zn-B). **Hematite encapsulated in zirconia** [128] proved to be stable in LT applications (T*~77 at 980°C). Lilac colors were developed exploiting **$(Ba,Sr)Zn_2Si_2O_7$** and **$BaMg_2Si_2O_7$** with melilite structure: color is originated by Ni^{2+} in tetrahedral coordination [157,158]; their thermal stability was not tested yet. Purple dyes were obtained by $(Mn,Mg)_2P_2O_7$ solid solutions with **thortveitite** structure. Once thortveitite breaks down during firing, manganese is released to the glaze, which turns colored (50<T*<65 at 1080°C) by the effect of Mn^{3+} ion dissolved in the glassy phase [159]. Another dye consisting of **Co phosphate** was described as purple, but final coloration in glaze is blue [160,161].

5.2. Yellow and orange colorants

There is a limited number of yellow colorants utilized in IT and HT-VHT applications that increases considerably once LT is concerned (Fig. 15). Only yellow zircon is employed in BO and DD technologies that makes it a "universal" pigment used in all the ceramic technologies. Mass-stone represents the main demand for orange colorants, mostly satisfied by rutile pigments, sometimes utilized in DD too.

Zircon doped with Pr provides a bright yellow (typically 60<T*<80 at 1100-1200°C) due to Pr^{4+} incorporated at the Zr site [162-164]. Developed also with other dopants, like Tb^{4+} and Ce^{4+}, but not at the industrial level [165-167]. Its synthesis is not straightforward, as solid, liquid and gas states are involved [168,169], with an important role played by mineralizers and calcination conditions [164,168-172]. It is highly stable in all applications, especially in Zr-rich and Zn-rich coatings [37]. Nevertheless, it is less performing in DD, due to detrimental effect of micronization on color, thus sometimes associated to other yellow or buff pigments [10,49].

Baddeleyite doped with V is a classic pigment with a characteristic yellow egg coloration (usually 40<T*<50 at 1100-1200°C) which can be tuned by doping with In, Y, Ti, or Al. Such a peculiar shade is related to the occurrence of tiny clusters of V^{5+} oxide included in ZrO_2 that makes it a sort of mordant pigment [173,174]. Its production is quite easy, also with alternatives to solid state synthesis [175-177]. The stability in glazes is generally good, but it is utilized especially in VHT applications [178]. Unsuitable for mass-stone (BO) because it tends to react with silica to form zircon. It is not used in DD, due to its color shade, not optimal in quadrichromy, and unsatisfactory tinctorial strength after micronization. Also, its high specific weight makes the ink more prone to pigment sedimentation.

Greenockite encapsulated in zircon provides a very brilliant yellow color (T*~90 at 1200°C). If encapsulation is complete and preserved during application, the stability in glazes is excellent [179]. As said for the analogous red pigment, the synthesis is complex. Indeed, in order to avoid the airtight container required by the ceramic method, the direct synthesis at low temperature by hydrothermal method is preferred. It entails the complex inclusion of cadmium sulfoselenide into a SiO_2-CeO_2 glassy phase, which have to be preserved during the zircon formation [113]. Since encapsulation is to some extent broken during micronization, it is not suitable for DD. A major issue is the high toxicity of cadmium, which imposes a standard control on Cd release from finished ceramic products [114].

Cassiterite doped with V is another classic among yellow colorants, but less used than baddeleyite [2], despite good tinctorial strength (typically 50<T*<75 at 1100-1200°C). The yellow color is originated by multiple chromophores, among which the dominating effect is by clusters of V^{5+} oxide included in tin oxide [2,180]. Co-doping with Ti and/or Al is a common practice to get color variants. Although still used in LT applications and sometimes in IT glazes, it is not employed in DD, as this pigment suffers from higher cost and worse tinctorial strength when compared to zircon-Pr. In addition, the high specific weight of tin oxide makes the ink more prone to sedimentation problems.

Rutile doped with Ni is a bright yellow pigment (commonly 50<T*<60 below 1150°C) needing a counterion that can be Sb, Nb, W or Mo [181,182]. Its synthesis is easy and can be performed also as solid solution with tin oxide [183,184]. It is employed more in other sectors than in ceramic production because of technological and safety issues. In fact, its stability is ensured only in LT applications, even though it would perform satisfactorily also in IT and as mass-stone. Nonetheless, the classification of nickel oxide as toxic and carcinogenic turned to be a major concern for pigment manufacturers.

Priderite doped with Ni is a traditional yellow pigment characterized by a peculiar primrose hue, not shown in Figure 16 [16,185]. Color is due to Ni^{2+} ion at one of the octahedral sites present in the hollandite-type structure [186]. The stability of $BaTi_8O_{17}$ in current glazes is limited, so the use of this pigment is restricted to some LT applications. As for rutile, the occurrence of nickel oxide is self-defeating, implying additional safety measures in the manufacturing cycle.

Srilankite doped with V gives a yellow color due to multiple chromophores: V^{4+} at a strongly distorted octahedral site, V^{4+}-V^{5+} intervalence charge transfer, and/or V-O charge transfer [178]. Its synthesis is not straightforward, as it needs the use of Al, In or Y, as counterions, and some Sn in substitution of Ti [187,188]. It is stable in most applications and exhibits a tinctorial strength (declining from T*~55 at 1000°C to T*~30 at 1200°C) midway from baddeleyite-V to zircon-Pr [178]. Although developed at industrial level, it had a very limited success, because of a worse benefit/cost ratio with respect to yellow zircon [188].

Rutile co-doped with Cr and Sb constitutes the reference pigment for orange colors (typically 60<T*<80 at 1100-1200°C). It can have Nb, Mo or Ta as counterion in replacement of Sb [189-191]. Synthesis is easy and can be performed in rotary furnaces [37]. Nonetheless, color stems from both crystal field (octahedrally-coordinated Cr^{3+}) and charge transfer (Cr-O) electronic transitions [181,182] that are affected by co-doping with Fe and Mn [37,192]. The color stability is good in LT and especially in BO applications, where it is largely used. Usually not employed in IT and HT glazes and not suitable for DD as primary pigment to be micronized. However, it is the pigment formed in-situ when soluble salts based on Ti-Cr-Sb organometallics are applied [104,193].

Pyrochlore $Pb_2Sb_2O_7$ (oxyplumboroméite) was widely used in the past, the so-called *Naples' yellow* [194], as an orange to yellow pigment, with color varying upon doping (Al, Ce, Fe, Sn, Zn). It is now completely abandoned by the ceramic industry for both technological and safety reasons. The former regard the poor thermal stability of the pigment, while the latter follow the ban of lead from modern ceramic manufacturing. This pigment is still used in some LT applications at level of craftsmanship.

There are other yellow and orange colorants proposed in the literature but never entered in the industrial use. For instance, **karrooite** doped with Ni or co-doped with Ni and Sb provides yellow to primrose shades (Fig. 16) rather stable in all applications (typically 30<T*<40 at 1100-1200°C) but DD [195,196]. Also, V doping was experimented, but it induces a complex structural rearrangement of karrooite crystal lattice, which implies a low purity of the final color, going from orange to buff [195]. For this reason, an employ for the V doping in the production of brown pigments with a T* ~80, is much more suggested [197].

Perovskites $SrSnO_3$ doped with V [198] or Cr and Tb [199], and $BaSnO_3$ doped with Tb [200] present pale yellow or light orange shades (Fig. 16). The color stability was tested at 1000-1050°C only with T* ~50 [199,200] or not verified at all [198].

Pyrochlore $Y_2Sn_2O_7$ co-doped with V and Ca [201,202] provides a yellow pigment (Fig. 16) that is stable only in double firing glazes at low temperature (T*~60 at 1000°C). The variants $Y_2Ti_2O_7$ [203] and $Dy_2Sn_2O_7$ [204] were proposed, also with V^{4+} as chromophore. In addition, lanthanide-based pyrochlores were investigated: $Y_2Ce_2O_7$ [205] and $Er_2Ce_2O_7$ [206] both doped with Mo. Such compounds have an orange color that revealed thermally instable even in a ceramic glaze at 1000°C. Their tinctorial strength is really too low (T*~30) to be taken into account as industrial pigment.

Geikielite $MgTiO_3$ doped with Ni requires high temperature for a successful calcination (i.e., 1400°C) and the synthesis is thermodynamically unfavored, leading to the co-existence of accessory phases [207]. This pigment shows a yellowish shade comparable to baddeleyite doped with V (Fig. 16) but is instable also in

low temperature glazes (50<T*<70 at 1000-1050°C). In order to improve the synthesis yield and the stability of this pigment a core-shell structure (consisting of TiO_2 core and outer ilmenite $NiTiO_3$ shell) obtained through sol-precipitation method was tested. Anyway, the color stability in low temperature glazes (1000°C) has been only qualitatively evaluated [208].

Powellite, $CaMoO_4$ doped with Cr, is characterized by a bright yellow color comparable to zircon-Pr (Fig. 16). It has excellent performances, with optimum tinctorial strength most of all in LT and IT technologies (75<T*<80 at 1000-1080°C), but good also in HT and BO applications (T*~65). Synthesis is easy, since pigment is obtained by a solid solution of Cr^{6+} substituting Mo^{6+} in the powellite lattice. Despite that, this pigment releases Cr^{6+} when washed, implying a strong safety hazard [209]. A pigment based on scheelite, $CaWO_4$ doped with Cr, isostructural with powellite, has a less intense yellow coloration [205].

Yttria doped with Tb^{4+} provides a pale yellow color, which requires Ca^{2+} or Ba^{2+} as counterion to balance Y^{3+} [210]. However, its synthesis is complex, as it involves solid, liquid and gas states and demands high control on the pigment stoichiometry [210]. Tests of this yellow pigment in industrial glazes at 1080°C indicate a good stability of Ca and Ba co-doped $Y_{1.86}Tb_{0.14}O_3$ (T*~65).

Zincite, i.e. ZnO doped with Co, Fe or V, was synthesized as a single phase with wurtzite structure that can give rise to different colors, depending on the dopant [211]. Nevertheless, to date, no tests on the pigments stability or tinctorial strength in glazes have been performed.

Rutile doped with Mo provides yellow to green tones, in accord with calcination temperatures. These compounds are characterized by low tinctorial strength already as calcinated powders (T*~50) and also suffer from color instability in glazes at intermediate temperatures, with a resulting T*~10 at 1165°C [212].

Orange colorants never entered in the industrial use consist essentially of cerianite and perovskite varieties.

Cerianite doped with Pr was extensively investigated and developed industrially, but its use is damped by high cost and specific weight of cerium oxide. The tinctorial strength is apparently good (70<T*<80) but, in reality, tested in the 1000-1100°C range only [213,214]. Similar coloration is achieved by doping with Tb, while using mixed lanthanides or other dopants (Cr, Eu, In) ensued a T*<50 [215]. Color can be tuned in various shades, at best resembling that of buff spinel and orange rutile. The synthesis of Pr-CeO_2, and to a lesser extent of Tb-CeO_2, has been profusely investigated in the last decade [216-218]: not only the classical ceramic method, but also by many non-conventional routes (*i.e.,* coprecipitation, flux method, combustion, pyrolysis, hydrothermal, microwave-assisted, and so forth). The results indicate that, opposite to the high temperature ceramic synthesis (1400-1500°C), the non-conventional way – especially the colloidal stabilization route with nitrates and the homogeneous coprecipitation route with oxalates and urea – allows to lower the calcination temperature down to 1100°C. Moreover, these methods enabled the formation of more homogeneous (single phase) solid solutions with optimal tinctorial strength in double-firing glaze (T*~80 at 1050°C). In addition, Pr-CeO_2 embedded in glass-ceramics was proposed as an encapsulated pigment [219].

Pyrochlore $Y_2Zr_2O_7$ doped with Pr and Fe, provides an orange to reddish brown color [155]. The synthesis by polymeric sol-gel method at 1400°C produced a defective fluorite structure able to confer high stability to the colorant in IT applications (68<T*<88 at 1080°C). As in the case of $Er_2(Zr,Ti)_2O_7$, the presence of Zr prevents the transition to an ordered pyrochlore structure with temperature, and allows to obtain an intense coloration of the pigment.

Finally, **gehlenite** $Ca_2Al_2SiO_7$ co-doped with Eu and Zn was proposed as an environment friendly yellow pigment [220].

5.3. Brown to maroon colorants

Brown and maroon colorants are important in ceramic decoration, because most graphics used in tile making are intended to reproduce natural surfaces, like stone, metal, skin and wood of various types, which have commonly a large range of brown shades. In addition, they are generally cheaper than “pure” colors. This makes brown pigments a viable substitute in DD of yellow, black and particularly magenta colorants (Fig. 17). Many brown pigments are based on the spinel structure, taking **chromite** as an archetype, which brownish color stems from Cr^{3+} and Fe^{2+} at the octahedral and tetrahedral sites, respectively. Numerous variants are achieved by the addition of Al, Mn, Ni, and especially Zn to modulate chromatic coordinates. In fact, Zn^{2+} occupies the tetrahedral site, forcing out chromophores like Mn^{2+}, Fe^{2+}, Fe^{3+}, Co^{2+} or Ni^{2+}, hence increasing the light transmittance in the yellow to red window. This category includes natural chromite, that is suitable only for mass-stone [221-222], as well as **franklinite** (Zn-Mn-Cr) and **jacobsite** (Mn-Fe-Cr), which ensure different shades, from light brown to coffee [37,223-225]. Doping with Ni (and/or Co) leads toward **trevorite** compositions (Zn-Ni-Fe-Cr) that provide a distinctly darker brown [226,227]. They are used in all applications, including sometimes BO, with tinctorial strength 75<T*<90 at 1200°C (Fig. 17). Redder shades of brown are widely exploited in DD, where they can replace magenta, despite color does not fit what theoretically required by quadrichromy. Another strategy with spinel pigments is the joint substitution of Zn^{2+} (tetrahedral site) and Al^{3+} and/or Fe^{3+} (octahedral site) that leads to light brown colors, extending to pale yellow or buff, like the case of **zincochromite** (Zn-Fe-Al-Cr). These are stable in all applications, having care to have some zinc in the matrix, and are common ingredients of yellow inks, together with other pigments [228-231]. They are useless in mass-stone since natural color of porcelain stoneware is a kind of light brown. Finally, dark brown is obtained by introducing Sn^{4+} and/or Ti^{4+} at the octahedral site and splitting Fe^{2+} in both four-fold and six-fold coordination in the inverse **ulvöspinel** pigment. Various shades are obtained by adding Cr, Al, and Zn [37], even though a careful control on synthesis is quite difficult. They are stable just in LT and IT applications [10,227].

Rutile co-doped with Cr and W gives a characteristic tobacco brown, appreciated in mass-stone (70<T*<85 at 1200°C) but seldom used in LT to IT firing cycles [181,182,185]. It is formed in-situ once Ti-Cr-W organometallics are applied with the soluble salts’ technology [103]. It exhibits a technological behavior similar to the orange rutile co-doped with Sb. Another dark brown pigment, but less common in use, is based on the rutile structure by combining Mn with a counterion (usually Sb, but also Nb or W can be used). Finally, titania doped with Cr, but without a proper counterion, was investigated: its tinctorial strength is worse than the above described rutile pigments [232].

Hematite is a popular brown pigment, which can assume many shades according to Fe:Cr:Al ratios and further dopings [233,234]. On the other hand, various shades of pure hematite appear, mainly due to the variation in crystallinity, particle size, shape and degree of aggregation [235,236]. Thus, the colour of this pigment depends on synthesis route [236]. Hematite is not stable in glazes, but in LT schedules it shows an excellent tinctorial strength, typically 75<T*<95 at 850-1000°C [237]. It is sometimes employed in mass-stone, but largely replaced by hematite-zircon and hematite-silica encapsulated pigments.

Iron, Nickel and Vanadium organometallics are applied, as penetrating soluble salts, to get a set of colors going from light brown (V) to brown with greenish (Ni) or reddish (Fe) shades [103]. In Ti-rich bodies, color changes to a brownish gray (Ni and Fe) or a chestnut brown (V).

Pseudobrookite can be easily synthetized by conventional ceramic route at 1300°C, with titania in moderate excess of the Fe_2TiO_5 stoichiometry [238,239]. This pigment exhibits a peculiar, intensely brown coloration

(Fig. 18) but its colouring performance depends on the chemico-physical properties of ceramic matrices: saturated brown shades achieved in low temperature glasses shift to a lighter brown in opacified glazes and fade to a light gray in wall tile glazes, where the high CaO and ZnO content contributes to rapidly dissolve pseudobrookite. Therefore, it is indicated in LT and IT applications (57<T*<63 at 1150°C).

Maroon and brown pigments not entered in the industrial use encompass, among others, many perovskites.

Perovskite **$CaTiO_3$ doped with Cr** provides light brown pigment due to the partial substitution of Ti^{4+} with Cr^{4+} in octahedral coordination sites. The synthesis of this colorant is easy, the classical solid-state ceramic route with or without the employ of mineraliser [240-243]. Both the color shade (Fig. 18) and stability strictly depend on the Cr doping of $Ca(Cr_xTi_{1-x})O_3$, and on the chemical system of the glaze. It demostrated to be stable only with low Cr doping (x=0.04 mol) in SiO_2-B_2O_3-CaO glaze systems, with a relatively good color yield, T*~66 at 1050°C [242]. On the other hand, its technological behavior becomes totally instable in SiO_2-ZnO-CaO glazes: at low Cr concentration (x≤0.05) the nuance of the pigment turns pink in glaze (57<T*<71 at 1050°C); while at higher Cr doping the color in glaze turns green for the crystallization of chromates, which dissolving in the melt impart this peculiar coloration. The use of mineraliser, in order to avoid the chromates formation, can further affect the color stability in glazes, leading to blue shades [240].

Perovskite **$CaTiO_3$ doped with V** gives brownish-pink shades, comparable to orange rutile (Fig. 18), thanks to the partial substitution of Ti^{4+} with V^{5+} [244]. The colorant obtained by conventional ceramic route has a relatively good performance in SiO_2-CaO-ZnO ceramic glazes (T*~70 at 1050°C) for a solid solution limit near x=0.2. Higher amounts of vanadium crystallize $Ca_2V_2O_7$, which dilutes the real amount of saturated $Ca(V_xTi_{1-x})O_3$ and diminishes the colour intensity.

Perovskite **$CaZrO_3$ doped with Cr** presents a brown color (T*~50 at 1050°C) due to the substitution of Zr^{4+} by Cr^{4+} [245]. The pigment proved to be unstable already at 820°C in highly aggressive alkali-boro-fluoro-silicate glazes, with dissolution in the molten glass. At the same time, Cr^{4+} is reduced to Cr^{3+}, responsible for the green color of the glaze. In the same way, **lanthanium aluminate doped with Cr**, $La(Al,Cr)O_3$, decomposes in aggressive glazes at low temperatures, entailing a colour degradation [246]. Another perovskite-like compound was proposed: Er_6MoO_{12} with a light brown color [247], which proved to be stable in a LT glaze (T*~55 at 1070°C).

Rare earth orthoferrites with a general formula $LnFeO_3$, provide brown to orange pigments. The addition of Ln^{3+} ions to Fe_2O_3 induces a change in color of perovskite. In particular, La and Gd form pigments of sienna or orange color, while adding Lu, Tm and Yb a dark reddish brown is achieved. However, they were not yet tested in ceramic glazes [248,249].

$Lu_3Ga_5O_{12}$ garnet doped with Cr and Ca shows a brownish pink color comparable to some brown spinels (Fig. 18). The pigment is formed by a solid solution of Ca^{2+} and Cr^{4+} substituting for Lu^{3+} in the dodecahedral site of $(Ca_xCr_xLu_{3-2x})Ga_5O_{12}$ and can be easily obtained by a solid state synthesis. Tests in single firing glaze at 1085°C indicated a good stability of the pigment, but a low final tinctorial strength, 50<T*<60 at 1085°C [250]. Also, the gallium-gadolinium garnet ($Gd_3Ga_5O_{12}$) doped with Cr was investigated, but no information was disclosed about its color in glazes [251].

Titanite doped with Cr is the titanium equivalent of the Cr-doped malayaite pigment, but instead of a burgundy, its color is a reddish brown [252-254]. No data about its behavior in glazes are available.

$BaFe_2O_4$ gives a light orange-brown tint. The employ of a polymeric precursor method leads to a high crystallinity material, avoiding the formation of secondary phases, otherwise occurring in the traditional ceramic synthesis. Pigment can be evaluated for LT application, since it showed good stability in ceramic

glaze at 1000°C, with T*~70 [255]. **$CaFe_2O_4$** and mostly **$MgFe_2O_4$** provide pigments with a darker brown color with respect to the $BaFe_2O_4$, but no tests on their stability in ceramic glaze are available to date [256,257].

Mg_2SnO_4 doped with Tb is an inverse spinel that shows a sandy yellow-buff color. The traditional ceramic synthesis is complicated by a difficult control on accessory phases [258]. Moreover, tests for LT applications (Fig. 16) revealed a low tinctorial strength (T*~40 at 1000°C). **$Zn_7Sb_2O_{12}$ doped with Co** may exhibit different colors, depending on which site – tetrahedral or octahedral – Co^{2+} occupies in substitution of Zn^{2+}. Based on doping, it is possible to obtain a yellow to black pigment. However, its behavior in ceramic glazes has not been tested yet [259].

Hibonite doped with Cr, Fe or Mn provides many different rosy-brown shades. Various substitutions are in fact possible at the Al sites in the $CaAl_{12}O_{19}$ host lattice. When Fe^{3+} is used as a chromophore, the color changes from yellow to red brown to dark chocolate by increasing the doping. When Mn is used, the color varies from burlywood to saddle brown. In the case of Cr-containing samples, the color changes from light rosy brown to grayish green with increasing Cr. Despite the great variety of colors obtainable with a simple solid-solution synthesis, no test on their stability in ceramic glazes is available yet [260].

Celsian doped with Fe in subtitution of Ba gives rise to a brownish-pink color [261]. The solid-solution is based on metal-doped $BaAl_2Si_2O_8$ lattice – where Fe^{3+} is expected to replace Al^{3+} in tetrahedral coordination – and is obtained by the conventional ceramic method. The resulting pigment is chemically stable in classical double firing glaze, but with a too low T*~35 (1050°C).

$FeNbO_4$ encapsulated in zircon can provide different shades (yellowish brown to earthy yellow) as the content of $FeNbO_4$ increases with respect to zircon [262]. Control on synthesis is not straightforward, as for complications to arrange a proper encapsulation, as because ixiolite is trimorphic and a phase transition occurs at 1085°C [263]. Anyway, the color of the pigments is not so intense (T*≤60) and no data are available on their chemical stability and final tinctorial strength in ceramic glazes.

$TiCeO_4$ doped with Pr obtained by solid-state reactions, with the substitution of Ce by Pr, has a color going from light pink to maroon, depending on the concentration of praseodymium. The color intensity of the different solid solutions is quite good, but their stability in ceramic matrix has not been investigated yet [264].

Further brown pigments developed at the lab scale include **willemite**, Zn_2SiO_4 doped with Cr [250] and **tialite**, Al_2TiO_5 doped with Mn [265]; both display a buff color (Fig. 18) stable in LT-IT applications, more intense in tialite (60<T*<64 at 1050°C) than in willemite (40<T*<47 at 1080°C). In addition, **cubic zirconia** takes a light brown color (T*~40 at 1100°C) once co-doped with Ca and Pr [266].

Recently, a range of **light brown phosphate-vanadate dyes** was investigated. They are based on $(Mg,Ni)_2P_2O_7$ [267]; $Ni_3(P,V)_2O_8$ and $Ni2(P,V)_2O_7$ [268]; $(Al,Fe)(P,V)O_4$ [269]; $(Ni,Co)_2P_2O_7$ [270] solid solutions. Their tinctorial strength in LT glazes is in between 60 and 82 at 1065°C (Fig. 16).

5.4. Green colorants

There is no all-season green in the ceramic palette, because the purest colorants have a limited thermal stability, while the most robust pigment – utilizable in every application – gives a coloration midway from green to blue (Fig. 19). In addition, these colorants are now relegated to occasional use in digital decoration, since green is not a basic color in quadrichromy and only special sets for hexachromy include a green ink.

Eskolaite pigments impart rather dull green colors with variable shades, according to doping with Al and/or Fe. In principle, it is highly refractory but suffers from a certain reactivity during firing. It is the reference colorant for mass-stone (70<T*<80 at 1200°C) and is still used in LT and occasionally in IT, max ~1100°C

[37]. However, its application in glazes is strongly constrained by the well-known incompatibility with Zn, Sn, and Ca [142,271,272]. Eskolaite is occasionally employed in DD as component of complex green inks.

Uvarovite, the so-called *Victoria green*, is based on $Ca_3Cr_2Si_2O_{12}$ garnet, possibly diluted with Al [273-276]. Unstable already in IT applications (unless in high calcium glazes) it provides the best color at LT (T*~70 at 1000°C). Its use is limited since decades, due to the hazards involved in solid-state synthesis, where $CaCrO_4$ forms and is responsible for high Cr^{6+} leaching in wastewaters [275].

Gahnite doped with Cr is a classic light green pigment [2,16,277]. Color can be easily tuned by the Al:Cr ratio and possible addition of Co, Fe, Mg, Mn, Sn and Ti as co-dopants. Although rather stable in all applications, it is seldom utilized, because coloration achievable is less saturated than other green pigments (T*~85 at 1080°C).

Cochromite is a spinel based on $CoCr_2O_4$ with various shades, according to the degree of occupancy of Co^{2+} at the tetrahedral site and Cr^{3+} at the octahedral site, which can be replaced by Mg, Zn, Al and Fe to get greenish blue to bluish green [37,278,279]. It has an excellent stability in glazes, but in Zn-rich ones (75<T*<80 at 1200°C); in bodies, its performance (65<T*<80 at 1200°C) in less satisfactory [37]. Sometimes used in DD, where the main hindrances are the cost (due to high amount of cobalt) and its hue far away from requirements of quadrichromy [10,280].

Green dyes are utilized exclusively as penetrating soluble salts in BO applications. Resulting colors vary from dark green-olive, based on Cr organometallics, to pale green-buff with Cu organometallics [103].

Liebenbergite, the nickel olivine Ni_2SiO_4, bestows a greenish yellow shade (Fig. 16) on LT glazes with fair tinctorial strength: 60<T*<75 at 1050°C [281,282]. It behaves likely as a dye: the color should derive from Ni^{2+} in multiple coordination (five-fold and six-fold) in the glass network. This colorant is not suited for DD and commonly not employed in IT and HT applications, mainly because of its high content of nickel (that makes it a hazardous material) and its color not pure.

Cobalt titanate is a green pigment with grayish-blue shades, based on the inverse spinel Co_2TiO_4. Although known at the industrial level, it has a poor technological performance (Fig. 19). Its use in LT technology, however, is tackled by high cost due to the amount of cobalt oxide [37].

There is a good number of green colorants not entered in the industrial practice yet.

$YCrO_3$ perovskite has an intense green color and a good performance in BO and LT, comparable with industrial pigments, but it is more expensive for the high yttria content [133,283,284].

Given by its stability at high temperatures and low thermal expansion coefficient, the **tialite** Al_2TiO_5 structure can be used for pigments production. The presence of metal cations into the two highly distorted octahedral sites inhibits the thermal decomposition of pure tialite and leads to the chromatic properties of pigment. The color is pale (40<T*<55 at 1050-1200°C) and may vary from green (Fig. 20) to greenish yellow (Fig. 16) passing from Co to Cr doping, respectively [265,285,286].

A less-pollutant and less-expensive alternative green pigment may be **karroite**, Co-doped $MgTi_2O_5$, an allochromatic solid solution for LT-IT applications [195,196]. This pigment exhibits a varied gamut of yellowish-green colors, showing a 55<T*<70 for calcined at 1200°C (Co molar content: 0–0.4). In glazes, a more turquoise coloration is developed, with a higher chromatic stability in Ca and Zn rich glasses [287].

Cr-doped $Y_2Ti_2O_7$ and $Y_2Sn_2O_7$ **pyrochlores** show rather similar optical properties. Given by the limited chromium solubility into the structure, any doping beyond 0.06-0.07 Cr atom/formula unit leads to green pigments with red shades, due to the presence of Cr^{4+} in the octahedral site of pyrochlore and of Cr^{3+} in the ternary perovskite side phase [152].

A wet chemical route – like Pechini, solution combustion or coprecipitation – can be used for the production of **zincite** doped at a molecular level [211,288-290]. The presence of Co or Fe into the flattened tetrahedral site, instead of zinc cations, determines a change in pigment color from greenish to yellowish, with a tinctorial strength of about 75 for 0.3 Co^{2+} molar content. In case of coprecipitation method, the solution pH and the precipitation agent nature can affect importantly the chromatic properties of the calcined pigment. In particular, the increase of pH from 7 to 10 by ammonia addition leads to an increase of both a* (i.e. from -16 to -8) and tinctorial strength (i.e. from 45 to 62). Similarly, the color changes from bright green to dark green by increase of calcination temperature (from 950 to 1200°C). The coprecipitated pigments can show high near-infrared reflectance, making them good candidates as cool pigments [288-290].

Yellow-green coloured pigments, with an intensity variation, can be obtained with **cuprates R_2BaCuO_5** (R = Y, Sm or Ho) having an ortorhombic structure, gettable by calcination (950-1050°C) or nitrate combustion. These superconducting ceramics contain isolated Cu^{2+} ions, interconnected by direct bonds through oxygen. The colour, given by d-d electronic transitions, is a light green. For Y_2BaCuO_5 obtained by combustion synthesis, the formed aggregates show a brighter color given by their higher surface area. Cuprates show a certain instability and reactivity with the glaze. After firing in ceramic glazes in IT conditions, a light-green to turquoise color is developed (Fig. 20) that can vary as a function of glaze formulation (52<T*<72 at 1070°C), leading to an important bubble formation in unleaded matrix [291,292].

Zircon matrix can be used as hosting structure for Cr^{3+} or Co^{2+} ions to produce thermally stable green pigments by aereosol hydrolysis and further synthetic routes [293-295]. The addition of mineralisers is required for the Cr containing systems, to reduce calcination temperature (1500°C) and to limit metal volatilization. The color saturation of pigments is different for Cr (T*~43) and Co (T*~51), the latter showing a greener shade, quite constant between 1100 and 1300°C [293].

The tetragonal **neodymium silicate** $Nd_2Si_2O_7$ can be prepared by the Pechini sol-gel method and subsequent thermal treatment. The addition of LiCl reduces the required calcination temperature (from 1300 to 1100°C), favoring the formation of the monoclinic structure, hence of a yellowish color. In glazes, the tinctorial strength goes from T*~53 at 1100°C toT*~45 at 1200°C [296].

$LnCrTeO_6$ has a structure AB_2O_6, with both A and B cations octahedrally coordinated to oxygen and Ln = La, Nd, Gd, Dy, Er, Tm or Yb. It can be used for a kind of “chromium green” for LT application (850-1000°C) having a color comparable to eskolaite (Fig. 20). Cr^{3+} in octahedral coordination acts as chromophore, leading to different shades that can be obtained by direct mixing of oxides and calcination at 1000°C. The colour changes from light to dark green passing from La to Yb, given by an increased crystal field splitting as a result of lattice parameters decreasing, maintaining the same colour shade also at high temperature. The presence of zincite must be controlled, given by its high reactivity with Cr. In presence of frits containing corrosive PbO, a dark green to yellowish hue is obtained. The coloration is rather intense (T*~80 at 1000°C) but thermal stability tested just for low temperatures [297].

For LT applications, also **$Pr_2Mo_2O_9$** can be used, where Pr is partially substituted by Ca in different amount. Synthesis was performed by both ceramic and wet nitrate routes [298]. The presence of Ca^{2+} instead of Pr^{3+} leads to a structural transition from cubic to monoclinic (when the Ca molar content is higher than 0.2) followed by a color change from green to yellow (25<T*<33 at 1050°C). The use of NaF as mineralizer results in a pale yellow that in glaze has just a greenish shadow (Figs. 16 and 20).

Co-Cr phosphates can be produced by simple calcination of precursors and addressed to IT applications. The increase of Co content implies a color change from yellowish green to bluish green [299]. Solid-state

reaction can be exploited also to dope iron oxide **Fe_2O_3** by progressive sobstitution of Fe^{3+} with Sc^{3+}, obtaining a colour change from reddish to greenish yellow [300].

5.5. Blue and turquoise colorants

Blue color in ceramics is commonly obtained by Co^{2+} in tetrahedral coordination in both pigment and dyes [301]. In fact, cobalt ions tend to assume the four-fold coordination also in glazes and glasses [302,303]. This circumstance explains the large recourse to cobalt dyes for the ceramic decoration. Cobalt colorants are characterized by the best performance per molar concentration, leading to brilliant and intense hue already for concentration lower than 1 %wt/wt. Blue colorants gained importance with the advent of inkjet printing as their use turned from occasional (only when necessary to have blue shades) to systematic in any graphics, even when no blue color is present, because of quadrichromy rules (Fig. 21). However, given by raising cost and limited reserves, cobalt became a strategic raw material and the ceramic industry has difficulty in the supply. Furthermore, cobalt shows toxic effects and is subjected to even more strictly environmental regulations. Cobalt appears to be hardly replaceable in order to achieve a deep blue coloration. Despite close to the cyan hue required by quadrichromy, turquoise pigments obtained with alternative chromophore, like V-doped zircon, are not used in DD.

Cobalt olivine is the reference for ultramarine blue. It consists of Co_2SiO_4 doped with Mg or Zn to lower the cobalt consumption [303,304]. It plays as a dye, being completely dissolved in glazes, so the original violet shade turns into a deep blue. It is widely used in glazes, in all the applications from LT to VHT ($90<T^*<100$ at 1200°C) but seldom as mass-stone (BO). This dye is the basic component of dark blue inks for DD [10].

Cobalt phosphates are quite popular blue dyes in LT and IT applications ($80<T^*<100$ at 1085°C). They are synthesized in crystalline form (sarcopside $Co_3(PO_4)_2$ and lithiophyllite $CoLiPO_4$ structures) but decompose during firing, releasing Co^{2+} in the glassy phase. Lithiophyllite is preferred because of the lower content of cobalt oxide. They are available in many variants, due to substitution of Co with Mg, Mn, Fe [305-308]. Magnesium borate is another blue dye, having the suanite $(Mg,Co)B_2O_5$ crystal structure, which behaves like phosphates during firing [2]. It is sometimes used in LT technology.

Cobalt organometallics are used in BO applications as penetrating soluble salts. They are based, as other cobalt dyes, on Co^{2+} ions dissolved in the glassy phase present in the porcelain stoneware bodies [103]. Color is a characteristic ultramarine blue, as for other dyes [101].

Cobalt aluminate spinel is the most important blue pigment, utilized in every application in glazes and bodies, and especially in DD [10,309]. Its color is purer than cobalt dyes and based on Co^{2+} at a regular tetrahedral site [301,303]. As $CoAl_2O_4$, it has a high tinctorial strength ($75<T^*<95$ at 1200°C) also in HT and BO applications [310]. There is a second pigment, $(Zn,Co)Al_2O_4$, which has similar technological properties ($70<T^*<80$ at 1200°C) but a distinctly greener shade (Fig. 22). Several variants are produced by doping with Cr, Fe, Ti and Zn to adjust hue and tinctorial strength [37,311]. It is a partially inverse spinel, implying that a small fraction of Co^{2+} is allocated at the octahedral site, depending on the cooling history [309]. This circumstance can explain color fluctuations in pigment production, since six-fold Co^{2+} provides a pink undertone. Available also in the encapsulated form [312]. A microemulsion-hydrothermal method can be used to obtain ultrafine pigments (~1 μm), reducing calcination temperature but increasing costs related to the synthesis [313].

Willemite doped with Co is an alternative blue pigment, even though less stable than spinel [303,314-316]. The color intensity scales with the cobalt concentration in $(Zn,Co)_2SiO_4$. Despite the good color saturation

(90<T*<100 at 1100-1200°C) it is seldom used in all applications. It is present in some complex blue inks for DD, together with other blue colorants [10].

Zircon doped with V is the reference pigment for turquoise shades. Its color stems from V^{4+} clusters hosted at an interstitial site of the zircon structure [317]. This circumstance explains the well-known difficulties in control and reproducibility of the synthesis [318-320]. It is stable in glazes, where can be used from LT to VHT applications, and in BO as well, with 50<T*<60 at 1200°C [37,321]. However, it is not utilized in DD yet, because its tinctorial strength is considerably reduced by micronization [40,41].

There are further blue and turquoise colorants that never entered in use.

Hardystonite doped with Co exhibits a blue shade similar to Co-gahnite (Fig. 22) and a tinctorial strength analogous to many cobalt dyes (T*~80 at 1150°C). It is stable in LT and IT firing cycles, but not in HT and BO, where it suffers from low-Ca glazes and bodies [322]. Not suitable in DD, likely because rapidly damaged during micronization. Another class of blue dyes based on calcium silicates is that of **clinopyroxenes**, where Co^{2+} can be accommodated at an octahedral site in substitution of Mg or Ca, giving rise to a violet color [323]. This phase is not stable in glazes and appears to be fully decomposed in IT to HT applications [324]. The chemical attack by the melt leads to the pyroxene breakdown and Co^{2+} ions diffusion, imparting a deep blue coloration and a tinctorial strength (90<T*<97 at 1200°C) as good as other dyes.

Celsian doped with Co was recently proposed as blue pigment [261]. In principle, it should be thermally stable, since $BaAl_2Si_2O_8$ is occasionally present in Ba-rich glazes [29], but polyphasic samples were obtained, where celsian, hexacelsian and unidentified phases occur together. Spectral features clearly indicate a tetrahedrally-coordinated Co^{2+}, which is likely present in some unidentified phase. The hue approaches that of blue spinels (Fig. 22) while tinctorial strength is, at best, T*~65 at 1050°C [261].

Hibonite, $CaAl_{12}O_{19}$, has a magnetoplumbite-type structure, which can accommodate a wide variety of ions with different valences and coordinations, making it interesting to pigment production [325]. It is the presence of Co^{2+} at a non-centrosymmetric tetrahedral site that ensures the intense blue color, particularly when Ti^{4+} or Sn^{4+} are used as counterion to compensate the Co^{2+}-Al^{3+} charge mismatch. Pigments can be prepared by solid state reaction at 1350-1400°C, also with Co-containing wastes [326]. The most intense hue was obtained for pigments calcined at 1350°C with a Co molar content of 0.3. In BO application, the bluish color (45<T*<70 at 1200°C) is similar to what obtained with willemite pigments (Fig. 22). On the contrary, in transparent glazes for IT production, chromatic differences are smaller, so suggesting that hibonite acts as a dye (80<T*<95 at 1050°C) for a Co content 0.15<x<0.45. **Hibonite doped with Ni** owes its color – a greenish shade of turquoise closer to cochromite (Fig. 20) than zircon-V (Fig. 22) – to Ni^{2+} at the tetrahedral site of the $CaAl_{12}O_{19}$ structure [327-329]. Apparently not stable in IT and HT glazes, it seems suitable only for LT (42<T*<47 at 1050°C) or BO applications (32<T*<35 at 1200°C) and was not considered for DD yet.

Turquoise shades can be imparted by using the nickel equivalent of known cobalt pigments, as the case of **spinel $NiAl_2O_4$** [330] and **willemite $(Zn,Ni)_2SiO_4$** [331,332] both exploiting a tetrahedrally-coordinated Ni^{2+}. However, while $NiAl_2O_4$ has a color similar to zircon-V, willemite-Ni approaches hibonite-Ni (Fig. 22). The calcination temperature modifies the colour by affecting both cations distribution at tedrahedral and octahedral sites and segregation of secondary phases, so limiting their applicability to LT. For instance, in nano-sized $Ni_xMg_{1-x}Al_2O_4$, different cation distribution and optical properties were found as a function of synthesis temperature and nickel content [333]. The higher is the calcination temperature, the greater is the degree of inversion in the spinel structure, with increasing Al^{3+} at the tetrahedral site and Ni^{2+} at the octahedral site. The resulting tetrahedral and octahedral splitting energies cause the change in the spectral

absorption (T* from 25 to 28 for 0.3<x<0.7). Tinctorial strength at 1085°C is T*~60 for $NiAl_2O_4$ and T*~35 for Ni-willemite [330,331]. Anyway, the presence of nickel can involve safety problems related to its toxicity.

A further class of turquoise pigments derives from the ancient Egyptian blue, i.e. **cuprorivaite** $BaCuSi_4O_{10}$, where Cu^{2+} occurs at a 5-fold coordinated site [334,335]. Barium can be replaced by Ca leading to a darkening of the color [336]. However, once in glaze, it takes a green shade (Fig. 20).

Recently, a different blue chromophore was pointed out: Mn^{3+} in 6-fold coordination in the **$YInO_3$ perovskite** [337,338]. The incorporation of Mn^{3+} at the trigonal bipyramidal site of In^{3+} leads to an ultramarine blue color, given by d−d transitions (E′→A′). The blue hue is darkened by an increase of Mn content (Mn/Y molar ratio 5<x<20). Colour is strongly influenced by glaze composition and firing temperature, fading away around 900°C in both B-containing glazes and plumbic frits [337]. This behavior severely restricts the end use to very low temperature applications. In any case, the industrial use is hindered by the prohibitive cost of indium and yttrium.

A blue colorant based on the **Y_2O_3-AlO_3-CoO** system was prepared by both solid-state reaction and mechanosynthesis [339]. The result is always multiphasic: YAP perovskite occurs admixed with spinel, YAG, YAM and yttria, in variable amounts depending on calcination temperature. The coloring performance is substantially related to the fraction of $CoAl_2O_4$ present in the mixture.

Amongst new **blue nanopigments**, the Al_2O_3/TiO_2 nanocomposite [340] and the spinel-like phase $Li_{1.33}Ti_{1.66}O_4$ [341] were both prepared by sol–gel methods. The former is doped by Co to obtain a blue colorant usable in DD technology. The color becomes more intense with the increase of Co^{2+} content, but is affected by the calcination temperature, with shift from blue to blue-green, thus limiting the pigment usage at LT and IT application [340]. The latter shows a bright turquoise color, attributed to Ti^{3+}-Ti^{4+} intervalence charge transfer, and a thermal stability up to 1000°C [341].

5.6. Black and gray colorants

In ceramics, black and gray are evaluated on a different basis with respect to other colors. Instead of a good tinctorial strength, the target is to have the lowest values of brightness and chroma. Therefore, the performance of black and gray colorants is assessed in the L*-C* diagram and not in the a*-b* plane.

There is a couple of universal black pigments that are industrially utilized in all the decoration technologies. In addition, few others are in use for BO or LT-IT applications (Fig. 23). In digital decoration, the black color is not used systematically, even if it is known its fundamental role to control the image quality in quadrichromy.

Among the best black colorants are **complex spinel compositions, based on cochromite** – also containing Fe and Mn – that are widely utilized in all decoration technologies, including inkjet printing, but rarely in bodies. A deep black color is achieved by the many optical bands due to multiple cations (Co^{2+}, Mn^{2+}, Mn^{3+}, Fe^{3+}, Cr^{3+} and sometimes Fe^{2+}, V^{3+}, Cu^{2+}) partitioned between the tetrahedral and octahedral sites [342-346]. The stability of these pigments is excellent, but in zinc-rich glazes, where they tend to assume a brownish nuance. A variant of the previous pigment is another **complex spinel based on nichromite**, used in every decoration technology as well, even though specifically addressed to withstand in Zn-rich environments. The larger affinity between the Jahn-Teller inactive Zn^{2+} (d^{10}) and Co^{2+} (d^7) ions compared to the Jahn-Teller active Ni^{2+} (d^8) ion in chromite spinel, where the strong preference on Cr^{3+} in octahedron prevents Ni^{2+} to be displaced from fourfold to sixfold coordination, provides a possible explanation of the less attitude for Zn to diffuse into nichromite than cochromite lattice. It should be noted that, similar to cochromite, nichromite compositions usually encompass other ions, namely Ni-Fe-Mn-Cr, and

occasionally Co-Cu-V and further elements. The complex interchange between these transition metal ions based on their different affinities related to their specific *d* orbitals configurations is likely to play a not fully clarified role on explanation of the above observation. The tinctorial strength is the best among black colorants [15,347-351]. Interestingly, nichromite pigments are characterized by C* on average lower than cochromite, even though L* values are fully comparable (Fig. 24). Further black spinels (e.g., binary Ni-Fe and Fe-Co or ternary Ni-Fe-Cr) exhibit higher L* values with respect to complex nichromite-cochromite formulations, but C* analogous to cochromite-based mixtures. At variance, the addition of Mg gives rise to dark gray pigments.

Another black pigment is **jacobsite**, i.e. a different solid solution of manganese and iron, which occur in multiple valences in both crystal sites of spinel [2], with respect to the brown variant in section 5.3. It is stable in LT-IT and BO applications, where is used because cheaper than complex black spinels, but unsuitable for porcelain stoneware glazes or digital decoration. A peculiar black pigment is **cuprospinel**, an antimagnet based on $CuCr_2O_4$ with limited doping from other metals [352]. It is stable just in LT and utilized when magnetic properties are needed.

Eskolaite-hematite is a well-known pigment that represents the reference black colorant for porcelain stoneware bodies [353,354]. Its stability in glazes and glassy coatings is limited, especially in presence of Zn, Ca, Ni, and Sn [37,355,356]. As the Cr_2O_3-Fe_2O_3 solid solution is complete, the pigment synthesis is easy over a wide range of compositions [357], which can give rise to reddish or greenish nuances, depending on the Cr:Fe ratio [358].

Ruthenium organometallics are the dye present in penetrating soluble salts to achieve a black color [103].

No universal gray colorant is able to satisfy all the different requirements of ceramic decoration (Fig. 23). Some pigments are used in traditional techniques (LT, IT, HT) but not in mass-stone or digital decoration, along with technological reasons, because in these applications the gray color is easy to be reproduced dosing properly a black colorant.

Cassiterite SnO_2 doped with Sb is an appreciated gray pigment, available in various shades depending on co-doping with Mn, Ti and Si [37,359,360]. It is a well-known semiconductor: the color stems from electronic transitions due to additional energy levels in the band linked to Sb^{3+} ions. Its electrical conductivity was exploited for special applications, as anti-electrostatic glazes [361,362]. The main limit to its use is the high cost of tin oxide.

Bunsenite encapsulated in zircon was a popular gray pigment, rather stable in all applications but DD. Various shades can be obtained, depending on the Co:Ni ratio and co-doping by Al, Fe, Mn, and Zn [37]. A strong limitation is the toxicity and carcinogenicity of NiO, which likely discouraged the registration in the REACH. In addition, the risk of Ni^{2+} leaching to glazes and bodies, if encapsulation is broken, prevented any use by inkjet printing, which requires micronized pigments.

Cobalt stannate is a gray pigment, with more or less accentuated greenish-blue shades, based on the inverse spinel Co_2SnO_4 (or sometimes a Co-doped cassiterite). Color derives from Co^{2+} at both tetrahedral and octahedral sites, giving rise to blue and pink colors, respectively, and a complex outcome of this mix with a blue prevalence. At variance of cochromite, it is not stable in HT applications [37] and not suited for DD. Its use in LT technology is contrasted by the high cost related to the large percentage of cobalt oxide.

Palladium organometallics are sometimes used to get gray shades by means of penetrating soluble salts [103].

Rutile doped with V and a proper counterion (generally Sb or Nb) is a well-known gray pigment that can show different tones, from bluish to reddish as a function of co-doping [181,182,363]. Its stability is ensured only in LT applications.

Black colorants never entered in use encompass perovskite **$LaCoO_3$**, which applications are limited to LT-IT. Its dark colour is given by crystal field, intevalence and Co-O charge transfer transitions ensured by different oxidation states of cobalt (Co^{2+} and Co^{3+}). The substitution of La with Ca allows reducing the pigment cost without importantly changes is L*, a* and b* parameters [364].

Sr-hexaferrite, $SrFe_{12}O_{19}$, in principle considered for its magnetic properties, was investigated (as BO and HT) in porcelain stoneware bodies. The addition of Co, Mn, Ni or Fe improved the light absorbance at lower wavenumbers, but resulted always in polyphasic products, containg also hematite and/or magnetite [365]. The color in fired bodies and glazes is a dark gray (L*~35 and C*~2.7) with greenish shades (Fig. 24).

Great interest has been devoted in the latest years to carbon-based pigments, instead heavy metals based ones, in order to reduce toxicity. The target is **carbon encapsulated in zircon**, composed of two insoluble structures: a carbon core and a transparent zircon coating to prevent pigment oxidation [366-370]. Soft-wet chemical routes were used to realize encapsulation, either by covering the carbonous particles or by direct in-situ carbon formation. In-situ carbon provided by carbon-containing precursors favors a homogeneous encapsulation. Many variables must be controlled, among which C/Zr molar ratio, layer thickness and deposition order of zircon precursors, and calcination schedule strongly affect the quality of pigments. A deep black can be obtained (down to L*~14) even though most literature data are in the 21<L*<42 range [370]. A particle size reduction brought about an undesired increase of L* that depends on synthesis parameters, which affect the final cover and pigment dimension. Correctly encapsulated pigments present an excellent color saturation (L*~34 and C*~0.9 at 900°C) in LT glazes [368].

An interesting candidate is **Al_2O_3-MoO_x**, a chemi-adsorbed pigment with a gray color and turquoise nuances (Fig. 22). Its peculiarity consists in clusters of molybdenum oxides that adhere on the corundum surface, where they are incorporated during calcination [371]. For this reason, high temperature annealing can cause a molybdenum volatilisation. Different valences (Mo^{4+}, Mo^{5+}, Mo^{6+}) contribute to a different extent to the final color, even if is the predominant Mo^{5+} the main responsible of the characteristic bluish gray. It displays a rather saturated color (60<T*<65 at 1200°C) in both HT and BO applications (Fig. 24).

5.7. White colorants

Opacifiers are extensively employed in all ceramic applications (Fig. 25) to get matt and semi matt glazes [2,372] as well as engobes [373] or white and “super white” porcelain stoneware bodies [37,374]. In contrast, the use of white inks is marginal in digital decoration [10]. White pigments have the basic role to mask the color of substrates by enhancing the light scattering [375]. For this purpose, a strict control on the amount, particle size and shape of white pigment is crucial [376,377] along with proper optical properties (see section 3.3). The final appearance may be dull to bright white, with a variable degree of translucency, and determined surface attributes (matt, semi matt, satin, translucent, etc). The color is usually evaluated by the CIE L* parameter (combined with a* and b* values as low as possible) or by the Kubelka-Munk formalism [39,378]. Opacifiers often fulfil additional functions, as damping the chemical attack to other pigments by saturation of the glaze (e.g., Zr^{4+} to improve the stability of Zr-colorants, see section 3.4). In other cases, white pigments are utilized to impart specific characteristics, like scratch resistance or anti-slip ability of ceramic surfaces [379].

Zirconium silicate, obtained by fine milling of natural zircon sands, is the most popular opacifier in all decoration techniques [380-382]. Its success stems from outstanding chemical stability in most ceramic matrices [383-387] and excellent optical properties (almost no light absorption in the visible spectrum, see Figure 7, joined to high refractive indices, Table 2). No significant interaction is known for $ZrSiO_4$ with other pigments [37]. In addition, it is able to improve the stability of Zr-bearing colorants, and rutile pigments as well (Table 5). The main limitation is a certain radioactivity [388] due to small amounts of U and Th in natural zircons (usually 50-100 $mg \cdot kg^{-1}$ each).

Baddeleyite is seldom utilized as opacifier in glazes, because it has good optical properties, but some disadvantages with respect to zirconium silicate [389]. ZrO_2 cannot be employed in mass-stone (zirconia reacts with silica to form zircon) or in digital inks (since they are micronized by zirconia microspheres, the milling yield is too low). In addition, more baddeleyite pigment is required to get the same whiteness, in force of its specific weight higher than zircon. Baddeleyite has a level of radioactivity analogous to zircon [388].

Cassiterite is a historical opacifier, widely used in ancient glazes [390,391]. SnO_2 exhibits the best optical characteristics for a white pigment: high refractive indices and negligible light absorbance in the visible range (Fig. 7). It has a good stability, ensured by its low solubility in ceramic glazes [392] and can be used to enhance the chemical resistance of tin-bearing pigments (malayaite, cassiterite doped with Cr, Sb or V). However, the occurrence of Sn^{4+} in the glaze is detrimental for eskolaite (green and black) and many spinel pigments [37]. Cassiterite is no longer used today, mainly because of its high cost (approximately 5 times that of zircon sand).

Corundum, although a common ingredient in ceramic frits, is seldom used as opacifier in glazes [393-395] but more frequently in engobes and “super white” bodies [37,374,396]. Its behavior is generally satisfactory in the various decoration techniques, and alumina is able to improve the chemical stability of many pigments (Table 5). However, the performance of α-Al_2O_3 as white pigment is lesser than other opacifiers in force of the low refractive indices (Table 2).

Zirconium, Cerium and Zinc organometallics provide the “white” color to the palette of soluble salts [103]. Although seldom employed in BO applications, their role has been revitalized by the chance to be used as white effect [397] or as primer in digital decoration.

Spinel $MgAl_2O_4$ is a white pigment proposed for glazes [398,399] where it never entered in use due to its low refractive index (Table 2). Nevertheless, it attracted the industrial interest for white-firing bodies, especially in times of zircon shortage [396]. Gahnite is a common component of Zn-rich glazes, as $ZnAl_2O_4$ and solid solutions with $MgAl_2O_4$. However, it usually occurs as a crystalline phase formed during firing by reaction of Zn and Al present in frits and raw glazes. The direct use of gahnite as white pigment is not carried out in the industrial practice, even though proposed in the literature [400,401].

Rutile and **cerianite** – although employed by the ceramic industry in the past [402-404] – have nowadays a limited use as opacifier in glazes, despite their very high refractive indices [405]. The main limitation is their unsatisfactory color purity, due to absorption of some violet-blue wavelengths that results in yellowish nuances (Fig. 7). In some glaze compositions, both titania and ceria undergo a rapid crystal growth, incompatible with the opacifier function [406,407]. This tendency is otherwise exploited to get peculiar aesthetic effects, as described in the following section.

There are some opacifiers that found just a limited use in the industrial production. Andalusite, wollastonite, and diopside are sporadically added as white pigments to glazes or porcelain stoneware bodies [29,408-

410]. Glass-ceramic frits (e.g., precipitating baghdadite, $Ca_3ZrSi_2O_9$) or even zincite are sometimes utilized in "super white" batches [411,412]. Sapphirine, $Mg_6Al_4Si_4O_{20}$, was proposed as opacifier in glazes [413].

5.8. Ceramic effects

The ceramic effects are used to impart peculiar optical, textural and functional properties to ceramic surfaces. Although utilized occasionally in LT, IT and HT applications, they have turned into a fundamental integration of quadrichromy (or hexachromy) in digital decoration. Recently, the pigment industry spent a considerable effort to search for new effects and develop proper suspensions for inkjet printing. This advancement is not mirrored in the scientific literature, where only few contributions deal with ceramic effects.

Account must be taken there is no classification of ceramic effects and no general agreement on criteria and terminology for their description. Therefore, the range of attributes that can be part of ceramic effects is rather wide, especially in the field of surface functionalization of ceramics. In the present review, we consider only the effects commonly utilized in ceramic manufacturing or candidates developed at least to the the industrial level (see some examples in Fig. 25).

The **gloss** or **matt** appearance, as bestowed on ceramic surfaces by inkjet decoration, is achieved by micronized transparent glasses or opacified glazes. These materials are formulated according to the conventional glaze technology, conveniently modified to account for the consequence of their small particle size. In fact, the firing behavior of micronized glazes is substantially changed in the kinetics of "melting", densification and crystallization, if any [414]. It is not disclosed which crystalline phases form in digital inks, among the ones known in ceramic glazes [28,415]. Further effects may be used to realize specific optical appearances (e.g., satin, transluscent) by tuning opportunely the amount and features of crystalline compounds and bubbles dispersed in the glaze [28,416]. In particular, translucency can be obtained by using BAS frits ($BaO\text{-}Al_2O_3\text{-}SiO_2$) that precipitate celsian, $BaAl_2Si_2O_8$ [411].

A classical way to realize a bas-relief pattern on the glaze surface is by a **sink** effect. It is achieved by applying low melting point compounds, typically based on V and Bi. The quintessential sink is vanadium pentoxide, but the incoming restrictions about V_2O_5 (connected with its toxicity and carcinogenity) have recently moved the industrial interest to bismuth vanadate, a well-known yellow colorant [417-420]. However, the color is lost on melting, leaving just the desired sink.

Lustre effects are pursued since antiquity [421] and for long time fulfilled by noble metal nanoparticles: Au, Pt, Ag, Cu [422-426]. Such applications are nowadays limited to third fire decoration of fine tableware. The metallic appearance on ceramic tiles is typically reproduced by surface precipitation of iron phosphate crystals in appropriate glazes [427]. However, this lustre is difficult to be realized by DD and is characterized by a poor chemical and tribological resistance. Therefore, to overcome these limitations, new solutions were developed in recent years, based on cerianite CeO_2 [428], tenorite CuO [429], scheelite $CaWO_4$ [430], powellite $CaMoO_4$ [416] or even stainless steel and a NiCoCrAlY alloy [431]. Gold lustre can be simulated in LT (third fire) also using pearlescent pigments, like TiO_2-coated mica [432].

The **glittering** effect is since long time known in ceramic decoration and often referred to as *aventurine* [433]. The mechanism behind shimmering glazes was disclosed, consisting of tiny crystal inclusions preferencially oriented in a translucent matrix [434,435]. By this way, light reflection depends on the incident angle, giving rise to a form of goniochromatism [436]. Industrially, the aventurine effect in glazes is imparted through precipitation of hematite in properly designed glazes [435-439].

The creation of a casual **speckle** effect, now easily reproduced by digital decoration graphics, was easily obtained by applying on the glaze colored refractory minerals (e.g., chromite) or man-made colored grains, like titania slag [440].

Phosphorescent glazes have been realized for ceramic tiles by introducing a phosphor, like Eu^{2+}-doped $SrAl_2O_4$ [441-443]. The main challenge is twice: i) having a sufficiently long afterglow of a proper color, and ii) preserving the phosphor during firing from the chemical attack of glaze. Since efficient phosphors have a limited thermal stability, satisfactory solutions were developed for LT or at most IT firings, best as thrid fire applications.

Cool pigments are characterized by a high solar reflectance (300-2500 nm) combined with a high thermal emissivity (4000-40000 nm). They are employed to get solar-reflective surfaces, which represent an effective countermeasure to the Urban Heat Island effect [444]. To be suitable for ceramic applications, such pigments must fulfil all requirements listed at sections 3 and 4. For this reason, the attention has been initially focused on current industrial colorants [444-447]. Recently, new cool pigments were proposed, including: yellow chromium-doped scheelite [205]; cyan cobalt-doped celsian, magenta chromium-doped armalcolite, yellow nickel-geikielite, green $CrNdO_3$ perovskite [447]; iron and tungsten co-doped lanthanum cerium oxide [448]; red-orange Tb-Fe and Pr-Fe co-doped pyrochlore $Y_2Zr_2O_7$ [155,449].

The performance improvement of ceramic products attracted a remarkable industrial interest in the last decade. It has been primarily pursued by surface functionalization through application of functional films or addition of the active compounds to glazes and glassy coatings. Three are the main industrial achievements, amongst the many proposals: **scratch resistant surfaces** have been developed adding soluble salts providing zirconium [396] or titanium and silver [450]; or alternatively nanoparticles of aluminium and zirconium oxides [451]. **Self-cleaning surfaces** have been realized by exploiting the photocatalytic effect of titania nanoparticles [452,453]. Attempts to achieve photocatalytic surfaces in the usual manufacturing conditions were unsuccessful, because of the anatase to rutile transition and concurrent crystal growth during firing at high temperatures [454,455]. Thus, photocatalytic tiles are currently produced by a second fire at low temperature [454,456]. New pigments have been proposed in order to improve both the photocatalytic efficiency and activity under visible light irradiation: they consist of anatase doped with N [457], Nb [458], W [459], rare earths and transition metals [460] or composites of titania and silica [461] and silver [450,462-464]. **Antibacterial activity** has been basically pursued through the application of silver compounds on ceramic surfaces. The challenge is to have enough Ag^+ ions available in the long run, but both silver oxidation and incorporation into the glass network of glazes must be prevented. For this purpose, various composites were proposed: Ag-silica [465], Ag-ZnO [466], Ag-nepheline [467] or Ag with calcium phosphate [468] as well as titania-coated silver nanoparticles [462-464]. However, the direct application of a thin film containing a sufficiently heat-resistant silver compound is at present preferred by the ceramic industry: e.g., Ag_2WO_4 [469], even though the best compromise of cost and performance was achieved with Nasicon-type solid solutions, like $(Na,Ag)Zr_2(PO_4)_3$ [470].

6. Lines of future research

The advent of digital decoration not only has revolutionized how pigments and dyes are manufactured and applied onto ceramic surfaces, but also the manner by which colorants are designed, formulated, and tested. Technological innovation brought about a groundbreaking change, both conceptual and practical, in the way colorant manufacturers conceive and carry out research and development activities.

From the conceptual point of view, the design of ceramic colorants underwent a paradigm shift, with emphasis moving to inks and related matters. This circumstance saw unexpected issues to stand out, such as the behavior of pigments during micronization or the interactions of colorants with organic carriers and additives, among others. At the same time, well-known aspects of decoration technology had to be reappraised at the light of the new characteristics of digital pigments and dyes. For instance, the relationship between color saturation and particle size of pigments, or the increased reactivity of micronized colorants in touch with glazes and glassy coatings. These questions have been magnified by the task to understand phenomena occurring at the scale of the ink drop, with all complications stemming from techniques used for color reproduction (quadrichromy typically plots four different ink drops on the same 64x64 µm target, with 400 dpi of native resolution).

In practice, the R&D laboratory was totally revamped, as new machinery and instrumentations are necessary to faithfully reproduce the industrial processes at the lab or pilot scale. This entails both ink-making (high-energy ball mill for micronization) and decoration (inkjet plotter to print test charts). Not to mention all techniques for ink characterization (including submicronic particle size, viscosity, surface tension) and measurement of the colorimetric coordinates on test charts. At the end of the day, the industry-academia distance increased a lot: before the digital decoration would take place, it was simple – in any ceramic laboratory – to simulate the manufacturing cycle of pigments and dyes. This because all the operations (solid-state synthesis in refractory crucibles, successive washing and milling, application by screen printing, spraying or pouring on ceramic substrates) could be run practically at the same scale of the industrial processes.

Notwithstanding the global diffusion of digital decoration in the ceramic tile industry (and its spreading through other ceramic and glass fields) not every technological question found a fully satisfactory answer yet. Further R&D efforts are necessary to overcome specific technological challenges of inkjet printing of pigments, dyes and effects. Hereafter, the main technological challenges still on the table are shortly reviewed, along with the evergreen issue of the search for new colorants. It is not an exhaustive list, but a summary of hot topics that can represent lines of future research. They pertain to the three pillars aimed at improving: the process efficiency, the performance of colorants, and the environmental sustainability.

Improving the efficiency of the ink-making process, from the colorant viewpoint, means essentially a better control on the micronization step. This task requires a deeper comprehension on the behavior of pigments and glasses during comminution, e.g. which mechanisms are active during high-energy milling in industrial conditions. Key points seem to be: i) the degree of pigment amorphization that is likely the cause of the loss of color saturation in digital inks; ii) the occurrence of plastic deformation and particle agglomeration phenomena during milling of vitreous materials, which is probably behind the current high energy consumption and very low efficiency to get submicronic glazes.

The performance of digital colorants can be improved by various routes, even though R&D investments are now hindered by the low price of digital inks. Two main strategies can be envisaged to enhance the colorant stability in ceramic matrices: i) shielding the pigment from the chemical attack of glaze, or ii) weakening the chemical aggressiveness of glaze against the pigment. The shield option primarily consists in a protective coating applied on a high-performance pigment: the challenge is to go beyond current encapsulation techniques in order to have a proper core-shell structure with the particle size imposed by inkjet printing. The option to damp the glaze aggressiveness needs to understand in depth the mechanisms of decomposition which pigments undergo during firing. This is the only way to improve the dual approach followed in DD, now

entirely empirical. On one hand, the pigment dissolution is minimized by an inert glass (the "protective coating") or a primer (able to "saturate" the glaze in some ingredients of the pigment) applied respectively after and prior inkjet decoration. On the other hand, undesired color shades, due to a given transition metal ion incorporated in the glaze after pigment leaching, are counterbalanced through another cation (absorbing further visible wavelengths) intentionally released to the glaze by a reformulation of the ink composition.

Reducing the impact of digital decoration on the Environment and Human health is a constant concern pursued by ink-makers and colorant manufacturers through a set of actions on well-defined aspects of pigment manufacturing and application. Sustainability implies also research to ban or minimize the use of toxic ingredients and mitigate the risks all along the chain from colorant synthesis to end use. New questions recently arose and need investigation to prevent possible problems. For instance, any chemical interaction of pigments with the organic compounds constituting the digital ink, particularly during the very early stage of firing, might catalyze the formation of undesired byproducts released to the flue gases.

Finally, the *search for new colorants* should be better focused on the actual (and foreseeable) needs of the ceramic industry. First of all, a complete technological characterization of candidate ceramic colorants is recommended, especially to include the most popular applications (DD with firing temperatures always above 1000°C and commonly close to 1200°C). The industrial interest seems now polarized by new effects and new functionalities (e.g., cool pigments). Looking at present-day color palette, new pigments and dyes should approach the chromatic coordinates of industrial cyan, magenta, yellow and black colorants. Another issue is to prevent problems in the access to colorant raw materials, e.g. by shortage and/or increasing price of some commodities. Considering that DD currently rests on a restricted variety of colorants, suitable alternatives should be actively searched, especially for cobalt (cyan and black inks) and praseodymium (yellow ink) which are likely to turn into critical raw materials in the future.

It must be clear that the lines of research illustrated above have been envisaged from a strictly technological point of view. Therefore, this industry-oriented perspective cannot cover all the possible subjects of investigation on ceramic dyes and pigments. First and foremost, basic research is crucial to provide that solid scientific background for any industrial development, particularly in a manufacturing sector – like ceramic colorants production is – still massively relying on an empirical approach. From this standpoint, investigating basic properties and synthesis processes is essential to improve the knowledge base necessary to understand in depth many facts occurring in the industrial production and ceramic application of pigments, dyes and effects. For instance, relating optical properties with crystal chemistry and structure turns fundamental to an efficacious pigment design. On the other hand, disclosing single and mutual effects of different parameters in the synthesis process is the key to improve industrial-scale operations. Last, but not least, it comes modelling, as a pressing request from colorant-makers to predict and design both physical or chemical features (e.g., optical properties) and behavior during synthesis or ceramic applications of pigments, dyes and effects.

References

[1] Bell, B. T. (1993). Ceramic colorants. Journal of the Society of Dyers and Colourists, 109(3), 101-105.

[2] Dondi, M., & Eppler, R. A. (2000). Ceramic colorants. Ullmann's Encyclopedia of Industrial Chemistry, 1-18.

[3] Dondi, M., Raimondo, M., & Zanelli, C. (2014). Clays and bodies for ceramic tiles: Reappraisal and technological classification. Applied Clay Science, 96, 91-109.

[4] Enrique, J. E., Amorós, J. L., & Moreno, A. (1996). Evolution of ceramic tile glazes. International Ceramics Journal, 20-26.

[5] Sánchez, E., García-Ten, J., Sanz, V., & Moreno, A. (2010). Porcelain tile: almost 30 years of steady scientific-technological evolution. Ceramics International, 36(3), 831-845.

[6] Nassetti, G., & Palmonari, C. (1997). Decoration of porcelain stoneware tiles. Ceram. Acta, 9(5), 15-21.

[7] Gardini, D., Dondi, M., Costa, A.L., Matteucci, F., Blosi, M., Galassi, C., Baldi, G. & Cinotti, E. (2008). Nano-sized ceramic inks for drop-on-demand ink-jet printing in quadrichromy. Journal of nanoscience and nanotechnology, 8(4), 1979-1988.
[8] Hutchings, I. (2010). Ink-jet printing for the decoration of ceramic tiles: technology and opportunities. Proc. XI World Congress on the Quality of Ceramic Tiles, Qualicer 2010, 16 p., Castellon (Spain).
[9] Solana Sanz, V. (2014). Inkjet printing technology for ceramic tile decoration. Proceedings XIII World Congress on the Quality of Ceramic Tiles, Qualicer 2014, 15 p., Castellon (Spain).
[10] Dondi, M., Blosi, M., Gardini, D., & Zanelli, C. (2012). Ceramic pigments for digital decoration inks: an overview. Ceramic Forum International, 89(8-9), E59-E64.
[11] Gardini, D., Blosi, M., Zanelli, C., & Dondi, M. (2015). Ceramic ink-jet printing for digital decoration: physical constraints for ink design. Journal of Nanoscience and Nanotechnology, 15(5), 3552-3561.
[12] Williams, E. S., Panko, J., & Paustenbach, D. J. (2009). The European Union's REACH regulation: a review of its history and requirements. Critical Reviews in Toxicology, 39(7), 553-575.
[13] Applegate, J. S. (2008). Synthesizing TSCA and REACH: practical principles for chemical regulation reform. Ecology LQ, 35, 721.
[14] Gualtieri, A. F., Mazzucato, E., Venturelli, P., Viani, A., Zannini, P., & Petras, L. (1999). Determination of nickel (II) oxide in ceramic pigments by in situ X-ray diffraction quantitative analysis. Journal of the American Ceramic Society, 82(9), 2566-2568.
[15] Calbo, J., Sorlí, S., Llusar, M., Tena, M. A., & Monrós, G. (2004). Minimisation of toxicity in nickel ferrite black pigment. British Ceramic Transactions, 103(1), 3-9.
[16] Eppler, R. A. (1987). Selecting ceramic pigments. Am. Ceram. Soc. Bull., 66(11) 1600-1604.
[17] Ardit M., Cruciani G., Dondi M., Zanelli C. (2016). Pigments based on perovskites. In: Perovskites and related mixed oxides: concepts and applications, V.I. Parvulescu, S. Kaliaguine, P. Granger, and W. Prellier (eds.), chapter 12, 259-288, Wiley-VCH Verlag GmbH & Co.
[18] Eppler, D. R., & Eppler, R. A. (1997). The relative stability of ceramic pigments. Ceramic Engineering and Science Proceedings, 18(2), 139-149.
[19] Eppler, R. A., & Eppler, D. R. (1994). Which colors can and cannot be produced in ceramic glazes? Ceramic Engineering and Science Proceedings, 15, 281-288.
[20] Murdock, S. H., Wise, T. D., & Eppler, R. A. (1990). Predicting the color of a ceramic glaze. American Ceramic Society Bulletin, 69(2), 228-30.
[21] Westland, S. (2003). Review of the CIE system of colorimetry and its use in dentistry. Journal of Esthetic and Restorative Dentistry, 15, S5-S12.
[22] Schanda, J., Ed. (2007). Colorimetry: understanding the CIE system. John Wiley & Sons, p. 453.
[23] Glaze stains – Body stains. Esmalglass-Itaca. https://www.esmalglass-itaca.com/en/products-and-solutions/colors (last access: March 19, 2020).
[24] Nassau, K. (2001). The fifteen causes of colour. John Wiley & Sons, New York, p. 481.
[25] Lever, A. P. (1984). Inorganic electronic spectroscopy. Elsevier, Amsterdam-New York, p. 863.
[26] Burns, R. G., & Burns, R. G. (1993). Mineralogical applications of crystal field theory. Cambridge University Press, Cambridge, p. 551.
[27] Henderson, B., & Imbusch, G. F. (2006). Optical spectroscopy of inorganic solids. Oxford University Press, Oxford, p. 662.
[28] Eppler, R. A., & Eppler, D. R. (2000). Glazes and glass coatings. American Ceramic Society.
[29] Casasola, R., Rincón, J. M., & Romero, M. (2012). Glass-ceramic glazes for ceramic tiles: a review. Journal of Materials Science, 47(2), 553-582.
[30] Katz, M., Gebhart, T., & Carty, W. (2003). The reevaluation of the unity molecular formula limits for glazes. Ceramic Engineering and Science Proceedings, 24(2), 13-24.
[31] Henderson, C. M. B., Charnock, J. M., & Plant, D. A. (2007). Cation occupancies in Mg, Co, Ni, Zn, Al ferrite spinels: a multi-element EXAFS study. Journal of Physics: Condensed Matter, 19(7), 076214.
[32] Malavergne, V., Guyot, F., Wang, Y., & Martinez, I. (1997). Partitioning of nickel, cobalt and manganese between silicate perovskite and periclase: a test of crystal field theory at high pressure. Earth and planetary science letters, 146(3-4), 499-509.
[33] Linton, J., Navrotsky, A., & Fei, Y. (1998). The thermodynamics of ordered perovskites on the $CaTiO_3$-$FeTiO_3$ Join. Physics and Chemistry of Minerals, 25(8), 591-596.
[34] Štemprok, M. (1990). Solubility of tin, tungsten and molybdenum oxides in felsic magmas. Mineralium Deposita, 25(3), 205-212.
[35] Dickinson Jr, J. E., & Hess, P. C. (1982). Zircon saturation in lunar basalts and granites. Earth and Planetary Science Letters, 57(2), 336-344.
[36] Ryerson, F. J., & Watson, E. B. (1987). Rutile saturation in magmas: implications for Ti-Nb-Ta depletion in island-arc basalts. Earth and Planetary Science Letters, 86(2-4), 225-239.
[37] Italian Ceramic Society (2003). Colour, Pigments and Colouring in Ceramics. SALA, Modena.
[38] Murdock, S. H., Wise, T. D., & Eppler, R. A. (1989). The effect of pigment particle size on glaze color. Ceramic Engineering and Science Proceedings, 9, 55-64.
[39] Schabbach, L. M., Bondioli, F., Ferrari, A. M., Manfredini, T., Petter, C. O., & Fredel, M. C. (2008). Color in ceramic glazes: Analysis of pigment and opacifier grain size distribution effect by spectrophotometer. Journal of the European Ceramic Society, 28(9), 1777-1781.
[40] Güngor, G.L., Kara, A., Blosi, M., Gardini, D., Guarini, G., Zanelli, C., Dondi, M. (2015). Micronizing ceramic pigments for inkjet printing: Part I. Grindability and particle size distribution. Ceramics International, 41, 6498-6506.

[41] Zanelli, C., Güngor, G.L., Kara, A., Blosi, M., Gardini, D., Guarini, G., Dondi, M. (2015). Micronizing ceramic pigments for inkjet printing: Part II. Effect on phase composition and color. Ceramics International, 41, 6507-6517
[42] Wang Y. & Forssberg E. 2007. Enhancement of energy efficiency for mechanical production of fine and ultra-fine particles in comminution. China Particuol., 5, 193-201.
[43] Holdich, R.G. (2002). Fundamentals of Particle Technology. Midland Information Technology and Publishing.
[44] Hukki, R.T. (1962). Proposal for a Solomonic settlement between the theories of Von Rittinger, Kick, and Bond. AIME Transactions, 223, 403-408.
[45] Walker W.H., Lewis W.K., McAdams W.H., Gilliland E.R. (1937). Principles of Chemical Engineering. McGraw-Hill, New York.
[46] Voller V.R. (1983). A note on energi-size reduction relationships in comminution. Powder Technology, 36, 281-286.
[47] Tanaka T. (1966). Comminution laws. I&EC Process Design and Development, 5, 353-358.
[48] Yüngevis H. & Ozel E. (2013). Effect of the milling process on the properties of $CoFe_2O_4$ pigment. Ceramics International, 39, 5503-5511.
[49] Guo D., Yang Q., Chen P., Chu Y., Zhang Y., Rao P. (2018). The influence of micronization on the properties of Pr-$ZrSiO_4$ pigment. Dyes and Pigments, 153, 74-83.
[50] Wang Y., Wang Q., Chang Q., Hu S., Wang X., Yang K. (2018). Effect of particle size on the blue chromate pigment $CoAl_2O_4$. Journal of Ceramic Science and Technology, 9, 43-46.
[51] Liu H., Wang Q., Chang Q., Wang C., Wang Y., Wang Y., Zhang X. (2019). Relationship between the colour and particle size of the ultrafine V-$ZrSiO_4$ and Pr-$ZrSiO_4$ pigments and their mixture. Materials Research Express, 6, 075214: 1-12.
[52] Ardit M., Cruciani G., Di Benedetto F., Sorace L., Dondi M. (2018). New spectroscopic and diffraction data to solve the vanadium-doped zircon pigment conundrum. Journal of the European Ceramic Society, 38, 5234-5245.
[53] Richet P. & Gillet P. (1997). Pressure-induced amorphization of minerals: a review. European Journal of Mineralogy, 9, 907-933.
[54] Anderson D. L. (1989). Theory of the Earth. Blackwell Scientific Publications, Oxford, 367 p.
[55] Angel R. J. (2000). Equations of State. In "High-Temperature and High-Pressure Crystal Chemistry", Hazen R. M. & Downs R. T. eds., Reviews in Mineralogy and Geochemistry, 41, 35-59.
[56] Finger, L. W. & Hazen, R. M. (1978). Crystal structure and compression of ruby to 46 kbar. Journal of Applied Physics, 49, 5823-5826.
[57] d'Amour, H., Schiferl, D., Denner, W., Schulz, H., & Holzapfel, W. B. (1978). High-pressure single-crystal structure determinations for ruby up to 90 kbar using an automatic diffractometer. Journal of Applied Physics, 49, 4411-4416.
[58] Richet, P., Xu, J.-A., & Mao, H.-K. (1988). Quasi-hydrostatic compression of ruby to 500 kbar. Physics and Chemistry of Minerals, 16, 207-211.
[59] Kim-Zajonz, J., Werner, S., & Schulz, H. (1999). High-pressure single crystal X-ray diffraction study on ruby up to 31 GPa. Zeitschrift für Kristallographie, 214, 331-336.
[60] Holland, T. J. B., & Powell, R. (2011). An improved and extended internally consistent thermodynamic dataset for phases of petrological interest, involving a new equation of state for solids. Journal of Metamorphic Geology, 29, 333-383.
[61] Catti, M., & Pavese, A. (1998). Equation of state of α-Al_2O_3 (Corundum) from Quasi-Harmonic atomistic simulations. Acta Crystallographica B, 54, 741-749.
[62] Goto, T., Anderson, O. L., Ohno, I., & Yamamoto, S., (1989). Elastic constants of corundum up to 1825 K. Journal of Geophysical Research, 94, 7588-7602.
[63] Pavese, A. (2002). Pressure-volume-temperature equation of state: a comparative study based on numerical simulation. Physics and Chemistry of Minerals, 29, 43-51.
[64] Özkan, H., Cartz, L., & Jamieson, J. C. (1974). Elastic constants of non-metamict zirconium silicate. Journal of Applied Physics, 45, 556-562.
[65] Özkan, H., & Jamieson, J. C. (1978). Pressure dependence of the elastic constants of non-metamict zircon. Physics and Chemistry of Minerals, 2, 215-224.
[66] Hazen, R. M., & Finger, L. W. (1979). Crystal structure and compressibility of zircon at high pressure. American Mineralogist, 64, 196-201.
[67] Ríos, S., & Boffa-Ballaran, T. (2003). Microstructure of radiation-damaged zircon under pressure. Journal of Applied Crystallography, 36, 1006-1012.
[68] Özkan, H. (2008). Correlations of the temperature and pressure dependencies of the elastic constants of zircon. Journal of the European Ceramic Society, 28, 3091-3095.
[69] Manghnani, M. H. (1969). Elastic constants of single-crystal rutile under pressures to 7.5 kilobars. Journal of Geophysical Research, 74, 4317-4328.
[70] Ming, L.-C., & Manghnani, M. H. (1979). Isothermal compression of TiO_2 (rutile) under hydrostatic pressure to 106 kbar. Journal of Geophysical Research, 84, 4777-4779.
[71] Hazen, R. M., & Finger, L. W. (1981). Bulk moduli and high-pressure crystal structures of rutile-type compounds. Journal of Physics and Chemistry of Solids, 42, 143-151.
[72] Mo, S.-D., & Ching, W. Y. (1995). Electronic and optical properties of three phases of titanum dioxide: rutile, anatase, and brookite. Physical Review B, 51, 13023-13032.
[73] Staun Olsen, J., Gerward, L., & Jiang, J. Z. (1999). On the rutile/α-PbO_2-type phase boundary of TiO_2. Journal of Physics and Chemistry of Solids, 60, 229-233.
[74] Staun Olsen, J., Gerward, L., & Jiang, J. Z. (2002). High-pressure behaviour of nano titanium dioxide. High Pressure Research, 22, 385-389.

[75] Haines, J., & Léger, J. M. (1997). X-ray diffraction study of the phase transitions and structural evolution of tin dioxide at high pressure: Relationships between structure types and implications for other rutile-type dioxides. Physical Review B, 55, 11144-11154.
[76] Liebermann, R. C. (1973). Elastic properties of polycrystalline SnO_2 and GeO_2: Comparison with stishovite and rutile data. Physics of the Earth and Planetary Interiors, 7, 461-465.
[77] Chang, E., & Graham, E. K. (1975). The elastic constants of cassiterite SnO2 and their pressure and temperature dependence. Journal of Geophysical Research, 80, 2595-2599.
[78] Ross, N. L., Zhao, J., & Angel, R. J., (2004). High-pressure single-crystal X-ray diffraction study of YAlO3 perovskite. Journal of Solid State Chemistry, 177, 1276-1284.
[79] Ross, N. L. (1996). Distortion of $GdFeO_3$-type perovskites with pressure: A study of $YAlO_3$ to 5 GPa. Phase Transitions, 58, 27-41.
[80] Wu, X., Qin, S., & Wu, Z. (2006). Generalized gradient approximation calculations of the pressure-induced phase transition of $YAlO_3$ perovskite. Journal of Physics: Condensed Matter, 18, 3907-3916.
[81] Li, Z., Fisher, E. S., Liu, J. Z., & Nevitt M. V. (1991). Single-crystal elastic constants of Co-Al and Co-Fe spinels. Journal of Materials Science, 26, 2621-2624.
[82] Akbudaka, S., Kushwahab, A. K., Uğurc, G., Uğurc, Ş., & Yaşar Ocak, H. (2018). Structural, electronic, elastic, optical and vibrational properties of MAl_2O_4 (M = Co and Mn) aluminate spinels. Ceramics International, 44, 310-316.
[83] Blasco, J., Subías, G., García, J., Popescu, C., & Cuartero, V. (2015). High-pressure transformation in the cobalt spinel ferrites. Journal of Solid State Chemistry, 221, 173-177.
[84] Levy, D., Diella, V., Pavese, A, Dapiaggi, M., & Sani, A. (2005). P-V equation of State, thermal expansion, and P-T stability of synthetic ($ZnCr_2O_4$ spinel). American Mineralogist, 90, 1157-1162.
[85] Zhang, Y., Liu, X., Xiong, Z., & Zhang, Z. (2016). Compressional behavior of $MgCr_2O_4$ spinel from first-principles simulation. Science China Earth Sciences, 59, 989-996.
[86] Liu, Y., Xing, J., Lia, Y., Tan, J., Sun, L., & Yan, J. (2016). Mechanical properties and anisotropy of thermal conductivity of $Fe_{3-x}Cr_xO_4$ (x = 0-3). Journal of Materials Research, 31, 3805-3813.
[87] Angel, R. J., Kunz, M., Miletich, R., Woodland, A. B., Koch, M., & Xirouchakis, D. (1999). High-pressure phase transition in $CaTiOSiO_4$ titanite. Phase Transitions, 68, 533-543.
[88] Rath, S., Kunz, M., & Miletich, R. (2003). Pressure-induced phase transition in malayaite, $CaSnOSiO_4$. American Mineralogist, 88, 293-300.
[89] Akdemir, S., Ozel, E., & Suvaci, E. (2011). Solubility of blue $CoAl_2O_4$ ceramic pigments in water and diethylene glycol media. Ceramics International, 37(3), 863-870.
[90] Ferrari, G., & Zannini, P. (2016). Thermal behavior of vehicles and digital inks for inkjet decoration of ceramic tiles. Thermochimica Acta, 639, 41-46.
[91] Ferrari, G., & Zannini, P. (2017). VOCs monitoring of new materials for ceramic tiles decoration: GC–MS analysis of emissions from common vehicles and inkjet inks during firing in laboratory. Boletín de la Sociedad Española de Cerámica y Vidrio, 56(5), 226-236.
[92] Escardino, A., Mestre, S., Feliu, C., Jodar, P., & Díaz, L. (2002). Stability of (Cr)CaO.SnO_2.SiO_2 pink pigment in ceramic frits. British Ceramic Transactions, 101(5), 213-220.
[93] Harisanov, V., Pavlov, R. S., Marinova, I. T., Kozhukharov, V., & Carda, J. B. (2003). Influence of crystallinity on chromatic parameters of enamels coloured with malayaite pink pigments. Journal of the European Ceramic Society, 23(3), 429-435.
[94] Cruciani G., Dondi M., Stoyanova T., Matteucci F., Carda J., Costa A.L., Malayaite ceramic pigments: a combined optical spectroscopy and neutron/X-ray diffraction study. Materials Research Bulletin, 44 (2009) 1778-1785.
[95] Lopez-Navarrete, E., Caballero, A., Orera, V. M., Lázaro, F. J., & Ocaña, M. (2003). Oxidation state and localization of chromium ions in Cr-doped cassiterite and Cr-doped malayaite. Acta Materialia, 51(8), 2371-2381.
[96] D[95oménech, A., Torres, F. J., Ruiz de Sola, E., & Alarcón, J. (2006). Electrochemical detection of high oxidation states of chromium (IV and V) in chromium-doped cassiterite and tin-sphene ceramic pigmenting systems. European Journal of Inorganic Chemistry, 2006(3), 638-648.
[97] Cordoncillo, E., Del Rio, F., Carda, J., Llusar, M., & Escribano, P. (1998). Influence of some mineralizers in the synthesis of sphene-pink pigments. Journal of the European Ceramic Society, 18(8), 1115-1120.
[98] Lee, H. S., & Lee, B. H. (2008). Colouring effect of malayaite formation and synthesis sphene-pink pigment. Journal of the Korean Ceramic Society, 45(3), 172.
[99] Lee, H. S., Park, J. S., & Lee, B. H. (2009). Synthesis of sphene-pink pigment under various firing conditions. Journal of the Korean Ceramic Society, 46(6), 615-620.
[100] Cavalcante P.M.T., Dondi M., Guarini G., Raimondo M., Baldi G., Colour performance of ceramic nano-pigments. Dyes and Pigments, 80 (2009) 226-232.
[101] Lambertson, R. H., Lacy, C. A., Gillespie, S. D., Leopold, M. C., & Coppage, R. H. (2017). Gold nanoparticle colorants as traditional ceramic glaze alternatives. Journal of the American Ceramic Society, 100(9), 3943-3951.
[102] Colomban, P. (2009). The use of metal nanoparticles to produce yellow, red and iridescent colour, from bronze age to present times in lustre pottery and glass: solid state chemistry, spectroscopy and nanostructure. Journal of Nano Research, 8, 109-132.
[103] Vignali, G. (2003). Soluble salts: organometallic complexes for colouring and decoration of porcelain gres tiles. In: “Colour, Pigments and Colouring in Ceramics”, chapter 10, pp. 163-182, Italian Ceramic Society and SALA, Modena, Italy.
[104] Mestre, S., Palacios, M. D., & Agut, P. (2012). Synthesis of a red pigment from gold nanoparticles. Boletin de la Sociedad Española de Ceramica y Vidrio, 51(2), 75-82.

[105] Saket, S., Rasouli, S., Arabic, A. M., & Sani, M. F. (2016). A novel approach to the synthesis of a wide range of ink jet printer pigment from yellow to magenta for tiles via gold nanoparticles. Journal of Ceramic Processing Research, 17(3), 246-252.
[106] Blosi M., Gatti F., Albonetti S., Baldi G., Dondi M., Au-Ag nanoparticles as red pigment in ceramic inks. Dyes and Pigments, 94 (2012) 355-362.
[107] Mestre, S., Chiva, C., Palacios, M. D., & Amorós, J. L. (2012). Development of a yellow ceramic pigment based on silver nanoparticles. Journal of the European Ceramic Society, 32(11), 2825-2830.
[108] López-Navarrete, E., González-Elipe, A. R., & Ocana, M. (2003). Non-conventional synthesis of Cr-doped SnO_2 pigments. Ceramics international, 29(4), 385-392.
[109] Julián, B., Beltrán, H., Cordoncillo, E., Escribano, P., Folgado, J. V., Vallet-Regí, M., & Real, R. P. D. (2002). A study of the method of synthesis and chromatic properties of the Cr-SnO_2 pigment. European Journal of Inorganic Chemistry, 2002(10), 2694-2700.
[110] Tena, M. A., Meseguer, S., Gargori, C., Forés, A., Badenes, J. A., & Monrós, G. (2007). Study of Cr-SnO_2 ceramic pigment and of Ti/Sn ratio on formation and coloration of these materials. Journal of the European Ceramic Society, 27(1), 215-221.
[111] Trojan, J., Luxová, J., & Šulcová, P. (2018). The effect of transition metals and rare-earth metals admixtures on the pigmentary properties of the cassiterite pigments. Scientific papers of the University of Pardubice. Series A, Faculty of Chemical Technology. 24/2018.
[112] Liu, H. F., Dai, W. B., Wang, H., Zeng, L. K., & Wang, Y. M. (2015). Study on the preparation of the $CdS_xSe_{1-x}@ZrSiO_4$ red ceramic pigments and its properties. Journal of Sol-Gel Science and Technology, 75(1), 198-205.
[113] Zhang, Y., Zeng, D., Rao, P., Cao, A., & Wu, J. (2008). Hydrothermal synthesis of cadmium sulfoselenide inclusion pigment. Journal of Sol-Gel Science and Technology, 48(3), 289-293.
[114] Zannini, P. (2019). Degradation due to milling of Cd, Se, Pr and Sn based pigments for ceramic inks. XVI Conference of the European Ceramic Society, Torino, Italy.
[115] Berry, F. J., Eadon, D., Holloway, J., & Smart, L. E. (1999). Iron-doped zircon: the mechanism of formation. Journal of Materials Science, 34(15), 3631-3638.
[116] Llusar, M., Badenes, J. A., Calbo, J., Tena, M. A., & Monros, G. (2000). Environmental and colour optimisation of mineraliser addition in synthesis of iron zircon ceramic pigment. British Ceramic Transactions, 99(1), 14-22.
[117] Ardizzone, S., Binaghi, L., Cappelletti, G., Fermo, P., & Gilardoni, S. (2002). Iron doped zirconium silicate prepared by a sol–gel procedure. The effect of the reaction conditions on the structure, morphology and optical properties of the powders. Physical Chemistry Chemical Physics, 4(22), 5683-5689.
[118] Cappelletti, G., Ardizzone, S., Fermo, P., & Gilardoni, S. (2005). The influence of iron content on the promotion of the zircon structure and the optical properties of pink coral pigments. Journal of the European Ceramic Society, 25(6), 911-917.
[119] Chu, H. L., Wang, C. L., Hwang, W. S., Lee, K. C., Zhou, X., & Wang, M. C. (2014). Kinetics of phase transformation and optical property of pink coral zirconia powders. Journal of Alloys and Compounds, 601, 307-318.
[120] Zumaquero, E., Orts, M. J., Sanz, V., & Mestre, S. (2017). Iron zircon pigment synthesis: Proposal of a mixing index for the raw materials mixtures. Boletín de la Sociedad Española de Cerámica y Vidrio, 56(4), 177-185.
[121] Wang, Y., Wang, Q., Chang, Q., Wang, Y., Zhao, Y., Wang, X., & Wang, Y. (2019). Chromatic study on the coloration mechanism of iron zircon pigment. Materials Chemistry and Physics, 121740.
[122] Sempio, A., & Gualtieri, A. (2002). Mineralogy of the “Grès de Thiviers” (Northern Aquitaine, France). Periodico di Mineralogia, 71(1), 65-84.
[123] Gualtieri, A. (2003). Different applications of “Grès de Thiviers”, a red pigment for traditional ceramics. Bulletin of European Ceramic Society, 1, 14-18.
[124] Bondioli, F., Ferrari, A. M., Leonelli, C., & Manfredini, T. (1998). Syntheses of Fe_2O_3/silica red inorganic inclusion pigments for ceramic applications. Materials Research Bulletin, 33(5), 723-729.
[125] Hosseini-Zori, M., Bondioli, F., Manfredini, T., & Taheri-Nassaj, E. (2008). Effect of synthesis parameters on a hematite–silica red pigment obtained using a coprecipitation route. Dyes and Pigments, 77(1), 53-58.
[126] Hosseini-Zori, M., Taheri-Nassaj, E., & Mirhabibi, A. R. (2008). Effective factors on synthesis of the hematite–silica red inclusion pigment. Ceramics International, 34(3), 491-496.
[127] Zhang, Y., Rao, P., Lü, M., Zeng, D., & Wu, J. (2009). Synthesis and color evolution of silica-coated hematite nanoparticles. Journal of the American Ceramic Society, 92(8), 1877-1880.
[128] Costa A.L., Zama I., Matteucci F., Dondi M., Albonetti S., Baldi G., Heterocoagulation-spray drying process for the inclusion of ceramic pigments. Journal of the European Ceramic Society 28 (2008) 169–176.
[129] Spinelli, A., Oliveira, A. P. N., Soledade, L. E. B., Paskocimas, C. A., Longo, E., Souza, A. G., Chicariano, C. A. & Flores, J. A. (2005). Propiedades ópticas del pigmento α-Fe_2O_3/SiO_2. Boletín de la Sociedad Española de Cerámica y Vidrio, 44(4), 223-227.
[130] Chen, S., Cheng, M., Lang, Y., Tian, C., Wei, H., & Wang, C. A. (2019). Preparation and characterization of monodispersed spherical $Fe_2O_3@SiO_2$ reddish pigments with core–shell structure. Journal of Advanced Ceramics, 8(1), 39-46.
[131] Baldi, G., Dolen, N., Barzanti, A., & Faso, V. (2004). Synthesis of a new class of red pigments based on perovskite-type lattice $A_xB_{2-xy}Cr_yO_3$ with $0.90<x<1$, $0.05<y<0.12$, A=Y, Lanthanides, B=Al for use in body stain and high temperature glazes. Key Engineering Materials, 264, 1545-1548.
[132] Marinova, Y., Hohemberger, J. M., Cordoncillo, E., Escribano, P., & Carda, J. B. (2003). Study of solid solutions, with perovskite structure, for application in the field of the ceramic pigments. Journal of the European Ceramic Society, 23(2), 213-220.

[133] Cruciani, G., Ardit, M., Dondi, M., Matteucci, F., Blosi, M., Dalconi, M. C., & Albonetti, S. (2009). Structural relaxation around Cr^{3+} in $YAlO_3$−$YCrO_3$ perovskites from electron absorption spectra. The Journal of Physical Chemistry A, 113(49), 13772-13778.

[134] Stobierska, E., Lis, J., Bućko, M. M., & Gubernat, A. (2006). Ceramic pigments with perovskite structure. Advances in Science and Technology, 45, 276-280.

[135] Shirpour, M., Sani, M. F., & Mirhabibi, A. (2007). Synthesis and study of a new class of red pigments based on perovskite YAlO3 structure. Ceramics International, 33(8), 1427-1433.

[136] Shin, K. H., & Lee, B. H. (2008). Synthesis of Cr-doped Y_2O_3-Al_2O_3 red pigments and their application. Journal of the Korean Ceramic Society, 45(8), 453.

[137] Matteucci F., Lepri Neto C., Dondi M., Cruciani G., Baldi G., Boschi A.O., Colour development of red perovskite pigment Y(Al,Cr)O_3 in various ceramic applications. Advances in Applied Ceramics, 105 [2] (2006) 99-106.

[138] Kato, M., & Takahashi, M. (2001). Synthesis of Cr-doped $NdAlO_3$-Al_2O_3 reddish pink pigment. Journal of Materials Science Letters, 20(5), 413-414.

[139] Shin, K. H., & Lee, B. H. (2009). Synthesis and Characterization of (Cr,Fe)-doped Y_2O_3-Al_2O_3 Red Pigments. Journal of the Korean Ceramic Society, 46(4), 350-356.

[140] Ianoş, R., Lazău, R., Băbuță, R., Muntean, E., Moacă, E. A., & Păcurariu, C. (2018). Solution combustion synthesis: a straightforward route for the preparation of chromium-doped lanthanum aluminate, $LaAl_{1-x}Cr_xO_3$, pink red pigments. Dyes and Pigments, 155, 218-224.

[141] Martos, M., Martínez, M., Cordoncillo, E., & Escribano, P. (2007). Towards more ecological ceramic pigments: Study of the influence of glass composition on the colour stability of a pink chromium-doped ceramic pigment. Journal of the European Ceramic Society, 27(16), 4561-4567.

[142] Bondioli, F., Ferrari, A. M., Leonelli, C., Manfredini, T., Linati, L., & Mustarelli, P. (2000). Reaction mechanism in alumina/chromia (Al_2O_3–Cr_2O_3) solid solutions obtained by coprecipitation. Journal of the American Ceramic Society, 83(8), 2036-2040.

[143] López-Navarrete, E., Caballero, A., González-Elipe, A. R., & Ocana, M. (2004). Chemical state and distribution of Mn ions in Mn-doped α-Al_2O_3 solid solutions prepared in the absence and the presence of fluxes. Journal of the European Ceramic Society, 24(10-11), 3057-3062.

[144] Lopez-Navarrete, E., & Ocana, M. (2004). Aerosol-derived Mn-doped Al_2O_3 pink pigments prepared in the absence of fluxes. Dyes and Pigments, 61(3), 279-286.

[145] Ricceri, R., Ardizzone, S., Baldi, G., & Matteazzi, P. (2002). Ceramic pigments obtained by sol-gel techniques and by mechanochemical insertion of color centers in Al_2O_3 host matrix. Journal of the European Ceramic Society, 22(5), 629-637.

[146] Maslennikova, G. N. (2001). Pigments of the spinel type. Glass and ceramics, 58(5-6), 216-220.

[147] Prim, S. R., Garcia, A., Galindo, R., Cerro, S., Llusar, M., Folgueras, M. V., & Monros, G. (2013). Pink ceramic pigments based on chromium doped $M(Al_{2-x}Cr_x)O_4$, M= Mg, Zn, normal spinel. Ceramics International, 39(6), 6981-6989.

[148] Fernández-Osorio, A., Pineda-Villanueva, E., & Chávez-Fernández, J. (2012). Synthesis of nanosized $(Zn_{1-x}Co_x)Al_2O_4$ spinels: new pink ceramic pigments. Materials Research Bulletin, 47(2), 445-452.

[149] Zhang, T., Huang, J., Yan, J., Pu, Z., Yin, X., & Wang, Y. (2019). The structural evolution and optical properties of $Mg_{1-x}Zn_xAl_{1.8}Cr_{0.2}O_4$ pink ceramic pigments. Ceramics International, 45, 16848-16854.

[150] Pavlov, R. S., Castelló, J. B. C., Marzá, V. B., & Hohembergerger, J. M. (2002). New red-shade ceramic pigments based on $Y_2Sn_{2-x}Cr_xO_{7-\delta}$ pyrochlore solid solutions. Journal of the American Ceramic Society, 85(5), 1197-1202.

[151] López-Navarrete, E., Orera, V. M., Lázaro, F. J., Carda, J. B., & Ocaña, M. (2004). Preparation through aerosols of cr-doped $Y_2Sn_2O_7$ (Pyrochlore) red-shade pigments and determination of the Cr oxidation state. Journal of the American Ceramic Society, 87(11), 2108-2113.

[152] Matteucci F., Cruciani G., Dondi M., Baldi G., Barzanti A. (2007). Crystal structural and optical properties of Cr-doped $Y_2Ti_2O_7$ and $Y_2Sn_2O_7$ pyrochlores. Acta Materialia, 55, 2229-2238.

[153] Martos, M., Julián-López, B., Cordoncillo, E., & Escribano, P. (2008). Structural and spectroscopic study of a novel erbium titanate pink pigment prepared by sol−gel methodology. Journal of Physical Chemistry B, 112(8), 2319-2325.

[154] Martos, M., Julián-López, B., Cordoncillo, E., & Escribano, P. (2009). Structural and spectroscopic study of a new pink chromium-free $Er_2(Ti,Zr)_2O_7$ ceramic pigment. Journal of the American Ceramic Society, 92(12), 2987-2992.

[155] Jovaní, M., Fortuño-Morte, M., Beltrán-Mir, H., & Cordoncillo, E. (2018). Environmental-friendly red-orange ceramic pigment based on Pr and Fe co-doped $Y_2Zr_2O_7$. Journal of the European Ceramic Society, 38(4), 2210-2217.

[156] Lyubenova, T. S., Carda, J. B., & Ocaña, M. (2009). Synthesis by pyrolysis of aerosols and ceramic application of Cr-doped $CaYAlO_4$ red–orange pigments. Journal of the European Ceramic Society, 29(11), 2193-2198.

[157] Thieme, C., & Rüssel, C. (2014). Temperature resistant red and purple ceramic pigments based on the solid solution series $BaZn_{2-x}Ni_xSi_2O_7$ and $BaMg_{2-x}Ni_xSi_2O_7$. Dyes and Pigments, 111, 75-80.

[158] Thieme, C., Waurischk, T., Lin, C., & Rüssel, C. (2016). Lilac ceramic pigments based on $Ba_{0.5}Sr_{0.5}Zn_{2-x}Ni_xSi_2O_7$ solid solutions. Ceramics International, 42(11), 13035-13040.

[159] Llusar, M., García, A., Gargori, C., Galindo, R., Badenes, J. A., & Monrós, G. (2012). Synthesis of diphosphate $Mn_{2-x}Mg_xP_2O_7$ solid solutions with thortveitite structure: New pink ceramic dyes for the colouration of ceramic glazes. Journal of the European Ceramic Society, 32(4), 765-776.

[160] Gu, X. Y., Luo, W. Q., & Chen, Y. X. (2010). Study on Co-$KZr_2(PO_4)_3$-type crystalline purple ceramic pigments. Applied Mechanics and Materials, 34, 790-794.

[161] Hunault, M., Robert, J. L., Newville, M., Galoisy, L., & Calas, G. (2014). Spectroscopic properties of five-coordinated Co^{2+} in phosphates. Spectrochimica Acta Part A: Molecular and Biomolecular Spectroscopy, 117, 406-412.

[162] Badenes, J. A., Vicent, J. B., Llusar, M., Tena, M. A., & Monros, G. (2002). The nature of Pr-$ZrSiO_4$ yellow ceramic pigment. Journal of Materials Science, 37(7), 1413-1420.

[163] Kar, J. K., Stevens, R., & Bowen, C. R. (2005). Processing and characterisation of Pr–zircon pigment powder. Advances in Applied Ceramics, 104(5), 233-238.

[164] Del Nero, G., Cappelletti, G., Ardizzone, S., Fermo, P., & Gilardoni, S. (2004). Yellow Pr-zircon pigments: The role of praseodymium and of the mineralizer. Journal of the European Ceramic Society, 24(14), 3603-3611.

[165] Kar, J. K., Stevens, R., & Bowen, C. R. (2004). Novel terbium-zircon yellow pigment. Journal of materials science, 39(18), 5755-5763.

[166] Kar, J. K., Stevens, R., & Bowen, C. R. (2007). Effect of cerium oxide on colour hue of praseodymium–zircon yellow pigment. Advances in Applied Ceramics, 106(4), 175-179.

[167] Guo, D., Xie, M., Ma, N., Yang, Q., Luo, Z., Chu, Y., & Rao, P. (2019). Synthesis and characterization of (Pr, Ce)-$ZrSiO_4$ ceramic pigments: The properties of the pigments and the effect of Ce. Journal of the American Ceramic Society, 102(5), 2619-2628.

[168] Bondioli, F., Corradi, A. B., Ferrari, A. M., Manfredini, T., & Baldi, G. (2000). Environmental scanning electron microscopy (ESEM) investigation of the reaction mechanism in praseodymium-doped zircon. Journal of the American Ceramic Society, 83(6), 1518-1520.

[169] Montoya, N., & Alarcón, J. (2012). Microstructural Evolution from Praseodymium-Containing Zircon Gels to Pr-ZrSiO4 Solid Solutions. Journal of the American Ceramic Society, 95(4), 1255-1260.

[170] Ocaña, M., Caballero, A., González-Elipe, A. R., Tartaj, P., Serna, C. J., & Merino, R. I. (1999). The effects of the NaF flux on the oxidation state and localisation of praseodymium in Pr-doped zircon pigments. Journal of the European Ceramic Society, 19(5), 641-648.

[171] Hill, K., Lehman, R., & Swiler, D. (2000). Effects of selected processing variables on color formation in praseodymium-doped zircon pigments. Journal of the American Ceramic Society, 83(9), 2177-2182.

[172] Pyon, K. R., & Lee, B. H. (2009). The influence of firing conditions on the color properties of Pr-$ZrSiO_4$ pigments synthesized using rice husk ash. Journal of the Korean Ceramic Society, 46(4), 397-404.

[173] Ren, F., Ishida, S., & Takeuchi, N. (1993). Color and vanadium valency in V-doped ZrO_2. Journal of the American Ceramic Society, 76(7), 1825-1831.

[174] Monrós, G., García, A., Sorlí, S., Benet, P., & Tena, M. A. (2003). Quantum sized chromophores in vanadium ceramic pigments. Materials Science Forum, 426, 2423-2427.

[175] Alarcón, J. (2001). Synthesis and characterization of vanadium-containing ZrO_2 solid solutions pigmenting system from gels. Journal of materials science, 36(5), 1189-1195.

[176] Torres, F. J., Amigó, J. M., & Alarcón, J. (2003). X-ray powder diffraction study of monoclinic V^{4+}-ZrO_2 solid solutions obtained from gels. Journal of Solid State Chemistry, 173(1), 40-44.

[177] Calatayud, J. M., & Alarcón, J. (2017). V-containing ZrO_2 inorganic yellow nano-pigments prepared by hydrothermal approach. Dyes and Pigments, 146, 178-188.

[178] Dondi M., Matteucci F., Zama I., Cruciani G., High-performance yellow ceramic pigments $Zr(Ti_{1-x-y}Sn_{x-y}V_yM_y)O_4$ (M = Al, In, Y): crystal structure, colouring mechanism and technological properties. Materials Research Bulletin, 42 (2007) 64-79.

[179] Lei, B., Qin, W., Kang, G., Peng, C., & Wu, J. (2015). Modeling and evaluation for encapsulation efficiency of zircon-based heteromorphic encapsulation pigments. Dyes and Pigments, 112, 245-254.

[180] Joo, I. D., Hwang, D. H., Lee, H. S., Park, J. S., & Lee, B. H. (2009). Synthesis of SnO_2-TiO_2-V_2O_5 System Yellow Pigment. Journal of the Korean Ceramic Society, 46(6), 639-642.

[181] Matteucci F., Cruciani G., Dondi M., Raimondo M., The Role of Counterions (Mo, Nb, Sb, W) in Cr-, Mn-, Ni- and V-doped Rutile Ceramic Pigments. Part 1. Crystal Structure and Phase Transformations. Ceramics International, 32 (2006) 385-392.

[182] Dondi M., Cruciani G., Guarini G., Matteucci F., Raimondo M., The Role of Counterions (Mo, Nb, Sb, W) in Cr-, Mn-, Ni- and V-doped Rutile Ceramic Pigments. Part 2. Colour and Technological Properties. Ceramics International, 32 (2006) 393-405.

[183] Sorlí, S., Tena, M. A., Badenes, J. A., Calbo, J., Llusar, M., & Monrós, G. (2004). Structure and color of $Ni_xA_{1-3x}B_{2x}O_2$ (A= Ti, Sn; B= Sb, Nb) solid solutions. Journal of the European Ceramic Society, 24(8), 2425-2432.

[184] Martos, M., Julián, B., Dehouli, H., Gourier, D., Cordoncillo, E., & Escribano, P. (2007). Synthesis and characterization of $Ti_{1-2x}Nb_xNi_xO_{2-x/2}$ solid solutions. Journal of Solid State Chemistry, 180(2), 679-687.

[185] Maloney, J. (2009). Titanate pigments: colored rutile, priderite, and pseudobrookite structured pigments. In: High Performance Pigments, pp. 53-73, Wiley-VCH Verlag GmbH & Co., Weinheim, Germany.

[186] Carter, M. L., & Withers, R. L. (2005). A universally applicable composite modulated structure approach to ordered $Ba_xM_yTi_{8-y}O_{16}$ hollandite-type solid solutions. Journal of Solid State Chemistry, 178(6), 1903-1914.

[187] Siggel, A., & Jansen, M. (1990). $ZrSn_{0,5}Ti_{0,5}O_4$ als Wirtsstruktur für keramische Farbkörper Strukturuntersuchungen an ZrTiO4 und $ZrSn_{0,5}Ti_{0,5}O_4$. Zeitschrift für anorganische und allgemeine Chemie, 582(1), 93-102.

[188] Dondi M., Matteucci F., Cruciani G., Zirconium titanate ceramic pigments: Crystal structure, spectroscopy and technological properties. Journal of Solid State Chemistry, 179 (2006) 233-246.

[189] Tena, M. A., Monrós, G., Carda, J., Cordoncillo, E., Escribano, P., & Alarcón, J. (1994). Synthesis of CrxTi1−2xNbxO2 O 2 0≤ x≤ 0.5 rutile solid solutions from alkoxides. Journal of Materials Science, 29(14), 3817-3821.

[190] Tena, M. A., Llusar, M., Badenes, J. A., Vicente, M., & Monrós, G. (2000). Influence of precursors on formation of TiO_2–$CrTaO_4$ rutile solid solutions. British Ceramic Transactions, 99(5), 219-224.

[191] Tena, M. A., Escribano, P., Monrós, G., Carda, J., & Alarcón, J. (1992). Influence of niobate structures on the formation of rutile solid solutions [$M^{III}NbO_4$-1bTiO_2, where M^{III} = Al, Fe, Cr]. Materials Research Bulletin, 27(11), 1301-1308.

[192] Gargori, C., Cerro, S., Galindo, R., & Monrós, G. (2010). In situ synthesis of orange rutile ceramic pigments by non-conventional methods. Ceramics International, 36(1), 23-31.

[193] Večeřa, J., Dohnalová, Ž., Mikulášek, P., & Šulcová, P. (2014). The influence of concentration of doping elements on anatase–rutile transformation at the synthesis of rutile pigments $(Ti,Cr,Nb)O_2$ and their pigmentary properties. Journal of Thermal Analysis and Calorimetry, 116(2), 547-555.

[194] Dik, J., Tichelaar, F., Goubitz, K., Peschar, R., & Schenk, H. (2002). 19th Century Naples yellow re-examined. Zeitschrift für Kunsttechnol. Konserv., 16, 291-306.

[195] Matteucci F., Cruciani G., Dondi M., Gasparotto G., Tobaldi D.M., Crystal structure, optical properties and colouring performance of karrooite $MgTi_2O_5$ ceramic pigments. Journal of Solid State Chemistry, 180 (2007) 3196-3210.

[196] Llusar, M., García, E., García, M. T., Gargori, C., Badenes, J. A., & Monrós, G. (2015). Synthesis, stability and coloring properties of yellow–orange pigments based on Ni-doped karrooite $(Ni,Mg)Ti_2O_5$. Journal of the European Ceramic Society, 35(1), 357-376.

[197] Kim, G. & Lee, B.-H. (2011). Synthesis and characterization of V_2O-doped karrooite brown pigments. Journal of the Korean Ceramic Society, 48(4), 303-306.

[198] Adolfová, L., Dohnalová, Ž., & Šulcová, P. (2013). New inorganic pigments based on $SrSnO_3$ doped by V_2O_5. Journal of thermal analysis and calorimetry, 113(1), 161-167.

[199] Adolfová, L., Dohnalová, Ž., Šulcová, P., & Matušková, M. (2014). Ceramic pigments based on doped strontium stannates. Journal of Thermal Analysis and Calorimetry, 116(2), 709-714.

[200] Luňáková, P., Trojan, M., Luxová, J., & Trojan, J. (2013). $BaSn_{1-x}Tb_xO_3$: A new yellow pigment based on a perovskite structure. Dyes and Pigments, 96(1), 264-268.

[201] Ishida, S., Ren, F., & Takeuchi, N. (1993). New yellow ceramic pigment based on codoping pyrochlore-type $Y_2Ti_2O_7$ with V^{5+} and Ca^{2+}. Journal of the American Ceramic Society, 76(10), 2644-2648.

[202] Gargori, C., Galindo, R., Cerro, S., García, A., Llusar, M., & Monrós, G. (2010). Synthesis of a new $Ca_xY_{2-x}VxSn2-_xO_7$ yellow pigment. Physics Procedia, 8, 84-87.

[203] Pailhé, N., Gaudon, M., & Demourgues, A. (2009). (Ca^{2+}, V^{5+}) co-doped $Y_2Ti_2O_7$ yellow pigment. Materials Research Bulletin, 44(8), 1771-1777.

[204] Šulcová, P., Fukalová, P., Válek, L., & Trojan, M. (2009). Study of ceramic pigments based on $Dy_2Sn_{2-x}V_xO_7$. Scientific papers of the University of Pardubice. Series A, Faculty of Chemical Technology. 14 (2008).

[205] Cerro, S., Llusar, M., Gargori, C., & Monrós, G. (2019). Cool and photocatalytic yellow ceramic pigments; from lead-tin to Cr doped scheelite pigments. Ceramics International, 45(4), 4613-4625.

[206] Stránská, L., Šulcová, P., & Mouchová, J. (2012). Study of ceramic pigments based on $Er_2Ce_{2-x}Mo_xO_7$. Journal of thermal Analysis and Calorimetry, 109(2), 643-648.

[207] Llusar, M., García, E., García, M. T., Esteve, V., Gargori, C., & Monrós, G. (2015). Synthesis and coloring performance of Ni-geikielite $(Ni,Mg)TiO_3$ yellow pigments: Effect of temperature, Ni-doping and synthesis method. Journal of the European Ceramic Society, 35(13), 3721-3734.

[208] He, X., Wang, F., Liu, H., Li, J., & Niu, L. (2017). Synthesis and coloration of highly dispersed $NiTiO_3$@TiO_2 yellow pigments with core-shell structure. Journal of the European Ceramic Society, 37(8), 2965-2972.

[209] Galindo, R., Gargori, C., Fas, N., Llusar, M., & Monrós, G. (2015). New chromium doped powellite ($Cr–CaMoO_4$) yellow ceramic pigment. Ceramics International, 41(5), 6364-6372.

[210] De la Luz, V., Prades, M., Beltrán, H., & Cordoncillo, E. (2013). Environmental-friendly yellow pigment based on Tb and M (M = Ca or Ba) co-doped Y_2O_3. Journal of the European Ceramic Society, 33(15-16), 3359-3368.

[211] Milao, T. M., Oliveira, J. F. A., Araújo, V. D., & Bernardi, M. I. B. (2010). $Zn_{0.97}M_{0.03}O$ (M = Co, Fe, and V) pigments: thermal, structural, and optical characterization. Journal of thermal analysis and calorimetry, 103(3), 873-877.

[212] Silvestri, S., Kubaski, E. T., Sequinel, T., Pianaro, S. A., Varela, J. A., & Tebcherani, S. M. (2013). Optical properties of the MoO_3-TiO_2 particulate system and its use as a ceramic pigment. Particulate Science and Technology, 31(5), 466-473.

[213] Šulcová, P., Trojan, M., & Šolc, Z. (1998). Cerium dioxide fluorite type pigments. Dyes and Pigments, 37(1), 65-70.

[214] Llusar, M., Vitásková, L., Šulcová, P., Tena, M. A., Badenes, J. A., & Monrós, G. (2010). Red ceramic pigments of terbium-doped ceria prepared through classical and non-conventional coprecipitation routes. Journal of the European Ceramic Society, 30(1), 37-52.

[215] Topuz, H., Ozel, E., & Turan, S. (2004). Synthesis of the CeO_2 Based Pigments by Using Enriched Rare-earth Oxides Located at Eskişehir Kızılcaören Region. Key Engineering Materials, 264, 1553-1556.

[216] Bondioli, F., Ferrari, A. M., Leonelli, C., Siligardi, C., Hart, N. A., & Evans, N. G. (2001). The application of microwaves in the synthesis of $Ce_{0.9}Pr_{0.1}O_2$ nanostructured powders. Journal of Materials Chemistry, 11(10), 2620-2624.

[217] Ocaña, M. (2002). Preparation and properties of uniform praseodymium-doped ceria colloidal particles. Colloid and Polymer Science, 280(3), 274-281.

[218] Masó, N., Beltrán, H., Muñoz, R., Julián, B., Carda, J. B., Escribano, P., & Cordoncillo, E. (2003). Optimization of praseodymium-doped cerium pigment synthesis temperature. Journal of the American Ceramic Society, 86(3), 425-430.

[219] Bondioli, F., Manfredini, T., Siligardi, C., & Ferrari, A. M. (2005). New glass–ceramic inclusion pigment. Journal of the American Ceramic Society, 88(4), 1070-1071.

[220] Bae, B., Tamura, S., & Imanaka, N. (2016). Novel environmentally friendly inorganic yellow pigments based on gehlenite-type structure. Ceramics International, 42(13), 15104-15106.

[221] Bondioli, F., Ferrari, A. M., Leonelli, C., & Manfredini, T. (1997). Chromite as a pigment for fast-fired porcelain tiles. Ceramic Engineering and Science Proceedings, 18, 44-58.
[222] Ozel, E., Kucuk, I., & Turan, S. (2002). Synthesis of an iron-chromium ceramic pigment by using limonite and chromite mixtures. Key Engineering Ceramics, 206, 1827-1830.
[223] Aly, M. H., Ismael, I. S., & Bondioli, F. (2010). Synthesis of coloured ceramic pigments by using chromite and manganese ores mixtures. Cerâmica, 56(338), 156-161.
[224] Xavier, C. S., Candeia, R. A., Bernardi, M. I. B., Lima, S. J. G., Longo, E., Paskocimas, C. A., & Santos, I. M. (2007). Effect of the modifier ion on the properties of $MgFe_2O_4$ and $ZnFe_2O_4$ pigments. Journal of Thermal Analysis and Calorimetry, 87(3), 709-713.
[225] Dohnalová, Ž., Šulcová, P., & Trojan, M. (2009). Effect of Er^{3+} substitution on the quality of Mg-Fe spinel pigments. Dyes and Pigments, 80(1), 22-25.
[226] Gurbuz, N., Coskun, E., & Ozel, E. (2010). Production of Ni and Co-gahnite pigments using ZnO powder produced from metal slags. Journal of Ceramic Processing Research, 11(2), 184-190.
[227] Souza, S. C., Souza, M. A. F., Lima, S. J. G., Cassia-Santos, M. R., Fernandes Jr, V. J., Soledade, L. E. B., & Santos, I. M. (2005). The effects of Co, Ni and Mn on the thermal processing of Zn_2TiO_4 pigments. Journal of Thermal Analysis and Calorimetry, 79(2), 455-459.
[228] Bernardin, A. M. (2008). Diffusion of Cr–Fe–Al–Zn pigment in a zirconia glaze. Dyes and Pigments, 79(1), 54-58.
[229] Naghibzadeh, S., Faghihi-Sani, M. A., & Baghshahi, S. (2013). Synthesis of beige pigment on the basis of (Fe, Zn, Cr, Al) spinel. International Journal of Engineering and Advanced Technology, 2(3), 606-609.
[230] Caki, M., Karasu, B., & Kaya, G. Use of iron and zinc oxide based pigments in stoneware glazes. In: J.G.Heinrich and C. Aneziris (eds.), Proc. 10th ECerS Conf., Göller Verlag, Baden-Baden, 2007, 1784-1787.
[231] Andreozzi, G. B., Baldi, G., Bernardini, G. P., Di Benedetto, F., & Romanelli, M. (2004). ^{57}Fe Mössbauer and electronic spectroscopy study on a new synthetic hercynite-based pigment. Journal of the European Ceramic Society, 24(5), 821-824.
[232] Vieira, F. T. G., Melo, D. S., de Lima, S. J. G., Longo, E., Paskocimas, C. A., Júnior, W. S., de Souza, A. G. & dos Santos, I. M. G. (2009). The influence of temperature on the color of TiO_2:Cr pigments. Materials Research Bulletin, 44(5), 1086-1092.
[233] Turan, S., Inceefe, Y., & Ozel, E. (2004). Production and characterisation of pigments produced using grinding waste from cast iron foundry. Key Engineering Materials, 264, 2473-2476.
[234] Ozel, E., Unluturk, G., & Turan, S. (2006). Production of brown pigments for porcelain insulator applications. Journal of the European Ceramic Society, 26(4-5), 735-740.
[235] Katsuki, H., & Komarneni, S. (2003). Role of α-Fe_2O_3 Morphology on the Color of Red Pigment for Porcelain. Journal of the American Ceramic Society, 86(1), 183-185.
[236] Opuchovicn, O., Kareiva, A. (2015). Historical hematite pigment: Synthesis by an aqueous sol-gel method, characterization and application for the colouration of ceramic glazes. Ceramics International 41, 4504-4513.
[237] Rodrigues Fiuza, T. E., Marcelino Borges, J. F., Marimon da Cunha, J. B., Masetto Antunes, S. R., Chaves de Andrade, A. V., Celso Antunes, A., Ferreira de Souza, E. C. (2018). Iron-based inorganic pigments from residue: Preparation and application in ceramic, polymer, and paint. Dyes and Pigments 148, 319-328.
[238] Dondi M., Matteucci F., Cruciani G., Gasparotto G., Tobaldi D.M., Pseudobrookite ceramic pigments: crystal structural, optical and technological properties. Solid State Sciences, 9 (2007) 362-369.
[239] Mesíková, Ž., Šulcová, P., & Trojan, M. (2006). Yellow pigments based on Fe_2TiO_5 and TiO_2. Journal of Thermal Analysis and Calorimetry, 83(3), 561-563.
[240] Gargori, C., Cerro, S., Galindo, R., García, A., Llusar, M., & Monrós, G. (2012). Iron and chromium doped perovskite (CaMO3 M= Ti, Zr) ceramic pigments, effect of mineralizer. Ceramics International, 38(6), 4453-4460.
[241] García, A., Galindo, R., Gargori, C., Cerro, S., Llusar, M., & Monrós, G. (2013). Ceramic pigments based on chromium doped alkaline earth titanates. Ceramics International, 39(4), 4125-4132.
[242] Hajjaji, W., Zanelli, C., Seabraa, M.P., Dondi, M., Labrinchaa, J.A. (2011). Cr-doped perovskite and rutile pigments derived from industrial by-products. Chemical Engineering Journal 171, 1178– 1184.
[243] Zou, J., Zhang, T., & He, X. (2019). Dark brown Cr doped $CaTiO_3$ pigments with high NIR reflectance. Materials Letters, 248, 173-176.
[244] Gargori, C., Cerro, S., Galindo, R., García, A., Llusar, M., Badenes, J., & Monrós, G. (2011). New vanadium doped calcium titanate ceramic pigment. Ceramics International, 37(8), 3665-3670.
[245] Ianoş, R., & Lazău, R. (2014). Chromium-doped calcium zirconate–A potential red shade pigment: Preparation, characterization and testing. Dyes and Pigments, 105, 152-156.
[246] Ianoş, R., Muntean, E., Lazău, R., Băbuță, R., Moacă, E. A., Păcurariu, C., & Hulka, I. (2018). One-step synthesis of near-infrared reflective brown pigments based on iron-doped lanthanum aluminate, $LaAl_{1-x}Fe_xO_3$. Dyes and Pigments, 152, 105-111.
[247] Kar, J. K., Stevens, R., & Bowen, C. R. (2008). Processing and characterisation of various mixed oxide and perovskite-based pigments for high temperature ceramic colouring application. Journal of Alloys and Compounds, 461(1-2), 77-84.
[248] Dohnalová, Ž., Šulcová, P., & Trojan, M. (2008). Synthesis and characterization of $LnFeO_3$ pigments. Journal of Thermal Analysis and Calorimetry, 91(2), 559-563.
[249] Liu, L., Han, A., Ye, M., & Zhao, M. (2015). Synthesis and characterization of Al^{3+} doped $LaFeO_3$ compounds: a novel inorganic pigments with high near-infrared reflectance. Solar Energy Materials and Solar Cells, 132, 377-384.
[250] Galindo, R., Llusar, M., Tena, M. A., Monrós, G., & Badenes, J. A. (2007). New pink ceramic pigment based on chromium (IV)-doped lutetium gallium garnet. Journal of the European Ceramic Society, 27(1), 199-205.

[251] Monrós, G., Pinto, H., Badenes, J., Llusar, M., & Tena, M. A. (2005). Chromium (IV) stabilisation in new ceramic matrices by coprecipitation method: application as ceramic pigments. Zeitschrift für anorganische und allgemeine Chemie, 631(11), 2131-2135.
[252] Stoyanova Lyubenova T., Matteucci F., Costa A.L. Dondi, M., Carda J., Ceramic pigments with sphene structure obtained by both spray- and freeze-drying techniques. Powder Technology, 193 (2009) 1-5.
[253] Stoyanova Lyubenova T., Matteucci F., Costa A.L., Dondi M., Ocaña M., Carda J., Synthesis of Cr-Doped CaTiSiO5 pigments by spray drying. Materials Research Bulletin, 44 (2009) 918–924
[254] Lyubenova, T. S., Ocaña, M., & Carda, J. (2008). Brown ceramic pigments based on chromium (III)-doped titanite obtained by spray pyrolysis. Dyes and pigments, 79(3), 265-269.
[255] Candeia, R. A., Souza, M. A. F., Bernardi, M. I. B., Maestrelli, S. C., Santos, I. M. G., Souza, A. G., & Longo, E. (2007). Monoferrite $BaFe_2O_4$ applied as ceramic pigment. Ceramics International, 33(4), 521-525.
[256] Candeia, R. A., Souza, M. A. F., Bernardi, M. I. B., Maestrelli, S. C., Santos, I. M. G., Souza, A. G., & Longo, E. (2006). $MgFe_2O_4$ pigment obtained at low temperature. Materials Research Bulletin, 41(1), 183-190.
[257] Candeia, R. A., Bernardi, M. I. B., Longo, E., Santos, I. M. G., & Souza, A. G. (2004). Synthesis and characterization of spinel pigment $CaFe_2O_4$ obtained by the polymeric precursor method. Materials Letters, 58(5), 569-572.
[258] Dohnalová, Ž., Šulcová, P., & Trojan, M. (2010). Synthesis and colour properties of pigments based on terbium-dopped Mg_2SnO_4. Journal of thermal analysis and calorimetry, 101(3), 973-978.
[259] Gouveia, D. S., Soledade, L. E. B., Paskocimas, C. A., Longo, E., Souza, A. G., & Santos, I. M. G. (2006). Color and structural analysis of $Co_xZn_{7-x}Sb_2O_{12}$ pigments. Materials Research Bulletin, 41(11), 2049-2056.
[260] Medina, E. A., Li, J., & Subramanian, M. A. (2017). Colored oxides with hibonite structure II: structural and optical properties of $CaAl_{12}O_{19}$-type pigments with chromophores based on Fe, Mn, Cr and Cu. Progress in Solid State Chemistry, 45, 9-29.
[261] Gargori, C., Cerro, S., Fas, N., Llusar, M., & Monrós, G. (2018). Ceramization of heavy metals in $(Ba_{1-x}M_x)Al_2Si_2O_8$ celsian solid solutions and recycling as pigments. Materials Letters, 221, 187-191.
[262] Zhang, Q., Yang, Q., Sun, Y., & Wang, H. (2018). Low temperature synthesis of a new yellowish brown ceramic pigment based on $FeNbO_4$@$ZrSiO_4$. Ceramics International, 44(11), 12621-12626.
[263] Roth, R. S., & Waring, J. L. (1964). Ixiolite and other polymorphic types of $FeNbO_4$. American Mineralogist, 49(3-4), 242-246.
[264] Kumari, L. S., George, G., Rao, P. P., & Reddy, M. L. P. (2008). The synthesis and characterization of environmentally benign praseodymium-doped $TiCeO_4$ pigments. Dyes and Pigments, 77(2), 427-431.
[265] Dondi M., Stoyanova Lyubenova T., Carda J., Ocaña M., M-doped Al_2TiO_5 (M=Cr,Mn,Co) solid solutions and their use as ceramic pigments. Journal of the American Ceramic Society, 92 [9] (2009) 1972-1980.
[266] Badenes, J. A., Llusar, M., Tena, M. A., Calbo, J., & Monros, G. (2002). Praseodymium-doped cubic Ca–ZrO_2 ceramic stain. Journal of the European Ceramic Society, 22(12), 1981-1990.
[267] Tena, M. A. (2012). Characterization of MgxM2−xP2O7 (M= Cu and Ni) solid solutions. Journal of the European Ceramic Society, 32(2), 389-397.
[268] Tena, M. A., Mendoza, R., García, J. R., & García-Granda, S. (2017). Structural characterization and colour of $Ni_3V_xP_{2-x}O_8$ ($0 \le x \le 2$) and $Ni_2V_yP_{2-y}O_7$ ($0 \le y \le 2$) materials. Results in physics, 7, 1095-1105.
[269] Tena, M. A., Mendoza, R., Martínez, D., Trobajo, C., García, J. R., & García-Granda, S. (2019). Beige materials for the ceramic industry: $Al_xV_yFe_{1-x}P_{1-y}O_4$ ($0.0 \le x \le 0.3$, $0.0 \le y \le 0.1$) solid solutions. Ceramics International, 45(7), 8271-8278.
[270] Tena, M. Á., Mendoza, R., Trobajo, C., García, J. R., & García-Granda, S. (2019). $Co_2P_2O_7$–$Ni_2P_2O_7$ solid solutions: Structural characterization and color. Journal of the American Ceramic Society, 102(6), 3695-3704.
[271] Liang, S. T., Zhang, H. L., Luo, M. T., Luo, K. J., Li, P., Xu, H. B., & Zhang, Y. (2014). Colour performance investigation of a Cr_2O_3 green pigment prepared via the thermal decomposition of CrOOH. Ceramics International, 40(3), 4367-4373.
[272] Li, P., Xu, H. B., Zheng, S. L., Zhang, Y., Li, Z. H., & Bai, Y. L. (2008). A green process to prepare chromic oxide green pigment. Environmental science & technology, 42(19), 7231-7235.
[273] Carda, J., Monros, G., Escribano, P., & Alarcon, J. (1989). Synthesis of uvarovite garnet. Journal of the American Ceramic Society, 72(1), 160-162.
[274] Carda, J., Monrós, G., Tena, M. A., Marti, M. C., Cordoncillo, E., & Escribano, P. (1992). Profundizacíon en el estudio de la síntesis y microcaracterización del pigmento verde victoria ($Ca_3Cr_2Si_3O_{12}$) de aplicación en la industria cerámica. Boletín de la Sociedad Española de Cerámica y Vidrio, 31(1), 19-31.
[275] Llusar, M., Vicent, J. B., Tena, M. A., Badenes, J., Escribano, P., & Monrós, G. (1997). Environmental optimization of green Victoria ceramic pigment by sol-gel methods. Key Engineering Materials, 132, 2236-2239.
[276] Llusar, M., Monros, G., Tena MÁ, Vicent, J. B., & Badenes, J. A. (1999). Effect of synthesis methods and aging on synthesis of uvarovite garnet by ceramic and sol-gel processes. British Ceramic Transactions, 98(3), 113-121.
[277] Verger, L., Dargaud, O., Rousse, G., Cotte, M., & Cormier, L. (2017). The stability of gahnite doped with chromium pigments in glazes from the French manufacture of Sèvres. Journal of the American Ceramic Society, 100(1), 86-95.
[278] Catalan, L., Contreras, G., Ramos, F., Bedoya, D., Vicente, M., & Monros, G. (2000). Structural modification of cobalt chromite by doping with Mg^{2+} and Zn^{2+} ions and their effect on colour in glassy matrices. Proc. VI World Congress on the Quality of Ceramic Tiles, Qualicer 2000, Vol. 3, Castellon (Spain).
[279] Gilabert, J., Palacios, M.D., Sanz, V., Mestre, S. (2018). Effects of composition and furnace temperature on $(Ni,Co)(Cr,Al)_2O_4$ pigments synthesized by solution combustion route. Int J Appl Ceram Technol.,15, 179-190.
[280] Wang, Y., Wang, Q., Chang, Q., Hu, S., Wang, X., & Yang, K. (2018). Effect of particle size on the blue chromate pigment $CoAl_2O_4$. Journal of Ceramic Science and Technology, 9(1), 43-46.

[281] Esteves, D., Hajjaji, W., Seabra, M. P., & Labrincha, J. A. (2010). Use of industrial wastes in the formulation of olivine green pigments. Journal of the European Ceramic Society, 30(15), 3079-3085.
[282] El Hadri, M., Ahamdane, H., & Raghni, M. E. I. (2015). Sol gel synthesis of forsterite, M-doped forsterite (M= Ni,Co) solid solutions and their use as ceramic pigments. Journal of the European Ceramic Society, 35(2), 765-777.
[283] Pavlov, R. S., Marzá, V. B., & Carda, J. B. (2002). Electronic absorption spectroscopy and colour of chromium-doped solids. Journal of Materials Chemistry, 12(9), 2825-2832.
[284] Ardit M., Cruciani G., Dondi M., Matteucci F., Ti-Ca-Al-doped $YCrO_3$ pigments: an XRD and UV-vis-NIR investigation. Materials Research Bulletin, 44 (2009) 666-673
[285] Kim, Y. J., & Lee, B. H. (2011). Synthesis of tialite ceramic pigments and coloring in glazes. Korean Journal of Materials Research, 21(8), 450-455.
[286] Kim, Y. J., & Lee, B. H. (2011). Cr-doped Tialite Pigments. Korean Journal of Materials Research, 21(9), 515-519.
[287] Llusar, M., Bermejo, T., Primo, J. E., Gargori, C., Esteve, V., & Monrós, G. (2017). Karrooite green pigments doped with Co and Zn: Synthesis, color properties and stability in ceramic glazes. Ceramics International, 43(12), 9133-9144.
[288] Gaudon, M., Toulemonde, O., & Demourgues, A. (2007). Green coloration of Co-doped ZnO explained from structural refinement and bond considerations. Inorganic chemistry, 46(26), 10996-11002.
[289] Ekambaram, S. (2005). Combustion synthesis and characterization of new class of ZnO-based ceramic pigments. Journal of Alloys and Compounds, 390(1-2), L4-L6.
[290] Zhou, N., She , S., Zhang, Y. , Li, S., Xu, S., Luan, J. (2020). Coprecipitation synthesis of a green Co-doped wurtzite structure high near-infrared reflective pigments using ammonia as precipitant, Journal of Alloys and Compounds, 820, 153183.
[291] Fernandez, F., Colon, C., Duran, A., Barajas, R., d'Ors, A., Becerril, M., Llopisc, J., Pajec, S.E., Saez-Puche, R. & Julian, I. (1998). The Y2BaCuO5 oxide as green pigment in ceramics. Journal of Alloys and Compounds, 275, 750-753.
[292] Kar, J. K., Stevens, R., & Bowen, C. R. (2008). Rare-earth cuprates for ceramic colouring application—An investigation. Journal of Alloys and Compounds, 455(1-2), 121-129.
[293] Ocana, M., González-Elipe, A. R., Andrés-Vergés, M., Tartaj, P., Serna, C. J., & Orera, V. M. (1998). Preparation by hydrolysis of aerosols and colour properties of Cr-doped and Co-doped zircon powders. Journal of the European Ceramic Society, 18(7), 821-830.
[294] Trojan, M. (1990). Synthesis of a blue-green pigment from the mineral zircon. Ceramics international, 16(5), 295-299.
[295] Trojan, M. (1990). Synthesis of blue-violet and brown-green zirconium silicate pigments from zircon mineral. Dyes and Pigments, 13(4), 311-323.
[296] Ke, S., Wang, Y., & Pan, Z. (2014). Synthesis of $Nd_2Si_2O_7$ ceramic pigment with LiCl as a mineralizer and its color property. Dyes and Pigments, 108, 98-105.
[297] Gayo, G. X., Troncoso, F., & Lavat, A. E. (2014). Application of $LnCrTeO_6$ oxides as new ceramic pigments of the type “green chromium”. Ceramics International, 40(1), 611-617.
[298] Galindo Llorach, R., Gargori García, C., Llusar, M., García López, A., Badenes March, J. A., & Monrós Tomás, G. (2011). Ecopigmentos cerámicos verdes y amarillos de $Pr_2Mo_2O_9$ dopados con calcio obtenidos en presencia de mineralizadores y por coprecipitación química. Boletín de la Sociedad Española de Cerámica y Vidrio, 50, 5, 219-224.
[299] Luxová, J., Těšitelová, K., Podzemná, V., Šulcová, P., Bosacka, M., Błońska-Tabero, A., & Filipek, E. (2019). Components of the $Co_3Cr_4(PO_4)_6$-$Cr(PO_3)_3$ system and the compound $CoCr_2(P_2O_7)_2$ as new ceramic pigments. Materials Chemistry and Physics, 121763.
[300] Hashimoto, H., Sayo, K., Asoh, H., Fujii, T., Takano, M., & Masuno, A. (2019). Bright greenish-yellow pigments based on $Sc_{2-x}Fe_xO_3$ solid solutions with bixbyite structure. Materials Research Bulletin, 109, 190-194.
[301] Dondi M., Ardit M., Cruciani G., Zanelli C., Tetrahedrally coordinated Co^{2+} in oxides and silicates: Effect of local environment on optical properties. American Mineralogist, 99 (2014) 1736-1745.
[302] Keppler, H., & Bagdassarov, N. (1999). The speciation of Ni and Co in silicate melts from optical absorption spectra to 1500°C. Chemical Geology, 158(1-2), 105-115.
[303] Llusar, M., Forés, A., Badenes, J. A., Calbo, J., Tena, M. A., & Monrós, G. (2001). Colour analysis of some cobalt-based blue pigments. Journal of the European Ceramic Society, 21(8), 1121-1130.
[304] El Hadri, M., Ahamdane, H., & Raghni, M. E. I. (2017). Effect of sol–gel method on colour properties of the classical cobalt olivine (Co_2SiO_4) ceramic pigment. Bulletin of Materials Science, 40(2), 375-382.
[305] Meseguer, S., Tena, M. A., Gargori, C., Badenes, J. A., Llusar, M., & Monrós, G. (2007). Structure and colour of cobalt ceramic pigments from phosphates. Ceramics international, 33(5), 843-849.
[306] Meseguer, S., Tena, M. A., Gargori, C., Galindo, R., Badenes, J. A., Llusar, M., & Monrós, G. (2008). Development of blue ceramic dyes from cobalt phosphates. Ceramics International, 34(6), 1431-1438.
[307] Llusar, M., Zielinska, A., Tena, M. A., Badenes, J. A., & Monrós, G. (2010). Blue-violet ceramic pigments based on Co and $MgCo_{2-x}Mg_xP_2O_7$ diphosphates. Journal of the European Ceramic Society, 30(9), 1887-1896.
[308] Llusar, M., Badenes, J. A., García, A., Gargori, C., Galindo, R., & Monrós, G. (2011). Solid solutions of mixed metal $Mn_{3-x}Mg_xFe_4(PO_4)_6$ orthophosphates: Colouring performance within a double-firing ceramic glaze. Ceramics International, 37(2), 493-504.
[309] Ardit, M., Cruciani, G., & Dondi, M. (2012). Structural relaxation in tetrahedrally coordinated Co^{2+} along the gahnite-Co-aluminate spinel solid solution. American Mineralogist, 97(8-9), 1394-1401.
[310] Tang, Y., Wu, C., Song, Y., Zheng, Y., & Zhao, K. (2018). Effects of colouration mechanism and stability of $CoAl_2O_4$ ceramic pigments sintered on substrates. Ceramics International, 44(1), 1019-1025.

[311] Mesíková, Ž., Šulcová, P., & Trojan, M. (2006). Preparation and practical application of spinel pigment $Co_{0.46}Zn_{0.55}(Ti_{0.064},Cr_{0.91})_2O_4$. Journal of thermal Analysis and Calorimetry, 84(3), 733-736.
[312] He, X., Wang, F., Liu, H., Niu, L., & Wang, X. (2018). Synthesis and color properties of the $TiO_2@CoAl_2O_4$ blue pigments with low cobalt content applied in ceramic glaze. Journal of the American Ceramic Society, 101(6), 2578-2588.
[313] Wang, Q., Wang, Y., Liu, K., Liu, J., Wang, C., Wang, Y., & Chang, Q. (2020). Synthesis and characterization of high-performance spherical urchin-like $CoAl_2O_4$ pigment prepared via microemulsion-hydrothermal-precipitation method. Advanced Powder Technology. https://doi.org/10.1016/j.apt.2019.12.041
[314] Forés, A., Llusar, M., Badenes, J. A., Calbo, J., Tena, M. A., & Monrós, G. (2000). Cobalt minimisation in willemite ($Co_xZn_{2-x}SiO_4$) ceramic pigments. Green Chemistry, 2(3), 93-100.
[315] Pozas, R., Orera, V. M., & Ocana, M. (2005). Hydrothermal synthesis of Co-doped willemite powders with controlled particle size and shape. Journal of the European Ceramic Society, 25(13), 3165-3172.
[316] Ozel E., Yurdakul H., Turan S., Ardit M., Cruciani G., Dondi M. (2010). Co-doped willemite ceramic pigments: Technological behaviour, crystal structure and optical properties. Journal of the European Ceramic Society, 30, 3319-3329.
[317] Dondi M., Ardit M., Cruciani G., Sorace L., Di Benedetto F., New spectroscopic and diffraction data to solve the vanadium-doped zircon pigment conundrum. Journal of the European Ceramic Society, 38 (2018) 5234-5245.
[318] Monrós, G., Carda, J., Tena, M. A., Escribano, P., Sales, M., & Alarcón, J. (1993). Different kinds of solid solutions in the V_2O_5-$ZrSiO_4$-NaF system by sol-gel processes and their characterization. Journal of the European Ceramic Society, 11(1), 77-86.
[319] Ardizzone, S., Cappelletti, G., Fermo, P., Oliva, C., Scavini, M., & Scime, F. (2005). Structural and spectroscopic investigations of blue, vanadium-doped $ZrSiO_4$ pigments prepared by a sol-gel route. The Journal of Physical Chemistry B, 109(47), 22112-22119.
[320] Caselli, C., Lusvardi, G., Malavasi, G., Menabue, L., & Miselli, P. (2007). Multitechnique approach to V–$ZrSiO_4$ pigment characterization and synthesis optimization. Journal of the European Ceramic Society, 27(2-3), 1743-1750.
[321] Schabbach, L. M., Bondioli, F., Ferrari, A. M., Manfredini, T., Petter, C. O., & Fredel, M. C. (2007). Influence of firing temperature on the color developed by a $(Zr,V)SiO_4$ pigmented opaque ceramic glaze. Journal of the European ceramic society, 27(1), 179-184.
[322] Dondi M., Zanelli C., Ardit M., Cruciani G., Co-doped hardystonite, $Ca_2(Zn,Co)Si_2O_7$, a new blue ceramic pigment. Journal of the American Ceramic Society, 94 (2011) 1025-1030.
[323] Mantovani L., Tribaudino M., Dondi M., Zanelli C., Synthesis and color performance of $CaCoSi_2O_6$ pyroxene, a new ceramic colorant. Dyes and Pigments, 120 (2015) 118-125.
[324] Gori C., Mantovani L., Tribaudino M., Zanelli C., Dondi, M., Colour of $Ca(Co_xMg_{1-x})Si_2O_6$ pyroxenes and their technological behaviour as ceramic colorants. Ceramics International, 44 (2018) 12745-12753.
[325] Leite, A., Costa, G., Hajjaji, W., Ribeiro, M. J., Seabra, M. P., & Labrincha, J. A. (2009). Blue cobalt doped-hibonite pigments prepared from industrial sludges: Formulation and characterization. Dyes and Pigments, 81(3), 211-217.
[326] Hajjaji, W., Seabra, M. P., & Labrincha, J. A. (2009). Recycling of solid wastes in the synthesis of Co-bearing calcium hexaluminate pigment. Dyes and Pigments, 83(3), 385-390.
[327] Costa G., Ribeiro M.J., Labrincha J.A., Dondi M., Matteucci F., Cruciani G., Ni-doped hibonite ($CaAl_{12}O_{19}$): a new turquoise blue ceramic pigment. Journal of the European Ceramic Society, 29 (2009) 2671-2678.
[328] Li, J., Medina, E. A., Stalick, J. K., Sleight, A. W., & Subramanian, M. A. (2016). Colored oxides with hibonite structure: a potential route to non-cobalt blue pigments. Progress in Solid State Chemistry, 44(4), 107-122.
[329] Ardit M., Borcănescu S., Cruciani G., Dondi M., Lazău I., Păcurariu C., Zanelli C., Ni-Ti co-doped hibonite ceramic pigments by combustion synthesis: crystal structure and optical properties. Journal of the American Ceramic Society, 99 (2016) 1749-1760.
[330] Gaudon, M., Robertson, L. C., Lataste, E., Duttine, M., Ménétrier, M., & Demourgues, A. (2014). Cobalt and nickel aluminate spinels: blue and cyan pigments. Ceramics International, 40(4), 5201-5207.
[331] Forés, A., & Llusar, M. (2001). Alternative turquoise blue pigments for glazes. American Ceramic Society Bulletin, 80(5), 47-52.
[332] Lavat, A. E., & Gayo, G. X. (2014). In situ formation of coloured M(II)–doped Zn_2SiO_4–willemite in ceramic glazes (M = Mn, Co, Ni, Cu). Ceramics International, 40(8), 11947-11955.
[333] Yan, J., Huang, J., Zhang, T., Tian, H., Yu, J., Zhang, L., & Zhang, Y. (2019). Investigation of the microstructure, cation distribution and optical properties of nanoscale $Ni_xMg_{1-x}Al_2O_4$ spinel pigments. Ceramics International, 45(11), 14073-14083.
[334] Kendrick, E., Kirk, C. J., & Dann, S. E. (2007). Structure and colour properties in the Egyptian Blue Family, $M_{1-x}M'_xCuSi_4O_{10}$, as a function of M, M′ where M,M′ = Ca, Sr and Ba. Dyes and Pigments, 73(1), 13-18.
[335] Zhang, C., Zhang, N., Wang, X., & Zhang, L. (2018). Novel preparation of an ancient ceramic pigment $BaCuSi_4O_{10}$ and its performance investigation. Materials Research Bulletin, 101, 334-339.
[336] Kusumoto, K. (2018). Synthesis of Co-free inorganic blue pigments based on turquoise blue glaze. Journal of the Ceramic Society of Japan, 126(5), 408-411.
[337] Ocaña, M., Espinós, J. P., & Carda, J. B. (2011). Synthesis, through pyrolysis of aerosols, of $YIn_{1-x}Mn_xO_3$ blue pigments and their efficiency for colouring glazes. Dyes and Pigments, 91(3), 501-507.
[338] Li, J., & Subramanian, M. A. (2019). Inorganic pigments with transition metal chromophores at trigonal bipyramidal coordination: $Y(In,Mn)O_3$ blues and beyond. Journal of Solid State Chemistry, 272, 9-20.
[339] Dohnalová, Ž., Šulcová, P., & Gorodylova, N. (2014). Study of ceramic pigments based on cobalt doped Y_2O_3-Al_2O_3 system. Journal of Thermal Analysis and Calorimetry, 116(2), 647-654.

[340] Hafez, H. S., & El-Fadaly, E. (2012). Synthesis, characterization and color performance of novel Co^{2+}-doped alumina/titania nanoceramic pigments. Spectrochimica Acta Part A: Molecular and Biomolecular Spectroscopy, 95, 8-14.
[341] Fernández-Osorio, A., Jiménez-Segura, M. P., Vázquez-Olmos, A., & Sato-Berru, R. (2011). Turquoise blue nanocrystalline pigment based on $Li_{1.33}Ti_{1.66}O_4$: Synthesis and characterization. Ceramics International, 37(5), 1465-1471.
[342] Dondi M., Zanelli C., Ardit M., Cruciani G., Mantovani L., Tribaudino M., Andreozzi G.B., Ni-free, black ceramic pigments based on Co-Cr-Fe-Mn spinels: a reappraisal of crystal structure, optical properties and technological behaviour. Ceramics International, 39 (2013) 9533-9547.
[343] Shin, K. H., & Lee, B. H. (2007). Synthesis of Fe_2O_3−CoO−Cr_2O_3−MnO_2 pigments and coloring in glazes. Journal of the Korean Ceramic Society, 44(10), 554-561.
[344] Lee, K. H., Myung, M. S., & Lee, B. H. (2007). Development of black color spinel pigment for high temperature. Journal of the Korean Ceramic Society, 44(5), 160.
[345] Tanisan, B., & Turan, S. (2011). Black ceramic pigments for porcelain tile bodies produced with chromite ores and iron oxide waste. Journal of Ceramic Processing Research, 12(4), 462-467.
[346] Kim, J. H., Lee, S. H., Suh, M. C., & Lee, B. H. (2007). Synthesis of cobalt oxide free black color spinel pigment. Journal of the Korean Ceramic Society, 44(11), 639-644.
[347] Eliziário, S. A., de Andrade, J. M., Lima, S. J., Paskocimas, C. A., Soledade, L. E., Hammer, P., Longo, E., Souza, A.G., & Santos, I. M. (2011). Black and green pigments based on chromium–cobalt spinels. Materials Chemistry and Physics, 129(1-2), 619-624.
[348] Calbo, J., Tena, M., Monrós, G., Llusar, M., Galindo, R., & Badenes, J. A. (2005). Flux agent effect on nickel ferrite black pigment. American Ceramic Society Bulletin, 84(12), 9201-9206.
[349] Costa, G., Della, V. P., Ribeiro, M. J., Oliveira, A. P. N., Monrós, G., & Labrincha, J. A. (2008). Synthesis of black ceramic pigments from secondary raw materials. Dyes and Pigments, 77(1), 137-144.
[350] Gargori, C., Prim, S. R., Llusar, M., Folgueras, M. V., & Monrós, G. (2018). Recycling of Cr/Ni/Cu plating wastes as black ceramic pigments. Materials Letters, 218, 341-345.
[351] Lee, K. H., Lee, Y. S., Park, J. S., & Lee, B. H. (2008). Preparation and characterization of black zirconia ceramics by black color spinel pigment. Journal of the Korean Ceramic Society, 45(4), 214.
[352] Ye, M. Q., Han, A. J., Chu, Z. S., Che, J. F., & Wang, C. (2013). Synthesis and characterization of Mn-doped copper chromite black pigments. Advanced Materials Research, 602, 71-75.
[353] Mestre, S., Gómez-Tena, M. P., Gazulla, M. F., & Gozalbo, A. (2013). Interaction of the chromium–iron black pigment with porcelanised stoneware. Ceramics International, 39(7), 7453-7459.
[354] De la Torre, Á. G., Aranda, M. A., León-Reina, L., & Pérez, J. (2011). Ceramic pigments and the European REACH legislation: black Fe_2O_3–Cr_2O_3, a case study. International Journal of Applied Ceramic Technology, 8(4), 905-910.
[355] Ozel, E., & Turan, S. (2003). Production and characterisation of iron-chromium pigments and their interactions with transparent glazes. Journal of the European Ceramic Society, 23(12), 2097-2104.
[356] Yurdakul, H., Turan, S., & Ozel, E. (2011). The mechanism for the colour change of iron chromium black pigments in glazes through transmission electron microscopy techniques. Dyes and Pigments, 91(2), 126-133.
[357] Escardino, A., Mestre, S., Barba, A., Beltrán, V., & Blasco, A. (2000). Synthesis mechanism of an iron–chromium ceramic pigment. Journal of the American Ceramic Society, 83(1), 29-32.
[358] Escardino, A., Mestre, S., Barba, A., Monzo, M., Blasco, A., & Beltran, V. (2003). Colorimetric study of black $(Fe,Cr)_2O_3$ pigment synthesis reaction: relation between chromatic coordinates and synthesis conditions. British Ceramic Transactions, 102(6), 247-250.
[359] Tena, M. A., Sorlí, S., Llusar, M., Badenes, J. A., Forés, A., & Monrós, G. (2005). Study of Sb-doped SnO_2 gray ceramic pigment with cassiterite structure. Zeitschrift für anorganische und allgemeine Chemie, 631(11), 2188-2191.
[360] Bernardi, M., Leite, E., Longo, E., Conceição, M., & Souza, A. (2004). Development of SnO_2/Sb-based ceramic pigments. Journal of Thermal Analysis and Calorimetry, 75(2), 481-486.
[361] Carceller, J.V., Jovaní, M.A., Nebot, A., Soler, A., Carda, J.B., Gómez, J.J., Garcia, G. (1998). Study of electrical conductivity in ceramic floor tiles. Development of an antielectrostatic vitrifiable glaze. Proc. V World Congress on the Quality of Ceramic Tiles, Qualicer98, Castellón, Spain.
[362] Wang, Y., Wu, J., & Zhou, J. (2007). Antistatic ceramic tiles modified by Sb-doped SnO_2. Key Engeneering Materials, 280-283, 279-280.
[363] Tena, M. A., Mestre, A., García, A., Sorlí, S., & Monrós, G. (2003). Synthesis of gray ceramic pigments with rutile structure from alkoxides. Journal of sol-gel science and technology, 26(1-3), 813-816.
[364] Melo, D., Vieira, F. T. G., Costa, T. C. C., Soledade, L. E. B., Paskocimas, C. A., Melo, D. M. A., Longo, E., Marinho, E.P., Souza, A.G. & Santos, I. M. G. (2013). Lanthanum cobaltite black pigments with perovskite structure. Dyes and Pigments, 98(3), 459-463.
[365] Hajjaji W., Pullar R.C., Zanelli C., Seabra M.P., Dondi M., Labrincha J.A., Compositional and chromatic properties of strontium hexaferrite as pigment for ceramic bodies and alternative synthesis from wiredrawing sludge. Dyes and Pigments, 96 (2013) 659-664.
[366] Peng, C., Zhang, C., Lv, M., & Wu, J. (2013). Preparation of silica encapsulated carbon black with high thermal stability. Ceramics International, 39(6), 7247-7253.
[367] Chang, Q., Wang, X., Wang, Y., Bao, Q., Zhou, J. E., & Zhu, Q. (2014). Encapsulated carbon black prepared by sol–gel-spraying: A new black ceramic pigment. Journal of the European Ceramic Society, 34(13), 3151-3157.
[368] Tang, H., Hu, Q., Jiang, F., Jiang, W., Liu, J., Chen, T., & Luo, W. (2019). Size control of C@$ZrSiO_4$ pigments via soft mechano-chemistry assisted non-aqueous sol-gel method and their application in ceramic glaze. Ceramics International, 45(8), 10756-10764.

[369] Tang, H., Hu, Q., Jiang, W, Liu, J, Feng, G., Chen, T, Tan, G, Zhang, X, Miao, L., Facile non-aqueous synthesis of high color rendering C@$ZrSiO_4$ encapsulation pigment with carbon-containing precursors as in-situ carbon sources, Ceramic International 44 820189 16498-16506.
[370] Chen, S., Fu, S., Lang, Y., Tian, C., Wei, H., & Wang, C. A. (2020). Submicronic spherical inclusion black pigment by double-shell reaction sintering. Journal of the American Ceramic Society, 103(3), 1520-1526.
[371] Dondi M., Matteucci F., Baldi G., Barzanti A., Cruciani G., Zama I., Bianchi C.L., Gray-blue Al_2O_3-MoO_x ceramic pigments: crystal structure, colouring mechanism and technological performance. Dyes & Pigments, 76 (2008) 179-186.
[372] Levitskii, I. A., & Mazura, N. V. (2005). Opacified glazes produced by high-temperature firing for sanitary ceramicware. Glass and Ceramics, 62(7-8), 215-218.
[373] Moreno, A., Bou, E., Cabrera, M. J., & Quereda, P. (1998). Zirconium silicate opacification mechanism in ceramic engobes. Proc. XI World Congress on the Quality of Ceramic Tiles, Qualicer98, Castellon (Spain).
[374] Cavalcante, P. T., Dondi, M., Ercolani, G., Guarini, G., Melandri, C., Raimondo, M., & e Almendra, E. R. (2004). The influence of microstructure on the performance of white porcelain stoneware. Ceramics International, 30(6), 953-963.
[375] Thiele, E. S., & French, R. H. (1998). Light-scattering properties of representative, morphological rutile titania particles studied using a finite-element method. Journal of the American Ceramic Society, 81(3), 469-479.
[376] Snyders, E., Potgieter, J. H., & Nel, J. T. (2005). The upgrading of an inferior grade zircon to superior opacifier for sanitary ware and glazes. Journal of the Southern African Institute of Mining and Metallurgy, 105(7), 459-463.
[377] Wang, S., Peng, C., Huang, Z., Zhou, J., Lü, M., & Wu, J. (2014). Clustering of zircon in raw glaze and its influence on optical properties of opaque glaze. Journal of the European Ceramic Society, 34(2), 541-547.
[378] Schabbach, L. M., Bondioli, F., & Fredel, M. C. (2011). Colouring of opaque ceramic glaze with zircon pigments: formulation with simplified Kubelka–Munk model. Journal of the European Ceramic Society, 31(5), 659-664.
[379] Sarjahani, R., Sheikhattar, M., Javadpour, S., & Hashemi, B. (2016). The effect of opacifiers on surface roughness of ceramic glazes. Iranian Journal of Materials Science and Engineering, 13(1), 37-42.
[380] Jacobs, C. W. F., & Baldwin, W. J. (1954). Effects of zirconium-type opacifiers on properties of glazes. Journal of the American Ceramic Society, 37(6), 258-266.
[381] Bhushan, B., Das, B., & Sen, S. (1966). Zircon opacifiers: Their preparation and performance in glazes. Transactions of the Indian Ceramic Society, 25(1), 97-106.
[382] Castilone, R. J., Sriram, D., Carty, W. M., & Snyder, R. L. (1999). Crystallization of zircon in stoneware glazes. Journal of the American Ceramic Society, 82(10), 2819-2824.
[383] Blonski, R. (1993). The effect of zircon dissolution and reprecipitation on the color development of glazes. Ceramic Engineering Science Proceedings, 14(1-2) 176-189.
[384] Earl, D. A., & Clark, D. E. (2000). Effects of glass frit oxides on crystallization and zircon pigment dissolution in whiteware coatings. Journal of the American Ceramic Society, 83(9), 2170-2176.
[385] Assifaoui, A., Atmani, W., Daoudi, A., Moussa, R., & Blanchart, P. (2003). Grain growth of zircon pigment in tile glaze. British Ceramic Transactions, 102(2), 57-60.
[386] Wang, S., Peng, C., Xiao, H., & Wu, J. (2015). Microstructural evolution and crystallization mechanism of zircon from frit glaze. Journal of the European Ceramic Society, 35(9), 2671-2678.
[387] Atkinson, I., Smith, M. E., & Zaharescu, M. (2012). Examining correlations between composition, structure and properties in zircon-containing raw glazes. Ceramics International, 38(3), 1827-1833.
[388] Bruzzi, L., Baroni, M., Mazzotti, G., Mele, R., & Righi, S. (2000). Radioactivity in raw materials and end products in the Italian ceramics industry. Journal of Environmental Radioactivity, 47(2), 171-181.
[389] Atkinson, I., Teoreanu, I., Mocioiu, O. C., Smith, M. E., & Zaharescu, M. (2010). Structure property relations in multicomponent oxide systems with additions of TiO_2 and ZrO_2 for glaze applications. Journal of Non-Crystalline Solids, 356(44-49), 2437-2443.
[390] Tite, M., Pradell, T., & Shortland, A. (2008). Discovery, production and use of tin-based opacifiers in glasses, enamels and glazes from the late iron age onwards: A reassessment. Archaeometry, 50(1), 67-84.
[391] Matin, M. (2019). Tin-based opacifiers in archaeological glass and ceramic glazes: a review and new perspectives. Archaeological and Anthropological Sciences, 11(4), 1155-1167.
[392] Atkinson, I., Teoreanu, I., & Zaharescu, M. (2008). Correlation among composition properties of SnO_2 opacified glazes. UPB Sci Bull Ser B, 70(3), 11-22.
[393] Bou, E., Moreno, A., Escardino, A., & Gozalbo, A. (2007). Microstructural study of opaque glazes obtained from frits of the system: SiO_2-Al_2O_3-B_2O_3-(P_2O_5)-CaO-K_2O-TiO_2. Journal of the European Ceramic Society, 27(2-3), 1791-1796.
[394] Yildiz, B., Ozturk, Z., & Kara, A. (2015). Effects of alumina and white fused alumina addition on transparent wall and floor tile glazes. Acta Physica Polonica A, 4(127), 1090-1093.
[395] Ozturk, Z. B., Yıldız, B., & Kara, A. (2019). Effects of alumina and white fused alumina addition on technological properties of transparent floor tile glazes. Journal of Thermal Analysis and Calorimetry, 1-7.
[396] Tucci, A., Esposito, L., Malmusi, L., & Rambaldi, E. (2007). New body mixes for porcelain stoneware tiles with improved mechanical characteristics. Journal of the European Ceramic Society, 27(2-3), 1875-1881.
[397] Bondioli, F., Manfredini, T., Giorgi, M., & Vignali, G. (2010). Functionalization of ceramic tile surface by soluble salts addition: Part I. Journal of the European Ceramic Society, 30(1), 11-16.
[398] Cai, J., Lv, M., Guan, K., Sun, Q., Peng, C., Wu, J., & Liu, Y. (2018). Development of spinel opaque glazes for ceramic tiles. Journal of the European Ceramic Society, 38(1), 297-302.
[399] Nebot-Diaz, I., Sanchez-Muñoz, L., Bakali, J., & Carda, J. B. (1999). Spinel glass-ceramics glaze for porcelain stoneware. Br. Ceram. Proc., 60, 91-92.
[400] Gajek, M., Partyka, J., Leśniak, M., Rapacz-Kmita, A., & Wójcik, Ł. (2018). Gahnite white colour glazes in ZnO–R_2O–RO–Al_2O_3–SiO_2 system. Ceramics International, 44(13), 15845-15850.

[401] Cai, J., Lu, M., Guan, K., Li, W., He, F., Chen, P., & Wu, J. (2018). Effect of ZnO/MgO ratio on the crystallization and optical properties of spinel opaque glazes. Journal of the American Ceramic Society, 101(4), 1754-1764.
[402] Vincenzini, P., Biffi, G., & Ortelli, G. (1975). TiO_2 as an opacifier of ceramic glazes firing in the range 900-1000°C. Ceramurgia, 5(1), 3-12.
[403] Tellier, C. (1979). Opacification of glazes for sanitary ware by titanium dioxide and zinc oxide. Bull. Soc. Fr. Ceram., 125, p. 21.
[404] Bobkova, N. M., Boloban, L. V., & Gailevich, S. A. (1997). Phase formation in titanium glazes. Glass and ceramics, 54(1-2), 17-19.
[405] Teixeira, S., & Bernardin, A. M. (2009). Development of TiO_2 white glazes for ceramic tiles. Dyes and Pigments, 80(3), 292-296.
[406] Xia, Y. F., Huang, Z. H., Yuan, J. Z., Wang, L. J., & Xie, J. H. (2010). Preparation of rutile crystalline glaze. In Advanced Materials Research, 105, 778-781.
[407] Pekkan, K. (2015). The thermal and microstructural behavior of a R_2O–RO–(ZnO)–Al_2O_3–(TiO_2)–SiO_2 based macro-crystalline raw glaze system. Ceramics International, 41(6), 7881-7889.
[408] Safi, M., Khalili, N., & Arabi, M. (2012). Effect of various opacifiers on color parameters and gloss of glazed tiles. Journal of Color Science and Technology, 5, 261-253.
[409] Montazerian, M., Javadi, S., & Shahriyari, M. (2014). An investigation into the replacement of zircon with fluorspar, andalusite and wollastonite as whitening agent of the body. Proc. XIII World Congress on the Quality of Ceramic Tiles, Qualicer2014, p. 7, Castellon, Spain.
[410] Tarhan, M. (2019). Whiteness improvement of porcelain tiles incorporated with anorthite and diopside phases. Journal of Thermal Analysis and Calorimetry, 138(2), 929-936.
[411] Zanelli, C., Baldi, G., Dondi, M., Ercolani, G., Guarini, G., & Raimondo, M. (2008). Glass–ceramic frits for porcelain stoneware bodies: Effects on sintering, phase composition and technological properties. Ceramics International, 34(3), 455-465.
[412] Siligardi, C., Miselli, P., Lusvarghi, L., & Reginelli, M. (2011). Influence of CaO–ZrO_2–Al_2O_3–SiO_2 glass-ceramic frits on the technological properties of porcelain stoneware bodies. Ceramics International, 37(6), 1851-1858.
[413] Li, R., Lv, M., Cai, J., Guan, K., He, F., Li, W., & Wu, J. (2018). Development of sapphirine opaque glazes for ceramic tiles. Journal of the European Ceramic Society, 38(16), 5632-5636.
[414] Nieves, L. J. J., Lot, A. V., Melchiades, F. G., & Boschi, A. O. (2020). Digital decoration for ceramic tiles: The effect of glazes particle size distribution on the inkjet decoration. Boletín de la Sociedad Española de Cerámica y Vidrio, 59(1), 44-48.
[415] Dakhai, S., Orlova, L. A., & Mikhailenko, N. Y. (1999). Types and compositions of crystalline glazes. Glass and Ceramics, 56(5-6), 177-180.
[416] Sorlí, S., Tena, M. A., Mestre, A., Llusar, M., & Monrós, G. (2004). Effect of the major devitrifying phase on ceramic glaze microstructure and mechanical properties. Proceedings of VIII World Congress on Ceramic Tile Quality, Qualicer 2004, 99-110, Castellon, Spain.
[417] Tücks, A., & Beck, H. P. (2005). The photochromic effect of bismuth vanadate pigments. Part I: Synthesis, characterization and lightfastness of pigment coatings. Journal of Solid State Chemistry, 178(4), 1145-1156.
[418] Sameera, S. F., Rao, P. P., Kumari, L. S., & Koshy, P. (2009). New Scheelite-based Environmentally Friendly Yellow Pigments:(BiV)x(CaW)1−xO4. Chemistry Letters, 38(11), 1088-1089.
[419] Masui, T., Honda, T., & Imanaka, N. (2013). Novel and environmentally friendly (Bi,Ca,Zn)VO_4 yellow pigments. Dyes and Pigments, 99(3), 636-641.
[420] Dolić, S. D., Jovanović, D. J., Štrbac, D., Far, L. Đ., & Dramićanin, M. D. (2018). Improved coloristic properties and high NIR reflectance of environment-friendly yellow pigments based on bismuth vanadate. Ceramics International, 44(18), 22731-22737.
[421] Sciau, P., Noé, L., & Colomban, P. (2016). Metal nanoparticles in contemporary potters' master pieces: Lustre and red "pigeon blood" potteries as models to understand the ancient pottery. Ceramics International, 42(14), 15349-15357.
[422] Wynn, N. (1959). Platinum in the decoration of ceramic wares. Platinum Metals Review, 3(2), 60-65.
[423] Dvornichenko, I. N., & Matsenko, S. V. (2000). Production of iron-containing crystalline glazes. Glass and Ceramics, 57(1-2), 67-68.
[424] Bobin, O., Schvoerer, M., Miane, J. L., & Fabre, J. F. (2003). Coloured metallic shine associated to lustre decoration of glazed ceramics: a theoretical analysis of the optical properties. Journal of Non-Crystalline Solids, 332(1-3), 28-34.
[425] Fredrickx, P., Helary, D., Schryvers, D., & Darque-Ceretti, E. (2004). A TEM study of nanoparticles in lustre glazes. Applied Physics A, 79(2), 283-288.
[426] Pekkan, K., Başkırkan, H., & Çakı, M. (2018). Development of gold-bronze metallic glazes in a clay-based system for stoneware bodies. Ceramics International, 44(5), 4789-4794.
[427] Pekkan, K., Taşçı, E., & Uz, V. (2015). Production of metallic glazes and their industrial applications. Journal of The Australian Ceramic Society, 51(1), 110-115.
[428] Siligardi, C., Montecchi, M., Montorsi, M., & Pasquali, L. (2010). Ceria-containing frit for luster in modern ceramic glaze. journal of the american ceramic society, 93(9), 2545-2550.
[429] Siligardi, C., Montecchi, M., Montorsi, M., & Pasquali, L. (2009). Lead free Cu-containing frit for modern metallic glaze. Journal of the American Ceramic Society, 92(11), 2784-2790.
[430] Gualtieri, A. F., Canovi, L., Viani, A., Bertocchi, P., Corradini, C., Gualtieri, M. L., & Berthier, S. (2013). Mechanism of lustre formation in scheelite-based glazes. Journal of the European Ceramic Society, 33(11), 2055-2064.
[431] Siligardi, C., Tagliaferri, L., Lusvarghi, L., Bolelli, G., & Venturelli, D. (2014). Preparation of innovative metallic composite glazes for porcelainized stoneware tiles. Ceramics International, 40(1), 1821-1828.

[432] Tenorio Cavalcante P.M., Dondi M., Guarini G., Barros F.M., da Luz A.B., Ceramic application of mica titania pearlescent pigments. Dyes and Pigments, 74 (2007) 1-8.
[433] Parmelee, C. W., & Lathrop, J. S. (1924). Aventurine glazes. Journal of the American Ceramic Society, 7(7), 567-574.
[434] Levitskii, I. A. (2001). Mechanism of phase formation in aventurine glaze. Glass and Ceramics, 58(5-6), 223-226.
[435] Gozalbo, A., Orts, M. J., Mestre, S., Gómez, P., Agut, P., Lucas, F., & Blanco, C. (2006). Ceramic glazes with aventurine effect. Proceedings of IX World Congress on Ceramic Tile Quality, Qualicer 2006, 189-202, Castellon, Spain.
[436] Eliseev, S. Y., Rodtsevich, S. P., & Dostanko, E. V. (2000). Enamel with the aventurine effect. Glass and Ceramics, 57(3-4), 140-142.
[437] Casan, E., Lleo, E., Palomares, F., Rodriguez, V., Marti, V., Seores, J., & Cabrera, M. J. (2010). Goniochromatism study on metallized effects of aventurine enamels. Boletin de la Sociedad Espanola de Ceramica y Vidrio, 49(3), 142-146.
[438] Păcurariu, C., Lazău, R. I., Lazău, I., Tiţa, D., & Dumitrel, A. (2011). Non-isothermal crystallization kinetics of some aventurine decorative glaze. Journal of thermal Analysis and Calorimetry, 105(2), 435-441.
[439] Lazău, I., Borcănescu, S., Păcurariu, C., & Vancea, C. (2013). Kinetic study of the non-isothermal crystallization process of hematite in ceramic glazes obtained from CRT wastes. Journal of Thermal Analysis and Calorimetry, 112(1), 345-351.
[440] Dondi, M., Cruciani, G., Balboni, E., Guarini, G., & Zanelli, C. (2008). Titania slag as a ceramic pigment. Dyes and Pigments, 77(3), 608-613.
[441] Soares, F. D. S., & Valerio, M. E. G. (2017). Laser sintering of doped strontium aluminate via modified sol-gel for use as a ceramic pigment. Cerâmica, 63(365), 90-98.
[442] Kaya, S. Y., Karasu, B., & Karacaoğlu, E. (2009). General review of application of phosphorescence pigments in ceramic industry. Proceedings of SERES, 9, 608-616.
[443] Karacaoğlu, E., & Karasu, B. (2013). The effects of re-firing process under oxidizing atmosphere and temperatures on the properties of strontium aluminate phosphors. Materials Research Bulletin, 48(10), 3702-3706.
[444] Ferrari, C., Muscio, A., Siligardi, C., & Manfredini, T. (2015). Design of a cool color glaze for solar reflective tile application. Ceramics International, 41(9), 11106-11116.
[445] Ferrari, C., Muscio, A., & Siligardi, C. (2016). Development of a solar-reflective ceramic tile ready for industrialization. Procedia Engineering, 169, 400-407.
[446] Schabbach, L. M., Marinoski, D. L., Güths, S., Bernardin, A. M., & Fredel, M. C. (2018). Pigmented glazed ceramic roof tiles in Brazil: Thermal and optical properties related to solar reflectance index. Solar Energy, 159, 113-124.
[447] Gargori, G., Cerro, L., Fas, A., Llusar, V., & Monrós, T. (2017). Study of the photocatalytic activity and cool characteristics of a novel palette of pigments. Boletin de la Sociedad Espanola de Ceramica y Vidrio, 56(4), 166-176.
[448] Chen, J., Xiao, Y., Huang, B., & Sun, X. (2018). Sustainable cool pigments based on iron and tungsten co-doped lanthanum cerium oxide with high NIR reflectance for energy saving. Dyes and Pigments, 154, 1-7.
[449] Jovaní, M., Sanz, A., Beltrán-Mir, H., & Cordoncillo, E. (2016). New red-shade environmental-friendly multifunctional pigment based on Tb and Fe doped $Y_2Zr_2O_7$ for ceramic applications and cool roof coatings. Dyes and Pigments, 133, 33-40.
[450] Bondioli, F., Dinelli, M., Giovanardi, R., & Giorgi, M. (2010). Functionalization of ceramic tile surface by soluble salts addition: Part II. Titanium and silver addition. Journal of the European Ceramic Society, 30(9), 1873-1878.
[451] Rambaldi, E., Tucci, A., Esposito, L., Naldi, D., & Timellini, G. (2010). Nano-oxides to improve the surface properties of ceramic tiles. Boletín de la Sociedad Española de Cerámica y Vidrio, 49(4), 253-258.
[452] Shimohigoshi, M., & Saeki, Y. (2005). Development of photocatalyst tile and commercial production. In PRO 41: International RILEM Symposium on Environment-Conscious Materials and Systems for Sustainable Development, 41, p. 35.
[453] Tobaldi, D. M., Tucci, A., Camera-Roda, G., Baldi, G., & Esposito, L. (2008). Photocatalytic activity for exposed building materials. Journal of the European Ceramic Society, 28(14), 2645-2652.
[454] da Silva, A. L., Dondi, M., Raimondo, M., & Hotza, D. (2018). Photocatalytic ceramic tiles: Challenges and technological solutions. Journal of the European Ceramic Society, 38(4), 1002-1017.
[455] Tezza, V. B., Scarpato, M., Oliveira, L. F. S., & Bernardin, A. M. (2015). Effect of firing temperature on the photocatalytic activity of anatase ceramic glazes. Powder Technology, 276, 60-65.
[456] Raimondo, M., Guarini, G., Zanelli, C., Marani, F., Fossa, L., & Dondi, M. (2012). Printing nano TiO_2 on large-sized building materials: Technologies, surface modifications and functional behaviour. Ceramics International, 38(6), 4685-4693.
[457] Vaiano, V., Sarno, G., Ciambelli, P., & Sannino, D. (2014). Functionalization of ceramic tiles with N-doped TiO_2 and their photocatalytic function under UV or visible light irradiation. Journal of Advanced Oxidation Technologies, 17(2), 193-201.
[458] da Silva, A. L., Dondi, M., & Hotza, D. (2017). Self-cleaning ceramic tiles coated with Nb_2O_5-doped-TiO_2 nanoparticles. Ceramics International, 43(15), 11986-11991.
[459] Vaiano, V., Sarno, G., Sannino, D., & Ciambelli, P. (2014). Photocatalytic and antistain properties of ceramic tiles functionalized with tungsten-doped TiO2. Chemical Engineering Transactions, 39, 499-504.
[460] Tobaldi, D. M., Škapin, A. S., Pullar, R. C., Seabra, M. P., & Labrincha, J. A. (2013). Titanium dioxide modified with transition metals and rare earth elements: phase composition, optical properties, and photocatalytic activity. Ceramics International, 39(3), 2619-2629.

[461] Sciancalepore, C., & Bondioli, F. (2015). Durability of SiO_2–TiO_2 photocatalytic coatings on ceramic tiles. International Journal of Applied Ceramic Technology, 12(3), 679-684.
[462] Machida, M., Norimoto, K., & Kimura, T. (2005). Antibacterial activity of photocatalytic titanium dioxide thin films with photodeposited silver on the surface of sanitary ware. Journal of the American Ceramic society, 88(1), 95-100.
[463] de Niederhausern, S., Bondi, M., & Bondioli, F. (2013). Self-cleaning and antibacteric ceramic tile surface. International Journal of Applied Ceramic Technology, 10(6), 949-956.
[464] Gurbuz, M., Atay, B., & Dogan, A. (2015). Synthesis of high-temperature-stable TiO_2 and its application on Ag^+-activated ceramic tile. International Journal of Applied Ceramic Technology, 12(2), 426-436.
[465] Baheiraei, N., Moztarzadeh, F., & Hedayati, M. (2012). Preparation and antibacterial activity of Ag/SiO_2 thin film on glazed ceramic tiles by sol–gel method. Ceramics international, 38(4), 2921-2925.
[466] Zhang, Q., Xu, L. S., & Guo, X. (2017). Improvement of mechanical properties, microscopic structures, and antibacterial activity by Ag/ZnO nanocomposite powder for glaze-decorated ceramic. Journal of Advanced Ceramics, 6(3), 269-278.
[467] Ghafari-Nazari, A., Moztarzadeh, F., Rabiee, S. M., Rajabloo, T., Mozafari, M., & Tayebi, L. (2012). Antibacterial activity of silver photodeposited nepheline thin film coatings. Ceramics International, 38(7), 5445-5451.
[468] Uzgur, E., Bayrakci, F., Koparal, S., & Dogan, A. (2004). Applications of calcium phosphate based antibacterial ceramics on sanitary and tile wares. Key Engineering Materials, 264, 1573-1576.
[469] Wang, Q. P., Guo, X. X., Wu, W. H., & Liu, S. X. (2011). Preparation of fine Ag_2WO_4 antibacterial powders and its application in the sanitary ceramics. Advanced Materials Research, 284, 1321-1325.
[470] Anantharamulu, N., Rao, K. K., Rambabu, G., Kumar, B. V., Radha, V., & Vithal, M. (2011). A wide-ranging review on Nasicon type materials. Journal of Materials Science, 46(9), 2821-2837.

Ceramic Pigments and Dyes beyond the Inkjet Revolution: from Technological Requirements to Constraints in Colorant Design

Molinari C., Conte S., Zanelli C., Ardit M., Cruciani G., Dondi M.

FIGURE CAPTIONS

Figure 1. Technologies used in ceramic tiles manufacturing and related decoration techniques.

Figure 2. Decoration techniques utilized in ceramic tile manufacturing since 1960.

Figure 3. Evolution of ceramic tile decoration technologies: symbols refer to Figure 1.

Figure 4. Gamut of colors (a*-b* equatorial plane, CIE-L*a*b* coordinates) for industrially-manufactured ceramic pigments and dyes [modified after 2].

Figure 5. Tinctorial strength versus color hue of the main industrial ceramic pigments and dyes (for numbers 1 to 25 see Table 4) and candidate colorants proposed in the literature.

Figure 6. Tinctorial strength of ceramic pigments in transparent glaze versus opaque glaze (A) and as function of the amount of pigment into porcelain stoneware body (B). Data from [23].

Figure 7. Examples of optical spectra of industrial pigments and dyes used by the ceramic industry.

Figure 8. Approximate fields of chemical composition of glazes, glassy coatings and porcelain stoneware bodies used in the different decoration technologies (see Figure 1 for abbreviations). A) Ternary diagrams of fluxes (% weight) and B) Stull diagram of silica and alumina (Seger formula).

Figure 9. Particle size distribution of colorants: A) micronized pigments and effects in IJP inks (DD) compared with conventional (AP-IP) and encapsulated pigments (EP); B) relationship with specific surface area in micronized pigments (data after [40]).

Figure 10. Variation of the reciprocal of the pigment particle size (i.e., $(\frac{1}{x_2} - \frac{1}{x_1}) \propto \frac{E}{K}$) as a function of the total milling rounds for various ceramic pigments. Symbols refer to: Pr- (yellow squares) and V-doped (cyan squares) zircon pigments [40,49,51]; Co-aluminate (blue circles), Co-ferrite (empty circles), and CoFe-chromate (black circles) spinel pigments [40, 48,50]; Cr,Sb codoped rutile pigments (orange diamonds) [40]. Dashed lines are a reader's eye guide.

Figure 11. Variation of the reciprocal of the pigment particle size as a function of (A) the total milling rounds for spinel [40, 48,50], and (B) zircon [40,49,51] ceramic pigments. Dashed lines are a reader's eye guide.

Figure 12. Box-and-whisker diagram of the degree of pigment amorphization in commercial inks for digital decoration of ceramic tiles (unpublished data).

Figure 13. Technological properties of industrial red to purple ceramic pigments and dyes. Symbols: widely used (■); limited use (⊡); no longer in use (□); not entered in use (◪). Unsuitable because of: technological behavior (1), health hazard (2), cost (3), color saturation and purity (4).

Figure 14. Red and purple colors in glaze, plotted on the a*-b* plane (CIE-L*a*b*). Numbered fields represent the main industrial colorants, while symbols refer to colorants proposed in the literature but not entered in use yet.

Figure 15. Technological properties of industrial yellow to orange ceramic pigments and dyes. Symbols: widely used (■); limited use (⊡); no longer in use (□); not entered in use (◪). Unsuitable because of: technological behavior (1), health hazard (2), cost (3), color saturation and purity (4).

Figure 16. Yellow colors in glaze, plotted on the a*-b* plane (CIE-L*a*b*). Numbered fields represent the main industrial colorants, while symbols refer to colorants proposed in the literature but not entered in use yet.

Figure 17. Technological properties of industrial light brown to maroon ceramic pigments and dyes. Symbols: widely used (■); limited use (⊡); no longer in use (□); not entered in use (◪). Unsuitable because of: technological behavior (1), health hazard (2), cost (3), color saturation and purity (4).

Figure 18. Brown, maroon and orange colors in glaze, plotted on the a*-b* plane (CIE-L*a*b*). Numbered fields represent the main industrial colorants, while symbols refer to colorants proposed in the literature but not entered in use yet.

Figure 19. Technological properties of industrial green ceramic pigments and dyes. Symbols: widely used (■); limited use (⊡); no longer in use (□); not entered in use (◪). Unsuitable because of: technological behavior (1), health hazard (2), cost (3), color saturation and purity (4).

Figure 20. Green colors in glaze, plotted on the a*-b* plane (CIE-L*a*b*). Numbered fields represent the main industrial colorants, while symbols refer to colorants proposed in the literature but not entered in use yet.

Figure 21. Technological properties of industrial blue to turquoise ceramic pigments and dyes. Symbols: widely used (■); limited use (⊡); no longer in use (□); not entered in use (◪). Unsuitable because of: technological behavior (1), health hazard (2), cost (3), color saturation and purity (4).

Figure 22. Blue and turquoise colors in glaze, plotted on the a*-b* plane (CIE-L*a*b*). Numbered fields represent the main industrial colorants, while symbols refer to colorants proposed in the literature but not entered in use yet.

Figure 23. Technological properties of industrial black to gray ceramic pigments and dyes. Symbols: widely used (■); limited use (⊡); no longer in use (□); not entered in use (◪). Unsuitable because of: technological behavior (1), health hazard (2), cost (3), color saturation and purity (4).

Figure 24. Black and gray colors in glaze, plotted on the L*-C* plane (CIE-L*a*b*).

Figure 25. Technological properties of industrial white pigments (opacifiers) and some ceramic effects. Symbols: widely used (■); limited use (⊡); no longer in use (□); not entered in use (⊘). Unsuitable because of: technological behavior (1), health hazard (2), cost (3), color saturation and purity (4).

Table 1. Definition of pigment, dye, and effect for ceramic applications and various types currently used by the industry.

Colorant		Definition in the ceramic sector
Pigment		Pigments are colored, black or white particulate inorganic solids which are largely insoluble in, and essentially physically and chemically unaffected by, the matrix in which they are incorporated (including the melt present in bodies and glazes during firing). They alter appearance by selective absorption and/or by scattering of light. Pigments are usually dispersed in vehicles for application, as for instance in the manufacture of colored powder agglomerates or ceramic inks to decorate glazes and bodies. Pigments retain their crystal structure throughout the ceramic process. Modified after the CPMA[1] definition.
IP	Idiochromatic	or "self-colored" pigments, where the chromophore is a major ingredient of the crystal structure, *e.g.* chromite spinel, $FeCr_2O_4$, or uvarovite garnet, $Ca_3Cr_2Si_3O_{12}$.
AP	Allochromatic	or "other colored" pigments, where the chromophore is present as dopant of the host crystal structure, *e.g.* praseodymium in zircon, $(Zr,Pr)SiO_4$, or chromium in malayaite, $Ca(Sn,Cr)(Si,Cr)O_5$.
MP	Mordant	pigments, where chromophore occurs as tiny inclusions in the host crystal structure, *e.g.* vanadium pentoxide into baddeleyite, $ZrO_2[V_2O_5]$. The size of inclusions is smaller than the domain of coherent diffraction, thus the chromophore cannot be detected by X-ray diffraction.
EP	Encapsulated	pigments, where the chromophore agent is coated by a protective layer because heat-liable or chemically attacked by the melt present in glazes and bodies, *e.g.* cadmium sulfide in zircon, $ZrSiO_4[CdS]$. They are sometimes called "occlusion" or "inclusion" pigments. The size of inclusions is larger than the domain of coherent diffraction, thus the pigment may be detected by X-ray diffraction.
Dye		Dyes are colored, black or white organometallic complexes or inorganic substances that are destroyed during firing, thus dissolved into glazes and glasses and the melt present in ceramic bodies. They impart color to a substrate by selective absorption of light. They are soluble complexes or particulates dispersed in vehicles for application, as for instance in the manufacture of soluble salts and ceramic inks to decorate glazes and bodies. Dyes do not retain their crystal structure but may promote crystallization/precipitation of other crystalline substances that occur at the end of the ceramic process. Modified after the ETAD[2] definition.
SD	Soluble salts	are dyes consisting of organometallic complexes in aqueous solutions or solvents, which are decomposed during firing, *e.g.* Co^{2+}-carboxylate complex. Transition metal ions impart color to the ceramic matrix in which are incorporated.
RD	Reactive dyes	are soluble salts that, reacting during firing with the ceramic matrix, induce the crystallization of colored crystalline phases. Reaction products usually incorporate the transition metal ions provided by the dye, *e.g.* Ti-Cr-Sb organometallic complexes that lead to the formation of rutile, $(Ti,Cr,Sb)O_2$.
PD	Crystalline particulates	are inorganic solids, which are dissolved during firing and incorporated into the ceramic matrix. Color is bestowed by transition metal ions migrated in the vitreous phase of bodies and glazes, *e.g.* Co^{2+} of $LiCoPO_4$.
Effect		Effects are particulate inorganic solids that confer peculiar optical and textural features to ceramic surfaces. They typically react during firing with the matrix in which are incorporated, generally ceramic glazes and glasses. They alter appearance by scattering of light and/or by modifying gloss, iridescence or texture of surfaces. Effects are usually dispersed in vehicles for application, as for instance in the manufacture of ceramic inks to decorate glazes. Effects do not retain their crystal structure but may promote the formation of other crystalline and amorphous phases.
SE	Sink	inducing a bas-relief texture, consisting of slightly depressed zones developed during firing by enhanced fusibility.
BE	Gloss/Matt	turning the surface either shiny (gloss) or opaque (matt) by changing refractive index or precipitating crystals, respectively.
GE	Glitter	sparkling effect, simulating the aventurine glass, achieved by precipitation of properly oriented crystals.
LE	Luster	simulating the brilliance and iridescence of metallic surfaces (steel and precious metals).

[1]CPMA: Color Pigments Manufacturers Association. [2]ETAD: Ecological and Toxicological Association of Dyes and organic pigments manufacturers.

Table 2. Crystallographic and physical characteristics of the main substances used as ceramic pigments.

Crystal structure	Formula	Symmetry	Space Group	Density ($Mg \cdot m^{-3}$)	Melting point (°C)	Refractive indices (adim.)			
Baddeleyite	ZrO_2	monoclinic	$P2_1/c$	5.75	2710	B	2.13	2.19	2.20
Bunsenite	NiO	cubic	$Fm3m$	7.45	1955	I	1.74		
Cassiterite	SnO_2	tetragonal	$P4_2/mnm$	6.95	1630	U	1.97	2.02	
Cerianite	CeO_2	cubic	$Fm3m$	7.22	2400	I	2.13		
Corundum	Al_2O_3	trigonal	$R-3c$	4.05	2050	U	1.76	1.77	
Garnet	$Ca_3Cr_2Si_3O_{12}$	cubic	$Ia3d$	3.59	1370	I	1.86		
Hematite	Fe_2O_3	trigonal	$R-3c$	5.30	1540	U	2.91	3.19	
Hibonite	$CaAl_{12}O_{19}$	hexagonal	$P6_3/mmc$	3.84	1910	U	1.79	1.81	
Malayaite	$CaSnSiO_5$	monoclinic	$A2/a$	4.42	1330	B	1.77	1.78	1.80
Perovskite	$YAlO_3$	orthorhombic	$Pbnm$	4.56	1870	B	1.92	1.94	1.95
Priderite	$BaNiTi_7O_{16}$	tetragonal	$I4/m$	3.86	1400	U	2.35	2.37	
Pseudobrookite	Fe_2TiO_5	orthorhombic	$Bbmm$	4.40	1550	B	2.37	2.38	2.40
Pyrochlore	$Pb_2Sb_2O_7$	cubic	$Fd3m$	5.94	1310	I	1.86		
Rutile	TiO_2	tetragonal	$P4_2/mnm$	4.25	1850	U	2.87	2.58	
Spinel	$MgAl_2O_4$	cubic	$Fd3m$	3.64	2140	I	1.76		
Srilankite	$ZrTiO_4$	orthorhombic	$Pbcn$	4.77	1840	B	2.33	2.38	2.41
Willemite	Zn_2SiO_4	trigonal	$R-3$	4.05	1510	B	1.71	1.72	
Wurtzite	CdS	hexagonal	$P6_3mc$	4.49	1290	B	2.53	2.51	
Zircon	$ZrSiO_4$	tetragonal	$I4_1/amd$	4.65	2550	B	1.92	1.97	

Note: I, U, and B stand for optically Isotropic (a single refractive index), Uniaxial (two refractive indices), and Biaxial (three refractive indices), respectively.

Table 3. Chemical and physical characteristics of the main substances used as ceramic dyes and effects.

Compound	Formula	Structure	Density ($Mg \cdot m^{-3}$)	Melting point (°C)	Type Table 1	Color/Effect
Cerianite	CeO_2	cubic, *Fm3m*	6.95	1630	LE	metallic luster
Chromium	Cr^{3+}	organometallic complex	—	—	SD	green or light brown
Chromium-Antimony	$Cr^{3+} + Sb^{5+}$	organometallic complex	—	—	RD	yellow
Clinobisvanite	$BiVO_4$	monoclinic, *I2/a*	6.95	~900	SE	sink
Cobalt olivine	Co_2SiO_4	orthorhombic, *Pbnm*	4.04	1420	PD	blue
Cobalt lithiophylite	$LiCoPO_4$	orthorhombic, *Pbnm*	3.76	~800	PD	blue
Cobalt sarcopside	$Co_3(PO_4)_2$	monoclinic, $P2_1/c$	3.82	1120	PD	blue
Cobalt suanite	$MgCoB_2O_5$	monoclinic, $P2_1/c$	2.35	~1100	PD	blue
Cobalt	Co^{2+}	organometallic complex	—	—	SD	blue
Copper	Cu^{+}	organometallic complex	—	—	SD	green
Ferroalluaudite	$NaFe_3(PO_4)_3$	monoclinic, *C12/c*	3.60	~900	LE	metallic luster
Frit (glossy)	Si-B-Na-K-Ca-Ba-O	borosilicate glass	2.4÷2.6	700÷1200[1]	BE	glossy surface
Frit (matt)	Si-B-Na-K-Ca-Zn-Mg-O	borosilicate glass	2.4÷2.6	700÷1200[1]	BE	opaque surface
Gold	Au^0	organometallic complex	—	—	RD	magenta or metallic gold
Hematite	Fe_2O_3	trigonal, *R*−3*c*	5.30	1540	LE	metallic luster
Iron	Fe^{3+}	organometallic complex	—	—	SD	brown
Iron phosphate	$Fe_2Fe(P_2O_7)_2$	orthorhombic, *Pnma*	3.07	940	LE	metallic luster
Liebenbergite	Ni_2SiO_4	orthorhombic, *Pbnm*	4.60	1650	PD	green
Nickel	Ni^{2+}	organometallic complex	—	—	SD	brown
Palladium	Pd^0	organometallic complex	—	—	RD	gray
Platinum	Pt^0	organometallic complex	—	—	RD	metallic platinum
Ruthenium	Ru^0	organometallic complex	—	—	RD	black
Scheelite	$CaWO_4$	tetragonal, $I4_1/a$	6.01	1580	GE	aventurine
Shcherbinaite	V_2O_5	orthorhombic, *Pmmn*	3.28	690	SE	sink
Silver	Ag^0	organometallic complex	—	—	RD	yellow or metallic silver
Tenorite	CuO	monoclinic, *C2/c*	6.50	1240	GE	aventurine
Vanadium	V^{3+}	organometallic complex	—	—	SD	light brown
Zirconium	Zr^{4+}	organometallic complex	—	—	RD	white, matt

[1]Softening (maturing) temperature.

Table 4. Color of the main ceramic pigments and dyes. Color Index number and code (Society of Dyers and Colourists). Chromophore: [ion coordination number]. Color origin: Crystal Field theory (CF); Metal Oxygen Charge Transfer (MOCT); Inter-Valence Charge Transfer (IVCT); Band theory (BT); Cooperative Transitions (COT); Paired spin Exchange transitions (PE).

no.	Structure/Name	Formula	Type	C.I. #	C.I. CODE	Chromophore	Origin	Reference
1	Cassius' purple	Au	IP	77482	RED 109	Au nanoparticles	plasmonics	
2	Malayaite	$Ca(Sn,Cr)(Si,Cr)O_5$	AP	77301	RED 233	Cr^{4+}[4] Cr^{4+}[6]	CF	
3	Perovskite	$Y(Al,Cr)O_3$	AP	—	—	Cr^{3+}[6]	CF COT	
4	Cadmoselite *(in zircon)*	$ZrSiO_4$[Cd(Se,S)]	EP	77196	RED 108	band gap	BT	
5	Hematite *(in zircon)*	$ZrSiO_4$[Fe_2O_3]	EP	77996	RED 232	$Fe^{3+}\leftrightarrow Fe^{3+}$[6]	PE CF	
	Hematite	Fe_2O_3	IP	77491	RED 101	$Fe^{3+}\leftrightarrow Fe^{3+}$[6]	PE CF	
6	Spinel Jacobsite	$(Mn,Fe)(Mn,Fe)_2O_4$ $(Mn,Fe)(Fe,Cr)_2O_4$	IP	77494 774945	BLACK 26 BROWN 46	Mn^{2+}[4] Fe^{3+}[4] Mn^{3+}[6] Cr^{3+}[6]	CF MOCT	
	Spinel Chromite	$FeCr_2O_4$	IP	77500	BROWN 29	Cr^{3+}[6] Fe^{2+}[4]	CF MOCT	
7	Rutile	$(Ti,Cr,Sb)O_2$ $(Ti,Cr,Nb)O_2$	AP	77310 77896	BROWN 24 YELLOW 162	Cr^{3+}[6]	CF MOCT	
8	Rutile	$(Ti,Cr,W)O_2$	AP	77897	YELLOW 163	Cr^{3+}[6]	CF MOCT	
9	Baddeleyite	$ZrO_2[V_2O_5]$	MP	77991	YELLOW 160	V_2O_5 V^{4+}[8]	MOCT CF	
	Oxyplumboroméite	$Pb_2Sb_2O_7$	IP	77588	YELLOW 41	band gap	BT	
10	Rutile	$(Ti,Ni,Sb)O_2$ $(Ti,Ni,Nb)O_2$ $(Ti,Ni,W)O_2$	AP	77788 77895 77902	YELLOW 53 YELLOW 161 YELLOW 189	Ni^{2+}[6]	CF MOCT	
	Pyrochlore	$Y_2(Sn,V)_2O_7$	AP	—	—	V^{4+}[6]	CF	
	Srilankite	$(Zr,Sn,Ti,V,In)O_2$	AP	—	—	V^{4+}[6]	CF	
11	Zircon	$(Zr,Pr)SiO_4$	AP	77997	YELLOW 159	Pr^{4+}[8]	CF	
12	Greenockite *(in zircon)*	$ZrSiO_4$[CdS] $ZrSiO_4$[Cd(S,Se)]	EP	77205 —	YELLOW 35 ORANGE 20	band gap	BT	
	Spinel Gahnite	$Zn(Al,Cr)_2O_4$	AP	77290	RED 235	Cr^{3+}[6]	CF	
	Corundum	$(Al,Cr)_2O_3$ $(Al,Mn)_2O_3$	AP	77003 77005	RED 230 RED 231	Cr^{3+}[6] Mn^{3+}[6]	CF CF	
13	Spinel Zincochromite	$(Zn,Fe)(Cr,Fe,Al)_2O_4$ $Zn(Fe,Cr)_2O_4$	IP	77496 77503	YELLOW 119 BROWN 33	Cr^{3+}[6]	CF	
14	Cassiterite	$(Sn,V)O_2[V_2O_5]$	MP	77862	YELLOW 158	V_2O_5 V^{4+}[6]	MOCT CF	
15	Priderite	$Ba(Ti,Ni)_8O_{16}$	AP	77900	YELLOW 157	Ni^{2+}[6]	CF	
16	Garnet Uvarovite	$Ca_3Cr_2(SiO_4)_3$	IP	77300	GREEN 51	Cr^{3+}[6]	CF	
17	Eskolaite	Cr_2O_3	IP	77288	GREEN 17	Cr^{3+}[6]	CF	
	Olivine Liebensbergite	Ni_2SiO_4	PD	77850	—	Ni^{2+}[6] Ni^{2+}[5] *in glass*	CF	
18	Spinel Co-Ti	Co_2TiO_4 $(Co,Al)_2(Al,Ti)O_4$	IP	77377 773465	GREEN 50 BLUE 81	Co^{2+}[4] Co^{2+}[6]	CF MOCT	
19	Spinel Cochromite	$CoCr_2O_4$ $(Zn,Co)Cr_2O_4$	IP	77344 77343	GREEN 26 BLUE 36	Co^{2+}[4] Cr^{3+}[6]	CF	
20	Zircon	$ZrSiO_4$:V	AP	77998	BLUE 71	V^{4+}-V^{4+}[4]	CF	
21	Cassiterite	$(Sn,Sb)O_2$	AP	77865	BLACK 23	band gap	BT	
	Spinel Hercynite	$Fe(Al,Ti)_2O_4$	AP	—	—	Fe^{2+}+$Ti^{4+}\leftrightarrow Fe^{3+}$+$Ti^{3+}$[6]	IVCT	
	Spinel Co-Sn	Co_2SnO_4	IP	77368	BLUE 35	Co^{2+}[4] Co^{2+}[6]	CF MOCT	
22	Spinel Gahnite	$CoAl_2O_4$ $(Co,Zn)Al_2O_4$	IP	77346 77347	BLUE 28 BLUE 72	Co^{2+}[4]	CF MOCT	
23	Willemite	$(Zn,Co)_2SiO_4$	AP	77366	BLUE 74	Co^{2+}[4]	CF MOCT	
24	Olivine	Co_2SiO_4	PD	77364	BLUE 73	Co^{2+}[4] Co^{2+}[5] *in glass*	CF MOCT	
	Perovskite	$Y(Mn,In)O_3$	IP	—	BLUE 86	Mn^{3+}[6] In^{3+}[6]		
	Lithiophylite	$CoLiPO_4$	PD	77362	VIOLET 14	Co^{2+}[4] Co^{2+}[5] *in glass*	CF MOCT	
	Sarcopside	$Co_3(PO_4)_2$	PD	77363	VIOLET 47	Co^{2+}[4] Co^{2+}[5] *in glass*	CF MOCT	
	Suanite	$MgCoB_2O_5$	DY	77352	VIOLET 48	Co^{2+}[4] Co^{2+}[5] *in glass*	CF MOCT	
25	Cassiterite	$(Sn,Cr)O_2[CrO_2]$	PD	77863	RED 236	CrO_2 Cr^{4+}[6] Cr^{3+}-Cr^{3+}[6]	IVCT CF	
	Rutile	$(Ti,Mn,Sb)O_2$	AP	77899	YELLOW 164	Mn^{2+}[6] Mn^{3+}[6]	CF MOCT	
	Pseudobrookite	Fe_2TiO_5 $(Al,Fe)_2TiO_5$	IP	77501 775435	BROWN 35 BROWN 48	Fe^{3+}[6]	CF MOCT	
	Spinel Chromite	$FeCr_2O_4$	IP	77500	BROWN 29	Fe^{2+}[4] Cr^{2+}[6]	CF MOCT	
	Spinel Ulvospinel	Fe_2TiO_4	IP	77543	BLACK 12	Fe^{2+}[4] Fe^{2+}[6] $Fe^{2+}\leftrightarrow Fe^{3+}$	CF IVCT	
26	Periclase Bunsenite	(Ni,Co)O	IP	77332	BLACK 25	Ni^{2+}[6] Co^{2+}[6]	CF MOCT	
27	Rutile	$(Ti,V,Sb)O_2$	AP	77898	BLACK 24	V^{4+}[6] V^{3+}[6]	CF MOCT	
28	Eskolaite-Hematite	$(Cr,Fe)_2O_3$	IP	77288	—	Cr^{3+}[6] Fe^{3+}[6]	CF MOCT	
	Spinel Cuprospinel	$CuCr_2O_4$	IP	77428	BLACK 28	Cr^{3+}[6] Cu^{2+}[4]	CF MOCT	
	Spinel Nichromite	$Ni(Cr,Fe)_2O_4$	IP	77504	BLACK 30	Ni^{2+}[4] Fe^{3+}[4] Fe^{3+}[6] Cr^{3+}[6]	CF MOCT	
29	Spinel Co-ferrite	$CoFe_2O_4$ $Co(Fe,Cr)_2O_4$	IP	77498 77502	BLACK 29 BLACK 27	Co^{2+}[4] Fe^{3+}[4] Fe^{3+}[6] Cr^{3+}[6]	CF MOCT	
30	Spinel complex	(Ni,Co,Mn) $(Cr,Mn,Fe)_2O_4$	IP	—	—	Ni^{2+}[4] Co^{2+}[4] Mn^{2+}[4] Fe^{3+}[4] Fe^{3+}[6] Mn^{3+}[6] Cr^{3+}[6]	CF MOCT	

Table 5. Chemical stability of ceramic pigments in contact with glazes and bodies: incompatibility (or improved stability) with single components and maximum temperature allowed for industrial firing.

Pigment	Formula	Incompatible with	Improved stability with	T_{max} °C
Baddeleyite	$ZrO_2[V_2O_5]$	B *Pb*	Zr Ca Mg Ba	1300
Bunsenite	$[(Ni,Co)O]ZrSiO_4$	Zn Na K B *Pb*	Zr	1350
Cassiterite	$(Sn,Cr)O_2[CrO_2]$	Zn Mg (Na K B)	Sn Ca	1300
Cassiterite	$(Sn,V)O_2[V_2O_5]$	Al	Sn B *Pb*	1300
Cassiterite	$(Sn,Sb)O_2$	Na K B	Sn	1250
Corundum	$(Al,Cr)_2O_3$	Ca B *Pb*	Al Zn	1400
Corundum	$(Al,Mn)_2O_3$	B Zn *Pb*	Al	1400
Eskolaite	$(Cr,Fe)_2O_3$	Ca Zn Sn Ni	Al	1250
Garnet	$Ca_3Cr_2Si_3O_{12}$	Zn *Pb*	Ca	1200
Hematite	$ZrSiO_4[Fe_2O_3]$		Zr	1250
Malayaite	$Ca(Sn,Cr)(Si,Cr)O_5$	Mg Zn Na K B	Ca Sn	1250
Olivine	Co_2SiO_4	Mg		1350
Perovskite	$Y(Al,Cr)O_3$	Ca Na K B	Al	1350
Pyrochlore	$Pb_2Sb_2O_7$	Na K B	*Pb* Zn Al	1050
Rutile	$(Ti,Cr,Sb)O_2$	Na K B	Ti Zn Zr	1300
Spinel	$CoAl_2O_4$	Na K B *Pb*	Al Zn	1350
Spinel	$CoCr_2O_4$	Zn Sn Ni	Al	1300
Spinel	Zn-Fe-Al-Cr-Mn	Sn	Zn Al	1400
Spinel	Co-Ni-Mn-Fe-Cr	Zn (Sn Zr)		1400
Willemite	Zn_2SiO_4	Ca	Zn	1200
Wurtzite	$ZrSiO_4[Cd(Se,S)]$	*Pb*	Cd	1200
Zircon	$(Zr,Pr)SiO_4$		Zr Zn *Pb*	1300
Zircon	$ZrSiO_4$:V		Zr	1300

Table 6. Coloration stemming from dissolution of transition metal ions into a silicate glass. In **bold** the most common colors developed in glazes and bodies.

Transition metal ion	Oxygen coordination	Color
Co^{2+}	4	**dark blue**
Co^{2+}	6	pink
Cr^{3+}	6	**emerald green**
Cr^{6+}	4	yellow
Cu^{+}	6	red
Cu^{2+}	6 (distorted)	**green to blue-green**
Fe^{2+}	4 to 5	green-blue to green-brown
Fe^{3+}	4	**reddish brown**
Fe^{3+}	6	**yellow-orange**
Mn^{2+}	4 to 6	**green to blue-green**
Mn^{3+}	6 (distorted)	pale red to purplish brown
Ni^{2+}	4	deep purple
Ni^{2+}	5	**brown**
Ni^{2+}	6	yellow
V^{3+}	6	**greenish brown**
V^{4+}	4 to 5	blue-green
V^{5+}	4	yellowish green

Table 7. Isothermal bulk modulus (K_{T0}, in GPa) for the crystal structures of the ceramic pigments under comparison along with its range of variation.

Structure formula	Structure type	Averaged K_{T0} [GPa]	K_{T0} range [GPa]	Reference
Al_2O_3	corundum	251	242 - 257	[56-63]
$ZrSiO_4$	zircon	226	225 - 228	[64-68]
TiO_2	rutile	212	209 - 216	[69-74]
SnO_2	cassiterite	210	203 - 212	[69,75-77]
$YAlO_3$	Y-aluminate (perovskite)	195	188 - 205	[78-80]
$CoAl_2O_4$	Co-aluminate (spinel)	207	203 - 210	[81,82]
$CoFe_2O_4$	Co-ferrite (spinel)	180	175 - 186	[81,83]
$(A)Cr_2O_4$ where A: Zn, Mg, Fe	chromite (spinel)	183	181 - 189	[84-86]
$CaTiOSiO_4$	titanite	131	-	[87]
$CaSnOSiO_4$	malayaite	121	-	[88]

Note: the reported isothermal bulk moduli derive from high-pressure X-ray diffraction experiments of single-crystal and powder samples [56-59,66,67,70,71,73-75,78,79,83,84,87,88], elastic constant measurements of single-crystal and powder samples [62,64,65,68,69,76,77,81], and theoretical calculations through various computational methods [60,61,63,72,80,82,85,86].

Technology	Ceramic product	Decoration techniques	Colorant applied as	Firing	Firing reactions with	Pigment size distribution
LT Low Temperature	third-fire applications classic slow double-fired products	rotogravure (silicon roller) screen printing (rotary or flat) flexography airless spraying (see Figure 2)	powder dispersed in paste or glaze	slow double third fire 700-950°C	low temperature glaze	**micrometric pigments** d_{50}=3-7 µm d_{90}=7-15 µm **encapsulated pigments** d_{50}=10-20 µm d_{90}=15-30 µm
IT Intermediate Temperature	porous (*monoporosa, birapida*) and semi-vitrified tiles (*stoneware*)			fast single (double) 1080-1160°C 30-50 min	intermediate temperature glaze	
HT High Temperature	highly vitrified tiles (*glazed porcelain stoneware*)		powder in slip or stuck on granules soluble salt	fast single 1180-1220°C 50-90 min	high temperature glaze	
BO Body (unglazed)	highly vitrified tiles (*unglazed porcelain stoneware*)			fast single 1190-1230°C 60-90 min	porcelain stoneware body	
VHT Very High Temperature	highly vitrified products (*vitreous china, porcelain*)	decal screen printing painting	powder dispersed in paste or stuck on decal	slow single or double 1250-1400°C	very high temperature glaze	
DD Digital Decoration	all tile types: stoneware, porcelain stoneware, third-fire, birapida, monoporosa	DOD inkjet printing	ink	fast single 700-1240°C 30-90 min	all glazes and bodies	**micronized pigments** d_{50}=0.3-0.7 µm d_{90}=0.6-1.0 µm

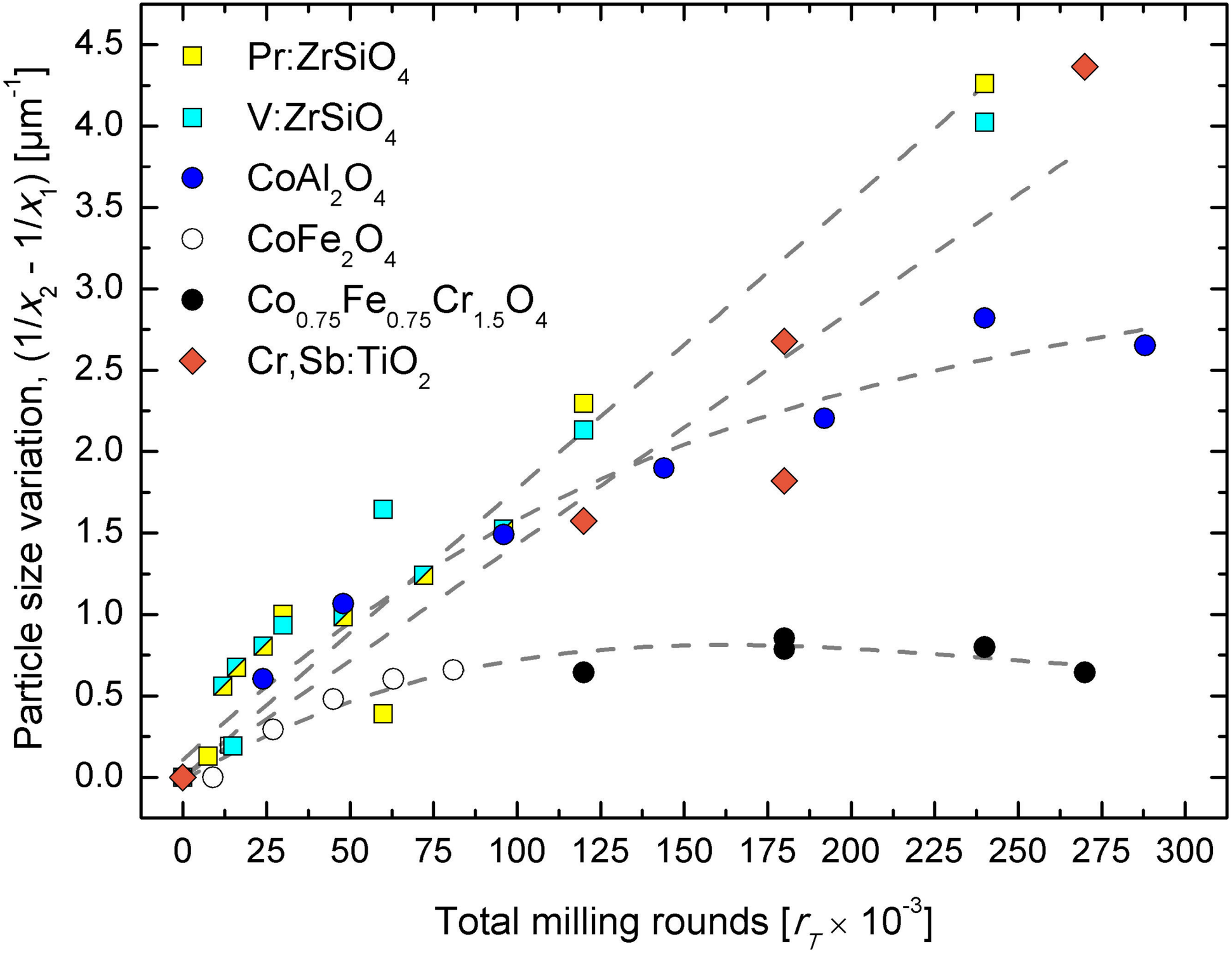
Pr:ZrSiO4
V:ZrSiO4
CoAl2O4
CoFe2O4
Co0.75Fe0.75Cr1.5O4
Cr,Sb:TiO2
Particle size variation, (1/x2 - 1/x1) [μm-1]
Total milling rounds [rT × 10-3]
0.0
0.5
1.0
1.5
2.0
2.5
3.0
3.5
4.0
4.5
0
25
50
75
100
125
150
175
200
225
250
275
300

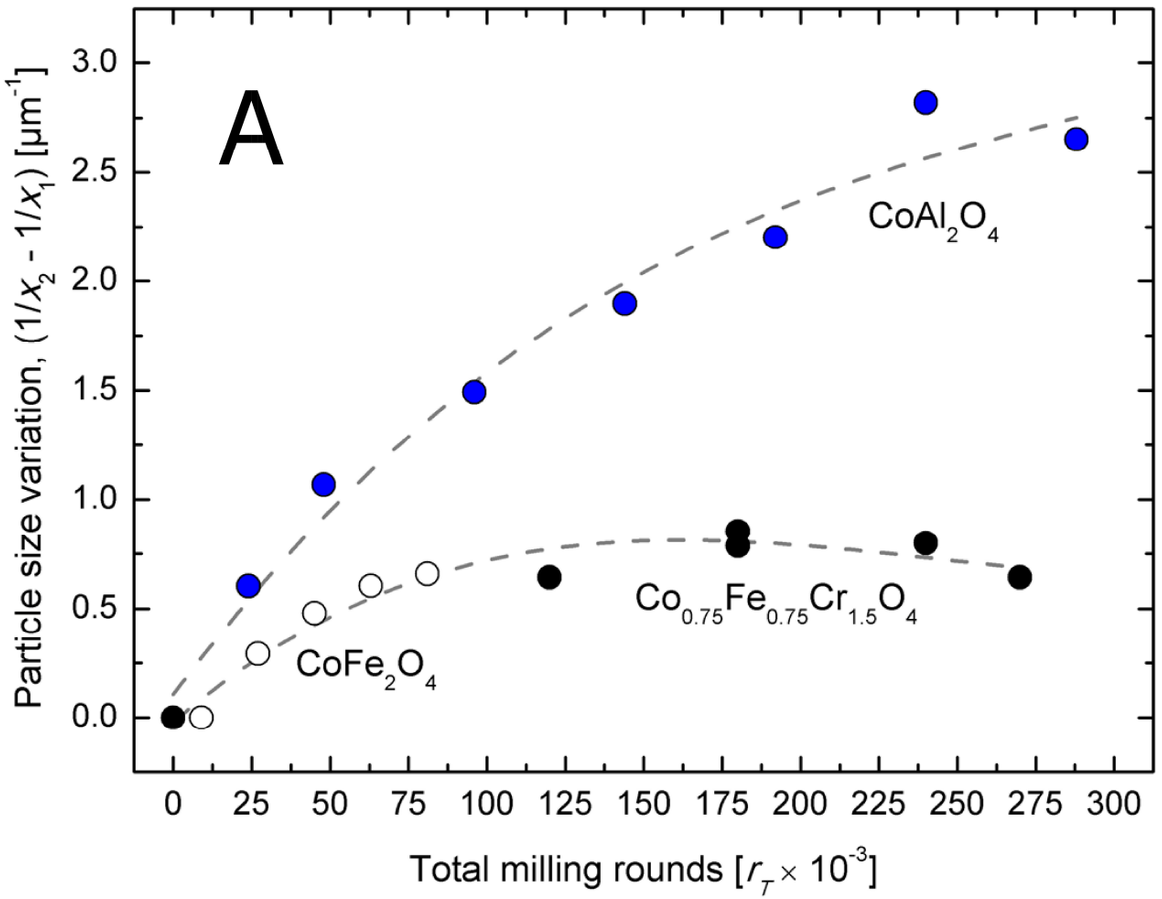

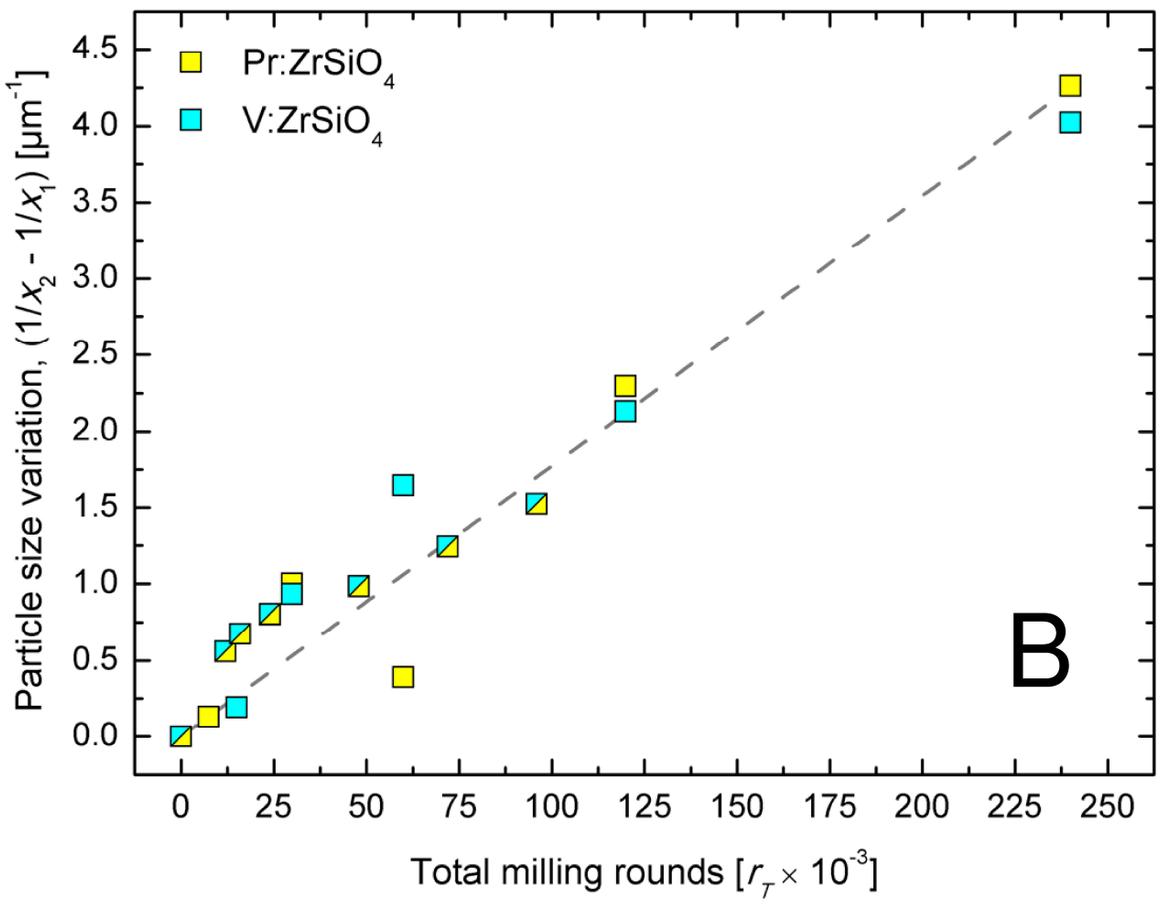

ZIRCON (yellow or turquoise) **RUTILE** (orange) **MALAYAITE** (burgundy) — — — — — **SPINEL** (blue) (black) (brown) (beige) — — — — —

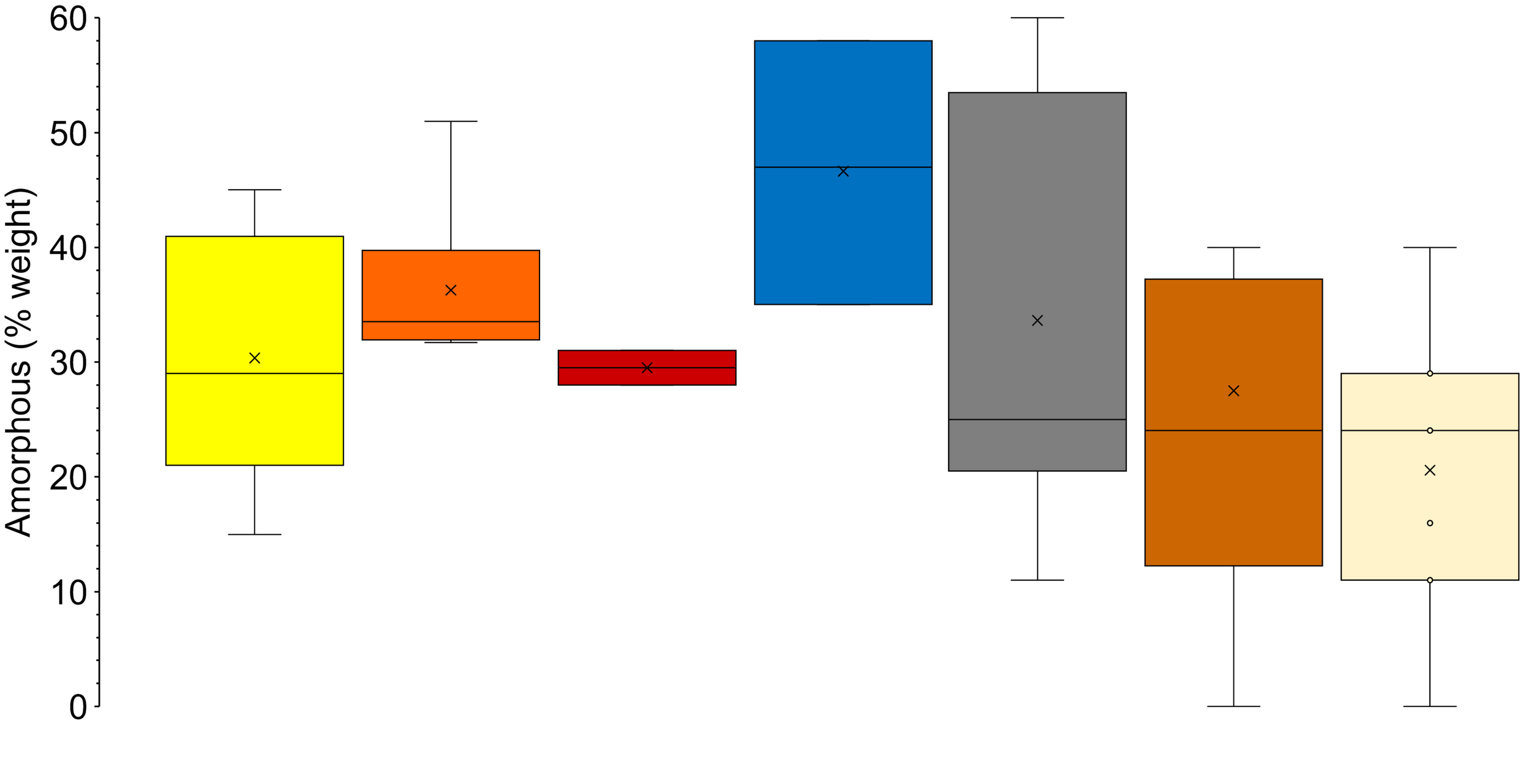

Colorant	Formula	Color	Application – Technology (see Fig. 1)				
			LT	**IT**	**HT-VHT**	**BO**	**DD**
Cassius' purple	Au	magenta RED 109	■	□ 3	□ 3	◉	◉
Malayaite	$Ca(Sn,Cr)(Si,Cr)O_5$	burgundy RED 233	■	■	■	⊘ 1	■
Pyrochlore	$Y_2(Sn,Cr)_2O_7$	burgundy not filed	⊘ 3 4	⊘ 3 4	⊘ 3 4	⊘ 3 4	⊘ 3 4
Cadmoselite	$ZrSiO_4[Cd(Se,S)]$	red RED108	■	■	■	⊘ 3	⊘ 1 2
Perovskite	$Y(Al,Cr)O_3$	red not filed	◉	⊘ 1	■	◉	⊘ 1
Hematite *(in zircon)*	$ZrSiO_4[Fe_2O_3]$	coral pink RED 232	■	■	◉	◉	⊘ 1
Hematite *(in silica)*	$SiO_2[Fe_2O_3]$	coral pink not filed	⊘ 1	⊘ 1	⊘ 1	■	⊘ 1
Corundum	$(Al,Mn)_2O_3$	pink RED 231	■	◉	◉	■	⊘ 4
Corundum	$(Al,Cr)_2O_3$	pink RED 230	■	◉	◉	⊘ 4	⊘ 4
Spinel	$Zn(Al,Cr)_2O_4$	pink RED 235	■	◉	◉	⊘ 1	⊘ 4
Cassiterite	$(Sn,Cr)O_2[CrO_2]$	purple RED 236	■	■	■	⊘ 3	◉

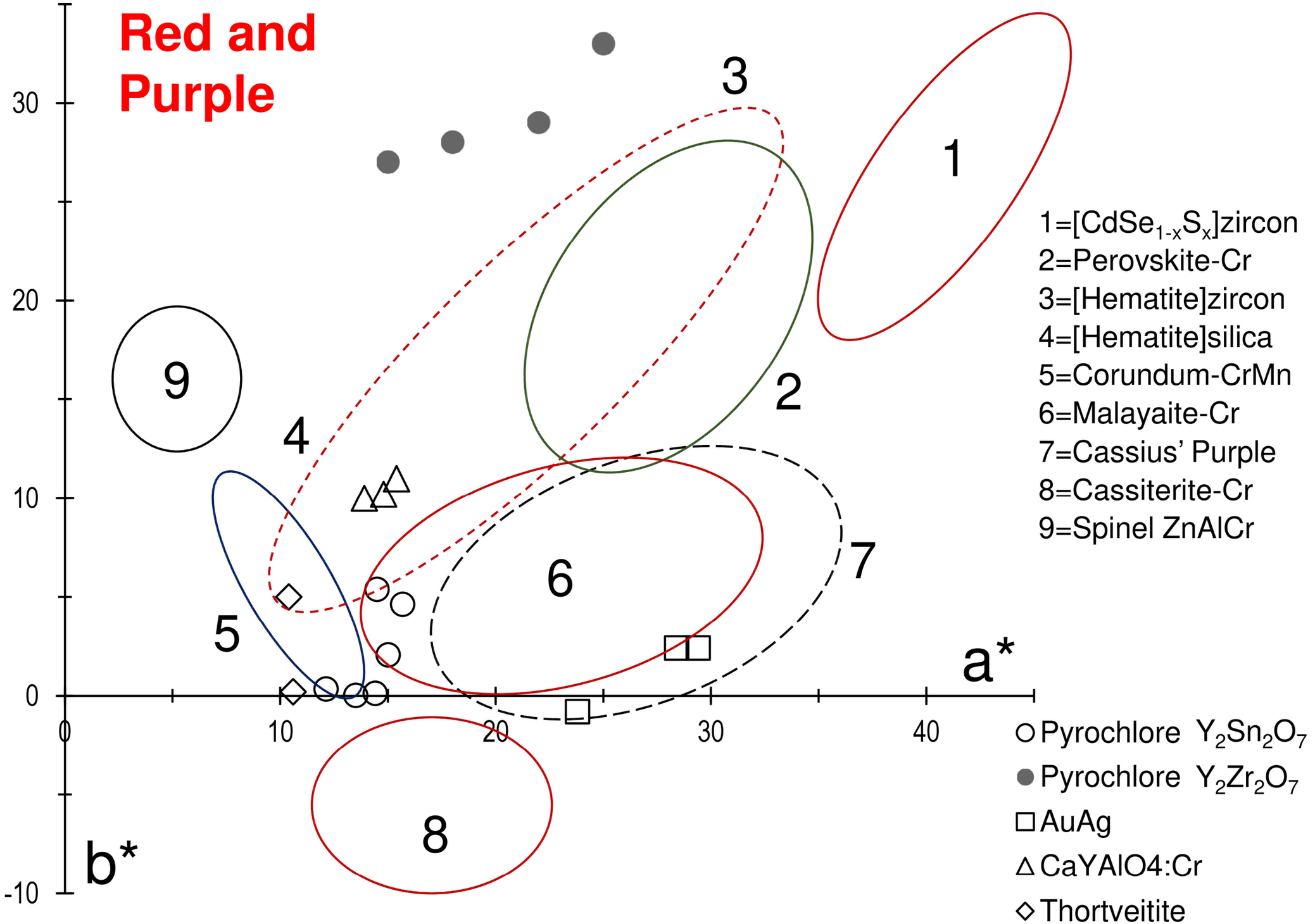
Red and Purple
30
20
10
0
-10
0
10
20
30
40
b*
a*
1
2
3
4
5
6
7
8
9
1=[CdSe1-xSx]zircon
2=Perovskite-Cr
3=[Hematite]zircon
4=[Hematite]silica
5=Corundum-CrMn
6=Malayaite-Cr
7=Cassius' Purple
8=Cassiterite-Cr
9=Spinel ZnAlCr
Pyrochlore Y2Sn2O7
Pyrochlore Y2Zr2O7
AuAg
CaYAlO4:Cr
Thortveitite

Colorant	Formula	Color	Application – Technology (see Fig. 1)				
			LT	**IT**	**HT-VHT**	**BO**	**DD**
Zircon	$(Zr,Pr)SiO_4$	yellow YELLOW 159	■	■	■	■	■
Rutile	$(Ti,Ni,Sb)O_2$	yellow YELLOW 53	◉	⊘ 1 2	⊘ 1 2	⊘ 2	⊘ 1 2
Greenockite	$ZrSiO_4[CdS]$	yellow YELLOW 35	■	■	◉	⊘ 3	⊘ 1 2
Srilankite	$Zr(Ti,Sn,V,In)O_4$	yellow not filed	⊘ 3	⊘ 3	⊘ 3	⊘ 3	⊘ ?
Perovskite	$Sr(Sn,V)O_3$ $Ba(Sn,Tb)O_3$	yellow not filed	⊘ 3	⊘ 1 3	⊘ 1 3	⊘ 1 3	⊘ 1 3
Baddeleyite	$ZrO_2[V_2O_5]$	yellow YELLOW 160	■	■	■	⊘ 1 3	⊘ 1 4
Cassiterite	$(Sn,V)O_2[V_2O_5]$	yellow YELLOW 158	■	□ 3	□ 3	⊘ 3	⊘ 1 4
Priderite	$Ba(Ti,Ni)_8O_{16}$	primrose YELLOW 157	◉	⊘ 1 4	⊘ 1 4	⊘ 1 4	⊘ 1 4
Pseudobrookite *(Karrooite)*	$Mg(Ti,V)_2O_5$	primrose not filed	⊘ 1 4	⊘ 1 4	⊘ 1 4	⊘ 1 4	⊘ 1 4
Pyrochlore	$Pb_2Sb_2O_7$	orange YELLOW 41	■	□ 1 2	⊘ 1 2	⊘ 1 2	⊘ 1 2 4
Cerianite	$(Ce,Pr)O_2$	orange-pink not filed	⊘ 1 3	⊘ 1 3	⊘ 3	⊘ 3	⊘ 1
Rutile	$(Ti,Cr,Sb)O_2$	orange BROWN 24	■	⊘ 1	⊘ 1	■	⊘ 1
Rutile (*formed in situ*)	Cr+Sb-organomet and Ti-primer	orange not filed	⊘ 1 4	⊘ 1 4	⊘ 1 4	■	◉

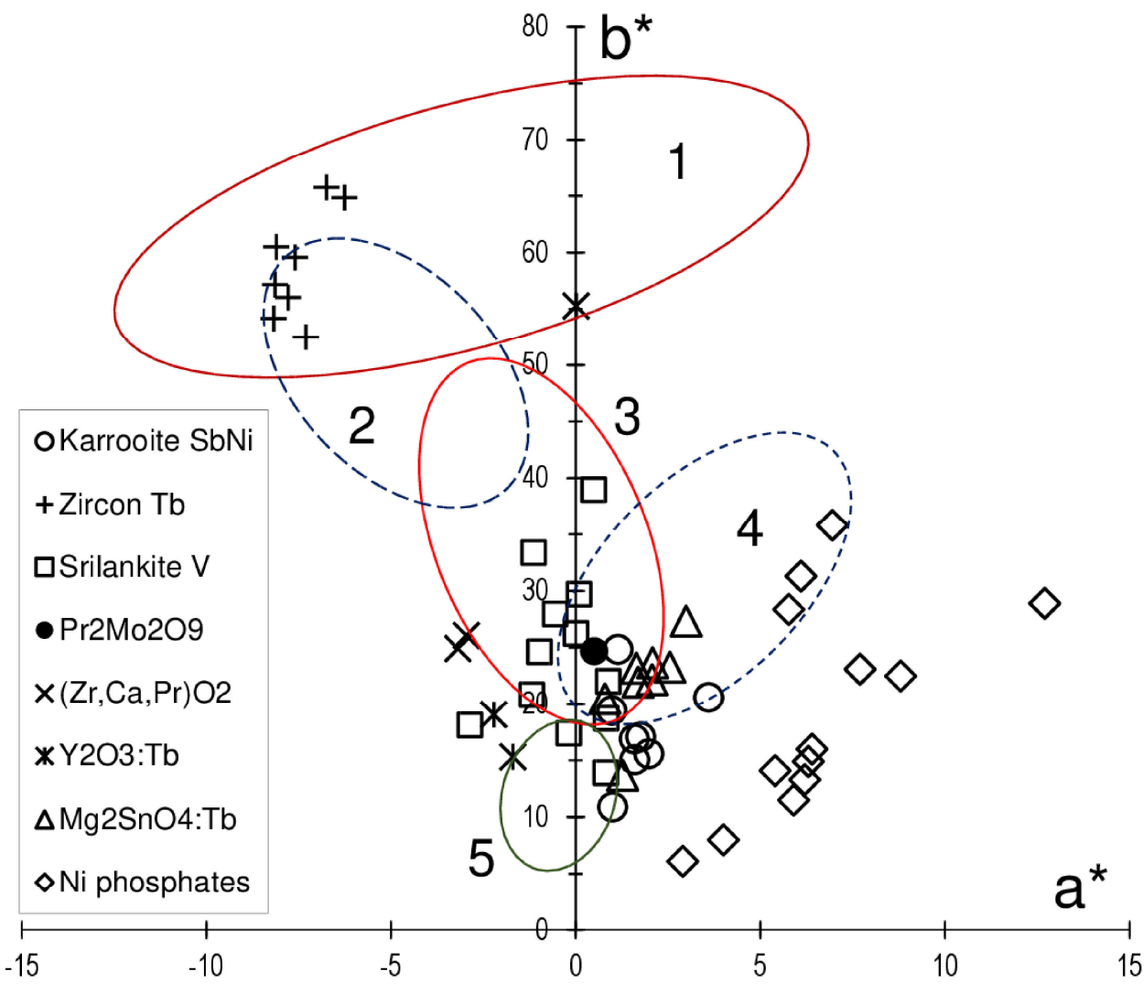
b*
a*
1
2
3
4
5
Karrooite SbNi
Zircon Tb
Srilankite V
Pr2Mo2O9
(Zr,Ca,Pr)O2
Y2O3:Tb
Mg2SnO4:Tb
Ni phosphates

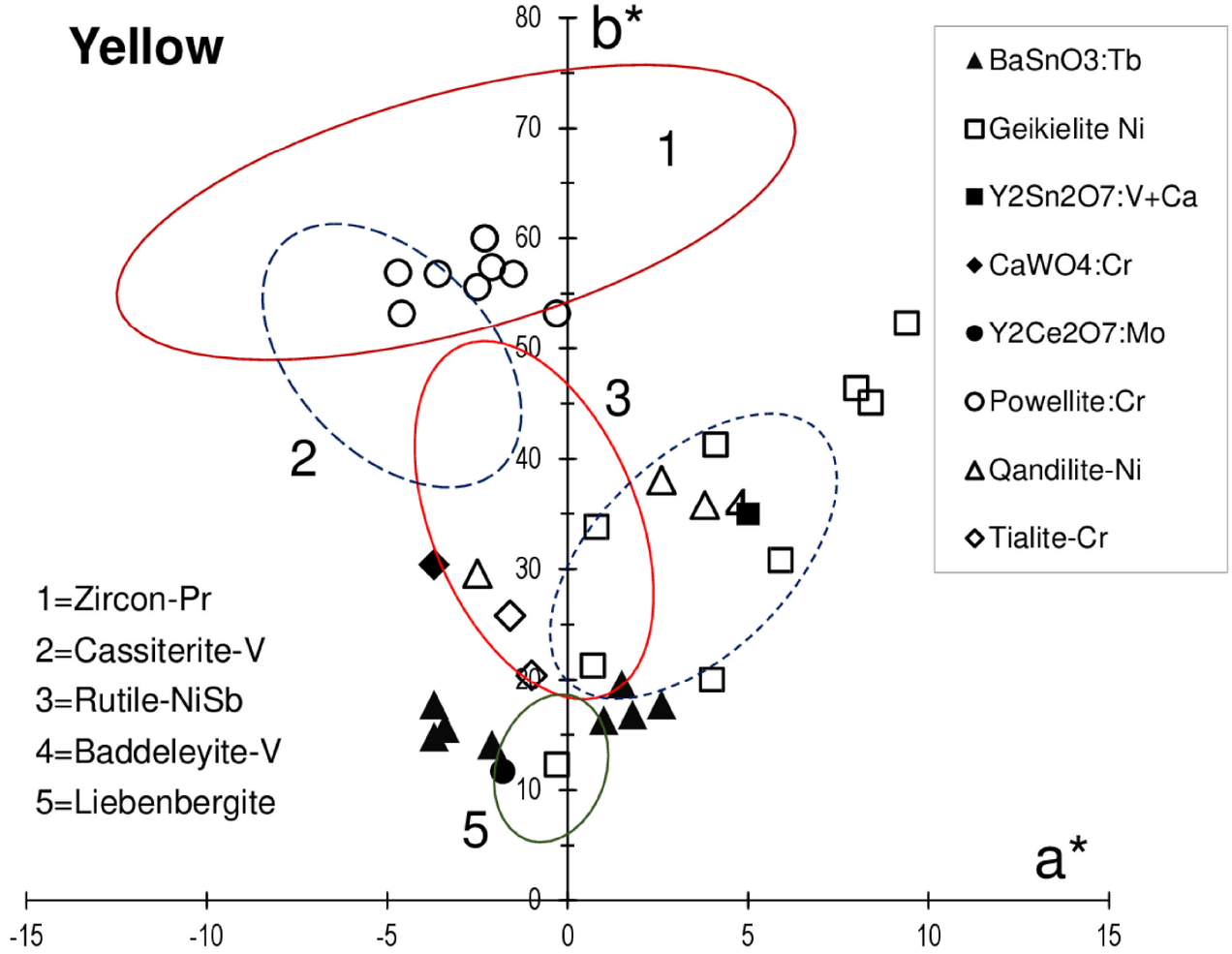
Yellow
b*
a*
1
2
3
4
5
1=Zircon-Pr
2=Cassiterite-V
3=Rutile-NiSb
4=Baddeleyite-V
5=Liebenbergite
BaSnO3:Tb
Geikielite Ni
Y2Sn2O7:V+Ca
CaWO4:Cr
Y2Ce2O7:Mo
Powellite:Cr
Qandilite-Ni
Tialite-Cr

Colorant	Formula	Color	Application – Technology (see Fig. 1)				
			LT	**IT**	**HT-VHT**	**BO**	**DD**
Spinel (*Zincochromite*) Zn(Fe,Cr)$_2$O$_4$ Zn(Fe,Al,Cr)$_2$O$_4$		buff BROWN 33	■	■	■	⊘ 1	■
Cr soluble salt V soluble salt	Cr-organometallic V-organometallic	buff not filed	⊘ 1 4	⊘ 1 4	⊘ 1 4	■	◉
Spinel (*Franklinite*)	(Zn,Mn)(Cr,Mn)$_2$O$_4$	brown not filed	◉	◉	◉	⊘ 1	⊘ 1 4
Fe soluble salt Ni soluble salt	Fe-organometallic Ni-organometallic	brown not filed	⊘ 1 4	⊘ 1 4	⊘ 1 4	■	◉
Perovskite	Ca(Ti,Cr)O$_3$	brown not filed	⊘ 1 4	⊘ 1 4	⊘ 1 4	⊘ 1 4	⊘ 1 4
Spinel (*Chromite*)	$Fe^{2+}Cr_2O_4$	brown BROWN 29	⊘ 1	⊘ 1	⊘ 1	◉	⊘ 1 4
Hematite	(Fe,Cr,Al)$_2$O$_3$	maroon not filed	◉	⊘ 1	⊘ 1	◉	⊘ 1 4
Pseudobrookite	$Fe^{3+}{}_2TiO_5$ $(Fe^{3+},Al)_2TiO_5$	maroon BROWN 35-48	◉	◉	⊘ 1	⊘ 1	⊘ 1
Titanite Karrooite	Ca(Ti,Cr)SiO$_5$ Mg(Ti,Cr)SiO$_5$	maroon not filed	⊘ 1	⊘ 1	⊘ 1	⊘ 1	⊘ 1
Spinel (*Trevorite*)	(Zn,Ni)(Fe,Cr)$_2$O$_4$ (Zn,Ni)Fe$_2$O$_4$	maroon not filed	■	■	■	⊘ 1	■
Spinel (*Jacobsite*)	(Mn,Fe)(Fe,Cr)$_2$O$_4$	coffee BROWN 46	■	■	■	◉	⊘ 1 4
Rutile	(Ti,Cr,W)O$_2$	tobacco YELLOW 163	◉	⊘ 1	⊘ 1	■	⊘ 1
Rutile	(Ti,Mn,Sb)O$_2$	dark brown YELLOW 164	◉	□ 1	⊘ 1	□ 1	⊘ 1
Perovskite	LaFeO$_3$	dark brown not filed	⊘ 1	⊘ 1	⊘ 1	⊘ 1	⊘ 1
Spinel (*Ulvöspinel*)	$Fe^{2+}{}_2TiO_4$	dark brown BLACK 12	□ 1	□ 1	⊘ 1	⊘ 1	⊘ 1

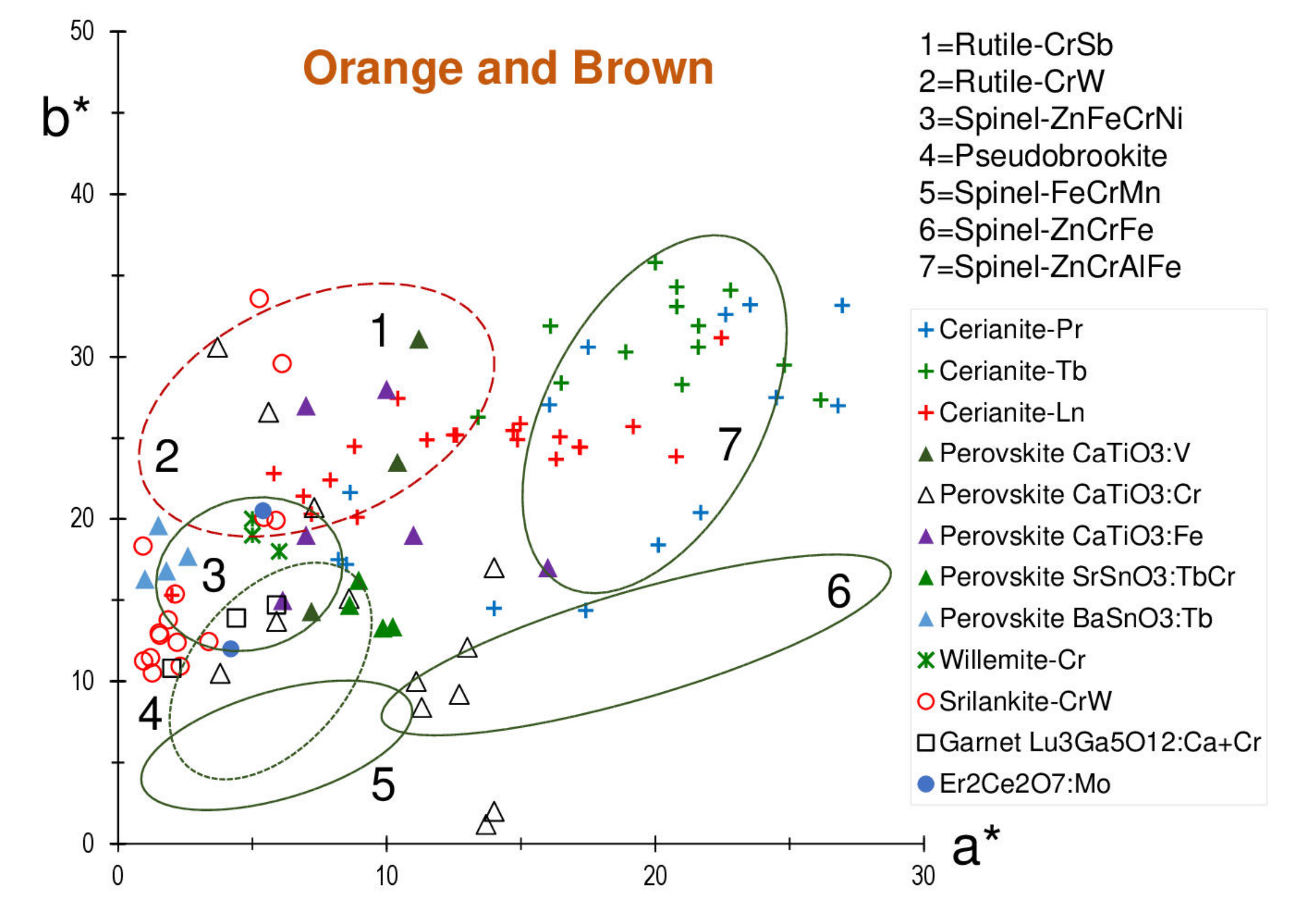
Orange and Brown
b*
a*
0
10
20
30
40
50
1=Rutile-CrSb
2=Rutile-CrW
3=Spinel-ZnFeCrNi
4=Pseudobrookite
5=Spinel-FeCrMn
6=Spinel-ZnCrFe
7=Spinel-ZnCrAlFe
Cerianite-Pr
Cerianite-Tb
Cerianite-Ln
Perovskite CaTiO3:V
Perovskite CaTiO3:Cr
Perovskite CaTiO3:Fe
Perovskite SrSnO3:TbCr
Perovskite BaSnO3:Tb
Willemite-Cr
Srilankite-CrW
Garnet Lu3Ga5O12:Ca+Cr
Er2Ce2O7:Mo

Colorant	Formula	Color	Application – Technology (see Fig. 1)				
			LT	**IT**	**HT-VHT**	**BO**	**DD**
Spinel	$CoCr_2O_4$	blue-green BLUE 36	■	■	■	⊘ 1	■
Eskolaite	$(Cr,Al)_2O_3$	green GREEN 17	◉	□ 1	⊘ 1	■	⊘ 1
Garnet (*Uvarovite*)	$Ca_3Cr_2(SiO_4)_3$	green GREEN 51	◉	□ 1 2	□ 1 2	⊘ 1 2	⊘ 1 2
Co-Ti Spinel	Co_2TiO_4	green GREEN 50	◉	□ 1 3	⊘ 1	⊘ 1	⊘ 1 4
Perovskite	$YCrO_3$	green not filed	⊘ 3	⊘ 1 3	⊘ 1 3	⊘ 3	⊘ 1 4
Olivine (*Liebenbergite*)	Ni_2SiO_4	yellow-green not filed	◉	⊘ 2	⊘ 1 2	⊘ 1 2	⊘ 2 4
Cr soluble salt Cu soluble salt	Cr-organometallic Cu-organometallic	green not filed	⊘ 1 4	⊘ 1 4	⊘ 1 4	■	⊘ 4

Decoration techniques used in ceramic tiles production

INK-JET PRINTING

soluble salts

SILICON ROLLER

flexography

ROTARY SCREEN PRINTING

airbrush – chalcography

FLAT SCREEN PRINTING

decal – pad printing

1960 1970 1980 1990 2000 2010 2020

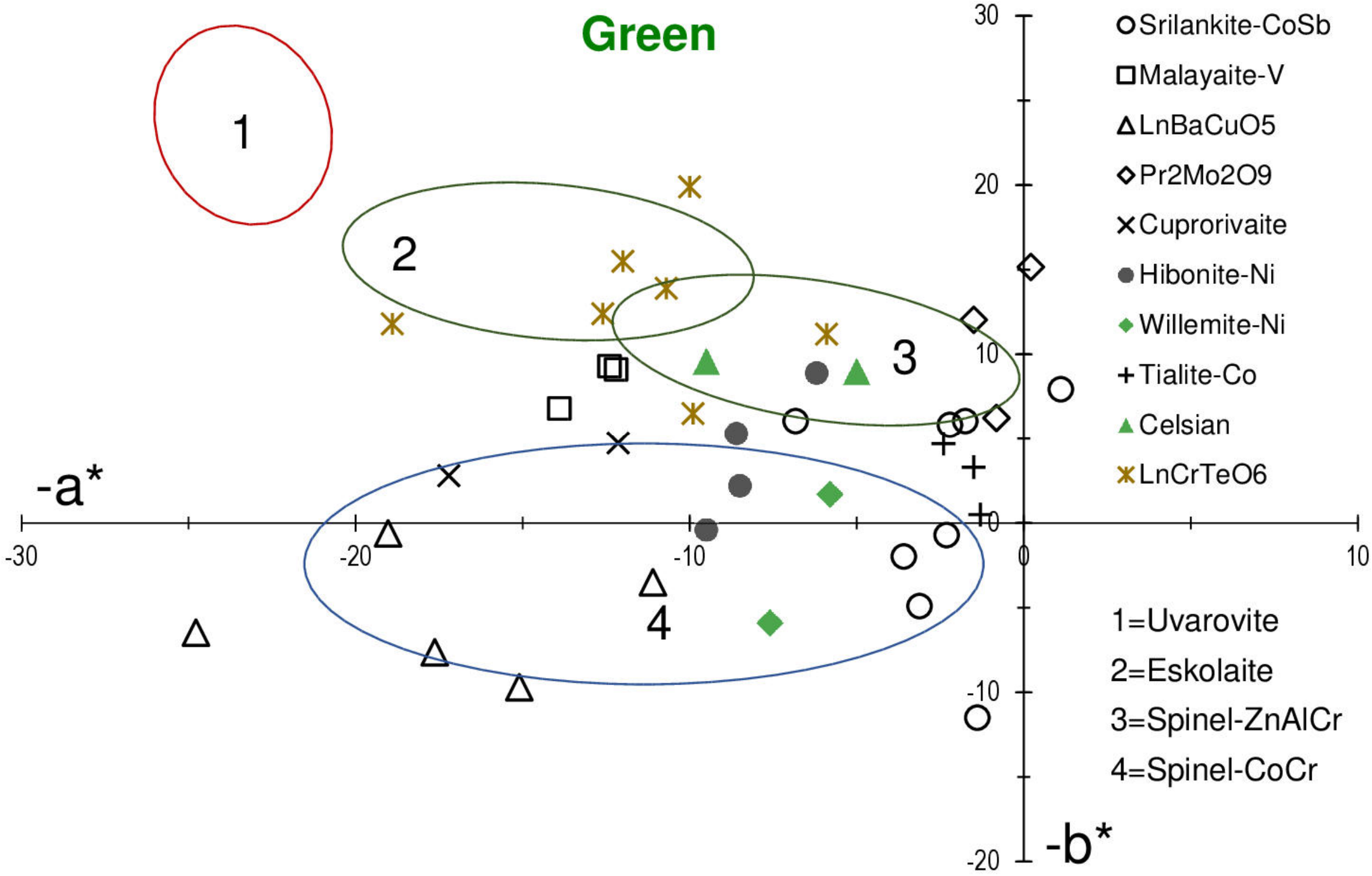
Green
1
2
3
4
-a*
-b*
-30
-20
-10
0
10
30
20
10
0
-10
-20
Srilankite-CoSb
Malayaite-V
LnBaCuO5
Pr2Mo2O9
Cuprorivaite
Hibonite-Ni
Willemite-Ni
Tialite-Co
Celsian
LnCrTeO6
1=Uvarovite
2=Eskolaite
3=Spinel-ZnAlCr
4=Spinel-CoCr

Colorant	Formula	Color	Application – Technology (see Fig. 1)				
			LT	**IT**	**HT-VHT**	**BO**	**DD**
Olivine	Co_2SiO_4	dark blue BLUE 73	■	■	■	◉	■
Sarcopside Lithiophylite	$Co_3(PO_4)_2$ $CoLiPO_4$	dark blue VIOLET 14+47	■	◉	⊘ 1	⊘ 1	⊘ 1
Suanite	$(Mg,Co)B_2O_5$	dark blue VIOLET 48	◉	⊘ 1	⊘ 1	⊘ 1	⊘ 1
Co soluble salt	Co-organometallic	blue not filed	⊘ 1 4	⊘ 1 4	⊘ 1 4	■	◉
Spinel	$CoAl_2O_4$ $(Zn,Co)Al_2O_4$	blue BLUE 28+72	■	■	■	■	■
Willemite	$(Zn,Co)_2SiO_4$	blue BLUE 74	◉	◉	◉	◉	◉
Hardystonite	$Ca_2(Zn,Co)Al_2O_7$	blue not filed	⊘ 3	⊘ 3	⊘ 1	⊘ 1	⊘ 1
Perovskite	$Y(Mn,In)O_3$	blue BLUE 86	⊘ 3	⊘ 3	⊘ 3	⊘ 3	⊘ 1 3
Zircon	$ZrSiO_4$:V	turquoise BLUE 71	■	■	■	■	⊘ 1
Hibonite	$Ca(Al,Ni)_{12}O_{19}$	turquoise not filed	⊘ 3	⊘ 1	⊘ 1	⊘ 1	⊘ 1

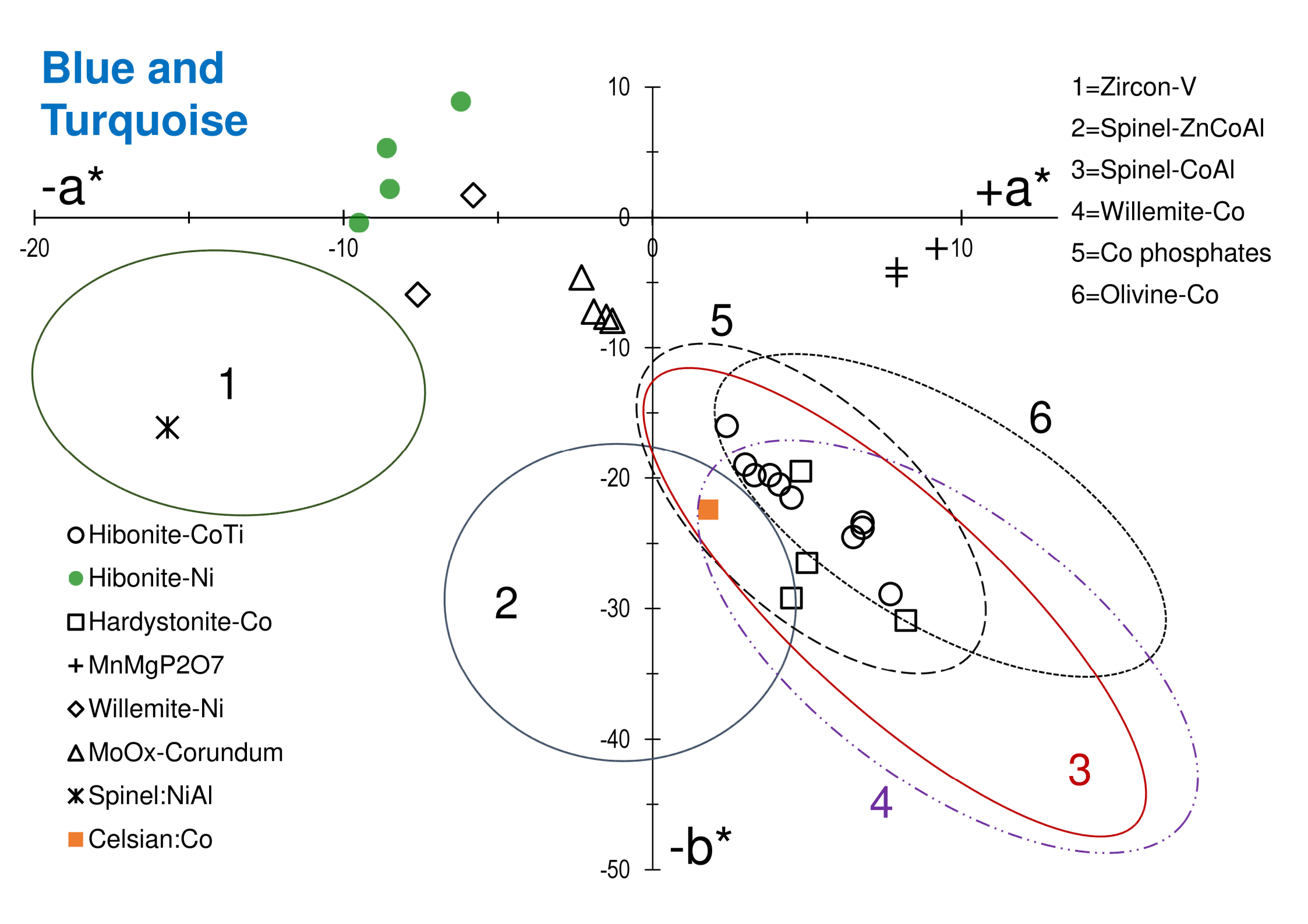
Blue and Turquoise
-a*
+a*
-b*
10
0
-10
-20
-30
-40
-50
-20
-10
0
10
1=Zircon-V
2=Spinel-ZnCoAl
3=Spinel-CoAl
4=Willemite-Co
5=Co phosphates
6=Olivine-Co
1
2
3
4
5
6
Hibonite-CoTi
Hibonite-Ni
Hardystonite-Co
MnMgP2O7
Willemite-Ni
MoOx-Corundum
Spinel:NiAl
Celsian:Co

Colorant	Formula	Color	Application – Technology (see Fig. 1)				
			LT	**IT**	**HT-VHT**	**BO**	**DD**
Spinel (*Nichromite*)	$(Ni,Fe)(Cr,Fe)_2O_4$ $(Ni,Co,Mn)(Cr,Fe)_2O_4$	black BLACK 30	■	■	■	◉	■
Spinel (*Cochromite*)	$(Co,Fe)(Cr,Fe)_2O_4$ $Co(Cr,Fe)_2O_4$	black BLACK 27-29	■	■	■	◉	■
Eskolaite-Hematite	$(Cr,Fe)_2O_3$	black not filed	◉	□ 1	□ 1	■	⊘ 1
Spinel (*Cuprospinel*)	$CuCr_2O_4$	black BLACK 28	◉	⊘ 1	⊘ 1	⊘ 1	⊘ 1
Spinel (*Jacobsite*)	$(Mn,Fe)(Mn,Fe)_2O_4$	black BLACK 26	◉	◉	⊘ 1	◉	⊘ 1 4
Perovskite	$LaCoO_3$	black not filed	⊘ 1	⊘ 1	⊘ 1	⊘ 1	⊘ 1
Ru soluble salt	Ru-organometallic	black not filed	⊘ 1 4	⊘ 1 4	⊘ 1 4	■	◉
Cassiterite	$(Sn,Sb)O_2$	gray BLACK 23	■	■	■	⊘ 1 3	⊘ 4
Co-Sn Spinel	Co_2SnO_4	gray BLUE 81	■	◉	◉	⊘ 3	⊘ 4
Bunsenite	(Ni,Co)O	gray BLACK 25	◉	◉	◉	⊘ 2	⊘ 2 4
Rutile	$(Ti,V,Sb)O_2$	gray BLACK 24	■	□ 1	⊘ 1	⊘ 1	⊘ 1
Corundum	$Al_2O_3[MoO_x]$	gray not filed	⊘ 3	⊘ 1	⊘ 1	⊘ 3	⊘ 4
Pd soluble salt	Pd-organometallic	gray not filed	⊘ 1 4	⊘ 1 4	⊘ 1 4	◉	⊘ 1 4

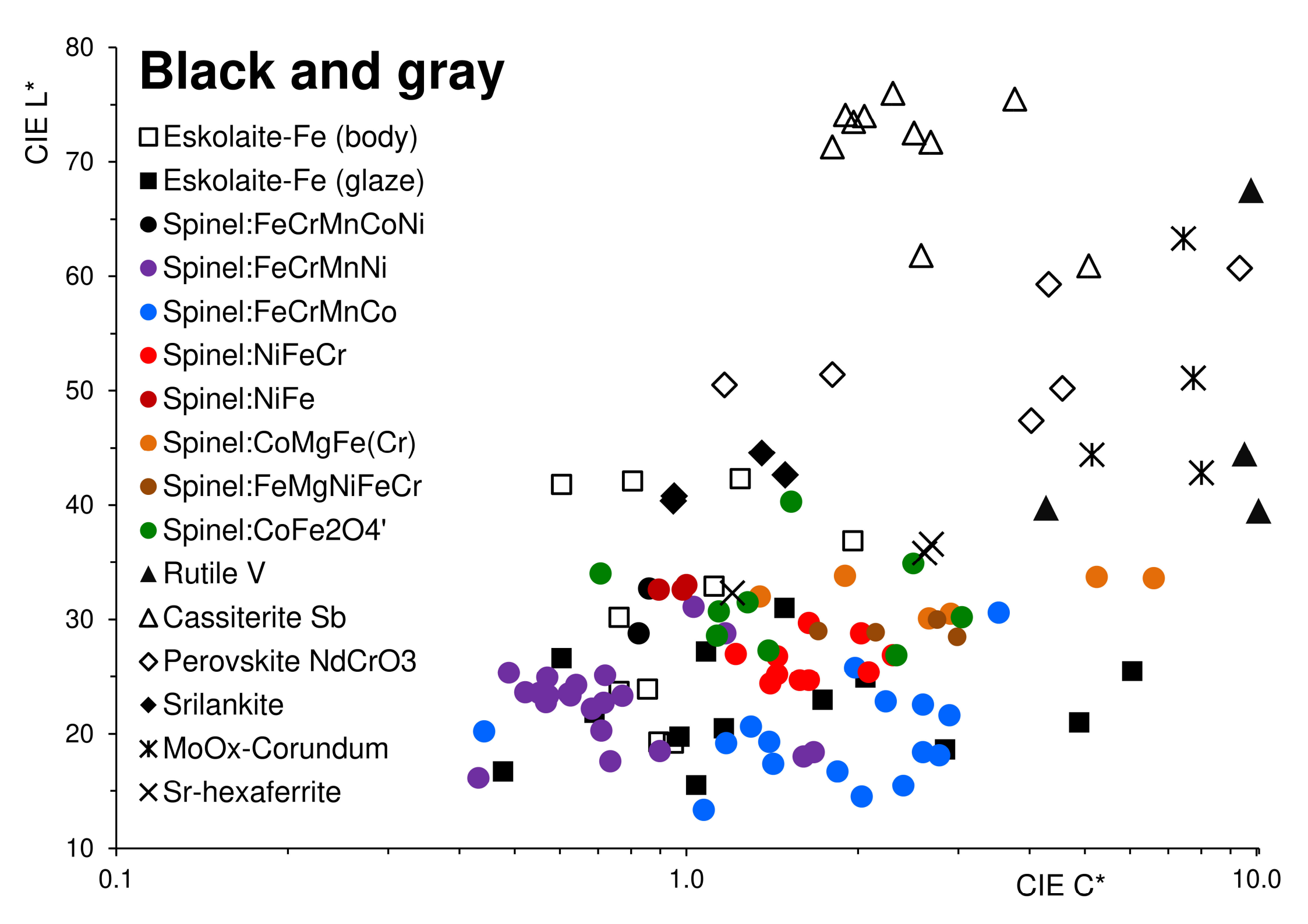
Black and gray
Eskolaite-Fe (body)
Eskolaite-Fe (glaze)
Spinel:FeCrMnCoNi
Spinel:FeCrMnNi
Spinel:FeCrMnCo
Spinel:NiFeCr
Spinel:NiFe
Spinel:CoMgFe(Cr)
Spinel:FeMgNiFeCr
Spinel:CoFe2O4'
Rutile V
Cassiterite Sb
Perovskite NdCrO3
Srilankite
MoOx-Corundum
Sr-hexaferrite
CIE L*
80
70
60
50
40
30
20
10
0.1
1.0
10.0
CIE C*

Pigment, Dye, Effect	Formula	Color	Application – Technology (see Fig. 1)				
			LT	**IT**	**HT-VHT**	**BO**	**DD**
Zircon	$ZrSiO_4$	white not filed	◉	■	■	■	■
Cassiterite	SnO_2	white WHITE 15	■	□ 3	▨ 3	▨ 3	▨ 3
Corundum	Al_2O_3	white,effect not filed	▨ 4	◉	◉	◉	◉
Baddeleyite	ZrO_2	white,effect WHITE 12	◉	◉	◉	▨ 1	▨ 1
Zr soluble salt	Zr-organometallic	white,effect not filed	▨ 1 4	▨ 1 4	▨ 1 4	◉	◉
Rutile	TiO_2	white WHITE 6	◉	▨ 1	▨ 1	□ 3	▨ 1
Spinel	$MgAl_2O_4$	white not filed	▨ 4	▨ 4	▨ 4	▨ 3	▨ 4
Cerianite	CeO_2	effect(white) not filed	◉	◉	■	▨ 3	◉
Fe phosphates	$Fe_2Fe(P_2O_7)_2$ $NaFe_3(PO_4)_3$	metallic luster	■	■	□ 1	▨ 1	▨ 1
Scheelite	$CaWO_4$	metallic luster	■	■	◉	▨ 1	▨ 1
Hematite	Fe_2O_3	aventurine	◉	■	■	▨ 1	▨ 1
Shcherbinaite	V_2O_5	sink effect	■	■	■	▨ 1	■
Clinobisvanite	$BiVO_4$	sink effect YELLOW 184	■	■	■	▨ 1	■
Mica (*coated by metal oxide*)	$KAl_3Si_3O_4(OH)_2$ @TiO_2 or Fe_2O_3	pearlescent luster	■	▨ 1	▨ 1	◉	▨ 1
Titania slag	Ti-rich slag	speckle effect	◉	▨ 1	▨ 1	◉	▨ 1 4

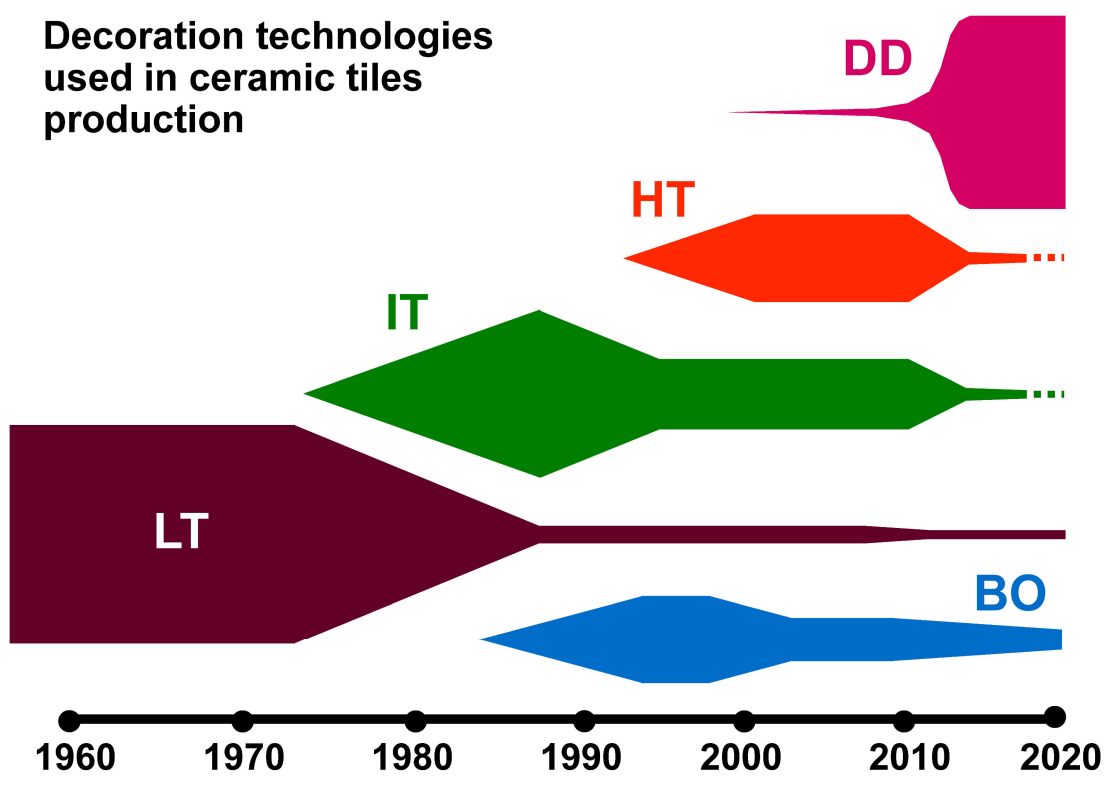
Decoration technologies used in ceramic tiles production
DD
HT
IT
LT
BO
1960
1970
1980
1990
2000
2010
2020

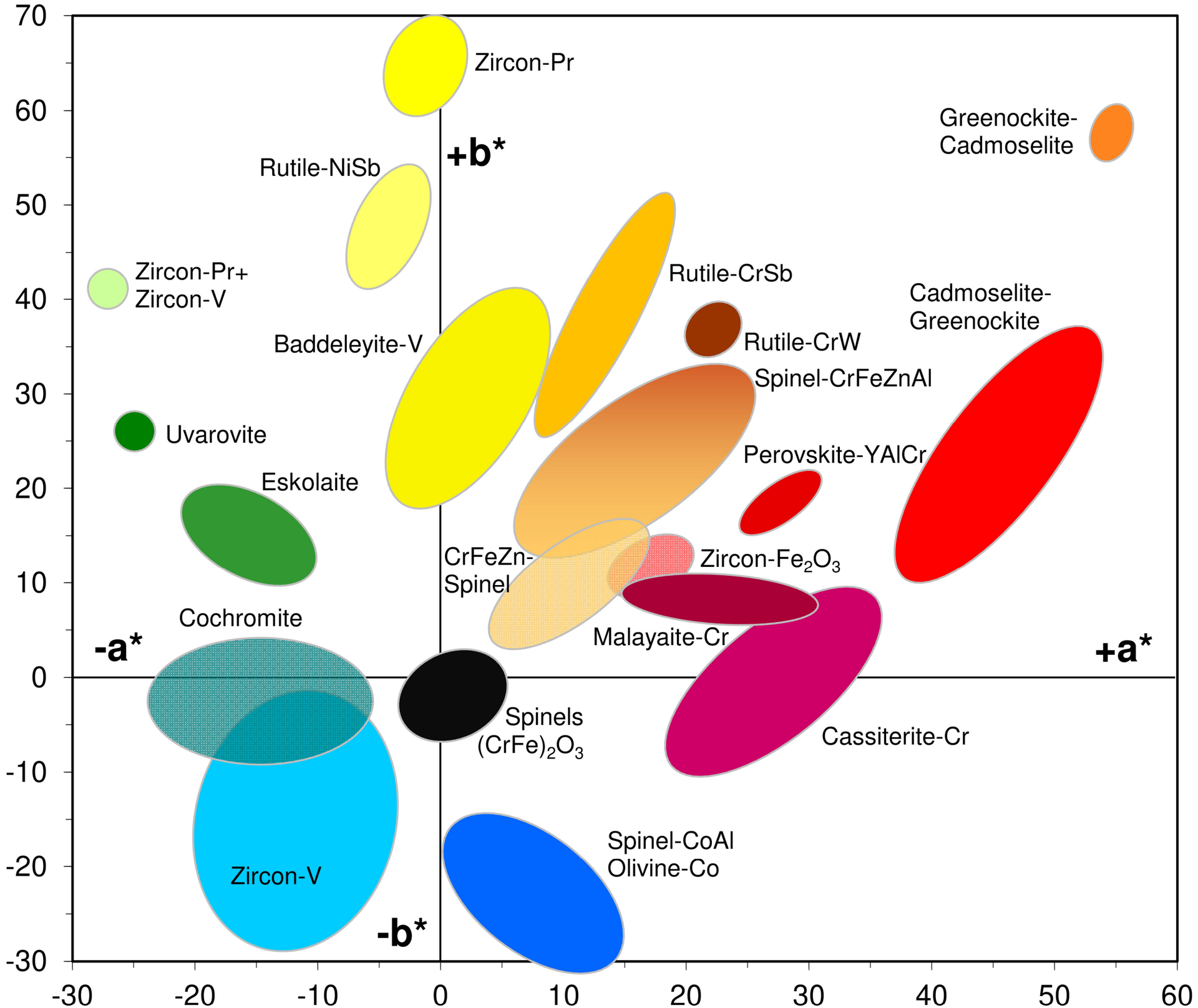
Zircon-Pr
+b*
Rutile-NiSb
Greenockite-
Cadmoselite
Zircon-Pr+
Zircon-V
Rutile-CrSb
Cadmoselite-
Greenockite
Baddeleyite-V
Rutile-CrW
Spinel-CrFeZnAl
Uvarovite
Perovskite-YAlCr
Eskolaite
CrFeZn-
Spinel
Zircon-Fe2O3
Cochromite
Malayaite-Cr
-a*
+a*
Spinels
(CrFe)2O3
Cassiterite-Cr
Zircon-V
Spinel-CoAl
Olivine-Co
-b*
70
60
50
40
30
20
10
0
-10
-20
-30
-30
-20
-10
0
10
20
30
40
50
60

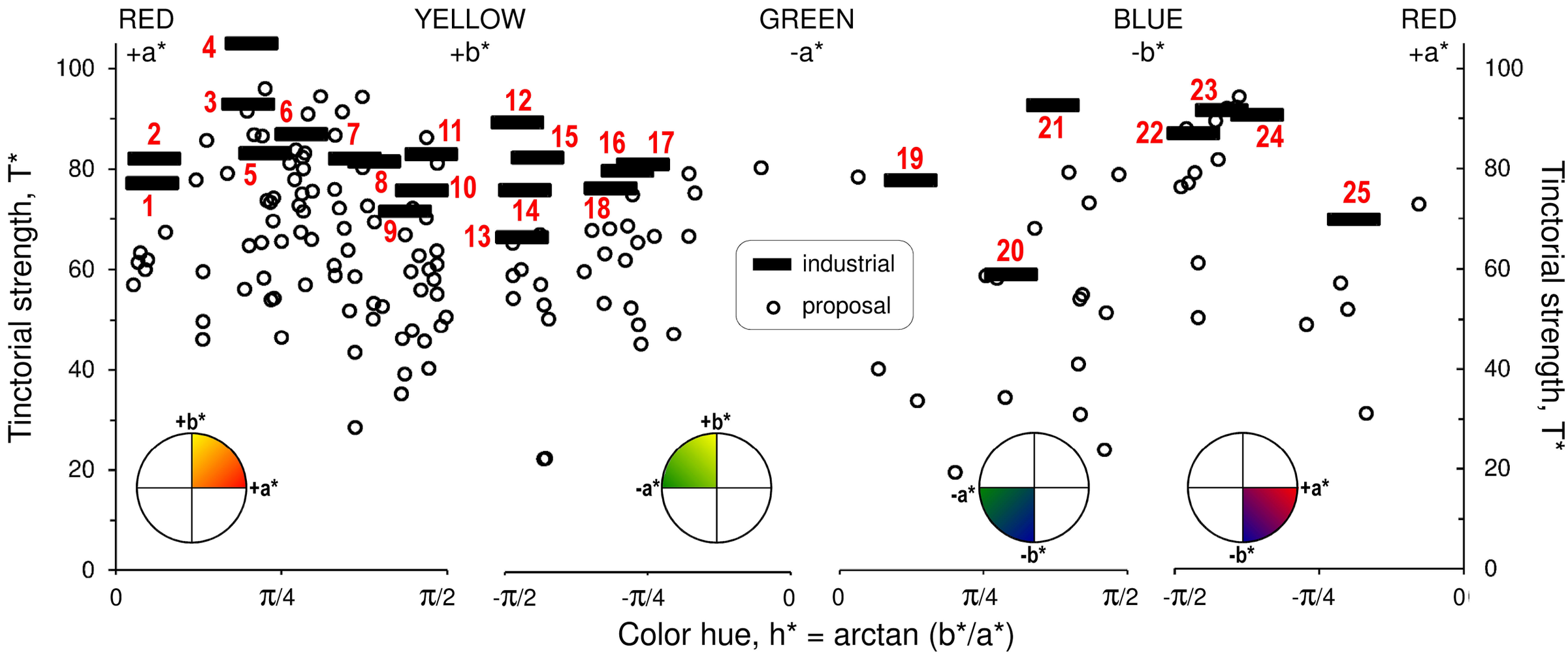

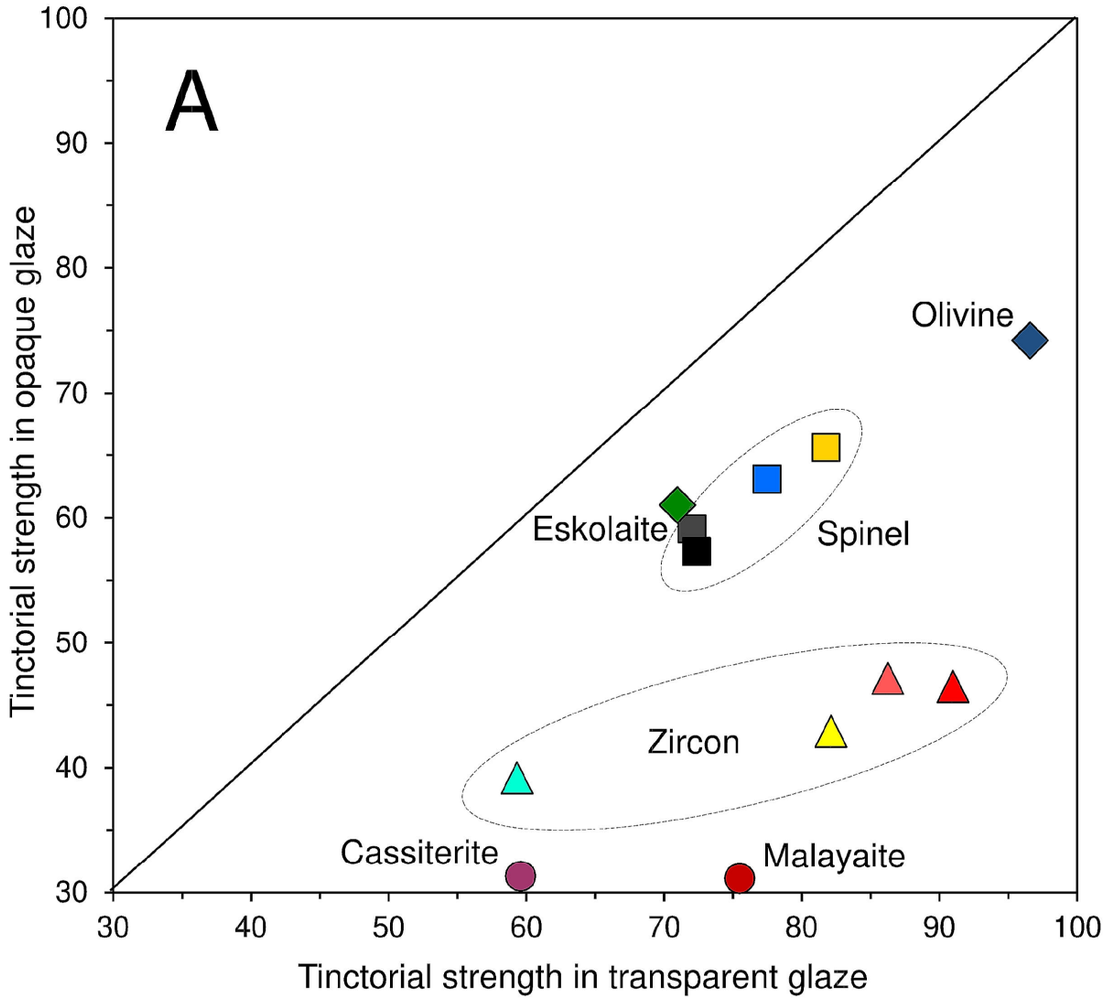

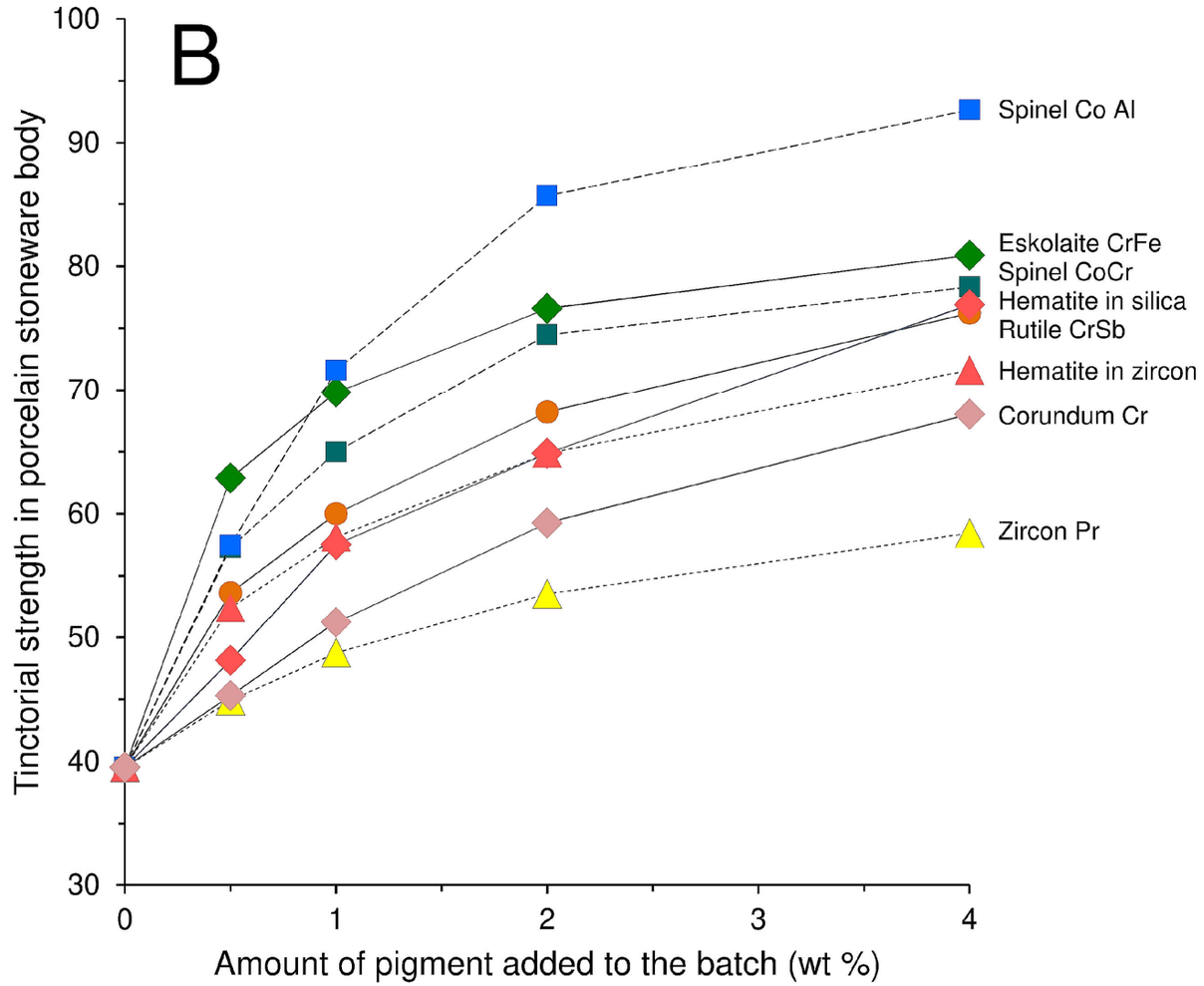

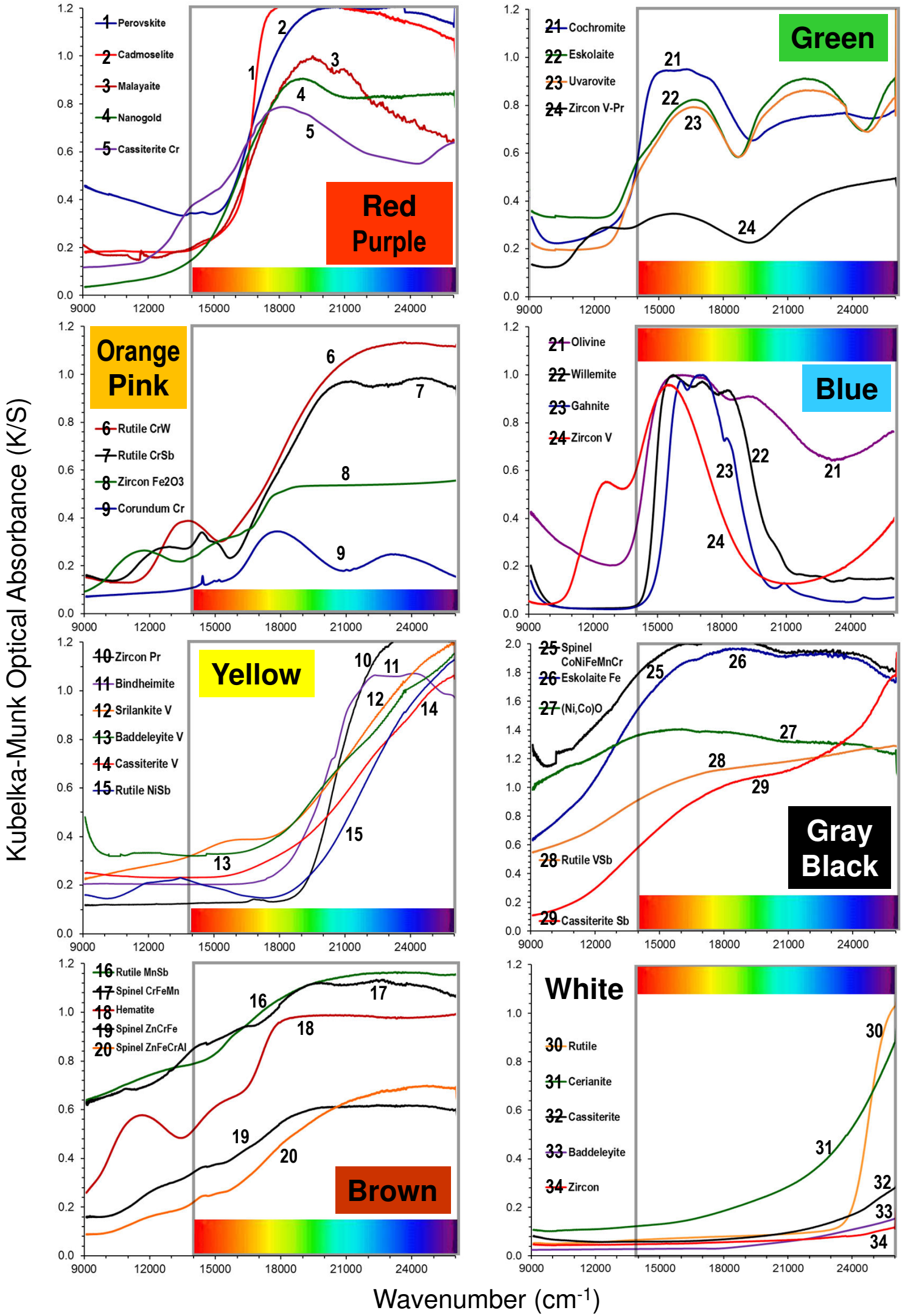
Kubelka-Munk Optical Absorbance (K/S)
Wavenumber (cm-1)
1 Perovskite
2 Cadmoselite
3 Malayaite
4 Nanogold
5 Cassiterite Cr
Red Purple
21 Cochromite
22 Eskolaite
23 Uvarovite
24 Zircon V-Pr
Green
Orange Pink
6 Rutile CrW
7 Rutile CrSb
8 Zircon Fe2O3
9 Corundum Cr
21 Olivine
22 Willemite
23 Gahnite
24 Zircon V
Blue
10 Zircon Pr
11 Bindheimite
12 Srilankite V
13 Baddeleyite V
14 Cassiterite V
15 Rutile NiSb
Yellow
25 Spinel CoNiFeMnCr
26 Eskolaite Fe
27 (Ni,Co)O
28 Rutile VSb
29 Cassiterite Sb
Gray Black
16 Rutile MnSb
17 Spinel CrFeMn
18 Hematite
19 Spinel ZnCrFe
20 Spinel ZnFeCrAl
Brown
30 Rutile
31 Cerianite
32 Cassiterite
33 Baddeleyite
34 Zircon
White

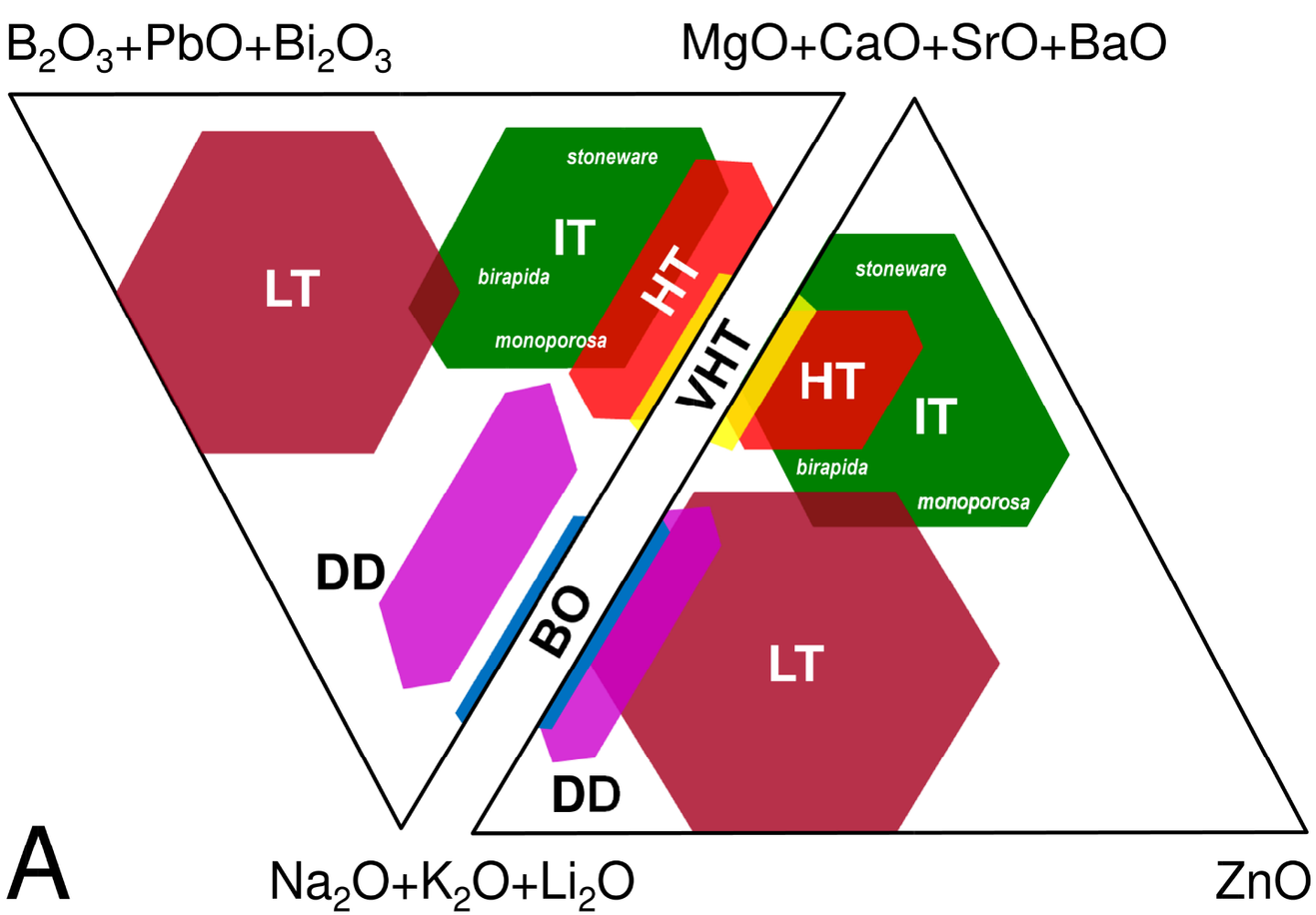
B_2O_3+PbO+Bi_2O_3
MgO+CaO+SrO+BaO
stoneware
IT
birapida
monoporosa
LT
HT
VHT
stoneware
HT
IT
birapida
monoporosa
DD
BO
LT
DD
A
Na_2O+K_2O+Li_2O
ZnO

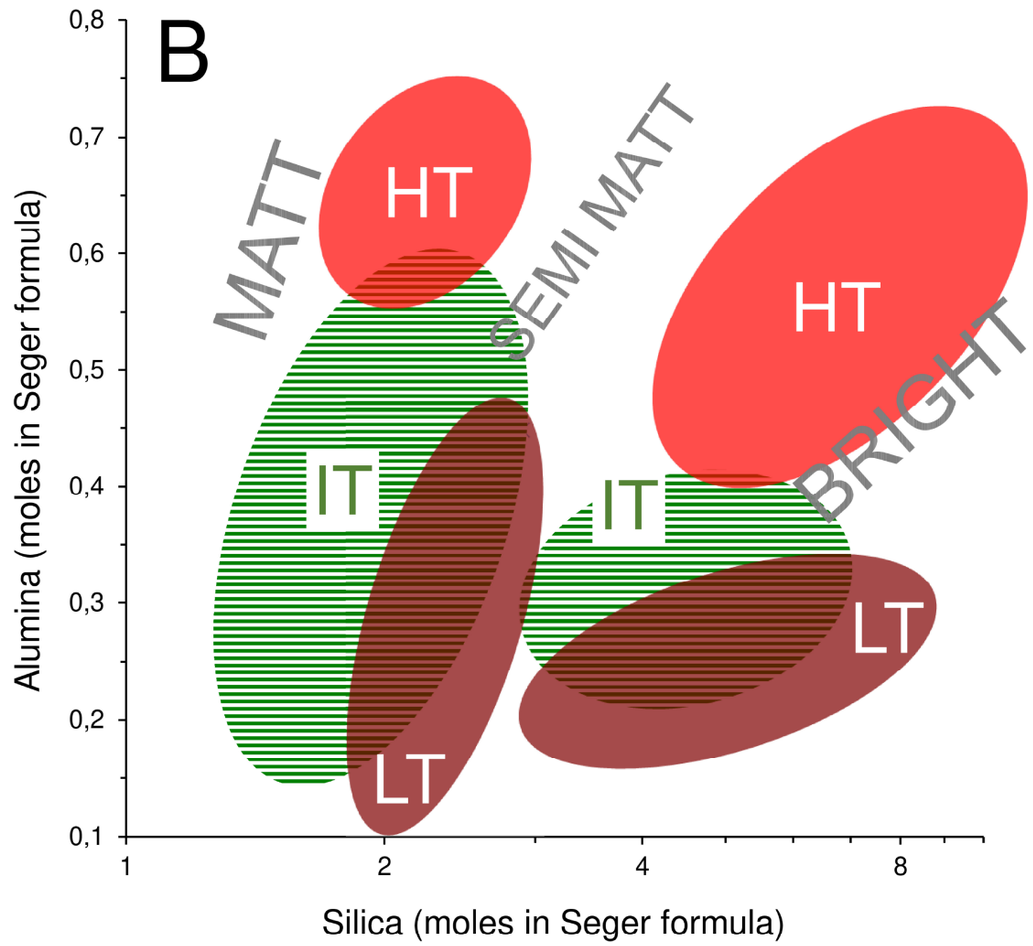
B
MATT
HT
SEMI MATT
HT
BRIGHT
IT
IT
LT
LT
Alumina (moles in Seger formula)
0,8
0,7
0,6
0,5
0,4
0,3
0,2
0,1
1
2
4
8
Silica (moles in Seger formula)

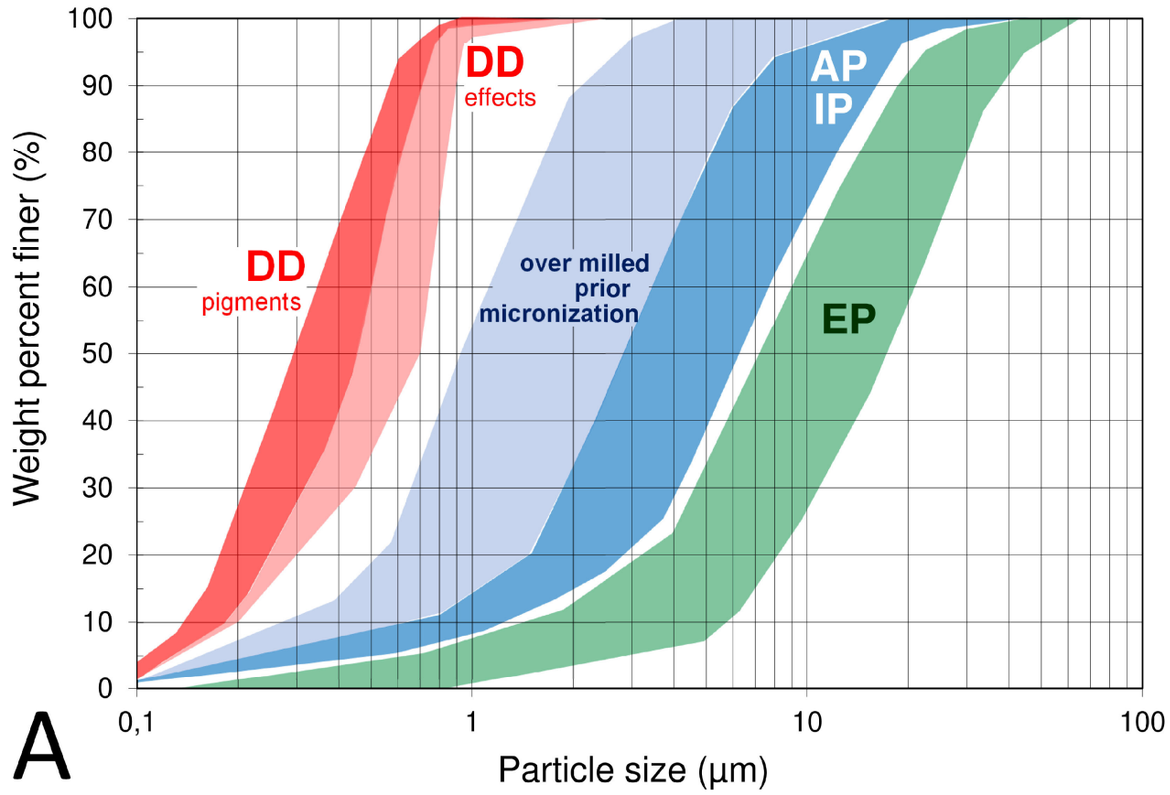
100
90
80
70
60
50
40
30
20
10
0
Weight percent finer (%)
DD
effects
DD
pigments
over milled
prior
micronization
AP
IP
EP
0,1
1
10
100
Particle size (µm)
A

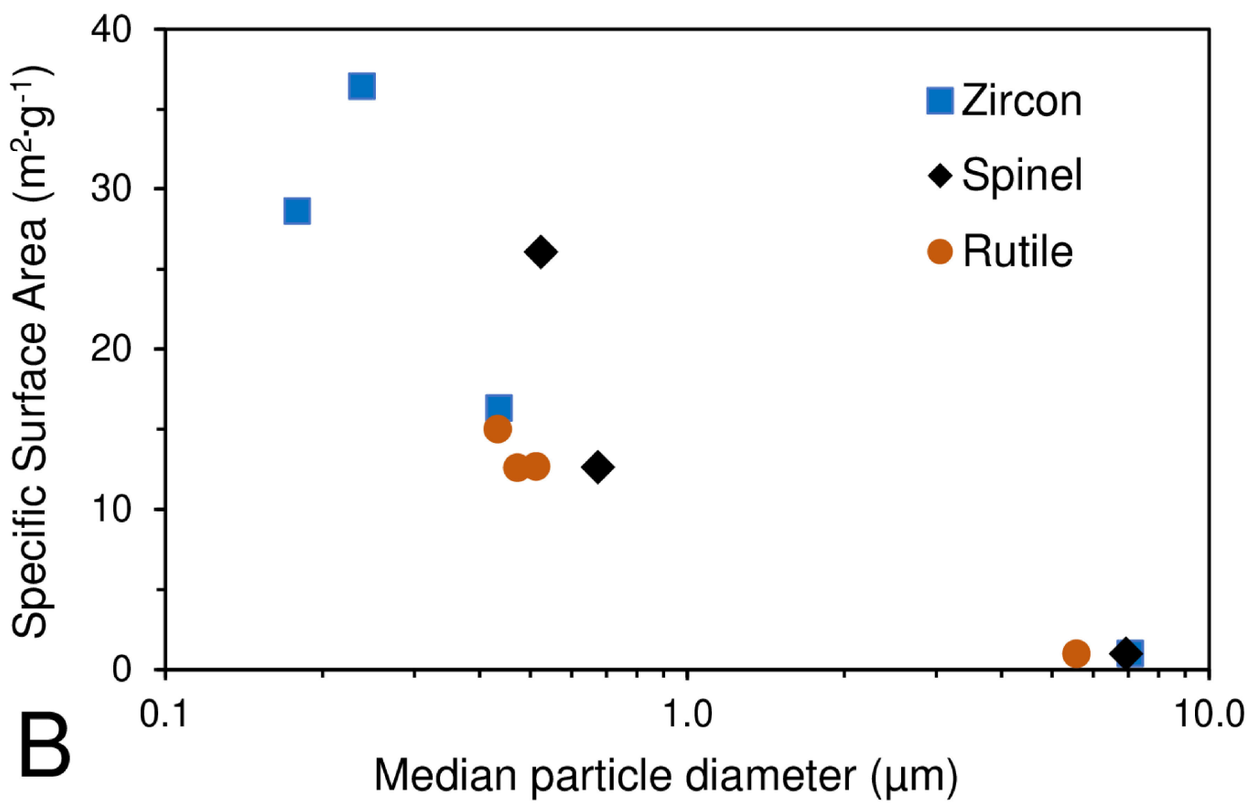
40
30
20
10
0
Specific Surface Area (m²·g⁻¹)
Zircon
Spinel
Rutile
0.1
1.0
10.0
Median particle diameter (µm)
B

Ceramic Pigments and Dyes beyond the Inkjet Revolution: from Technological Requirements to Constraints in Colorant Design

Molinari C.[1,*], Conte S.[1,*], Zanelli C.[1], Ardit M.[2], Cruciani G.[2], Dondi M.[1,§]

[1] CNR-ISTEC, Institute of Science and Technology for Ceramics, Via Granarolo 64, 48018 Faenza, Italy
[2] Physics and Earth Sciences Department, University of Ferrara, Via Saragat 1, 44122 Ferrara, Italy

Abstract

The advent of digital decoration has changed the technological requirements of colorants and the way they are applied onto ceramic substrates. This technological revolution has introduced additional steps in colorant production (ink micronization) and new constraints in application (ink-jet printing) that cannot be reproduced in a standard ceramic laboratory, so stretching the distance between academic and industrial research. The goal of this work is to provide an up-to-date picture of ceramic pigments, dyes and effects, with emphasis on their behavior in the current decoration technologies, which are shortly reviewed. Technological performance expected for ceramic colorants and new requirements imposed by digital decoration are discussed in detail. An extensive overview of both industrially used and candidate pigments, dyes and effects is focused on the suitability to different ceramic applications and firing conditions. Finally, lines of future research are outlined and commented.

Key-words: ceramics, colorant, dye, effect, glaze, pigment.

INDEX

1. Introduction

Coloration of ceramic materials implies the use of technologies that are different from many other applications, mainly because of the high temperature treatment that imposes specific requirements to colorants. This peculiarity makes it advisable to reappraise the conventional definitions and classification of *colorants* (hereafter used as a comprehensive term for pigments and dyes) in order to explain the terminology commonly utilized in the ceramic industry (Table 1).

The industry of ceramic colorants is apparently a mature sector: almost all pigments, currently on the market, entered in use since the 19th century to 1960 [1,2]. Ceramic pigments and dyes are utilized to bestow color on wall and floor tiles, tableware, sanitaryware, art wares, roof tiles, and enamels (for metallic wares). However, the quantity of colorants globally used in ceramic tile production is much larger (and it grew faster in the last decades) than in all the other sectors and at present represents over 80% of the global demand for ceramic pigments and dyes. For this reason, trends in colorant manufacturing have been essentially driven by the ceramic tile industry.

The strong technological innovation in tile-making that occurred in the 1980s (introduction of fast single firing) and the 1990s (development of porcelain stoneware) had limited effects on the range of pigments and dyes actually used in the industrial practice.

* Both authors equally contributed to the study.
§ Corresponding author.

Table 1. Definition of pigment, dye, and effect for ceramic applications and various types currently used by the industry.

Colorant	Definition in the ceramic sector	
Pigment	Pigments are colored, black or white particulate inorganic solids which are largely insoluble in, and essentially physically and chemically unaffected by, the matrix in which they are incorporated (including the melt present in bodies and glazes during firing). They alter appearance by selective absorption and/or by scattering of light. Pigments are usually dispersed in vehicles for application, as for instance in the manufacture of colored powder agglomerates or ceramic inks to decorate glazes and bodies. Pigments retain their crystal structure throughout the ceramic process. Modified after the CPMA[1] definition.	
IP	Idiochromatic	or "self-colored" pigments, where the chromophore is a major ingredient of the crystal structure, *e.g.* chromite spinel, $FeCr_2O_4$, or uvarovite garnet, $Ca_3Cr_2Si_3O_{12}$.
AP	Allochromatic	or "other colored" pigments, where the chromophore is present as dopant of the host crystal structure, *e.g.* praseodymium in zircon, $(Zr,Pr)SiO_4$, or chromium in malayaite, $Ca(Sn,Cr)(Si,Cr)O_5$.
MP	Mordant	pigments, where chromophore occurs as tiny inclusions in the host crystal structure, *e.g.* vanadium pentoxide into baddeleyite, $ZrO_2[V_2O_5]$. The size of inclusions is smaller than the domain of coherent diffraction, thus the chromophore cannot be detected by X-ray diffraction.
EP	Encapsulated	pigments, where the chromophore agent is coated by a protective layer because heat-liable or chemically attacked by the melt present in glazes and bodies, *e.g.* cadmium sulfide in zircon, $ZrSiO_4[CdS]$. They are sometimes called "occlusion" or "inclusion" pigments. The size of inclusions is larger than the domain of coherent diffraction, thus the pigment may be detected by X-ray diffraction.
Dye	Dyes are colored, black or white organometallic complexes or inorganic substances that are destroyed during firing, thus dissolved into glazes and glasses and the melt present in ceramic bodies. They impart color to a substrate by selective absorption of light. They are soluble complexes or particulates dispersed in vehicles for application, as for instance in the manufacture of soluble salts and ceramic inks to decorate glazes and bodies. Dyes do not retain their crystal structure but may promote crystallization/precipitation of other crystalline substances that occur at the end of the ceramic process. Modified after the ETAD[2] definition.	
SD	Soluble salts	are dyes consisting of organometallic complexes in aqueous solutions or solvents, which are decomposed during firing, *e.g.* Co^{2+}-carboxylate complex. Transition metal ions impart color to the ceramic matrix in which are incorporated.
RD	Reactive dyes	are soluble salts that, reacting during firing with the ceramic matrix, induce the crystallization of colored crystalline phases. Reaction products usually incorporate the transition metal ions provided by the dye, *e.g.* Ti-Cr-Sb organometallic complexes that lead to the formation of rutile, $(Ti,Cr,Sb)O_2$.
PD	Crystalline particulates	are inorganic solids, which are dissolved during firing and incorporated into the ceramic matrix. Color is bestowed by transition metal ions migrated in the vitreous phase of bodies and glazes, *e.g.* Co^{2+} of $LiCoPO_4$.
Effect	Effects are particulate inorganic solids that confer peculiar optical and textural features to ceramic surfaces. They typically react during firing with the matrix in which are incorporated, generally ceramic glazes and glasses. They alter appearance by scattering of light and/or by modifying gloss, iridescence or texture of surfaces. Effects are usually dispersed in vehicles for application, as for instance in the manufacture of ceramic inks to decorate glazes. Effects do not retain their crystal structure but may promote the formation of other crystalline and amorphous phases.	
SE	Sink	inducing a bas-relief texture, consisting of slightly depressed zones developed during firing by enhanced fusibility.
BE	Gloss/Matt	turning the surface either shiny (gloss) or opaque (matt) by changing refractive index or precipitating crystals, respectively.
GE	Glitter	sparkling effect, simulating the aventurine glass, achieved by precipitation of properly oriented crystals.
LE	Luster	simulating the brilliance and iridescence of metallic surfaces (steel and precious metals).

[1]CPMA: Color Pigments Manufacturers Association. [2]ETAD: Ecological and Toxicological Association of Dyes and organic pigments manufacturers.

This occurred despite the complete change in chemical composition of bodies, frits and glazes [3-5] which now need much higher firing temperatures (from ~900-1000°C of traditional fire to 1100-1160°C for porous tiles and 1180-1240°C for vitrified tiles). Also, the way by which pigments and dyes are applied on ceramic tiles has evolved over time [4-6].

Such a steady picture was revolutionized by the advent of digital decoration of ceramic tiles that took place on a large scale since 2009 [7-9]. The introduction of inkjet printing (IJP) has completely changed both the way colorants are applied onto the ceramic tiles and the technological requirements for pigments and dyes [9-11]. By this way, pigment manufacturers had to face a paradigm shift: the finished product is no longer a powdered colorant (to be admixed with vehicles in the customer's factory) but turned into an ink (encompassing colorant, carrier and additives) with a proper technological behavior certified for each type of inkjet print head and printer. Nowadays, digital decoration is spreading through other ceramic sectors (tableware, decals, etc) and allied industries (glass, artificial stone).

This new situation has important repercussions on the R&D of ceramic colorants. As a matter of fact, the requirements that pigment must fulfil have changed in the last decade: old issues have been readdressed (*e.g.*, reaction kinetics during firing) and new targets appeared (*e.g.*, behavior during micronization). The goal of the present overview is to provide an up-to-date picture of ceramic pigments, dyes and effects, with special attention to technological requirements and suitability of different colorants for the current decoration technologies, in order to shorten the distance between academic research and industry needs.

The paper is structured as follows: technologies used in ceramic decoration are briefly described (section 2) to introduce the technological performance required to ceramic colorants (section 3) with emphasis on the new requirements of digital decoration (section 4). The suitability of both industrially used and candidate pigments and dyes to different ceramic applications is discussed in detail (section 5). Finally, open questions and lines of future research are addressed in section 6.

<table>
<tr><th>Technology</th><th>Ceramic product</th><th>Decoration techniques</th><th>Colorant applied as</th><th>Firing</th><th>Firing reactions with</th><th>Pigment size distribution</th></tr>
<tr><td>LT
Low Temperature</td><td>third-fire applications classic slow double-fired products</td><td rowspan="4">rotogravure (silicon roller)
screen printing (rotary or flat)
flexography
airless spraying
(see Figure 2)</td><td rowspan="2">powder dispersed in paste or glaze</td><td>slow double third fire 700-950°C</td><td>low temperature glaze</td><td rowspan="5">micrometric pigments
d_{50}=3-7 µm
d_{90}=7-15 µm
encapsulated pigments
d_{50}=10-20 µm
d_{90}=15-30 µm</td></tr>
<tr><td>IT
Intermediate Temperature</td><td>porous (monoporosa, birapida) and semi-vitrified tiles (stoneware)</td><td>fast single (double) 1080-1160°C 30-50 min</td><td>intermediate temperature glaze</td></tr>
<tr><td>HT
High Temperature</td><td>highly vitrified tiles (glazed porcelain stoneware)</td><td rowspan="2">powder in slip or stuck on granules
soluble salt</td><td>fast single 1180-1220°C 50-90 min</td><td>high temperature glaze</td></tr>
<tr><td>BO
Body (unglazed)</td><td>highly vitrified tiles (unglazed porcelain stoneware)</td><td>fast single 1190-1230°C 60-90 min</td><td>porcelain stoneware body</td></tr>
<tr><td>VHT
Very High Temperature</td><td>highly vitrified products (vitreous china, porcelain)</td><td>decal
screen printing
painting</td><td>powder dispersed in paste or stuck on decal</td><td>slow single or double 1250-1400°C</td><td>very high temperature glaze</td></tr>
<tr><td>DD
Digital Decoration</td><td>all tile types: stoneware, porcelain stoneware, third-fire, birapida, monoporosa</td><td>DOD inkjet printing</td><td>ink</td><td>fast single 700-1240°C 30-90 min</td><td>all glazes and bodies</td><td>micronized pigments
d_{50}=0.3-0.7 µm
d_{90}=0.6-1.0 µm</td></tr>
</table>

Figure 1. Technologies used in ceramic tiles manufacturing and related decoration techniques.

2. Technological evolution in the ceramic tile industry

A continuous technological upgrading occurred in ceramic tile manufacturing and deeply influenced the way colorants are applied by different decoration techniques and the conditions they undergo during firing [3,5,6]. Basically, five technologies have been utilized to decorate ceramic tiles of different kinds: they are distinguished by application techniques, firing schedules, ceramic matrices, and pigment features, particularly particle size (Fig. 1).

In this framework, the decoration department underwent an evolution over the last decades regarding the application techniques (Fig. 2). In particular, the digital decoration caused two disruptive innovations [9-10]:

i) IJP replaced almost totally the preceding means of decoration, as only the technological solutions for unglazed bodies survived (at variance of previous advancements that always saw the coexistence for long time of various techniques).

ii) IJP requires a further step of micronization to get particle size in the submicronic range, while the other techniques make use of standard ceramic pigments, that have the particle size in the micrometer range (Fig. 1). This implies a considerable change in specific surface area of colorants, which in turn affects the color saturation and reaction kinetics during firing.

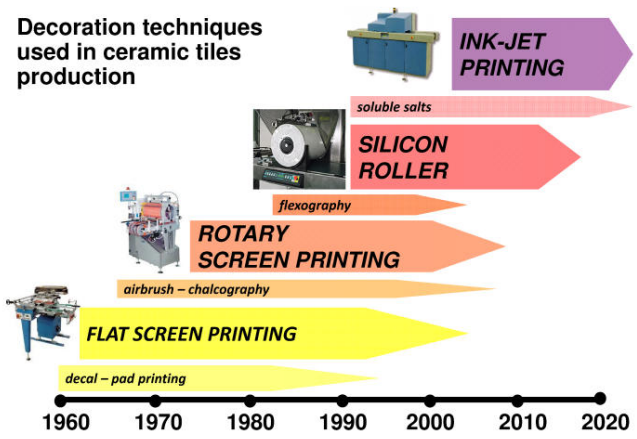

Fig. 2. Decoration techniques utilized in ceramic tile manufacturing since 1960.

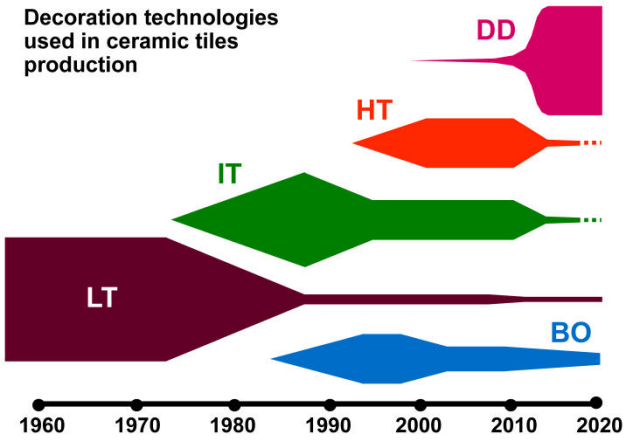

Fig. 3. Evolution of ceramic tile decoration technologies: symbols refer to Figure 1.

Figure 3 illustrates how ceramic technologies evolved along the last sixty years, starting from low temperature treatments: slow double-firing, now disappeared, and present day third fire applications (LT). Next step was the fast single-firing at intermediate temperature to produce porous and semi-vitrified tiles (IT). The follow-up was at high temperature for unglazed porcelain stoneware (BO) and then glazed porcelain stoneware (HT). Both the IT and HT decoration technologies are going to be completely replaced by the novel solutions developed to implement IJP and further digital techniques on ceramic tiles (DD).

Further factors have been playing a crucial role, beyond the technological aspects, in the design of ceramic colorants. They are connected with the growing concern on health and safety issues all along the colorant value chain, entailing effluents, gaseous emissions, hazardous substances and, in general, the reduction of chemical risk. Current regulations – like REACH in the EU [12] or TSCA in the USA [13] – may determine the fate or a given colorant. For instance, the occurrence of a carcinogenic ingredient among precursors may turn the manufacture too costly, because of all the preventive measures and controls imposed to the pigment industry [14,15].

3. Technological requirements for ceramic colorants

Pigments and dyes must fulfil a set of technical requirements to be applied in ceramic manufacturing [2,16]. These specifications concerned – in the pre-IJP technologies – essentially refractoriness, color saturation, optical properties, resistance to chemical attack, and particle size distribution. Such requirements will be henceforward discussed in some detail for industrial pigments, which basic crystallographic and physical features are summarized in Table 2, and for industrial dyes and effects as well, which general features are described in Table 3.

Table 2. Crystallographic and physical characteristics of the main substances used as ceramic pigments.

Crystal structure	Formula	Symmetry	Space Group	Density ($Mg \cdot m^{-3}$)	Melting point (°C)	Refractive indices (adim.)			
Baddeleyite	ZrO_2	monoclinic	$P2_1/c$	5.75	2710	B	2.13	2.19	2.20
Bunsenite	NiO	cubic	$Fm3m$	7.45	1955	I	1.74		
Cassiterite	SnO_2	tetragonal	$P4_2/mnm$	6.95	1630	U	1.97	2.02	
Cerianite	CeO_2	cubic	$Fm3m$	7.22	2400	I	2.13		
Corundum	Al_2O_3	trigonal	$R–3c$	4.05	2050	U	1.76	1.77	
Garnet	$Ca_3Cr_2Si_3O_{12}$	cubic	$Ia3d$	3.59	1370	I	1.86		
Hematite	Fe_2O_3	trigonal	$R–3c$	5.30	1540	U	2.91	3.19	
Hibonite	$CaAl_{12}O_{19}$	hexagonal	$P6_3/mmc$	3.84	1910	U	1.79	1.81	
Malayaite	$CaSnSiO_5$	monoclinic	$A2/a$	4.42	1330	B	1.77	1.78	1.80
Perovskite	$YAlO_3$	orthorhombic	$Pbnm$	4.56	1870	B	1.92	1.94	1.95
Priderite	$BaNiTi_7O_{16}$	tetragonal	$I4/m$	3.86	1400	U	2.35	2.37	
Pseudobrookite	Fe_2TiO_5	orthorhombic	$Bbmm$	4.40	1550	B	2.37	2.38	2.40
Pyrochlore	$Pb_2Sb_2O_7$	cubic	$Fd3m$	5.94	1310	I	1.86		
Rutile	TiO_2	tetragonal	$P4_2/mnm$	4.25	1850	U	2.87	2.58	
Spinel	$MgAl_2O_4$	cubic	$Fd3m$	3.64	2140	I	1.76		
Srilankite	$ZrTiO_4$	orthorhombic	$Pbcn$	4.77	1840	B	2.33	2.38	2.41
Willemite	Zn_2SiO_4	trigonal	$R–3$	4.05	1510	B	1.71	1.72	
Wurtzite	CdS	hexagonal	$P6_3mc$	4.49	1290	B	2.53	2.51	
Zircon	$ZrSiO_4$	tetragonal	$I4_1/amd$	4.65	2550	B	1.92	1.97	

Note: I, U, and B stand for optically Isotropic (a single refractive index), Uniaxial (two refractive indices), and Biaxial (three refractive indices), respectively.

3.1. Refractoriness

Ceramic pigments must have a high melting point, consistently above the firing temperature they have to withstand in the industrial kiln. Indeed, the melting point reasonably matches the colorant behavior usually recognized in the industrial practice. Significantly, all the pigment structures widely used in large-scale ceramic production melt above 1600°C (Table 2), with the single exception of malayaite, that means at least 400°C above the highest temperature of industrial kilns for ceramic tiles (~1240°C). In particular, melting temperatures above 2000°C correspond to highly stable structures – like baddeleyite, zircon, spinel, or corundum – that are known to withstand high firing temperatures in a wide range of ceramic matrices [2,16]. On the other hand, a melting point in the 1800-2000°C range characterizes reliable host structures – such as periclase-bunsenite, perovskite or rutile – which, however, denote some instability either at the highest firing temperatures or in touch with aggressive glazes [16-18]. Certain stability problems are recognized when the melting occurs below 1800°C – as for garnet, hematite, willemite and wurtzite – which are generally used in low temperature applications or once encapsulated by protective layers [18-19]. Thus, melting point should be considered as a basic prerequisite in the pigment design.

Table 3. Chemical and physical characteristics of the main substances used as ceramic dyes and effects.

Compound	Formula	Structure	Density ($Mg \cdot m^{-3}$)	Melting point (°C)	Type Table 1	Color/Effect
Cerianite	CeO_2	cubic, *Fm3m*	6.95	1630	LE	metallic luster
Chromium	Cr^{3+}	organometallic complex	—	—	SD	green or light brown
Chromium-Antimony	$Cr^{3+} + Sb^{5+}$	organometallic complex	—	—	RD	yellow
Clinobisvanite	$BiVO_4$	monoclinic, *I2/a*	6.95	~900	SE	sink
Cobalt olivine	Co_2SiO_4	orthorhombic, *Pbnm*	4.04	1420	PD	blue
Cobalt lithiophylite	$LiCoPO_4$	orthorhombic, *Pbnm*	3.76	~800	PD	blue
Cobalt sarcopside	$Co_3(PO_4)_2$	monoclinic, $P2_1/c$	3.82	1120	PD	blue
Cobalt suanite	$MgCoB_2O_5$	monoclinic, $P2_1/c$	2.35	~1100	PD	blue
Cobalt	Co^{2+}	organometallic complex	—	—	SD	blue
Copper	Cu^{+}	organometallic complex	—	—	SD	green
Ferroalluaudite	$NaFe_3(PO_4)_3$	monoclinic, *C12/c*	3.60	~900	LE	metallic luster
Frit (glossy)	Si-B-Na-K-Ca-Ba-O	borosilicate glass	2.4÷2.6	700÷1200[1]	BE	glossy surface
Frit (matt)	Si-B-Na-K-Ca-Zn-Mg-O	borosilicate glass	2.4÷2.6	700÷1200[1]	BE	opaque surface
Gold	Au^0	organometallic complex	—	—	RD	magenta or metallic gold
Hematite	Fe_2O_3	trigonal, *R–3c*	5.30	1540	LE	metallic luster
Iron	Fe^{3+}	organometallic complex	—	—	SD	brown
Iron phosphate	$Fe_2Fe(P_2O_7)_2$	orthorhombic, *Pnma*	3.07	940	LE	metallic luster
Liebenbergite	Ni_2SiO_4	orthorhombic, *Pbnm*	4.60	1650	PD	green
Nickel	Ni^{2+}	organometallic complex	—	—	SD	brown
Palladium	Pd^0	organometallic complex	—	—	RD	gray
Platinum	Pt^0	organometallic complex	—	—	RD	metallic platinum
Ruthenium	Ru^0	organometallic complex	—	—	RD	black
Scheelite	$CaWO_4$	tetragonal, $I4_1/a$	6.01	1580	GE	aventurine
Shcherbinaite	V_2O_5	orthorhombic, *Pmmn*	3.28	690	SE	sink
Silver	Ag^0	organometallic complex	—	—	RD	yellow or metallic silver
Tenorite	CuO	monoclinic, *C2/c*	6.50	1240	GE	aventurine
Vanadium	V^{3+}	organometallic complex	—	—	SD	light brown
Zirconium	Zr^{4+}	organometallic complex	—	—	RD	white, matt

[1]Softening (maturing) temperature.

Completely different is the case of dyes, since a low melting point is needed to ensure an easy and complete dissolution into the ceramic matrix. Particulate dyes exhibit melting temperatures usually in the 900-1100°C range (Table 3), thus well below the firing temperatures of the IT and HT technologies (Fig. 1). A separate case is that of silicate dyes (Cobalt olivine and liebenbergite) that melt over 1400°C, though are readily dissolved in most glazes. Low melting temperatures (600 to 900°C) are typical of the sink effect, which is obtained by drastically boosting the fusibility in order to locally drop the viscosity of glazes or glassy coatings. On the other hand, glitter and luster effects imply crystallization that may occur either during sintering or cooling. Therefore, the melting points of crystallizing phases vary in a wide range: from 900 to 1650°C.

3.2. Color saturation

The typical color palette obtainable with standard ceramic colorants can be plotted in the a*-b* equatorial plane of CIE-L*a*b* coordinates (Fig. 4) where +a* is red, –a* is green, +b* is yellow and –b* is blue [2,16,19-20]. The sector between the +a* and +b* axes is rather crowded by several pigments of warm color, going from red to orange and yellow. Less numerous are the industrial colorants in the yellow to green quarter (+b* to –a*) and some plot in the green to blue (–a* to –b*) and blue to purple (–b* to +a*) quarters. It deserves to be noticed there are “pure colors” (i.e., those approaching the highest value of chroma) and “pastel colors” (plotting somehow midway to the origin of axes).

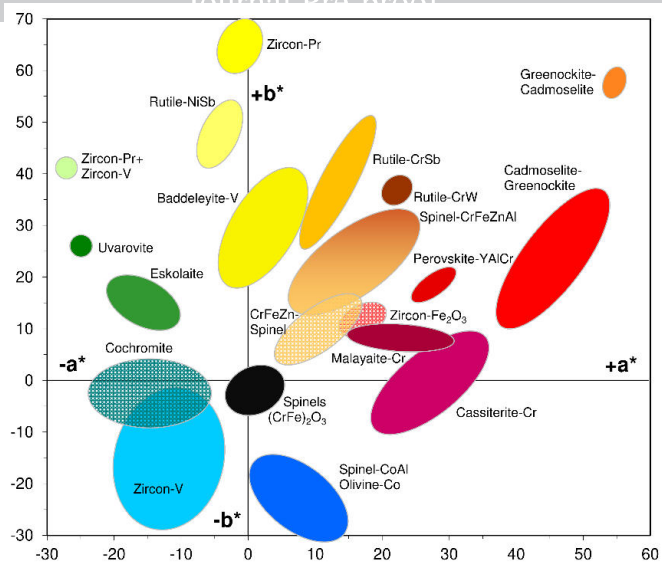

Fig. 4. Gamut of colors (a*-b* equatorial plane, CIE-L*a*b* coordinates) for industrially-manufactured ceramic pigments and dyes [modified after 2].

However, it must be emphasized that the concept of color intensity for ceramic applications involves both color saturation and brightness [1,19-20], so it should not be merely expressed by the chromatic coordinates of Figure 4. In order to overcome this limit, the *tinctorial strength* index is proposed for the first time:

$$T^* = (100 - L^*) + C^* = (100 - L^*) + (a^{*2} + b^{*2})^{1/2}$$

where L* is lightness (0=white, 100=black) and C* is chroma. It should not be confused with the *tinting strength* (used in paints), the *color strength* (applied in the textile sector) or the *tinctorial power* (utilized in the food industry) all based on the Kubelka-Munk equation.

From this standpoint, the industrial pigments and dyes exhibit tinctorial strength that, in most cases, is in between T*~70 and T*~100 (Fig. 5). These values can be devised as another basic requirement for ceramic pigments and dyes to enter in the industrial practice. Significantly, most of the pigment candidates proposed in the literature – that did not find an industrial application yet – exhibit a tinctorial strength that is lower than the industrial colorant of similar hue. A detailed discussion on the colorant suitability for present day applications is in section 5.

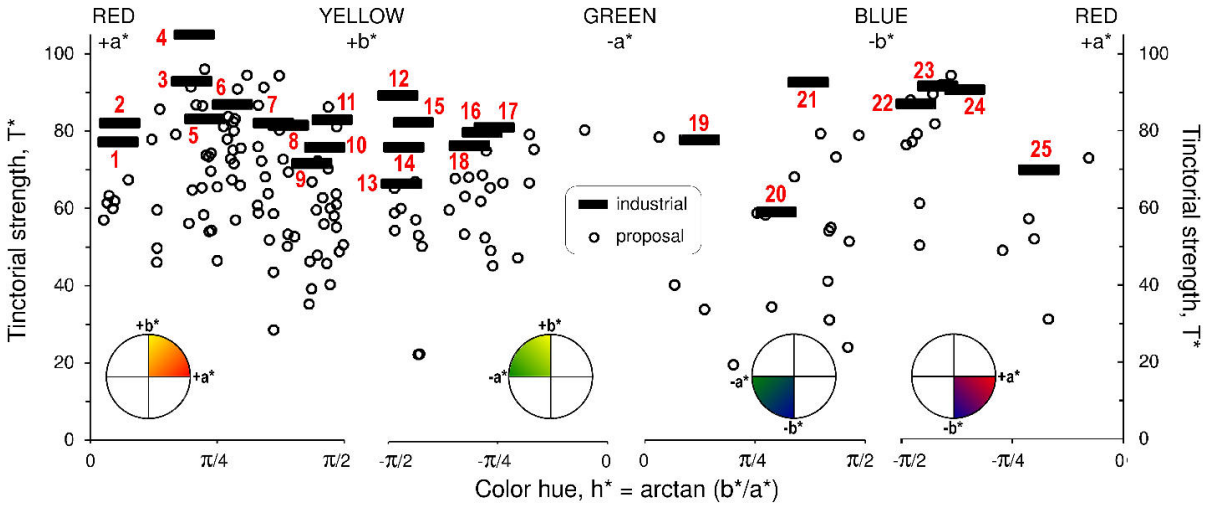

Fig. 5. Tinctorial strength versus color hue of the main industrial ceramic pigments and dyes (for numbers 1 to 25 see Table 4) and candidate colorants proposed in the literature.

Table 4. Color of the main ceramic pigments and dyes. Color Index number and code (Society of Dyers and Colourists). Chromophore: [ion coordination number]. Color origin: Crystal Field theory (CF); Metal Oxygen Charge Transfer (MOCT); Inter-Valence Charge Transfer (IVCT); Band theory (BT); Cooperative Transitions (COT); Paired spin Exchange transitions (PE).

no.	Structure/Name	Formula	Type	C.I. #	C.I. CODE	Chromophore	Origin	Reference
1	Cassius' purple	Au	IP	77482	RED 109	Au nanoparticles	plasmonics	
2	Malayaite	$Ca(Sn,Cr)(Si,Cr)O_5$	AP	77301	RED 233	Cr^{4+}[4] Cr^{4+}[6]	CF	
3	Perovskite	$Y(Al,Cr)O_3$	AP	—	—	Cr^{3+}[6]	CF COT	
4	Cadmoselite *(in zircon)*	$ZrSiO_4$[Cd(Se,S)]	EP	77196	RED 108	band gap	BT	
5	Hematite *(in zircon)*	$ZrSiO_4$[Fe_2O_3]	EP	77996	RED 232	$Fe^{3+}\leftrightarrow Fe^{3+}$[6]	PE CF	
	Hematite	Fe_2O_3	IP	77491	RED 101	$Fe^{3+}\leftrightarrow Fe^{3+}$[6]	PE CF	
6	Spinel Jacobsite	$(Mn,Fe)(Mn,Fe)_2O_4$ $(Mn,Fe)(Fe,Cr)_2O_4$	IP	77494 774945	BLACK 26 BROWN 46	Mn^{2+}[4] Fe^{3+}[4] Mn^{3+}[6] Cr^{3+}[6]	CF MOCT	
	Spinel Chromite	$FeCr_2O_4$	IP	77500	BROWN 29	Cr^{3+}[6] Fe^{2+}[4]	CF MOCT	
7	Rutile	$(Ti,Cr,Sb)O_2$ $(Ti,Cr,Nb)O_2$	AP	77310 77896	BROWN 24 YELLOW 162	Cr^{3+}[6]	CF MOCT	
8	Rutile	$(Ti,Cr,W)O_2$	AP	77897	YELLOW 163	Cr^{3+}[6]	CF MOCT	
9	Baddeleyite	$ZrO_2[V_2O_5]$	MP	77991	YELLOW 160	V_2O_5 V^{4+}[8]	MOCT CF	
	Oxyplumboroméite	$Pb_2Sb_2O_7$	IP	77588	YELLOW 41	band gap	BT	
10	Rutile	$(Ti,Ni,Sb)O_2$ $(Ti,Ni,Nb)O_2$ $(Ti,Ni,W)O_2$	AP	77788 77895 77902	YELLOW 53 YELLOW 161 YELLOW 189	Ni^{2+}[6]	CF MOCT	
	Pyrochlore	$Y_2(Sn,V)_2O_7$	AP	—	—	V^{4+}[6]	CF	
	Srilankite	$(Zr,Sn,Ti,V,In)O_2$	AP	—	—	V^{4+}[6]	CF	
11	Zircon	$(Zr,Pr)SiO_4$	AP	77997	YELLOW 159	Pr^{4+}[8]	CF	
12	Greenockite *(in zircon)*	$ZrSiO_4$[CdS] $ZrSiO_4$[Cd(S,Se)]	EP	77205 —	YELLOW 35 ORANGE 20	band gap	BT	
	Spinel Gahnite	$Zn(Al,Cr)_2O_4$	AP	77290	RED 235	Cr^{3+}[6]	CF	
	Corundum	$(Al,Cr)_2O_3$ $(Al,Mn)_2O_3$	AP	77003 77005	RED 230 RED 231	Cr^{3+}[6] Mn^{3+}[6]	CF CF	
13	Spinel Zincochromite	$(Zn,Fe)(Cr,Fe,Al)_2O_4$ $Zn(Fe,Cr)_2O_4$	IP	77496 77503	YELLOW 119 BROWN 33	Cr^{3+}[6]	CF	
14	Cassiterite	$(Sn,V)O_2[V_2O_5]$	MP	77862	YELLOW 158	V_2O_5 V^{4+}[6]	MOCT CF	
15	Priderite	$Ba(Ti,Ni)_8O_{16}$	AP	77900	YELLOW 157	Ni^{2+}[6]	CF	
16	Garnet Uvarovite	$Ca_3Cr_2(SiO_4)_3$	IP	77300	GREEN 51	Cr^{3+}[6]	CF	
17	Eskolaite	Cr_2O_3	IP	77288	GREEN 17	Cr^{3+}[6]	CF	
	Olivine Liebensbergite	Ni_2SiO_4	PD	77850	—	Ni^{2+}[6] Ni^{2+}[5] *in glass*	CF	
18	Spinel Co-Ti	Co_2TiO_4 $(Co,Al)_2(Al,Ti)O_4$	IP	77377 773465	GREEN 50 BLUE 81	Co^{2+}[4] Co^{2+}[6]	CF MOCT	
19	Spinel Cochromite	$CoCr_2O_4$ $(Zn,Co)Cr_2O_4$	IP	77344 77343	GREEN 26 BLUE 36	Co^{2+}[4] Cr^{3+}[6]	CF	
20	Zircon	$ZrSiO_4$:V	AP	77998	BLUE 71	V^{4+}-V^{4+}[4]	CF	
21	Cassiterite	$(Sn,Sb)O_2$	AP	77865	BLACK 23	band gap	BT	
	Spinel Hercynite	$Fe(Al,Ti)_2O_4$	AP	—	—	Fe^{2+}+$Ti^{4+}\leftrightarrow Fe^{3+}$+$Ti^{3+}$[6]	IVCT	
	Spinel Co-Sn	Co_2SnO_4	IP	77368	BLUE 35	Co^{2+}[4] Co^{2+}[6]	CF MOCT	
22	Spinel Gahnite	$CoAl_2O_4$ $(Co,Zn)Al_2O_4$	IP	77346 77347	BLUE 28 BLUE 72	Co^{2+}[4]	CF MOCT	
23	Willemite	$(Zn,Co)_2SiO_4$	AP	77366	BLUE 74	Co^{2+}[4]	CF MOCT	
24	Olivine	Co_2SiO_4	PD	77364	BLUE 73	Co^{2+}[4] Co^{2+}[5] *in glass*	CF MOCT	
	Perovskite	$Y(Mn,In)O_3$	IP	—	BLUE 86	Mn^{3+}[6] In^{3+}[6]		
	Lithiophylite	$CoLiPO_4$	PD	77362	VIOLET 14	Co^{2+}[4] Co^{2+}[5] *in glass*	CF MOCT	
	Sarcopside	$Co_3(PO_4)_2$	PD	77363	VIOLET 47	Co^{2+}[4] Co^{2+}[5] *in glass*	CF MOCT	
	Suanite	$MgCoB_2O_5$	DY	77352	VIOLET 48	Co^{2+}[4] Co^{2+}[5] *in glass*	CF MOCT	
25	Cassiterite	$(Sn,Cr)O_2[CrO_2]$	PD	77863	RED 236	CrO_2 Cr^{4+}[6] Cr^{3+}-Cr^{3+}[6]	IVCT CF	
	Rutile	$(Ti,Mn,Sb)O_2$	AP	77899	YELLOW 164	Mn^{2+}[6] Mn^{3+}[6]	CF MOCT	
	Pseudobrookite	Fe_2TiO_5 $(Al,Fe)_2TiO_5$	IP	77501 775435	BROWN 35 BROWN 48	Fe^{3+}[6]	CF MOCT	
	Spinel Chromite	$FeCr_2O_4$	IP	77500	BROWN 29	Fe^{2+}[4] Cr^{2+}[6]	CF MOCT	
	Spinel Ulvospinel	Fe_2TiO_4	IP	77543	BLACK 12	Fe^{2+}[4] Fe^{2+}[6] $Fe^{2+}\leftrightarrow Fe^{3+}$	CF IVCT	
26	Periclase Bunsenite	$(Ni,Co)O$	IP	77332	BLACK 25	Ni^{2+}[6] Co^{2+}[6]	CF MOCT	
27	Rutile	$(Ti,V,Sb)O_2$	AP	77898	BLACK 24	V^{4+}[6] V^{3+}[6]	CF MOCT	
28	Eskolaite-Hematite	$(Cr,Fe)_2O_3$	IP	77288	—	Cr^{3+}[6] Fe^{3+}[6]	CF MOCT	
	Spinel Cuprospinel	$CuCr_2O_4$	IP	77428	BLACK 28	Cr^{3+}[6] Cu^{2+}[4]	CF MOCT	
	Spinel Nichromite	$Ni(Cr,Fe)_2O_4$	IP	77504	BLACK 30	Ni^{2+}[4] Fe^{3+}[4] Fe^{3+}[6] Cr^{3+}[6]	CF MOCT	
29	Spinel Co-ferrite	$CoFe_2O_4$ $Co(Fe,Cr)_2O_4$	IP	77498 77502	BLACK 29 BLACK 27	Co^{2+}[4] Fe^{3+}[4] Fe^{3+}[6] Cr^{3+}[6]	CF MOCT	
30	Spinel complex	(Ni,Co,Mn) $(Cr,Mn,Fe)_2O_4$	IP	—	—	Ni^{2+}[4] Co^{2+}[4] Mn^{2+}[4] Fe^{3+}[4] Fe^{3+}[6] Mn^{3+}[6] Cr^{3+}[6]	CF MOCT	

Even more important are the chromatic coordinates of pigments once applied in the various types of ceramic bodies and glazes. Indeed, the performance of ceramic colorants depends to a large extent on the matrix and decreases moving from transparent glazes/glasses to opaque glazes to bodies [19-20]. On the other hand, it is well known that the color yield varies upon the amount of colorant added. Examples for the main ceramic pigments are given in Figure 6. Any direct comparison of the tinctorial strength of different colors, nonetheless, is not fully reliable, because the colorimetric system in use in the ceramic sector, i.e. CIE L*a*b* [21], does not reproduce the intensity of all the colors in the same way [22].

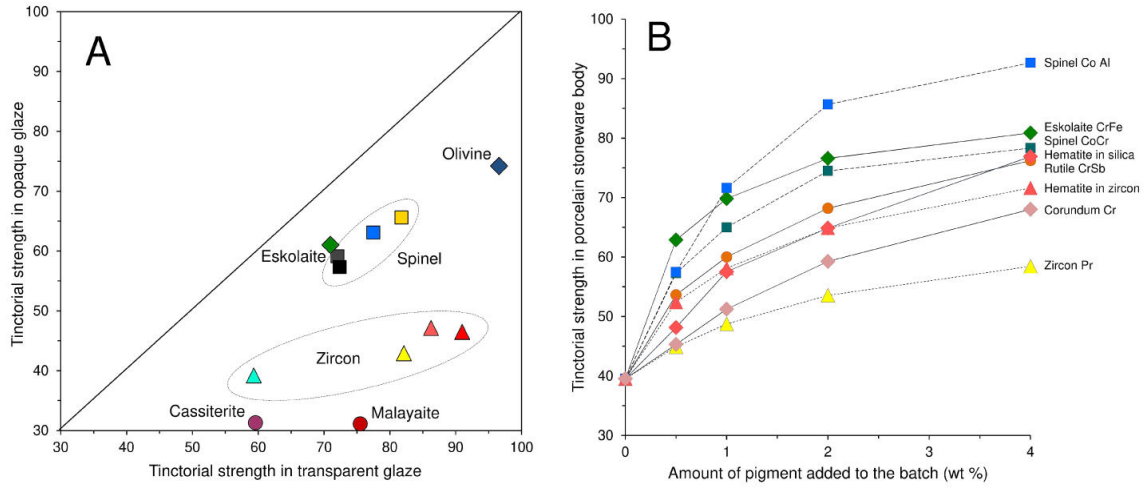

Fig. 6. Tinctorial strength of ceramic pigments in transparent glaze versus opaque glaze (A) and as function of the amount of pigment into porcelain stoneware body (B). Data from [23].

Color has a strong dependence on optical properties and particle size distribution of pigments, which role will be discussed in detail in the next sections. However, the behavior of ceramic dyes is different, since it entails the efficiency by which the metal ions are incorporated – with the desired oxygen coordination number – into the vitreous phase of bodies and glazes.

3.3. Optical properties

Besides the knowledge of the origin of color in ceramics is fundamental for pigment design, a detailed discussion of optical spectra goes beyond the scope of the present overview. Here, *chromophores* (metal ions responsible for coloration once coordinated by a given number of oxygens) are summarized in Table 4. Reference is done to mechanisms behind color development that encompass the crystal field, ligand, and band theories, for which the Reader is addressed to specific treatises [24-27]. These formalisms may be associated to cooperative phenomena, like intervalence charge transfer or paired spin exchange transitions.

The chromatic coordinates, by which the tinctorial strength is calculated, are affected by both the refractive indexes and the main absorption bands in the visible spectrum. The difference in refractive indexes between pigments (see Table 2) and the vitreous phase in which they are incorporated determines the degree of light scattering that is often seen as the ability to “cover” the substrate [28-29]. It consequently affects the brightness of color. The refractive index of ceramic glazes and glasses is usually in the 1.50-1.55 range [29]. The difference in refractive indexes between pigment and matrix should be at least 0.2 to ensure an adequate light scattering and therefore a satisfactory covering effect. This requirement implies a threshold for effective pigments as high as 1.75 or so. Indeed, industrial pigments always exhibit refractive indexes over 1.7 and the best performance is found for values over 1.9.

Looking at the optical spectra of the main ceramic pigments and dyes (Fig. 7) it can be appreciated that absorbance bands shift leftwards when colorants are considered in the order: white, yellow, orange, and red.

White pigments (so called *opacifiers*) have indeed a negligible absorbance in the visible range – as for zircon, baddeleyite and cassiterite – or may induce a yellowish shade, due to a slight absorption of violet wavelengths, as usually occurs with cerianite and rutile.

Yellow pigments absorb intensely all wavelengths above the ~20,000 cm^{-1}, so leaving a wide transmittance window (250-500 nm) that ensures bright colors. Two distinct kinds of optical band occur: steep in zircon-Pr and bindheimite pigments and less abrupt in baddeleyite-V, rutile-NiSb, and cassiterite-V pigments. The color shade depends on the wavelength of minimum absorbance, which can shift from the yellow region (where it gives rise to "cold" colors, like zircon-Pr and rutile-NiSb) towards the orange one, determining "warm" yellows, as those of bindheimite, baddeleyite-V, or cassiterite-V pigments.

Red pigments are featured by sharp bands absorbing most of the orange to violet wavelengths, *i.e.* above the ~16,000 cm^{-1} (below ~600 nm) as shown by cadmium sulfoselenide and Cr-doped yttrium aluminate perovskite. By this way, the transmitted light is limited to the red-orange region, resulting in rather dark colors. Magenta to burgundy shades, as those of malayaite-Cr and the so called Cassius' purple (gold nanoparticles), are originated by an additional transmittance in the blue-violet region, while purple colors require a second minimum of absorbance in the violet region, like that at ~24,000 cm^{-1} (~420 nm) of the cassiterite-Cr pigment. On the other hand, pink colors have an absorbance band that occurs at the same wavenumber of red pigments (onset at ~16,000 cm^{-1}) but with a distinctly weaker intensity, as the case of hematite encapsulated in zircon. The spectrum of Cr-doped corundum reveals, in addition, the transmission of some blue and violet wavelengths, justifying the typical ruby shade.

Orange pigments exhibit optical features intermediate between yellow and red colorants. Cr-doped rutile pigments, for instance, are characterized by a slope not so steep and a rather wide transmittance window, by which light is increasingly absorbed moving from orange (minimum around 15,500 cm^{-1}) to green regions of the visible spectrum.

Optical features different from the shutter-like bands observed in red to yellow pigments are necessary in order to get the remaining colors. For instance, a selective wavelength absorption that allows the transmission of either the green or the blue light only. On the other hand, dark colors are obtained through a non-selective light absorption over the whole visible spectrum, but with different intensity for brown, gray and black shades.

Green pigments require a light absorption at both the red-orange and blue-violet extremes of the visible spectrum. The resulting transmission window has a minimal absorption at ~19,000 cm^{-1} that is more accentuated for green pigments (e.g., eskolaite, uvarovite) than for bluish-green ones (cochromite) which exhibit a plateau over the green and blue regions.

Blue colorants must absorb selectively the orange to green wavelengths (15,000 to 20,000 cm^{-1}, 500-650 nm) to achieve the desired blue hue, as in the case of the cobalt aluminate spinel pigment. Instead, cobalt dyes (olivine, but also phosphates and borate, see Table 4) are filters less selective, because they absorb also some blue and violet light, giving rise to a deep, ultramarine blue tint. Turquoise shades occur in case of a narrower absorption band – like that of zircon-V pigments, usually extended over the 14,000 to 17,500 cm^{-1} range (580-700 nm) – which let some green light to be transmitted, so the overall hue is between green and blue.

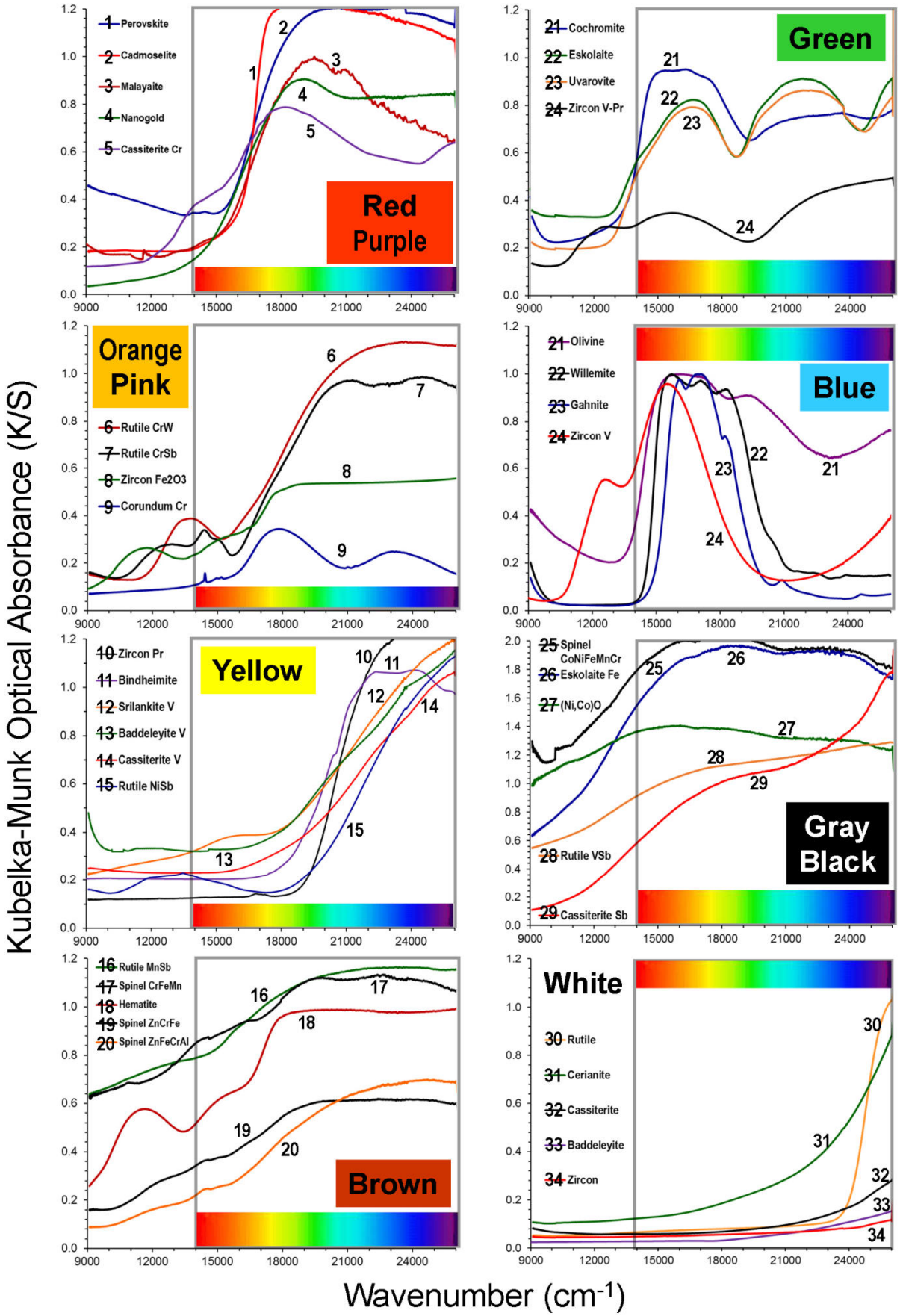

Fig. 7. Examples of optical spectra of industrial pigments and dyes used by the ceramic industry.

Brown pigments are a variegated family of compounds, exhibiting broad optical spectra, not easily attributable to single bands. A more or less accentuated light absorption is observed growing from red to violet wavelengths. It is the intensity of such an optical hump to discriminate between light brown (e.g., spinel Zn-Cr-Fe) and dark brown shades (e.g., spinel Mn-Cr-Fe and rutile Mn-Sb). The window transmitting in the low energy region of the visible spectrum accounts for brown colors with reddish to yellowish tints.

Black pigments should in principle absorb all the visible spectrum, as it practically occurs in the best cases (like complex Co-Ni-Fe-Cr-Mn spinels). In comparison, eskolaite-hematite pigments have a weak transmission in the red region, that is enough to justify some brownish shade. Gray colors are expected to differ from black just for the lower absorbance over the whole visible spectrum (e.g., bunsenite-Co). In reality, some selective absorption can lead to bluish, greenish or yellowish overprints.

3.4. Interaction of pigments and dyes with ceramic matrices

Ceramic pigments must be stable in contact with the melt formed during the firing of glazes and bodies. Therefore, the resistance to chemical attack is a relative concept, depending on the substrate composition (glaze or body) that varies upon the technology used in ceramic manufacturing. In practice, there are different arrays of 'chemical composition x firing schedule', which define a variable degree of aggressiveness of the liquid phase towards the pigment.

The differences in chemical composition among glazes and bodies used by the ceramic industry are illustrated in Figure 8 with reference to the decoration technologies of Figure 1. The main fluxes are arranged in Figure 8A according to their technological role and chemical action against the ceramic pigments [4,28,29]. Account must be taken since there are three basic mechanisms by which a ceramic pigment can be chemically attacked with permanent color deterioration [10]:

a) pigment dissolution in the liquid phase;

b) pigment transformation into another crystalline phase;

c) change in the crystal chemical composition of the pigment, which keeps its structure.

Alkaline fluxes, i.e. Na_2O, K_2O and Li_2O, enhance fusibility, so reducing the maturing temperature, and increase the brightness of glazes (but in the case of lithium a devitrification may occur). Alkali do not enter the crystal structure of pigments and usually do not promote the crystallization of phases hosting transition metal ions [28-29]. Thus, their action is principally to foster pigment dissolution by lowering viscosity and increasing surface tension of melt.

Alkaline-earth fluxes, i.e. MgO, CaO, SrO and BaO, play different roles, depending on concentration and firing conditions, with some variation from one element to another [19,28,30]. At high concentration, they promote devitrification, leading to opaque glazes, but at low percentages tend to improve brightness (useful for glassy coatings). On the other hand, they enhance fusibility at higher firing temperatures, whilst boost viscosity at lower temperatures. Therefore, alkaline-earth fluxes can take part into the chemical attack by various reactions, depending on the colorant. For instance, magnesium can affect spinel pigments, since Mg^{2+} ions compete with divalent transition metal ions (Co^{2+}, Mn^{2+}, Ni^{2+}) mainly to access the tetrahedral site [31]. Similarly, in bunsenite pigments Mg can replace both Ni and Co at the octahedral site [32]. On the other hand, calcium may have opposite functions: it stabilizes Ca-bearing pigments, like garnet and malayaite, but heavily attacks rutile, hematite, and eskolaite, as $CaTiO_3$, $CaFe_2O_4$ and $CaCr_2O_4$ phases turn to be thermodynamically favored with respect to simple oxides [33]. Eventually, all colorants are attained to some extent by dissolution into the melt, which is more effective at lower viscosity, thus with higher temperature and BaO content.

Strong fluxes, i.e. B_2O_3, PbO and Bi_2O_3, reduce viscosity and surface tension of the melt, thus promoting the diffusion in the liquid phase of other glaze components [30]. Account must be taken that present-day glazes are nominally leadless, while bismuth is utilized only in some third fire applications. Boron does not enter the crystal structure of ceramic pigments; thus, its role is essentially to enhance the fluxing effect of alkali.

Zinc oxide has a wide range of effects in glazes, including a fusibility enhancement through the reduction of viscosity and surface tension of the melt or, at high concentration, the tendency to crystallize Zn-phases (gahnite, willemite, hardystonite). Zinc can interfere with the coloration of glazes because it may be incorporated in the crystal structure of many pigments. In fact, it can replace transition metal ions at tetrahedrally- and octahedrally-coordinated sites, e.g. in spinel, periclase, malayaite. In addition, zinc easily reacts with TiO_2, Cr_2O_3, Al_2O_3, Fe_2O_3, and SnO_2 pigments, giving rise to Zn-rich phases [29].

The *silica-to-alumina ratio* governs many chemical and physical properties of glazes and glassy coatings [29,30]. Indeed, the amounts of silica and alumina determine the appearance (transparency and gloss) of glazes, which can be described as matt, semi matt, and bright (Fig. 8B).

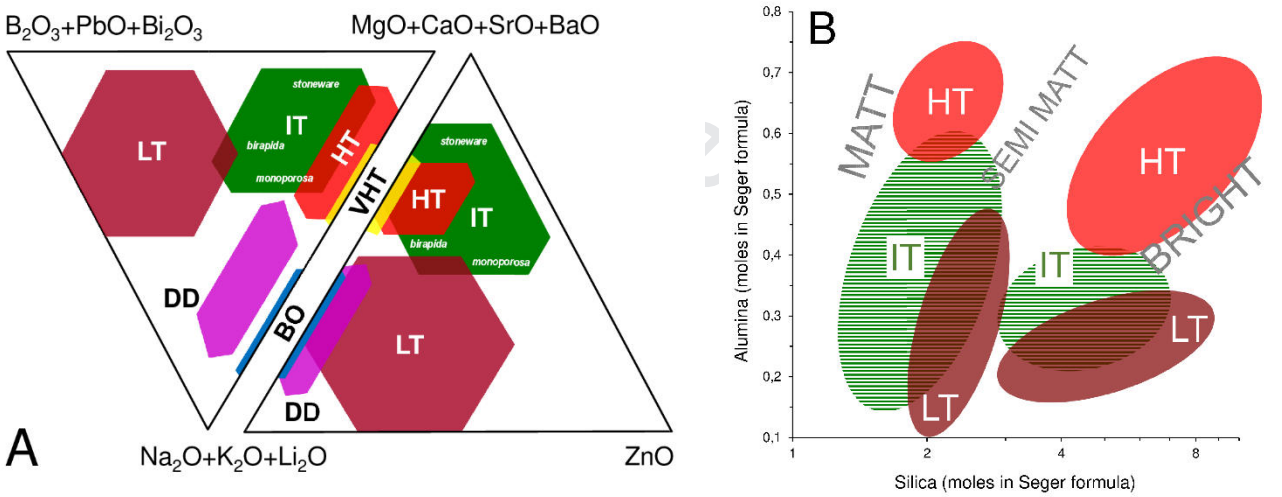

Fig. 8. Approximate fields of chemical composition of glazes, glassy coatings and porcelain stoneware bodies used in the different decoration technologies (see Figure 1 for abbreviations). A) Ternary diagrams of fluxes (% weight) and B) Stull diagram of silica and alumina (Seger formula).

Pigment dissolution in bodies and glazes always occurs to some extent, depending on both the phase refractoriness and its solubility in the melt. This phenomenon has commonly a twin effect: loss of the desired color (due to pigment breakdown) and onset of undesired shades due to element “leaching” (transition metal ions incorporated into the glassy phase). No data exist on pigment solubility into ceramic liquid phases, but information is available about some minerals in granitic melts, which can be somehow approximated to those present in porcelain stoneware bodies. The saturation concentration at 1200°C is below 1%wt for cassiterite [34], approximately 1.2%wt for zircon [35], and around 2%wt for rutile [36]. However, the solubility in ceramic melts is difficult to predict from phase diagrams, because of the remarkable complexity of glaze compositions. To overcome this problem, a common practice is to “saturate” the glaze with the major components of the pigment, in order to improve the chemical stability of colorants. This was typically an additional role of opacifiers, which are usually selected also to ensure the color yield, e.g. tin oxide for cassiterite pigments or zirconium silicate for zircon pigments [2,16]. This solution is no longer feasible with IJP, but it was revitalized in digital decoration by using “primers” and “protective” layers (i.e., glassy coatings with a very low amount of the most aggressive components, like ZnO and alkaline-earth oxides).

Pigment phase transformation is apparently a phenomenon restricted to specific circumstances, as in the classic example of the eskolaite green pigment, once applied on a zinc-bearing glaze: the reaction Cr_2O_3 + ZnO leads to the formation of the brown $ZnCr_2O_3$ spinel [16]. In reality, such reactions are easily overlooked, because the resulting chromatic change can be erroneously attributed to a pigment dissolution. These transformations typically occur when a thermodynamically favored crystalline phase exists in the relevant chemical system, which is usually hard to represent in a phase diagram due to the conspicuous complexity of glaze compositions.

A *change in the pigment crystal chemistry* can affect the chromatic coordinates, since factors that are fundamental in color development are usually modified. Such factors encompass the transition metal ion valence and oxygen coordination, as well as the metal-oxygen distances and distortion of the polyhedron where the cation is accommodated. These phenomena are governed by the partition equilibria, for each ion, between melt and pigment. In addition, the diffusion kinetics through the pigment crystal structure turns crucial. As a rule of thumb, structures with more than one crystallographic site, where transition metal ions can be allocated, are more prone to variation of crystal chemistry. A classic example is spinel: the Ni-free black spinel, once in touch with zinc-rich glazes, changes color by shifting towards a brown shade. This occurs because Zn^{2+} replaces Co^{2+} at the tetrahedral site; as a consequence, light absorption in the red-orange region no longer occurs and the outcome is a brown spinel.

Table 5. Chemical stability of ceramic pigments in contact with glazes and bodies [37]: incompatibility (or improved stability) with single components and maximum temperature allowed for industrial firing.

Pigment structure	Formula	Reduced stability with	Improved stability with	T_{max} °C
Baddeleyite	$ZrO_2[V_2O_5]$	B Zn (Pb)	Zr Ca Mg Ba	1300
Bunsenite	$[(Ni,Co)O]ZrSiO_4$	Zn B Pb (Na K)	Zr	1350
Cassiterite	$(Sn,Cr)O_2[CrO_2]$	Zn Mg B (Na K)	Sn Ca (Pb)	1300
Cassiterite	$(Sn,V)O_2[V_2O_5]$	(Al)	Sn (B Pb)	1300
Cassiterite	$(Sn,Sb)O_2$	Na K B Zn Zr	Sn Pb	1250
Corundum	$(Al,Cr)_2O_3$	Ca Mg B Pb	Al Zn Si	1400
Corundum	$(Al,Mn)_2O_3$	B Zn Pb	Al	1400
Eskolaite	$(Cr,Fe)_2O_3$	Ca Zn Sn Ni	Al	1250
Garnet	$Ca_3Cr_2Si_3O_{12}$	Zn	Ca Al	1200
Hematite	$ZrSiO_4[Fe_2O_3]$	Zn Na K B Pb	Zr	1250
Malayaite	$Ca(Sn,Cr)(Si,Cr)O_5$	Mg Zn B (Na K)	Ca Sn (Pb)	1250
Olivine	Co_2SiO_4	Mg	Zn	1350
Perovskite	$Y(Al,Cr)O_3$	Na K B Pb	Al	1350
Pyrochlore	$Pb_2Sb_2O_7$	Na K B	Pb Zn Al	1050
Rutile	$(Ti,Cr,Sb)O_2$	Na K B (Zn)	Ti Zr (Pb)	1300
Spinel	$CoAl_2O_4$	Na K B Pb	Al Zn	1350
Spinel	$CoCr_2O_4$	Zn Ni (Sn)	(Al)	1300
Spinel	Zn-Fe-Al-Cr-Mn	Sn	Zn Al	1400
Spinel	Co-Ni-Mn-Fe-Cr	Zn Al Zr (Sn)	Ca Na K	1400
Willemite	Zn_2SiO_4	Ca	Zn	1200
Wurtzite	$ZrSiO_4[Cd(Se,S)]$	Pb B Zn (Na K)	Zr Cd Si	1200
Zircon	$(Zr,Pr)SiO_4$	(Na K)	Zr Zn Pb	1300
Zircon	$ZrSiO_4$:V	(Na K)	Zr Sn	1300

Dye dissolution into the melt formed during firing is required and depends on the composition of ceramic matrices. The different compositional fields of glazes and bodies utilized in the various technologies are illustrated in Figure 8. They imply a spectrum of chemical environments and thermal treatments, hence conditions where dye melting (and the three causes of pigment deterioration) can play with a changing relative weight. This aspect must be considered when the chemical compatibility of a dye/pigment with single components of glazes and bodies is evaluated, as known from the industrial practice (Table 5). Some crystal structures suffer from the attack of alkaline fluxes and particularly strong fluxes (e.g., garnet, pyrochlore, bunsenite, baddeleyite, and cassiterite). It is not a case that the relevant pigments have a relatively low stability, as witnessed by the maximum temperatures allowed in the firing schedules that are among the lowest in industrial colorants. In contrast, pigments based on corundum and spinel structures are more exposed to phase transformations and/or change in their crystal chemistry, especially under the effect of element that can easily accommodated in the crystal sites (i.e., Zn, Mg, Sn).

Transition elements can be released to the liquid phase, present at high temperature in glazes and bodies, as a consequence of dye dissolution or pigment breakdown or even ion exchange between melt and pigment [2,16]. In case of pigments, such a leaching process determines the dissolution of transition metal ions into the glassy matrix with undesired repercussions on color purity [37]. Each transition metal ion will absorb in the visible light spectrum, depending on its valence and oxygen coordination in the silicate glass, giving rise to specific color shades, which is the mechanism exploited with dyes (Table 6). These more or less accentuated nuances, depending on the transition metal concentration, may significantly alter the original coloration due to the pigment.

Table 6. Coloration stemming from dissolution of transition metal ions in the vitreous phase formed in glazes and bodies. The most common occurrences are in bold.

Transition metal ion	Oxygen coordination	Color
Co^{2+}	4	**dark blue**
Co^{2+}	6	pink
Cr^{3+}	6	**emerald green**
Cr^{6+}	4	yellow
Cu^{+}	6	red
Cu^{2+}	6 (distorted)	**green to blue-green**
Fe^{2+}	4 to 5	green-blue to green-brown
Fe^{3+}	4	**reddish brown**
Fe^{3+}	6	**yellow-orange**
Mn^{2+}	4 to 6	**green to blue-green**
Mn^{3+}	6 (distorted)	pale red to purplish brown
Ni^{2+}	4	deep purple
Ni^{2+}	5	**brown**
Ni^{2+}	6	yellow
V^{3+}	6	**greenish brown**
V^{4+}	4 to 5	blue-green
V^{5+}	4	yellowish green

Ceramic effects behave either as a dye or a pigment. Sink effects (SE) and bright/matt glasses (BE) must dissolve in the glassy phase, as some speckle effects do. In contrast, glittering (GE) or phosphorescence require crystals dispersed in the glaze. Lusters (LE) are obtained by controlled crystallization during firing.

4. New technological requirements of ceramic colorants for digital decoration

The advent of IJP imposed to move from conventional pigments and dyes delivered as powders towards micronized colorants dispersed in a carrier (ink). This paradigm shift made some technical solutions no longer practicable and, at the same time, introduced new requirements (or emphasized some technological aspects).

For instance, the control on the pigment color saturation, which was commonly achieved through a careful addition of a filler [37], is unappropriated in inks. As a consequence, nowadays pigments must be even more constant in their color performance, because only the colorants (not diluted by filler) are used in inks [10]. On the other hand, no easy adjustment of color saturation by increasing the pigment concentration is possible in IJP, since it has immediate repercussions on the density, shear viscosity and surface tension of the suspension, hence on ink printability [9-11].

New requisites concern the behavior of ceramic pigments during micronization and their interactions with ink carriers and print head components. Particle size distribution assumed a crucial role in IJP, involving the micronization process adopted to make inks. Therefore, pigment grindability is now a key issue for both ink productivity and color saturation, and consequently the relevant parameters, such as the mechanical properties and the resistance to amorphization of the crystal structures of ceramic pigments. Further factors are the interactions between colorant and carrier, as electro-magnetic properties of pigments and dyes.

4.1. Particle size distribution

Most colorants are utilized as powders, directly or as feed in ink making. Therefore, pigments, effects and particulate dyes always undergo, after synthesis, a comminution or disaggregation stage to obtain the desired particle size distribution [37]. Such a process can be performed either by the dry route (typically through jet milling) or by the wet route (ball milling followed by spray-drying) depending on specific needs (e.g., washing any mineralizer residue out).

Particle size is the most important feature to keep under control in the industrial practice, because it affects both the optical properties and reaction kinetics during firing [38,39]. Thus, granulometry ultimately influences tinctorial strength in the various decoration technologies. For this reason, pigment-making companies spend considerable efforts to find out the best particle size distribution for every product to be applied as powder or entering the micronization process for ink-making [37,40].

Different requirements exist in the various applications, as exemplified in Figure 9A. The pigments utilized in conventional technologies (i.e., from LT to VHT and BO) are commonly milled to a median particle diameter in between 3 and 7 µm, irrespective of being allochromatic (AP) or idiochromatic (IP). The same pigments, once addressed to digital inks, undergo a more intensive comminution, down to approximately 1-2 µm or even less, in order to damp the cost of the high-energy micronization process. In contrast, encapsulated pigments are kept to a coarser particle size, in order to preserve the protective coating on the heat-liable pigment, so that the median particle diameter can span from 10 to 20 µm.

The micronization process, carried out in high-energy mills with Y-stabilized zirconia microspheres, leads to a narrow particle size distribution of the colorant dispersed in the ink medium. The median particle diameter for pigments is usually in the 0.3-0.6 µm range, with the d_{90} always below 1 µm [9-11], while micronized effects are slightly coarser, with a median particle diameter ordinarily from 0.6 to 1 µm. Such a drastic reduction of particle size brings about two different effects: a proportional increase of the specific surface area and a physical deterioration of pigments (see section 4.2 for a further discussion on pigment behavior

during milling). Both have relevant repercussions on the colorant performance of inks by two mechanisms: less intense light absorption (due to a loss of pigment) combined with undesired shades (due to transition metals migrating to the glaze or glassy coating, Table 6).

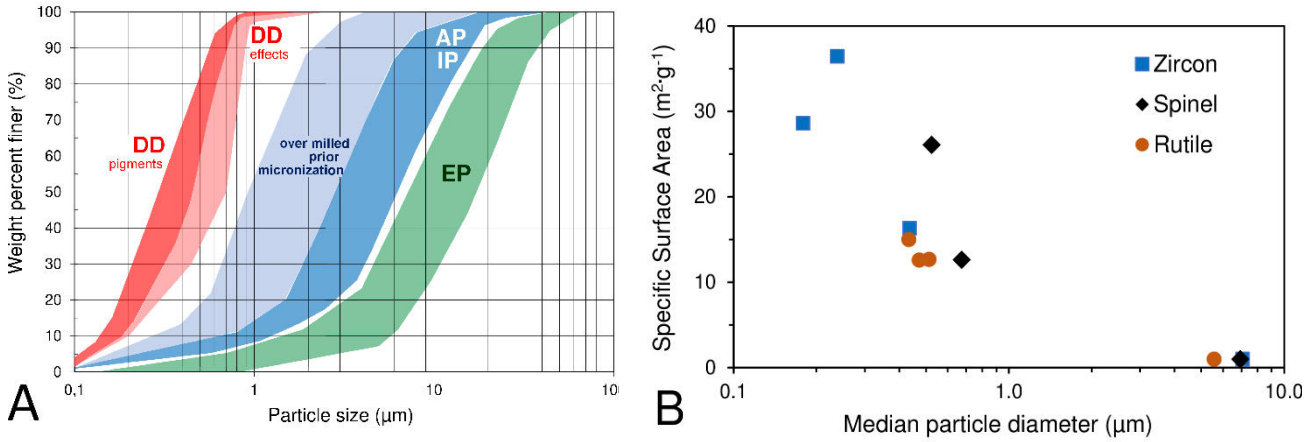

Fig. 9. Particle size distribution of colorants: A) micronized pigments and effects in IJP inks (DD) compared with conventional (AP-IP) and encapsulated pigments (EP); B) relationship with specific surface area in micronized pigments (data after [40]).

The specific surface area grows from conventional pigments, having normally values close to 1 $m^2 \cdot g^{-1}$, to 15-35 $m^2 \cdot g^{-1}$ in the resulting inks (Fig. 9B). Such an increased specific surface area implies an enhanced reactivity of pigments in touch with glazes and glassy coatings [40-41]. Thus, a much lower resistance to chemical attack is generally observed during firing. This fact reflects on color saturation, which is notoriously weaker in digital inks with respect to conventional pigments [10,41].

4.2. Pigment grindability

As introduced in the previous paragraph, DOD-IJP entails some strict requirements, among which ensuring that >99% of the pigment particles are less than 1 µm in diameter [8,9,11]. Being mainly dependent on the specific energy input (i.e., on the energy supplied to the grinding chamber in relation to the mass of product), pigments micronization down to the requested particles size proves to be the most energy-consuming comminution process per unit weight of product [42]. It derives that comminution of ceramic pigments is a key issue for ink production, which has strong repercussions on tinctorial strength, mechanical properties and resistance to amorphization of the pigment crystal structure.

In an ideal case, when a particle undergoes brittle fracture, a crack propagates through the particle creating new surface area. On the other hand, in the real cases, most of the energy supplied during comminution processes is dissipated into effects other than the new surface itself, *e.g.*, elastic deformations, friction between particles and/or between particles and apparatus walls, heat, vibrations, and so on [43]. Despite the effort in finding the best relationship that can rationalize the energy-dependent particle size variation during a comminution process and, at the same time, to account for all the above-mentioned secondary effects, the main relationship commonly used to describe a comminution processes of a brittle solid originates from a single differential equation of the general form [44]:

$$dE = -K\frac{dx}{x^{f(x)}} \quad (1)$$

where *dE* is the infinitesimal energy change per unit weight required during comminution, *dx* is the infinitesimal size change, *x* is the particle size, *K* and *f*(*x*) are a constant and a variable dependent on the particle size *x*, respectively, related with the material (*e.g.*, initial particles size, and particles physical properties) and with the size reduction method [44-47]. When particles fall at the boundary of the micrometric-submicrometric range, $f(x) \rightarrow 2$, and the Rittinger's law is considered the most suitable in describing the energy change in a comminution process [44,46,47]. Rittinger postulated that the energy per unit mass is proportional to the new surface area produced, and the Rittinger's relationship can be easily derived through the integration of equation 1 [44,46,47], such as:

$$E = K\left(\frac{1}{x_2} - \frac{1}{x_1}\right) \quad (2)$$

where *E* is the net energy (expressed in $J \cdot kg^{-1}$) required to micronize a particle from the initial (x_1) to the final (x_2) particle size (defined as the integrated mean particle size, in m [44,46]) in a given grinding cycle (*i.e.*, time × milling rounds), and *K* is expressed in the units of $J \cdot m \cdot kg^{-1}$ [43]. Once eqn. (1) and its derived form (2) have to be applied in fitting experimental data, a tough limitation occurs in finding the best fit values for *K* and *f*(*x*). In particular, the Rittinger's equation, eqn. (2), requires the values of *K* and *f*(*x*) to be known a priori [46]. In the case of ceramic pigments, the literature on their micronization is limited to few experimental investigations [40,48-51]. From these works, it emerges that the energy required to downsize a particle from x_1 to x_2 (*i.e.*, expressed as the variation of the median particle diameter, d_{50} in μm) is proportional to the total number of milling rounds, r_T [*e.g.*, 40], which is an experimental inference to what postulated by Hukki [44]. In figure 10, the variation of the reciprocal of the particles size (*i.e.*, $\left(\frac{1}{x_2} - \frac{1}{x_1}\right) \propto \frac{E}{K}$) for pigments micronized in a pilot plant is plotted as a function of the total milling rounds.

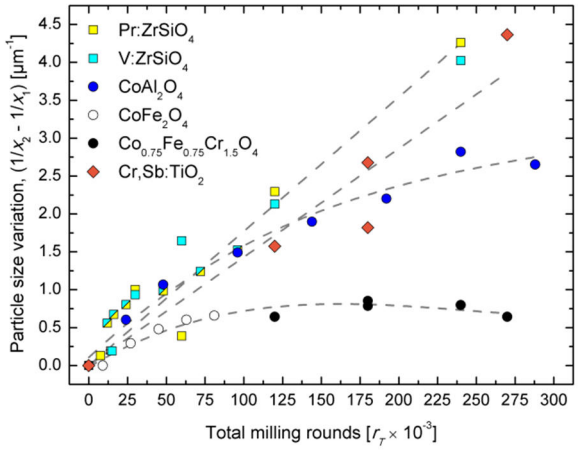

Fig. 10. Variation of the reciprocal of the pigment particle size (*i.e.*, $\left(\frac{1}{x_2} - \frac{1}{x_1}\right) \propto \frac{E}{K}$) as a function of the total milling rounds for various ceramic pigments. Symbols refer to: Pr- (yellow squares) and V-doped (cyan squares) zircon pigments [40,49,51]; Co-aluminate (blue circles), Co-ferrite (empty circles), and CoFe-chromate (black circles) spinel pigments [40, 48,50]; Cr,Sb codoped rutile pigments (orange diamonds) [40]. Dashed lines are a reader's eye guide.

Data in Figure 10 clearly show the strong dependence of particles size reduction on grinding cycles (by definition, proportional to the energy supplied during the comminution process). Along with this observation, a detailed inspection of data in Figure 10 reveals that the particles size reduction strongly depends on the structural features (*i.e.*, crystal structure and chemical composition) of the micronized ceramic pigments. Consistently to what reported by Güngör et al. [40], it appears that ceramic pigments with spinel structure are less grindable than those with rutile and zircon structure, respectively. In addition, while the particle size

variation of both zircon and rutile pigments scales almost linearly with the milling rounds, the particle size variation for spinel pigments undergoes a constant but gradual decreasing. In particular, above 2 × 10^5 and 2.5 × 10^5 milling rounds for Co-aluminate and CoFe-chromite, respectively, no appreciable particle size variation is observed.

The particles size variation for spinel and zircon ceramic pigments during micronization is highlighted in two distinct plots (A and B, respectively) in Figure 11.

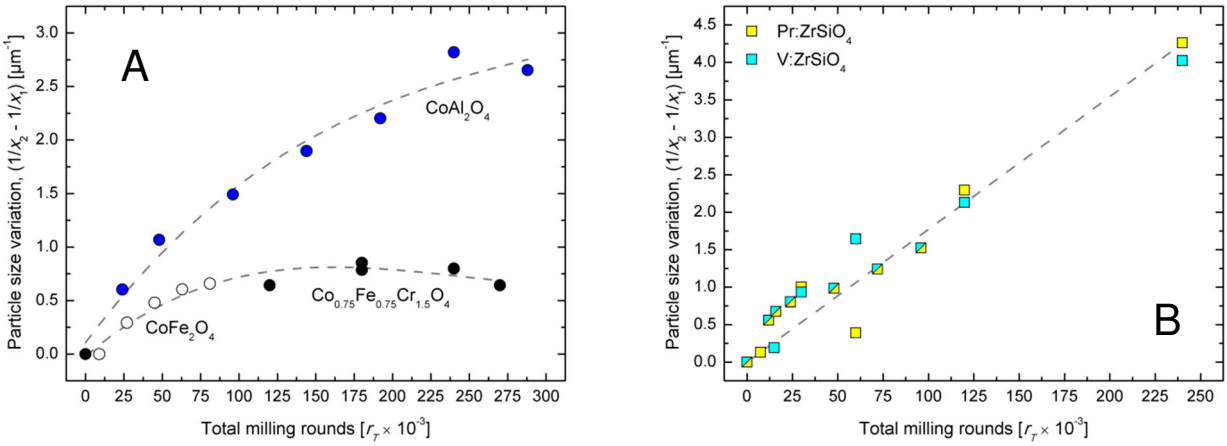

Fig. 11. Variation of the reciprocal of the pigment particle size as a function of (A) the total milling rounds for spinel [40, 48,50], and (B) zircon [40,49,51] ceramic pigments. Dashed lines are a reader's eye guide.

Beyond the general remarks of above, the comminution of spinel ceramic pigments returns different micronization trends depending on their crystal chemistry, with Co-aluminate pigments more grindable than Co-ferrite and CoFe-chromite spinel ceramic pigments, which in turn have a common particle downsizing (Fig. 11A).

This behavior apparently contrasts with that highlighted during the comminution of zircon ceramic pigments (Fig. 11B). Although purchased from different manufacturers and investigated at different laboratories [40, 48,50], data in Figure 11B unequivocally show that the zircon structure undergoes the same particles downsizing irrespective of the dopant cation nature. This fact can be readily explained because of the small substitution (or incorporation) of dopant cation within the zircon lattice. Pigment manufacturers produce yellow and turquoise zircon pigments by a doping of about 3% to 5% of Pr^{4+} and V^{4+}, respectively [49,51,52]. It derives that the presence of dopants in small amounts does not influence the grindability of zircon ceramic pigments.

The comparison of the selected data, at the micrometric scale, suggests that the energy supplied during a comminution process is used/dissipated by two main mechanisms related to two different energetic contributions. In the first mechanism, the energy supplied during the comminution process will be mainly devoted to the creation of new surface area, as in the ideal case entailed by the general comminution laws [43-47]. This energy is preserved as long as a particle undergoes brittle fractures: "energy conservation process". The second mechanism implicates a process for which the crystal structure of a particle loses long-range order by means of interatomic bonds breaking and lattice disorder, *i.e.*, the structure undergoes amorphization [53]. Hence, in terms of particle comminution, this process has a "dissipative/non-conservative" energetic contribution. Both mechanisms, and by consequence both energetic contributions,

mainly depend on the resistance of a crystal structure to an external compression, which is defined by its isothermal bulk modulus (K_{T0}, in GPa) [54,55].

The isothermal bulk modulus (or incompressibility) for the crystal structures of the ceramic pigments under comparison is listed in Table 7. The listed K_{T0}, is the average value among several from literature. For sake of clarity the range of variation of K_{T0} is also reported in Table 7.

Table 7. Isothermal bulk modulus (K_{T0}, in GPa) for the crystal structures of the ceramic pigments under comparison along with its range of variation.

Structure formula	Structure type	Averaged K_{T0} [GPa]	K_{T0} range [GPa]	Reference
Al_2O_3	corundum	251	242 - 257	[56-63]
$ZrSiO_4$	zircon	226	225 - 228	[64-68]
TiO_2	rutile	212	209 - 216	[69-74]
SnO_2	cassiterite	210	203 - 212	[69,75-77]
$YAlO_3$	Y-aluminate (perovskite)	195	188 - 205	[78-80]
$CoAl_2O_4$	Co-aluminate (spinel)	207	203 - 210	[81,82]
$CoFe_2O_4$	Co-ferrite (spinel)	180	175 - 186	[81,83]
$(A)Cr_2O_4$ where A: Zn, Mg, Fe	chromite (spinel)	183	181 - 189	[84-86]
$CaTiOSiO_4$	titanite	131	-	[87]
$CaSnOSiO_4$	malayaite	121	-	[88]

Note: the reported isothermal bulk moduli derive from high-pressure X-ray diffraction experiments of single-crystal and powder samples [56-59,66,67,70,71,73-75,78,79,83,84,87,88], elastic constant measurements of single-crystal and powder samples [62,64,65,68,69,76,77,81], and theoretical calculations through various computational methods [60,61,63,72,80,82,85,86].

Incompressibility data in Table 7 perfectly match with the grindability ranking derived from the particle size variation of micronized ceramic pigments (see Fig. 10), where the stiffest structure of zircon pigments has the highest rate of micronization, while the more compressible structures of Co-ferrite and CoFe-chromite spinel pigments show a little aptitude at micronizing.

Although the concept of resistance at the compression could be misleading, it results evident, when a crystal structure is stiffer than another, that the process of micronization can be prolonged at higher milling rounds. This means that a particle with a high bulk isothermal modulus undergoes brittle fracture when micronized, and the energy supplied during the comminution process will be largely devoted to the creation new surface area. Conversely, when the energy supplied to micronize a particle dissipates into other effects, the comminution efficiency will drastically decrease. Indeed, data on the phase composition for micronized ceramic pigments achieved by means of X-ray diffraction experiments highlighted a higher tendency to amorphization for spinel pigments than for zircon ceramic pigments [41]. In addition, the different trends for spinel and zircon ceramic pigments in Figure 11 are consistent, although qualitatively, with two different kinds of energy change. Indeed, the ball milling mechanical energy transforms into an energy process which is predominantly conservative in the case of zircon pigments, where the particle downsizing scales linearly with grinding cycles, while it changes into a largely dissipative energy process (*e.g.*, amorphization) in the case of spinel pigments, where the particle downsizing turns to be curvilinear.

Other bulk properties, such as density, which in turns is related with the pressure of amorphization [55], brittleness, hardness, etc. can play important roles during the comminution of ceramic pigments, but the driving force which governs the micronization of ceramic pigments is their resistance at the compression (i.e. the isothermal bulk modulus or incompressibility).

The high-energy micronization is able to progressively damage the crystal structure of colorants, leading eventually to a pigment loss due to amorphization [41]. This phenomenon brings about a lower yield at the end of the micronizing stage, which can vary widely from a few percent to 60% of the initial amount of pigment. The average loss in commercial inks, estimated by X-ray powder diffraction through Rietveld refinement with internal standard, is around 30% (Fig. 12). The differences amongst crystal structures – zircon, rutile, malayaite, and various spinel types – are just indicative, because data are not fully representative of ceramic inks, since the number of samples varies upon the different pigments.

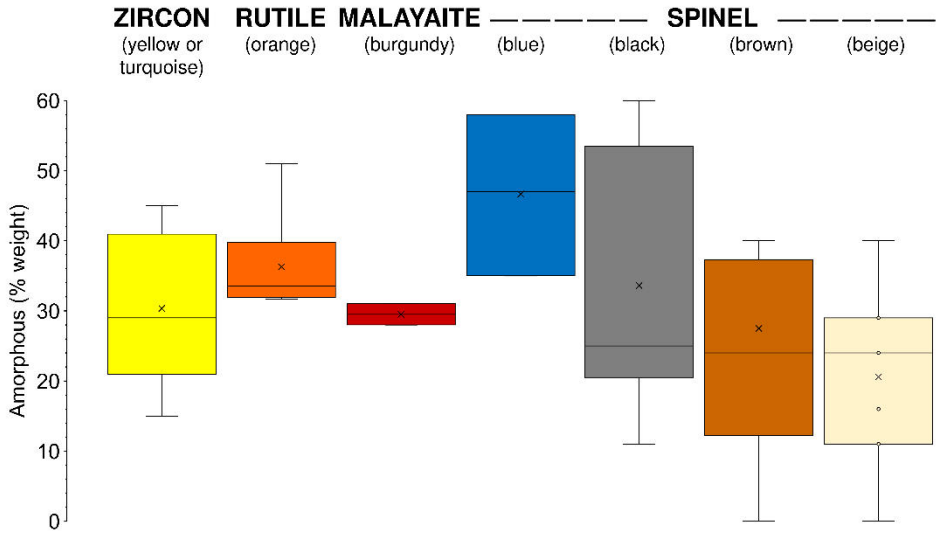

Fig. 12. Box-and-whisker diagram of the degree of pigment amorphization in commercial inks for digital decoration of ceramic tiles (unpublished data).

This picture lets the micronization of ceramic pigments to be a crucial stage to define quality, performance, yield and cost of digital inks. Key points for a better comprehension of this process are the dependence of results on the pigment crystal structure, and the chance of a direct estimation of the energy required for pigments comminution. On the other hand, the need of a direct measurement of the Rittinger's constant *K* and exponent *f(x)* still represents a challenging issue. Further relevant parameters to be considered during comminution of ceramic pigments encompass the feed size (starting particle diameter) and the evolution of particle size and shape, for increasing milling time, that can reveal the onset of agglomeration phenomena (which mechanism is not fully understood). In addition, type and amounts of additives (dispersant, block copolymers, etc.), grinding media, chamber mill dimension and rotation speed introduce variables that influence the comminution process. These aspects are only partially known and need to be furtherly investigated.

4.3. Colorant interaction with ink carriers

Colorants interact with the carrier and the additives in the various stages of the ink life: micronization, storage, inkjet application on the tile surface, drying and firing. Although, in principle, chemical reactions between the colorant and the organic components should be negligible, there are evidences of some interactions occurring mainly during long time storage and fast firing.

A prolonged contact of some effects (glazes and glassy coatings) with the carrier may turn into a partial solubilization, depending on the type (water, polar and non-polar organic media), pH, etc. Available data for the $CoAl_2O_4$ pigment point to high ion concentration (>800 $mg \cdot dm^{-3}$) in diethylene glycol, while the dissolution was less significant in aqueous medium [89].

The organic components of the ink deposited on the tile surface undergo a rapid thermal decomposition once entering the first module of roller kiln, where temperatures can be as high as 300 to 500°C. In these shocking conditions, organic compounds can be stripped by the water vapor stream coming out from tiles. Otherwise, they can undergo pyrolysis or combustion under the effect of the hot flue gases flowing from the heating zone of the roller kiln [90,91]. There are clues that the formation of the different organic by-products during combustion, pyrolysis or stripping are affected also by a sort of catalytic action attributable to the pigment present in the ink.

5. Suitability of colorants in the different ceramic technologies

In this section, the suitability of colorants in the various decoration technologies used in ceramic tile-making is overviewed by taking into account different issues: technological behavior, cost, and possible health hazards. The technological performance is considered under various viewpoints: chemical stability during firing, color saturation and purity, and behavior during micronization.

Along with pigments, dyes, and effects currently utilized by the ceramic tile industry, this analysis is extended to colorants under development that were proposed for ceramic applications in the literature. Reference to the Colour Index (C.I., by the Society of Dyers and Colourists) is given, when available. The list of candidate pigments and dyes is not exhaustive: only those with enough pieces of information on technological performance were included in the discussion.

For every colorant, the outcome is given for each decoration technology (as listed in Fig. 1): low temperature (LT), intermediate temperature (IT), high temperature (HT), unglazed body (BO), very high temperature (VHT), and digital decoration (DD). The verdict can be ‘suitable’ or ‘unsuitable’. If suitable, additional information is provided, as: currently in industrial use; no longer in use; never entered in use. If unsuitable, the main motive is indicated: technological reasons; insufficient tinctorial strength or color purity; possible environmental impact or health hazards; economic reasons (high cost of precursors).

Pigments and dyes are hereafter illustrated color by color. In few cases, the color definition is ambiguous (for instance, greenish yellow or yellowish green). As far as possible, it was followed the color attribution given in the literature, but sometimes the technological behavior (coloration in glaze) was in contrast. In this circumstance, technological data were plotted in the most appropriate color graph.

5.1. Red and purple colorants

There are no “universal” colorants able to impart red (or purple) shades with all the ceramic technologies. The rather wide array of colorants utilizable with the LT application turns to be progressively restricted with

IT, HT-VHT and BO applications (Fig. 13). The situation is critical in DD, where no frankly red colors can be achieved and burgundy to magenta and purple pigments are employed.

Malayaite doped with Cr is widely used, despite it suffers from some chemical instability in glazes that limits the maximum temperature attainable [92,93]. Control on burgundy color during synthesis is difficult, because different shades develop from relative abundance of multiple chromophores: octahedrally-coordinated Cr^{3+}, tetrahedrally-coordinated Cr^{4+}, and even some Cr^{5+} [94-96]. Color shades are also in accord with co-doping with La, Zn, Fe or Ti [37]. In addition, there is a strong influence of firing conditions and mineralizers on synthesis yield [97-99]. Overall, this pigment behaves best in glazes (typically T*~85 at 1100°C, T*~75 at 1200°C) – with several constraints (Table 5) – and is not suitable in bodies.

Colorant	Formula	Color	Application – Technology (see Fig. 1)				
			LT	IT	HT-VHT	BO	DD
Cassius' purple	Au	magenta RED 109	■	□ 3	□ 3	⊡	⊡
Malayaite	$Ca(Sn,Cr)(Si,Cr)O_5$	burgundy RED 233	■	■	■	⊘ 1	■
Pyrochlore	$Y_2(Sn,Cr)_2O_7$	burgundy not filed	⊘ 3 4	⊘ 3 4	⊘ 3 4	⊘ 3 4	⊘ 3 4
Cadmoselite	$ZrSiO_4[Cd(Se,S)]$	red RED108	■	■	■	⊘ 3	⊘ 1 2
Perovskite	$Y(Al,Cr)O_3$	red not filed	⊡	⊘ 1	■	⊡	⊘ 1
Hematite *(in zircon)*	$ZrSiO_4[Fe_2O_3]$	coral pink RED 232	■	■	⊡	⊡	⊘ 1
Hematite *(in silica)*	$SiO_2[Fe_2O_3]$	coral pink not filed	⊘ 1	⊘ 1	⊘ 1	■	⊘ 1
Corundum	$(Al,Mn)_2O_3$	pink RED 231	■	⊡	⊡	■	⊘ 4
Corundum	$(Al,Cr)_2O_3$	pink RED 230	■	⊡	⊡	⊘ 4	⊘ 4
Spinel	$Zn(Al,Cr)_2O_4$	pink RED 235	■	⊡	⊡	⊘ 1	⊘ 4
Cassiterite	$(Sn,Cr)O_2[CrO_2]$	purple RED 236	■	■	■	⊘ 3	⊡

Fig. 13. Technological properties of industrial red to purple ceramic pigments and dyes. Symbols: widely used (■); limited use (⊡); no longer in use (□); not entered in use (⊘). Unsuitable because of: technological behavior (1), health hazard (2), cost (3), color saturation and purity (4).

Purple of Cassius has a high potential as red pigment, due to an intense plasmonic band of gold nanoparticles (T*~80 at 1150°C). These are rather stable in most applications, even if the highest temperatures the magenta-red color turns into brown [100-102]. There are various synthesis procedures, including soluble salts [103] and ceramic inks [104,105]. The main hindrance is the very high cost, even if the red color can be achieved with diluted concentrations, connected with the growing price of gold. To overcome this limitation, Ag-Au alloys were industrially developed, but never used because the color has a strong yellowish shade [106,107].

Cassiterite doped with Cr was a pigment with a marginal importance in the conventional technologies that has been revitalized by the advent of digital decoration, even though handicapped by the high cost of tin oxide. It bestows a peculiar violet color on glazes (T*~60 at 1200°C) likely originated by a unique combination of different chromophores [95,96]. Color shades are achieved with further dopants (Co, Ce). For as concerns the synthesis, since the traditional ceramic one can cause serious environmental and health problems due to the formation of carcinogenic Cr^{6+} during the process, a wet method can be preferred. This

low temperature synthesis limits the Cr oxidation [108-111]. It has a fair stability in glazes [37] and rather good performance in DD.

Cadmoselite-greenockite solid solution, encapsulated in zircon, provides an unrivalled red color that is the reference colorant for all applications in glazes (90<T*<100 at 1200°C). Its stability is satisfactory, if encapsulation is complete, in all matrices but low viscosity glazes [37,112]. The synthesis is complex: the sulfo-selenide seeds must be incorporated in the silicate mass and preserved during formation of zircon [113]. Its utilization in DD is problematic, because micronization can break the encapsulation, leading to chemical attack of the pigment by glaze. However, some application was recently attempted by reducing the particle size prior micronization. A major issue is the high toxicity of cadmium and selenium that imposes a standard control on Cd release from finished ceramic products [114].

Hematite encapsulated in zircon can be used in all technologies but DD, because micronization causes the rupture of the protective envelope made of zircon. Nevertheless, it is mainly addressed to mass-stone and is the reference red pigment in BO application [115]. It has a characteristic pink coral hue (Fig. 14) that turns redder in Zn-bearing matrices (80<T*<90 at 1200°C). Encapsulation is a complex process depending on several variables, not straightforward to control, that was investigated in depth [116-121].

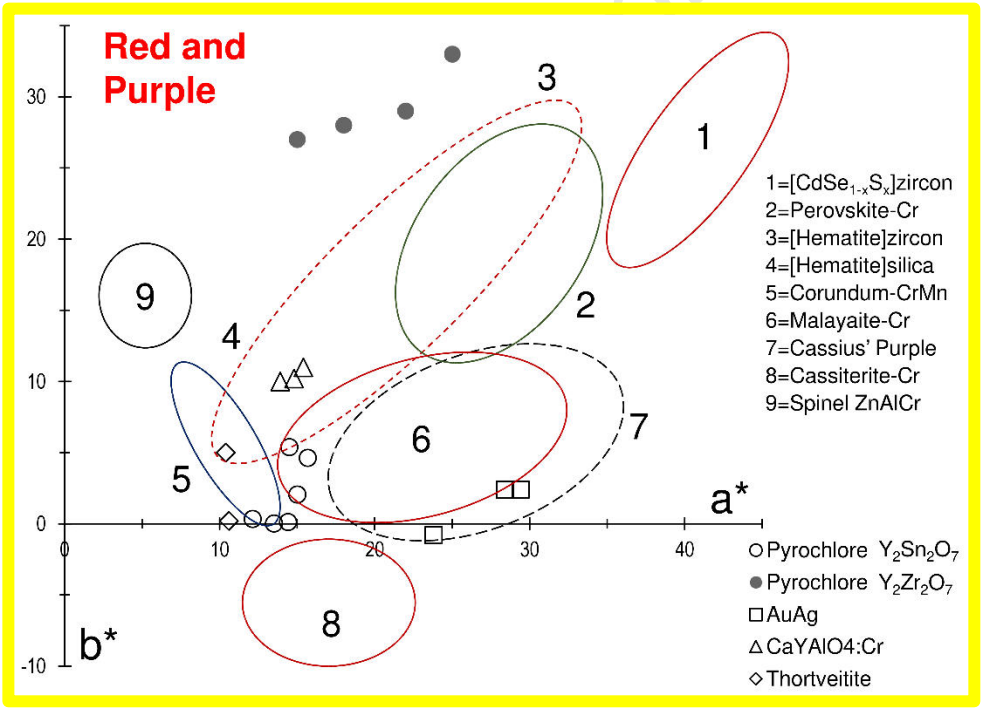

Fig. 14. Red and purple colors in glaze, plotted on the a*-b* plane (CIE-L*a*b*). Numbered fields represent the main industrial colorants, while symbols refer to colorants proposed in the literature but not entered in use yet.

Hematite encapsulated in silica presents analogies with the previous pigment: it has a pink color as well, but less performing in glazes (80<T*<88 at 1100°C) to the point it is used essentially in BO applications (60<T*<78 at 1200°C). A natural analogue is the *Grès de Thiviers* [122-123]. Its synthesis appears to be easier that the hematite-zircon encapsulation and seems possible by various routes [124-130]. It cannot be used in DD.

Yttrium-aluminium perovskite doped with Cr is the most recent ceramic pigment added to the industrial palette [131,132]. It exhibits a red color stemming from Cr^{3+}-Ca^{2+} pairs, where calcium can be substituted by other impurities coming from mineralizers, like Mg [17,132,133]. Its synthesis is not straightforward, because

of the crucial role played by mineralizers [131,134-136]. It is stable particularly in HT glazes (80<T*<90 at 1200°C) where it takes advantage by the high content of Ca and Al in these matrices [37,137]. No information exists about its performance in DD, where the high cost of yttrium represents a notable hindrance. Reddish perovskites have been synthesized also with lanthanides (e.g., La, Nd) and with mixed chromophores (Cr+Fe) but coloration is worse [138-140].

Corundum doped with Cr and/or Mn is the basis of two classic rose pigments, rather stable in most applications [141]. Now $(Al,Cr)_2O_3$ is utilized essentially for LT-IT (52<T*<62 at 1140°C) while $(Al,Mn)_2O_3$ for BO (60<T*<70 at 1200°C). Color stems from transitions due to the high crystal field of Cr^{3+} or Mn^{3+} in the Al site [142,143]. Color variants are obtained by co-doping Mn with Ca or P [37]. Not used in DD, both not suitable for quadrichromy and cost of micronization (due to its hardness). Easy synthesis by solid state, possible also in absence of mineralizers [144], and by mechanosynthesis [145].

Gahnite doped with Cr is another classic rose pigment [2,146]. $ZnAl_2O_4$ is a common phase in zinc-rich glazes, and the pigment is rather stable in all applications. Its synthesis is quite easy, in presence of borate mineralizers [37]. This spinel has been developed in many variants, with Mg, Fe, Ni, Cr, as co-dopants [147-149]. It is still used in LT (50<T*<60 at 1050°C) since its incompatibility with B, Ca, Mg and Ba precludes applications at higher temperatures. Peculiar colors – peach to salmon pink (Fig. 14) – are obtained and tend to exhibit some degree of metamerism [37].

There is a set of red and purple pigments not entered in the industrial practice, along with colorants used in the past but now completely abandoned. Modern production does not employ crocoite ($PbCrO_4$) or further chromate pigments. **Pyrochlore** $Y_2Sn_2O_7$ doped with Cr was developed as a burgundy to brown pigment [150,151]. Its color (60<T*<70 at 1080°C) is similar to the less intense shades of malayaite-Cr (Fig. 14) and similarly stems from multiple chromophores (Cr^{3+} and Cr^{4+} in octahedral coordination). Synthesis is complicated by an uneasy control on accessory phases [150,152]. Although stable in the main applications, it is handicapped by a higher cost and worse color with respect to industrial colorants. Other pyrochlores were investigated, as reddish brown $Y_2Ti_2O_7$ doped with Cr [152] and pink $Er_2(Zr,Ti)_2O_7$ doped with Cr [153,154] or $Y_2Zr_2O_7$ co-doped with Cr and Pr [155]. They all suffer from an insufficient tinctorial strength, most of all for as concerns pink $Er_2Ti_2O_7$ doped with Cr, which if prepared by solid-state synthesis presents a very pale pink shade whatever the temperature; otherwise, if prepared by sol-gel method shows an intense pink coloration when calcinated at 700°C [153]. The color stability significantly diminishes above this temperature, unless the sample contains zirconium, which stabilizes the fluorite structure and ensures a color intensity also at higher calcination temperature [154].

Further proposals include **$CaYAlO_4$ doped with Cr** that exhibits pink shades (55<T*<60 at 1050°C) comparable to the weakest achieved with encapsulated hematite (Fig. 14). Color stems from Cr^{3+} and Cr^{4+} in a distorted octahedral site [156] and its stability was tested at 1050°C in transparent frit (Ca-Zn-B). **Hematite encapsulated in zirconia** [128] proved to be stable in LT applications (T*~77 at 980°C). Lilac colors were developed exploiting **$(Ba,Sr)Zn_2Si_2O_7$** and **$BaMg_2Si_2O_7$** with melilite structure: color is originated by Ni^{2+} in tetrahedral coordination [157,158]; their thermal stability was not tested yet. Purple dyes were obtained by $(Mn,Mg)_2P_2O_7$ solid solutions with **thortveitite** structure. Once thortveitite breaks down during firing, manganese is released to the glaze, which turns colored (50<T*<65 at 1080°C) by the effect of Mn^{3+} ion dissolved in the glassy phase [159]. Another dye consisting of **Co phosphate** was described as purple, but final coloration in glaze is blue [160,161].

5.2. Yellow and orange colorants

There is a limited number of yellow colorants utilized in IT and HT-VHT applications that increases considerably once LT is concerned (Fig. 15). Only yellow zircon is employed in BO and DD technologies, that makes it a "universal" pigment used in all the ceramic technologies. Mass-stone represents the main demand for orange colorants, mostly satisfied by rutile pigments, sometimes utilized in DD too.

Zircon doped with Pr provides a bright yellow (typically 60<T*<80 at 1100-1200°C) due to Pr^{4+} incorporated at the Zr site [162-164]. Developed also with other dopants, like Tb^{4+} and Ce^{4+}, but not at the industrial level [165-167]. Its synthesis is not straightforward, as solid, liquid and gas states are involved [168,169], with an important role played by mineralizers and calcination conditions [164,168-172]. It is highly stable in all applications, especially in Zr-rich and Zn-rich coatings [37]. Nevertheless, it is less performing in DD, due to detrimental effect of micronization on color, thus sometimes associated to other yellow or buff pigments [10,49].

Colorant	Formula	Color	Application – Technology (see Fig. 1)									
			LT		IT		HT-VHT		BO		DD	
Zircon	$(Zr,Pr)SiO_4$	yellow YELLOW 159	■		■		■		■		■	
Rutile	$(Ti,Ni,Sb)O_2$	yellow YELLOW 53	◙		☒	1 2	☒	1 2	☒	2	☒	1 2
Greenockite	$ZrSiO_4[CdS]$	yellow YELLOW 35	■		■		◙		☒	3	☒	1 2
Srilankite	$Zr(Ti,Sn,V,In)O_4$	yellow not filed	☒	3	☒	3	☒	3	☒	3	☒	?
Perovskite	$Sr(Sn,V)O_3$ $Ba(Sn,Tb)O_3$	yellow not filed	☒	3	☒	1 3	☒	1 3	☒	1 3	☒	1 3
Baddeleyite	$ZrO_2[V_2O_5]$	yellow YELLOW 160	■		■		■		☒	1 3	☒	1 4
Cassiterite	$(Sn,V)O_2[V_2O_5]$	yellow YELLOW 158	■		□	3	□	3	☒	3	☒	1 4
Priderite	$Ba(Ti,Ni)_8O_{16}$	primrose YELLOW 157	◙		☒	1 4	☒	1 4	☒	1 4	☒	1 4
Pseudobrookite *(Karrooite)*	$Mg(Ti,V)_2O_5$	primrose not filed	☒	1 4	☒	1 4	☒	1 4	☒	1 4	☒	1 4
Pyrochlore	$Pb_2Sb_2O_7$	orange YELLOW 41	■		□	1 2	☒	1 2	☒	1 2	☒	1 2 4
Cerianite	$(Ce,Pr)O_2$	orange-pink not filed	☒	1 3	☒	1 3	☒	3	☒	3	☒	1
Rutile	$(Ti,Cr,Sb)O_2$	orange BROWN 24	■		☒	1	☒	1	■		☒	1
Rutile (*formed in situ*)	Cr+Sb-organomet and Ti-primer	orange not filed	☒	1 4	☒	1 4	☒	1 4	■		◙	

Fig. 15. Technological properties of industrial yellow to orange ceramic pigments and dyes. Symbols: widely used (■); limited use (◙); no longer in use (□); not entered in use (☒). Unsuitable because of: technological behavior (1), health hazard (2), cost (3), color saturation and purity (4).

Baddeleyite doped with V is a classic pigment with a characteristic yellow egg coloration (usually 40<T*<50 at 1100-1200°C) which can be tuned by doping with In, Y, Ti, or Al. Such a peculiar shade is related to the occurrence of tiny clusters of V^{5+} oxide included in ZrO_2 that makes it a sort of mordant pigment [173,174]. Its production is quite easy, also with alternatives to solid state synthesis [175-177]. The stability in glazes is generally good, but it is utilized especially in VHT applications [178]. Unsuitable for mass-stone (BO) because it tends to react with silica to form zircon. It is not used in DD, due to its color shade, not optimal in quadrichromy, and unsatisfactory tinctorial strength after micronization. Also, its high specific weight makes the ink more prone to pigment sedimentation.

Greenockite encapsulated in zircon provides a very brilliant yellow color (T*~90 at 1200°C). If encapsulation is complete and preserved during application, the stability in glazes is excellent [179]. As said for the analogous red pigment, the synthesis is complex. Indeed, in order to avoid the airtight container required by the ceramic method, the direct synthesis at low temperature by hydrothermal method is preferred. It entails the complex inclusion of cadmium sulfoselenide into a SiO_2-CeO_2 glassy phase, which have to be preserved during the zircon formation [113]. Since encapsulation is to some extent broken during micronization, it is not suitable for DD. A major issue is the high toxicity of cadmium, which imposes a standard control on Cd release from finished ceramic products [114].

Cassiterite doped with V is another classic among yellow colorants, but less used than baddeleyite [2], despite good tinctorial strength (typically 50<T*<75 at 1100-1200°C). The yellow color is originated by multiple chromophores, among which the dominating effect is by clusters of V^{5+} oxide included in tin oxide [2,180]. Co-doping with Ti and/or Al is a common practice to get color variants. Although still used in LT applications and sometimes in IT glazes, it is not employed in DD, as this pigment suffers from higher cost and worse tinctorial strength when compared to zircon-Pr. In addition, the high specific weight of tin oxide makes the ink more prone to sedimentation problems.

Rutile doped with Ni is a bright yellow pigment (commonly 50<T*<60 below 1150°C) needing a counterion that can be Sb, Nb, W or Mo [181,182]. Its synthesis is easy and can be performed also as solid solution with tin oxide [183,184]. It is employed more in other sectors than in ceramic production because of technological and safety issues. In fact, its stability is ensured only in LT applications, even though it would perform satisfactorily also in IT and as mass-stone. Nonetheless, the classification of nickel oxide as toxic and carcinogenic turned to be a major concern for pigment manufacturers.

Priderite doped with Ni is a traditional yellow pigment characterized by a peculiar primrose hue, not shown in Figure 16 [16,185]. Color is due to Ni^{2+} ion at one of the octahedral sites present in the hollandite-type structure [186]. The stability of $BaTi_8O_{17}$ in current glazes is limited, so the use of this pigment is restricted to some LT applications. As for rutile, the occurrence of nickel oxide is self-defeating, implying additional safety measures in the manufacturing cycle.

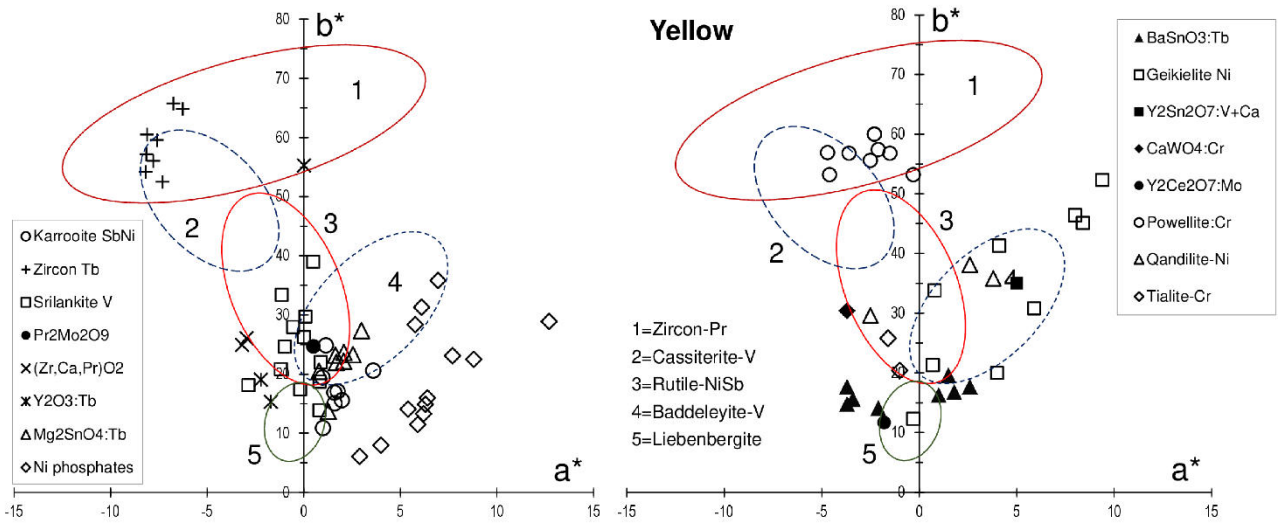

Fig. 16. Yellow colors in glaze, plotted on the a*-b* plane (CIE-L*a*b*). Numbered fields represent the main industrial colorants, while symbols refer to colorants proposed in the literature but not entered in use yet.

Srilankite doped with V gives a yellow color due to multiple chromophores: V^{4+} at a strongly distorted octahedral site, V^{4+}-V^{5+} intervalence charge transfer, and/or V-O charge transfer [178]. Its synthesis is not straightforward, as it needs the use of Al, In or Y, as counterions, and some Sn in substitution of Ti [187,188]. It is stable in most applications and exhibits a tinctorial strength (declining from T*~55 at 1000°C to T*~30 at 1200°C) midway from baddeleyite-V to zircon-Pr [178]. Although developed at industrial level, it had a very limited success, because of a worse benefit/cost ratio with respect to yellow zircon [188].

Rutile co-doped with Cr and Sb constitutes the reference pigment for orange colors (typically 60<T*<80 at 1100-1200°C). It can have Nb, Mo or Ta as counterion in replacement of Sb [189-191]. Synthesis is easy and can be performed in rotary furnaces [37]. Nonetheless, color stems from both crystal field (octahedrally-coordinated Cr^{3+}) and charge transfer (Cr-O) electronic transitions [181,182] that are affected by co-doping with Fe and Mn [37,192]. The color stability is good in LT and especially in BO applications, where it is largely used. Usually not employed in IT and HT glazes and not suitable for DD as primary pigment to be micronized. However, it is the pigment formed in-situ when soluble salts based on Ti-Cr-Sb organometallics are applied [104,193].

Pyrochlore $Pb_2Sb_2O_7$ (oxyplumboroméite) was widely used in the past, the so-called *Naples' yellow* [194], as an orange to yellow pigment, with color varying upon doping (Al, Ce, Fe, Sn, Zn). It is now completely abandoned by the ceramic industry for both technological and safety reasons. The former regard the poor thermal stability of the pigment, while the latter follow the ban of lead from modern ceramic manufacturing. This pigment is still used in some LT applications at level of craftsmanship.

There are other yellow and orange colorants proposed in the literature but never entered in the industrial use. For instance, **karrooite** doped with Ni or co-doped with Ni and Sb provides yellow to primrose shades (Fig. 16) rather stable in all applications (typically 30<T*<40 at 1100-1200°C) but DD [195,196]. Also, V doping was experimented, but it induces a complex structural rearrangement of karrooite crystal lattice, which implies a low purity of the final color, going from orange to buff [195]. For this reason, an employ for the V doping in the production of brown pigments with a T* ~80, is much more suggested [197].

Perovskites $SrSnO_3$ doped with V [198] or Cr and Tb [199], and $BaSnO_3$ doped with Tb [200] present pale yellow or light orange shades (Fig. 16). The color stability was tested at 1000-1050°C only with T* ~50 [199,200] or not verified at all [198].

Pyrochlore $Y_2Sn_2O_7$ co-doped with V and Ca [201,202] provides a yellow pigment (Fig. 16) that is stable only in double firing glazes at low temperature (T*~60 at 1000°C). The variants $Y_2Ti_2O_7$ [203] and $Dy_2Sn_2O_7$ [204] were proposed, also with V^{4+} as chromophore. In addition, lanthanide-based pyrochlores were investigated: $Y_2Ce_2O_7$ [205] and $Er_2Ce_2O_7$ [206] both doped with Mo. Such compounds have an orange color that revealed thermally instable even in a ceramic glaze at 1000°C. Their tinctorial strength is really too low (T*~30) to be taken into account as industrial pigment.

Geikielite $MgTiO_3$ doped with Ni requires high temperature for a successful calcination (i.e., 1400°C) and the synthesis is thermodynamically unfavored, leading to the co-existence of accessory phases [207]. This pigment shows a yellowish shade comparable to baddeleyite doped with V (Fig. 16) but is instable also in low temperature glazes (50<T*<70 at 1000-1050°C). In order to improve the synthesis yield and the stability of this pigment a core-shell structure (consisting of TiO_2 core and outer ilmenite $NiTiO_3$ shell) obtained through sol-precipitation method was tested. Anyway, the color stability in low temperature glazes (1000°C) has been only qualitatively evaluated [208].

Powellite, $CaMoO_4$ doped with Cr, is characterized by a bright yellow color comparable to zircon-Pr (Fig. 16). It has excellent performances, with optimum tinctorial strength most of all in LT and IT technologies ($75<T^*<80$ at 1000-1080°C), but good also in HT and BO applications (T^*~65). Synthesis is easy, since pigment is obtained by a solid solution of Cr^{6+} substituting Mo^{6+} in the powellite lattice. Despite that, this pigment releases Cr^{6+} when washed, implying a strong safety hazard [209]. A pigment based on scheelite, $CaWO_4$ doped with Cr, isostructural with powellite, has a less intense yellow coloration [205].

Yttria doped with Tb^{4+} provides a pale yellow color, which requires Ca^{2+} or Ba^{2+} as counterion to balance Y^{3+} [210]. However, its synthesis is complex, as it involves solid, liquid and gas states and demands high control on the pigment stoichiometry [210]. Tests of this yellow pigment in industrial glazes at 1080°C indicate a good stability of Ca and Ba co-doped $Y_{1.86}Tb_{0.14}O_3$ (T^*~65).

Zincite, i.e. ZnO doped with Co, Fe or V, was synthesized as a single phase with wurtzite structure that can give rise to different colors, depending on the dopant [211]. Nevertheless, to date, no tests on the pigments stability or tinctorial strength in glazes have been performed.

Rutile doped with Mo provides yellow to green tones, in accord with calcination temperatures. These compounds are characterized by low tinctorial strength already as calcinated powders (T^*~50) and also suffer from color instability in glazes at intermediate temperatures, with a resulting T^*~10 at 1165°C [212].

Orange colorants never entered in the industrial use consist essentially of cerianite and perovskite varieties.

Cerianite doped with Pr was extensively investigated and developed industrially, but its use is damped by high cost and specific weight of cerium oxide. The tinctorial strength is apparently good ($70<T^*<80$) but, in reality, tested in the 1000-1100°C range only [213,214]. Similar coloration is achieved by doping with Tb, while using mixed lanthanides or other dopants (Cr, Eu, In) ensued a $T^*<50$ [215]. Color can be tuned in various shades, at best resembling that of buff spinel and orange rutile. The synthesis of Pr-CeO_2, and to a lesser extent of Tb-CeO_2, has been profusely investigated in the last decade [216-218]: not only the classical ceramic method, but also by many non-conventional routes (*i.e.,* coprecipitation, flux method, combustion, pyrolysis, hydrothermal, microwave-assisted, and so forth). The results indicate that, opposite to the high temperature ceramic synthesis (1400-1500°C), the non-conventional way – especially the colloidal stabilization route with nitrates and the homogeneous coprecipitation route with oxalates and urea – allows to lower the calcination temperature down to 1100°C. Moreover, these methods enabled the formation of more homogeneous (single phase) solid solutions with optimal tinctorial strength in double-firing glaze (T^*~80 at 1050°C). In addition, Pr-CeO_2 embedded in glass-ceramics was proposed as an encapsulated pigment [219].

Pyrochlore $Y_2Zr_2O_7$ doped with Pr and Fe, provides an orange to reddish brown color [155]. The synthesis by polymeric sol-gel method at 1400°C produced a defective fluorite structure able to confer high stability to the colorant in IT applications ($68<T^*<88$ at 1080°C). As in the case of $Er_2(Zr,Ti)_2O_7$, the presence of Zr prevents the transition to an ordered pyrochlore structure with temperature, and allows to obtain an intense coloration of the pigment.

Finally, **gehlenite** $Ca_2Al_2SiO_7$ co-doped with Eu and Zn was proposed as an environment friendly yellow pigment [220].

5.3. Brown to maroon colorants

Brown and maroon colorants are important in ceramic decoration, because most graphics used in tile making are intended to reproduce natural surfaces, like stone, metal, skin and wood of various types, which have

commonly a large range of brown shades. In addition, they are generally cheaper than "pure" colors. This makes brown pigments a viable substitute in DD of yellow, black and particularly magenta colorants (Fig. 17). Many brown pigments are based on the spinel structure, taking **chromite** as an archetype, which brownish color stems from Cr^{3+} and Fe^{2+} at the octahedral and tetrahedral sites, respectively. Numerous variants are achieved by the addition of Al, Mn, Ni, and especially Zn to modulate chromatic coordinates. In fact, Zn^{2+} occupies the tetrahedral site, forcing out chromophores like Mn^{2+}, Fe^{2+}, Fe^{3+}, Co^{2+} or Ni^{2+}, hence increasing the light transmittance in the yellow to red window. This category includes natural chromite, that is suitable only for mass-stone [221-222], as well as **franklinite** (Zn-Mn-Cr) and **jacobsite** (Mn-Fe-Cr), which ensure different shades, from light brown to coffee [37,223-225]. Doping with Ni (and/or Co) leads toward **trevorite** compositions (Zn-Ni-Fe-Cr) that provide a distinctly darker brown [226,227]. They are used in all applications, including sometimes BO, with tinctorial strength 75<T*<90 at 1200°C (Fig. 17). Redder shades of brown are widely exploited in DD, where they can replace magenta, despite color does not fit what theoretically required by quadrichromy. Another strategy with spinel pigments is the joint substitution of Zn^{2+} (tetrahedral site) and Al^{3+} and/or Fe^{3+} (octahedral site) that leads to light brown colors, extending to pale yellow or buff, like the case of **zincochromite** (Zn-Fe-Al-Cr). These are stable in all applications, having care to have some zinc in the matrix, and are common ingredients of yellow inks, together with other pigments [228-231]. They are useless in mass-stone, since natural color of porcelain stoneware is a kind of light brown. Finally, dark brown is obtained by introducing Sn^{4+} and/or Ti^{4+} at the octahedral site and splitting Fe^{2+} in both four-fold and six-fold coordination in the inverse **ulvöspinel** pigment. Various shades are obtained by adding Cr, Al, and Zn [37], even though a careful control on synthesis is quite difficult. They are stable just in LT and IT applications [10,227].

Colorant	Formula	Color	Application – Technology (see Fig. 1)				
			LT	IT	HT-VHT	BO	DD
Spinel (*Zincochromite*)	$Zn(Fe,Cr)_2O_4$ $Zn(Fe,Al,Cr)_2O_4$	buff BROWN 33	■	■	■	⊘ 1	■
Cr soluble salt V soluble salt	Cr-organometallic V-organometallic	buff not filed	⊘ 1 4	⊘ 1 4	⊘ 1 4	■	⊙
Spinel (*Franklinite*)	$(Zn,Mn)(Cr,Mn)_2O_4$	brown not filed	⊙	⊙	⊙	⊘ 1	⊘ 1 4
Fe soluble salt Ni soluble salt	Fe-organometallic Ni-organometallic	brown not filed	⊘ 1 4	⊘ 1 4	⊘ 1 4	■	⊙
Perovskite	$Ca(Ti,Cr)O_3$	brown not filed	⊘ 1 4	⊘ 1 4	⊘ 1 4	⊘ 1 4	⊘ 1 4
Spinel (*Chromite*)	$Fe^{2+}Cr_2O_4$	brown BROWN 29	⊘ 1	⊘ 1	⊘ 1	⊙	⊘ 1 4
Hematite	$(Fe,Cr,Al)_2O_3$	maroon not filed	⊙	⊘ 1	⊘ 1	⊙	⊘ 1 4
Pseudobrookite	$Fe^{3+}{}_2TiO_5$ $(Fe^{3+},Al)_2TiO_5$	maroon BROWN 35-48	⊙	⊙	⊘ 1	⊘ 1	⊘ 1
Titanite Karrooite	$Ca(Ti,Cr)SiO_5$ $Mg(Ti,Cr)SiO_5$	maroon not filed	⊘ 1	⊘ 1	⊘ 1	⊘ 1	⊘ 1
Spinel (*Trevorite*)	$(Zn,Ni)(Fe,Cr)_2O_4$ $(Zn,Ni)Fe_2O_4$	maroon not filed	■	■	■	⊘ 1	■
Spinel (*Jacobsite*)	$(Mn,Fe)(Fe,Cr)_2O_4$	coffee BROWN 46	■	■	■	⊙	⊘ 1 4
Rutile	$(Ti,Cr,W)O_2$	tobacco YELLOW 163	⊙	⊘ 1	⊘ 1	■	⊘ 1
Rutile	$(Ti,Mn,Sb)O_2$	dark brown YELLOW 164	⊙	□ 1	⊘ 1	□ 1	⊘ 1
Perovskite	$LaFeO_3$	dark brown not filed	⊘ 1	⊘ 1	⊘ 1	⊘ 1	⊘ 1
Spinel (*Ulvöspinel*)	$Fe^{2+}{}_2TiO_4$	dark brown BLACK 12	□ 1	□ 1	⊘ 1	⊘ 1	⊘ 1

Fig. 17. Technological properties of industrial light brown to maroon ceramic pigments and dyes. Symbols: widely used (■); limited use (⊙); no longer in use (□); not entered in use (⊘). Unsuitable because of: technological behavior (1), health hazard (2), cost (3), color saturation and purity (4).

Rutile co-doped with Cr and W gives a characteristic tobacco brown, appreciated in mass-stone (70<T*<85 at 1200°C) but seldom used in LT to IT firing cycles [181,182,185]. It is formed in-situ once Ti-Cr-W organometallics are applied with the soluble salts technology [103]. It exhibits a technological behavior similar to the orange rutile co-doped with Sb. Another dark brown pigment, but less common in use, is based on the rutile structure by combining Mn with a counterion (usually Sb, but also Nb or W can be used). Finally, titania doped with Cr, but without a proper counterion, was investigated: its tinctorial strength is worse than the above described rutile pigments [232].

Hematite is a popular brown pigment, which can assume many shades according to Fe:Cr:Al ratios and further dopings [233,234]. On the other hand, various shades of pure hematite appear, mainly due to the variation in crystallinity, particle size, shape and degree of aggregation [235,236]. Thus, the colour of this pigment depends on synthesis route [236]. Hematite is not stable in glazes, but in LT schedules it shows an excellent tinctorial strength, typically 75<T*<95 at 850-1000°C [237]. It is sometimes employed in mass-stone, but largely replaced by hematite-zircon and hematite-silica encapsulated pigments.

Iron, Nickel and Vanadium organometallics are applied, as penetrating soluble salts, to get a set of colors going from light brown (V) to brown with greenish (Ni) or reddish (Fe) shades [103]. In Ti-rich bodies, color changes to a brownish gray (Ni and Fe) or a chestnut brown (V).

Pseudobrookite can be easily synthetized by conventional ceramic route at 1300°C, with titania in moderate excess of the Fe_2TiO_5 stoichiometry [238,239]. This pigment exhibits a peculiar, intensely brown coloration (Fig. 18) but its colouring performance depends on the chemico-physical properties of ceramic matrices: saturated brown shades achieved in low temperature glasses shift to a lighter brown in opacified glazes and fade to a light gray in wall tile glazes, where the high CaO and ZnO content contributes to rapidly dissolve pseudobrookite. Therefore, it is indicated in LT and IT applications (57<T*<63 at 1150°C).

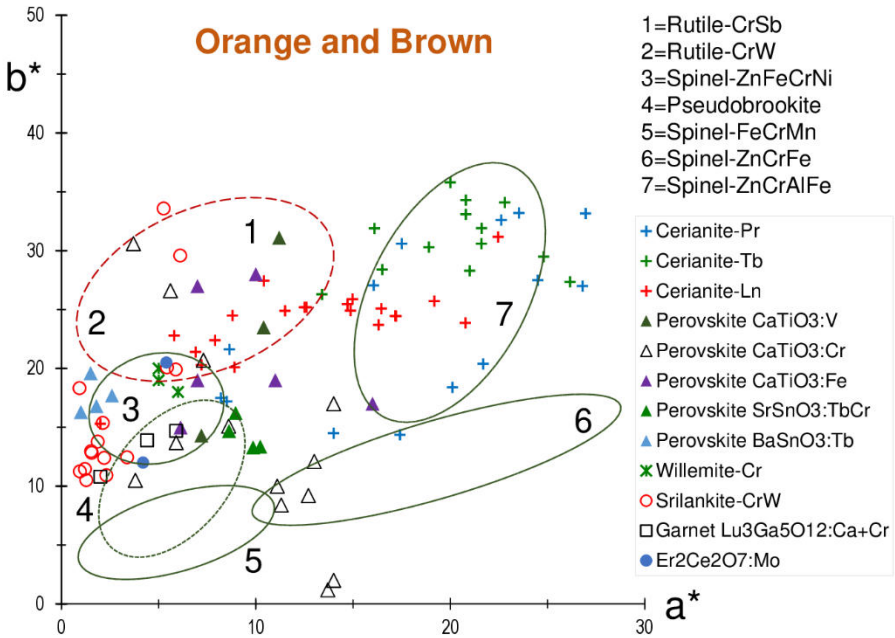

Fig. 18. Brown, maroon and orange colors in glaze, plotted on the a*-b* plane (CIE-L*a*b*). Numbered fields represent the main industrial colorants, while symbols refer to colorants proposed in the literature but not entered in use yet.

Maroon and brown pigments not entered in the industrial use encompass, among others, many perovskites.

Perovskite **$CaTiO_3$ doped with Cr** provides light brown pigment due to the partial substitution of Ti^{4+} with Cr^{4+} in octahedral coordination sites. The synthesis of this colorant is easy, the classical solid-state ceramic route with or without the employ of mineraliser [240-243]. Both the color shade (Fig. 18) and stability strictly depend on the Cr doping of $Ca(Cr_xTi_{1-x})O_3$, and on the chemical system of the glaze. It demostrated to be stable only with low Cr doping (x=0.04 mol) in SiO_2-B_2O_3-CaO glaze systems, with a relatively good color yield, T*~66 at 1050°C [242]. On the other hand, its technological behavior becomes totally instable in SiO_2-ZnO-CaO glazes: at low Cr concentration (x≤0.05) the nuance of the pigment turns pink in glaze (57<T*<71 at 1050°C); while at higher Cr doping the color in glaze turns green for the crystallization of chromates, which dissolving in the melt impart this peculiar coloration. The use of mineraliser, in order to avoid the chromates formation, can further affect the color stability in glazes, leading to blue shades [240].

Perovskite **$CaTiO_3$ doped with V** gives brownish-pink shades, comparable to orange rutile (Fig. 18), thanks to the partial substitution of Ti^{4+} with V^{5+} [244]. The colorant obtained by conventional ceramic route has a relatively good performance in SiO_2-CaO-ZnO ceramic glazes (T*~70 at 1050°C) for a solid solution limit near x=0.2. Higher amounts of vanadium crystallize $Ca_2V_2O_7$, which dilutes the real amount of saturated $Ca(V_xTi_{1-x})O_3$ and diminishes the colour intensity.

Perovskite **$CaZrO_3$ doped with Cr** presents a brown color (T*~50 at 1050°C) due to the substitution of Zr^{4+} by Cr^{4+} [245]. The pigment proved to be unstable already at 820°C in highly aggressive alkali-boro-fluoro-silicate glazes, with dissolution in the molten glass. At the same time, Cr^{4+} is reduced to Cr^{3+}, responsible for the green color of the glaze. In the same way, **lanthanium aluminate doped with Cr**, $La(Al,Cr)O_3$, decomposes in aggressive glazes at low temperatures, entailing a colour degradation [246]. Another perovskite-like compound was proposed: Er_6MoO_{12} with a light brown color [247], which proved to be stable in a LT glaze (T*~55 at 1070°C).

Rare earth orthoferrites with a general formula $LnFeO_3$, provide brown to orange pigments. The addition of Ln^{3+} ions to Fe_2O_3 induces a change in color of perovskite. In particular, La and Gd form pigments of sienna or orange color, while adding Lu, Tm and Yb a dark reddish brown is achieved. However, they were not yet tested in ceramic glazes [248,249].

$Lu_3Ga_5O_{12}$ garnet doped with Cr and Ca shows a brownish pink color comparable to some brown spinels (Fig. 18). The pigment is formed by a solid solution of Ca^{2+} and Cr^{4+} substituting for Lu^{3+} in the dodecahedral site of $(Ca_xCr_xLu_{3-2x})Ga_5O_{12}$ and can be easily obtained by a solid state synthesis. Tests in single firing glaze at 1085°C indicated a good stability of the pigment, but a low final tinctorial strength, 50<T*<60 at 1085°C [250]. Also, the gallium-gadolinium garnet ($Gd_3Ga_5O_{12}$) doped with Cr was investigated, but no information was disclosed about its color in glazes [251].

Titanite doped with Cr is the titanium equivalent of the Cr-doped malayaite pigment, but instead of a burgundy, its color is a reddish brown [252-254]. No data about its behavior in glazes are available.

$BaFe_2O_4$ gives a light orange-brown tint. The employ of a polymeric precursor method leads to a high crystallinity material, avoiding the formation of secondary phases, otherwise occurring in the traditional ceramic synthesis. Pigment can be evaluated for LT application, since it showed good stability in ceramic glaze at 1000°C, with T*~70 [255]. **$CaFe_2O_4$** and mostly **$MgFe_2O_4$** provide pigments with a darker brown color with respect to the $BaFe_2O_4$, but no tests on their stability in ceramic glaze are available to date [256,257].

Mg_2SnO_4 doped with Tb is an inverse spinel that shows a sandy yellow-buff color. The traditional ceramic synthesis is complicated by a difficult control on accessory phases [258]. Moreover, tests for LT applications

(Fig. 16) revealed a low tinctorial strength (T*~40 at 1000°C). **$Zn_7Sb_2O_{12}$ doped with Co** may exhibit different colors, depending on which site – tetrahedral or octahedral – Co^{2+} occupies in substitution of Zn^{2+}. Based on doping, it is possible to obtain a yellow to black pigment. However, its behavior in ceramic glazes has not been tested yet [259].

Hibonite doped with Cr, Fe or Mn provides many different rosy-brown shades. Various substitutions are in fact possible at the Al sites in the $CaAl_{12}O_{19}$ host lattice. When Fe^{3+} is used as a chromophore, the color changes from yellow to red brown to dark chocolate by increasing the doping. When Mn is used, the color varies from burlywood to saddle brown. In the case of Cr-containing samples, the color changes from light rosy brown to grayish green with increasing Cr. Despite the great variety of colors obtainable with a simple solid-solution synthesis, no test on their stability in ceramic glazes is available yet [260].

Celsian doped with Fe in subtitution of Ba gives rise to a brownish-pink color [261]. The solid-solution is based on metal-doped $BaAl_2Si_2O_8$ lattice – where Fe^{3+} is expected to replace Al^{3+} in tetrahedral coordination – and is obtained by the conventional ceramic method. The resulting pigment is chemically stable in classical double firing glaze, but with a too low T*~35 (1050°C).

$FeNbO_4$ encapsulated in zircon can provide different shades (yellowish brown to earthy yellow) as the content of $FeNbO_4$ increases with respect to zircon [262]. Control on synthesis is not straightforward, as for complications to arrange a proper encapsulation, as because ixiolite is trimorphic and a phase transition occurs at 1085°C [263]. Anyway, the color of the pigments is not so intense (T*≤60) and no data are available on their chemical stability and final tinctorial strength in ceramic glazes.

$TiCeO_4$ doped with Pr obtained by solid-state reactions, with the substitution of Ce by Pr, has a color going from light pink to maroon, depending on the concentration of praseodymium. The color intensity of the different solid solutions is quite good, but their stability in ceramic matrix has not been investigated yet [264].

Further brown pigments developed at the lab scale include **willemite**, Zn_2SiO_4 doped with Cr [250] and **tialite**, Al_2TiO_5 doped with Mn [265]; both display a buff color (Fig. 18) stable in LT-IT applications, more intense in tialite (60<T*<64 at 1050°C) than in willemite (40<T*<47 at 1080°C). In addition, **cubic zirconia** takes a light brown color (T*~40 at 1100°C) once co-doped with Ca and Pr [266].

Recently, a range of **light brown phosphate-vanadate dyes** was investigated. They are based on $(Mg,Ni)_2P_2O_7$ [267]; $Ni_3(P,V)_2O_8$ and $Ni2(P,V)_2O_7$ [268]; $(Al,Fe)(P,V)O_4$ [269]; $(Ni,Co)_2P_2O_7$ [270] solid solutions. Their tinctorial strength in LT glazes is in between 60 and 82 at 1065°C (Fig. 16).

5.4. Green colorants

There is no all-season green in the ceramic palette, because the purest colorants have a limited thermal stability, while the most robust pigment – utilizable in every application – gives a coloration midway from green to blue (Fig. 19). In addition, these colorants are now relegated to occasional use in digital decoration, since green is not a basic color in quadrichromy and only special sets for hexachromy include a green ink.

Eskolaite pigments impart rather dull green colors with variable shades, according to doping with Al and/or Fe. In principle, it is highly refractory but suffers from a certain reactivity during firing. It is the reference colorant for mass-stone (70<T*<80 at 1200°C) and is still used in LT and occasionally in IT, max ~1100°C [37]. However, its application in glazes is strongly constrained by the well-known incompatibility with Zn, Sn, and Ca [142,271,272]. Eskolaite is occasionally employed in DD as component of complex green inks.

Uvarovite, the so-called *Victoria green*, is based on $Ca_3Cr_2Si_2O_{12}$ garnet, possibly diluted with Al [273-276]. Unstable already in IT applications (unless in high calcium glazes) it provides the best color at LT (T*~70 at

1000°C). Its use is limited since decades, due to the hazards involved in solid-state synthesis, where $CaCrO_4$ forms and is responsible for high Cr^{6+} leaching in wastewaters [275].

Colorant	Formula	Color	Application – Technology (see Fig. 1)									
			LT		IT		HT-VHT		BO		DD	
Spinel	$CoCr_2O_4$	blue-green BLUE 36	■		■		■		⊘	1	■	
Eskolaite	$(Cr,Al)_2O_3$	green GREEN 17	⊡		□	1	⊘	1	■		⊘	1
Garnet (*Uvarovite*)	$Ca_3Cr_2(SiO_4)_3$	green GREEN 51	⊡		□	1 2	□	1 2	⊘	1 2	⊘	1 2
Co-Ti Spinel	Co_2TiO_4	green GREEN 50	⊡		□	1 3	⊘	1	⊘	1	⊘	1 4
Perovskite	$YCrO_3$	green not filed	⊘	3	⊘	1 3	⊘	1 3	⊘	3	⊘	1 4
Olivine (*Liebenbergite*)	Ni_2SiO_4	yellow-green not filed	⊡		⊘	2	⊘	1 2	⊘	1 2	⊘	2 4
Cr soluble salt Cu soluble salt	Cr-organometallic Cu-organometallic	green not filed	⊘	1 4	⊘	1 4	⊘	1 4	■		⊘	4

Fig. 19. Technological properties of industrial green ceramic pigments and dyes. Symbols: widely used (■); limited use (⊡); no longer in use (□); not entered in use (⊘). Unsuitable because of: technological behavior (1), health hazard (2), cost (3), color saturation and purity (4).

Gahnite doped with Cr is a classic light green pigment [2,16,277]. Color can be easily tuned by the Al:Cr ratio and possible addition of Co, Fe, Mg, Mn, Sn and Ti as co-dopants. Although rather stable in all applications, it is seldom utilized, because coloration achievable is less saturated than other green pigments (T*~85 at 1080°C).

Cochromite is a spinel based on $CoCr_2O_4$ with various shades, according to the degree of occupancy of Co^{2+} at the tetrahedral site and Cr^{3+} at the octahedral site, which can be replaced by Mg, Zn, Al and Fe to get greenish blue to bluish green [37,278,279]. It has an excellent stability in glazes, but in Zn-rich ones (75<T*<80 at 1200°C); in bodies, its performance (65<T*<80 at 1200°C) in less satisfactory [37]. Sometimes used in DD, where the main hindrances are the cost (due to high amount of cobalt) and its hue far away from requirements of quadrichromy [10,280].

Green dyes are utilized exclusively as penetrating soluble salts in BO applications. Resulting colors vary from dark green-olive, based on Cr organometallics, to pale green-buff with Cu organometallics [103].

Liebenbergite, the nickel olivine Ni_2SiO_4, bestows a greenish yellow shade (Fig. 16) on LT glazes with fair tinctorial strength: 60<T*<75 at 1050°C [281,282]. It behaves likely as a dye: the color should derive from Ni^{2+} in multiple coordination (five-fold and six-fold) in the glass network. This colorant is not suited for DD and commonly not employed in IT and HT applications, mainly because of its high content of nickel (that makes it a hazardous material) and its color not pure.

Cobalt titanate is a green pigment with grayish-blue shades, based on the inverse spinel Co_2TiO_4. Although known at the industrial level, it has a poor technological performance (Fig. 19). Its use in LT technology, however, is tackled by high cost due to the amount of cobalt oxide [37].

There is a good number of green colorants not entered in the industrial practice yet.

$YCrO_3$ perovskite has an intense green color and a good performance in BO and LT, comparable with industrial pigments, but it is more expensive for the high yttria content [133,283,284].

Given by its stability at high temperatures and low thermal expansion coefficient, the **tialite** Al_2TiO_5 structure can be used for pigments production. The presence of metal cations into the two highly distorted octahedral sites inhibits the thermal decomposition of pure tialite and leads to the chromatic properties of pigment. The color is pale ($40<T^*<55$ at 1050-1200°C) and may vary from green (Fig. 20) to greenish yellow (Fig. 16) passing from Co to Cr doping, respectively [265,285,286].

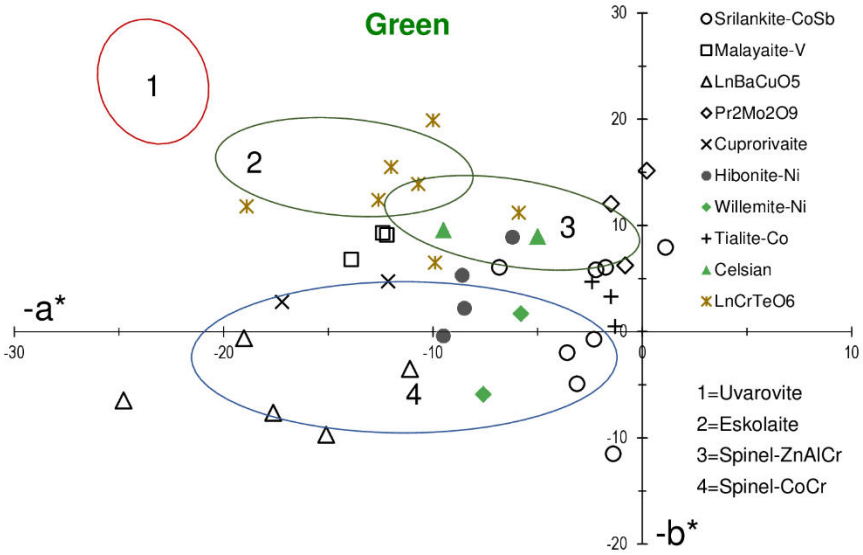

Fig. 20. Green colors in glaze, plotted on the a*-b* plane (CIE-L*a*b*). Numbered fields represent the main industrial colorants, while symbols refer to colorants proposed in the literature but not entered in use yet.

A less-pollutant and less-expensive alternative green pigment may be **karroite**, Co-doped $MgTi_2O_5$, an allochromatic solid solution for LT-IT applications [195,196]. This pigment exhibits a varied gamut of yellowish-green colors, showing a $55<T^*<70$ for calcined at 1200°C (Co molar content: 0–0.4). In glazes, a more turquoise coloration is developed, with a higher chromatic stability in Ca and Zn rich glasses [287].

Cr-doped $Y_2Ti_2O_7$ and $Y_2Sn_2O_7$ **pyrochlores** show rather similar optical properties. Given by the limited chromium solubility into the structure, any doping beyond 0.06-0.07 Cr atom/formula unit leads to green pigments with red shades, due to the presence of Cr^{4+} in the octahedral site of pyrochlore and of Cr^{3+} in the ternary perovskite side phase [152].

A wet chemical route – like Pechini, solution combustion or coprecipitation – can be used for the production of **zincite** doped at a molecular level [211,288-290]. The presence of Co or Fe into the flattened tetrahedral site, instead of zinc cations, determines a change in pigment color from greenish to yellowish, with a tinctorial strength of about 75 for 0.3 Co^{2+} molar content. In case of coprecipitation method, the solution pH and the precipitation agent nature can affect importantly the chromatic properties of the calcined pigment. In particular, the increase of pH from 7 to 10 by ammonia addition leads to an increase of both a* (i.e. from -16 to -8) and tinctorial strength (i.e. from 45 to 62). Similarly, the color changes from bright green to dark green by increase of calcination temperature (from 950 to 1200°C). The coprecipitated pigments can show high near-infrared reflectance, making them good candidates as cool pigments [288-290].

Yellow-green coloured pigments, with an intensity variation, can be obtained with **cuprates R_2BaCuO_5** (R = Y, Sm or Ho) having an ortorhombic structure, gettable by calcination (950-1050°C) or nitrate combustion. These superconducting ceramics contain isolated Cu^{2+} ions, interconnected by direct bonds through oxygen.

The colour, given by d-d electronic transitions, is a light green. For Y_2BaCuO_5 obtained by combustion synthesis, the formed aggregates show a brighter color given by their higher surface area. Cuprates show a certain instability and reactivity with the glaze. After firing in ceramic glazes in IT conditions, a light-green to turquoise color is developed (Fig. 20) that can vary as a function of glaze formulation (52<T*<72 at 1070°C), leading to an important bubble formation in unleaded matrix [291,292].

Zircon matrix can be used as hosting structure for Cr^{3+} or Co^{2+} ions to produce thermally stable green pigments by aereosol hydrolysis and further synthetic routes [293-295]. The addition of mineralisers is required for the Cr containing systems, to reduce calcination temperature (1500°C) and to limit metal volatilization. The color saturation of pigments is different for Cr (T*~43) and Co (T*~51), the latter showing a greener shade, quite constant between 1100 and 1300°C [293].

The tetragonal **neodymium silicate** $Nd_2Si_2O_7$ can be prepared by the Pechini sol-gel method and subsequent thermal treatment. The addition of LiCl reduces the required calcination temperature (from 1300 to 1100°C), favoring the formation of the monoclinic structure, hence of a yellowish color. In glazes, the tinctorial strength goes from T*~53 at 1100°C toT*~45 at 1200°C [296].

$LnCrTeO_6$ has a structure AB_2O_6, with both A and B cations octahedrally coordinated to oxygen and Ln = La, Nd, Gd, Dy, Er, Tm or Yb. It can be used for a kind of “chromium green” for LT application (850-1000°C) having a color comparable to eskolaite (Fig. 20). Cr^{3+} in octahedral coordination acts as chromophore, leading to different shades that can be obtained by direct mixing of oxides and calcination at 1000°C. The colour changes from light to dark green passing from La to Yb, given by an increased crystal field splitting as a result of lattice parameters decreasing, maintaining the same colour shade also at high temperature. The presence of zincite must be controlled, given by its high reactivity with Cr. In presence of frits containing corrosive PbO, a dark green to yellowish hue is obtained. The coloration is rather intense (T*~80 at 1000°C) but thermal stability tested just for low temperatures [297].

For LT applications, also **$Pr_2Mo_2O_9$** can be used, where Pr is partially substituted by Ca in different amount. Synthesis was performed by both ceramic and wet nitrate routes [298]. The presence of Ca^{2+} instead of Pr^{3+} leads to a structural transition from cubic to monoclinic (when the Ca molar content is higher than 0.2) followed by a color change from green to yellow (25<T*<33 at 1050°C). The use of NaF as mineralizer results in a pale yellow that in glaze has just a greenish shadow (Figs. 16 and 20).

Co-Cr phosphates can be produced by simple calcination of precursors and addressed to IT applications. The increase of Co content implies a color change from yellowish green to bluish green [299]. Solid-state reaction can be exploited also to dope iron oxide **Fe_2O_3** by progressive sobstitution of Fe^{3+} with Sc^{3+}, obtaining a colour change from reddish to greenish yellow [300].

5.5. Blue and turquoise colorants

Blue color in ceramics is commonly obtained by Co^{2+} in tetrahedral coordination in both pigment and dyes [301]. In fact, cobalt ions tend to assume the four-fold coordination also in glazes and glasses [302,303]. This circumstance explains the large recourse to cobalt dyes for the ceramic decoration. Cobalt colorants are characterized by the best performance per molar concentration, leading to brilliant and intense hue already for concentration lower than 1 %wt/wt. Blue colorants gained importance with the advent of inkjet printing as their use turned from occasional (only when necessary to have blue shades) to systematic in any graphics, even when no blue color is present, because of quadrichromy rules (Fig. 21). However, given by raising cost and limited reserves, cobalt became a strategic raw material and the ceramic industry has difficulty in the

supply. Furthermore, cobalt shows toxic effects and is subjected to even more strictly environmental regulations. Cobalt appears to be hardly replaceable in order to achieve a deep blue coloration. Despite close to the cyan hue required by quadrichromy, turquoise pigments obtained with alternative chromophore, like V-doped zircon, are not used in DD.

Colorant	Formula	Color	Application – Technology (see Fig. 1)									
			LT		IT		HT-VHT		BO		DD	
Olivine	Co_2SiO_4	dark blue BLUE 73	■		■		■		⊙		■	
Sarcopside Lithiophylite	$Co_3(PO_4)_2$ $CoLiPO_4$	dark blue VIOLET 14+47	■		⊙		⊘	1	⊘	1	⊘	1
Suanite	$(Mg,Co)B_2O_5$	dark blue VIOLET 48	⊙		⊘	1	⊘	1	⊘	1	⊘	1
Co soluble salt	Co-organometallic	blue not filed	⊘	1 4	⊘	1 4	⊘	1 4	■		⊙	
Spinel	$CoAl_2O_4$ $(Zn,Co)Al_2O_4$	blue BLUE 28+72	■		■		■		■		■	
Willemite	$(Zn,Co)_2SiO_4$	blue BLUE 74	⊙		⊙		⊙		⊙		⊙	
Hardystonite	$Ca_2(Zn,Co)Al_2O_7$	blue not filed	⊘	3	⊘	3	⊘	1	⊘	1	⊘	1
Perovskite	$Y(Mn,In)O_3$	blue BLUE 86	⊘	3	⊘	3	⊘	3	⊘	3	⊘	1 3
Zircon	$ZrSiO_4$:V	turquoise BLUE 71	■		■		■		■		⊘	1
Hibonite	$Ca(Al,Ni)_{12}O_{19}$	turquoise not filed	⊘	3	⊘	1	⊘	1	⊘	1	⊘	1

Fig. 21. Technological properties of industrial blue to turquoise ceramic pigments and dyes. Symbols: widely used (■); limited use (⊙); no longer in use (□); not entered in use (⊘). Unsuitable because of: technological behavior (1), health hazard (2), cost (3), color saturation and purity (4).

Cobalt olivine is the reference for ultramarine blue. It consists of Co_2SiO_4 doped with Mg or Zn to lower the cobalt consumption [303,304]. It plays as a dye, being completely dissolved in glazes, so the original violet shade turns into a deep blue. It is widely used in glazes, in all the applications from LT to VHT ($90<T^*<100$ at 1200°C) but seldom as mass-stone (BO). This dye is the basic component of dark blue inks for DD [10].

Cobalt phosphates are quite popular blue dyes in LT and IT applications ($80<T^*<100$ at 1085°C). They are synthesized in crystalline form (sarcopside $Co_3(PO_4)_2$ and lithiophyllite $CoLiPO_4$ structures) but decompose during firing, releasing Co^{2+} in the glassy phase. Lithiophyllite is preferred because of the lower content of cobalt oxide. They are available in many variants, due to substitution of Co with Mg, Mn, Fe [305-308]. Magnesium borate is another blue dye, having the suanite $(Mg,Co)B_2O_5$ crystal structure, which behaves like phosphates during firing [2]. It is sometimes used in LT technology.

Cobalt organometallics are used in BO applications as penetrating soluble salts. They are based, as other cobalt dyes, on Co^{2+} ions dissolved in the glassy phase present in the porcelain stoneware bodies [103]. Color is a characteristic ultramarine blue, as for other dyes [101].

Cobalt aluminate spinel is the most important blue pigment, utilized in every application in glazes and bodies, and especially in DD [10,309]. Its color is purer than cobalt dyes and based on Co^{2+} at a regular tetrahedral site [301,303]. As $CoAl_2O_4$, it has a high tinctorial strength ($75<T^*<95$ at 1200°C) also in HT and BO applications [310]. There is a second pigment, $(Zn,Co)Al_2O_4$, which has similar technological properties ($70<T^*<80$ at 1200°C) but a distinctly greener shade (Fig. 22). Several variants are produced by doping with Cr, Fe, Ti and Zn to adjust hue and tinctorial strength [37,311]. It is a partially inverse spinel, implying that a

small fraction of Co^{2+} is allocated at the octahedral site, depending on the cooling history [309]. This circumstance can explain color fluctuations in pigment production, since six-fold Co^{2+} provides a pink undertone. Available also in the encapsulated form [312]. A microemulsion-hydrothermal method can be used to obtain ultrafine pigments (~1 μm), reducing calcination temperature but increasing costs related to the synthesis [313].

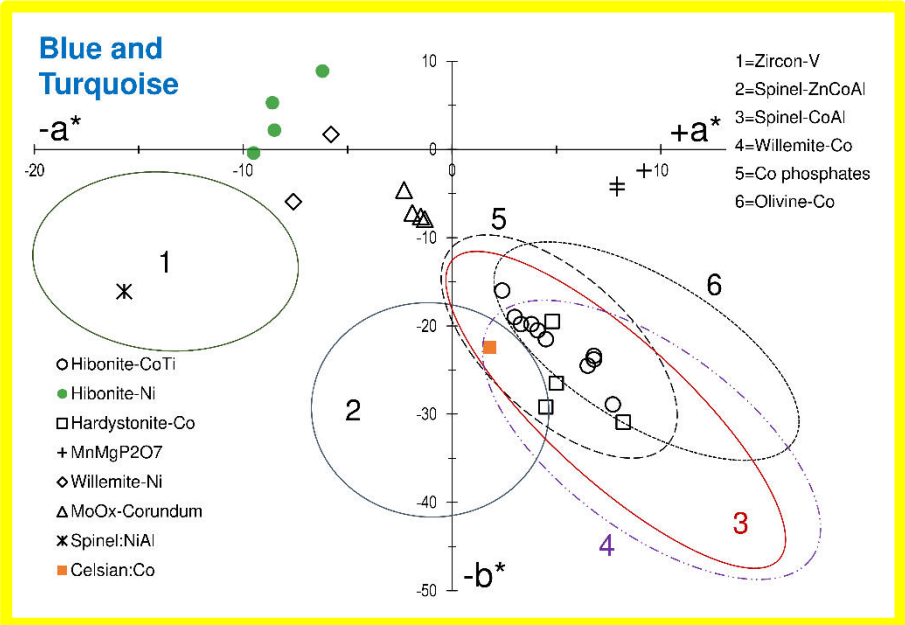

Fig. 22. Blue and turquoise colors in glaze, plotted on the a*-b* plane (CIE-L*a*b*). Numbered fields represent the main industrial colorants, while symbols refer to colorants proposed in the literature but not entered in use yet.

Willemite doped with Co is an alternative blue pigment, even though less stable than spinel [303,314-316]. The color intensity scales with the cobalt concentration in $(Zn,Co)_2SiO_4$. Despite the good color saturation ($90<T^*<100$ at 1100-1200°C) it is seldom used in all applications. It is present in some complex blue inks for DD, together with other blue colorants [10].

Zircon doped with V is the reference pigment for turquoise shades. Its color stems from V^{4+} clusters hosted at an interstitial site of the zircon structure [317]. This circumstance explains the well-known difficulties in control and reproducibility of the synthesis [318-320]. It is stable in glazes, where can be used from LT to VHT applications, and in BO as well, with $50<T^*<60$ at 1200°C [37,321]. However, it is not utilized in DD yet, because its tinctorial strength is considerably reduced by micronization [40,41].

There are further blue and turquoise colorants that never entered in use.

Hardystonite doped with Co exhibits a blue shade similar to Co-gahnite (Fig. 22) and a tinctorial strength analogous to many cobalt dyes (T^*~80 at 1150°C). It is stable in LT and IT firing cycles, but not in HT and BO, where it suffers from low-Ca glazes and bodies [322]. Not suitable in DD, likely because rapidly damaged during micronization. Another class of blue dyes based on calcium silicates is that of **clinopyroxenes**, where Co^{2+} can be accommodated at an octahedral site in substitution of Mg or Ca, giving rise to a violet color [323]. This phase is not stable in glazes and appears to be fully decomposed in IT to HT applications [324]. The chemical attack by the melt leads to the pyroxene breakdown and Co^{2+} ions diffusion, imparting a deep blue coloration and a tinctorial strength ($90<T^*<97$ at 1200°C) as good as other dyes.

Celsian doped with Co was recently proposed as blue pigment [261]. In principle, it should be thermally stable, since $BaAl_2Si_2O_8$ is occasionally present in Ba-rich glazes [29], but polyphasic samples were obtained, where celsian, hexacelsian and unidentified phases occur together. Spectral features clearly indicate a tetrahedrally-coordinated Co^{2+}, which is likely present in some unidentified phase. The hue approaches that of blue spinels (Fig. 22) while tinctorial strength is, at best, T*~65 at 1050°C [261].

Hibonite, $CaAl_{12}O_{19}$, has a magnetoplumbite-type structure, which can accommodate a wide variety of ions with different valences and coordinations, making it interesting to pigment production [325]. It is the presence of Co^{2+} at a non-centrosymmetric tetrahedral site that ensures the intense blue color, particularly when Ti^{4+} or Sn^{4+} are used as counterion to compensate the Co^{2+}-Al^{3+} charge mismatch. Pigments can be prepared by solid state reaction at 1350-1400°C, also with Co-containing wastes [326]. The most intense hue was obtained for pigments calcined at 1350°C with a Co molar content of 0.3. In BO application, the bluish color ($45<T^*<70$ at 1200°C) is similar to what obtained with willemite pigments (Fig. 22). On the contrary, in transparent glazes for IT production, chromatic differences are smaller, so suggesting that hibonite acts as a dye ($80<T^*<95$ at 1050°C) for a Co content $0.15<x<0.45$. **Hibonite doped with Ni** owes its color – a greenish shade of turquoise closer to cochromite (Fig. 20) than zircon-V (Fig. 22) – to Ni^{2+} at the tetrahedral site of the $CaAl_{12}O_{19}$ structure [327-329]. Apparently not stable in IT and HT glazes, it seems suitable only for LT ($42<T^*<47$ at 1050°C) or BO applications ($32<T^*<35$ at 1200°C) and was not considered for DD yet.

Turquoise shades can be imparted by using the nickel equivalent of known cobalt pigments, as the case of **spinel $NiAl_2O_4$** [330] and **willemite $(Zn,Ni)_2SiO_4$** [331,332] both exploiting a tetrahedrally-coordinated Ni^{2+}. However, while $NiAl_2O_4$ has a color similar to zircon-V, willemite-Ni approaches hibonite-Ni (Fig. 22). The calcination temperature modifies the colour by affecting both cations distribution at tedrahedral and octahedral sites and segregation of secondary phases, so limiting their applicability to LT. For instance, in nano-sized $Ni_xMg_{1-x}Al_2O_4$, different cation distribution and optical properties were found as a function of synthesis temperature and nickel content [333]. The higher is the calcination temperature, the greater is the degree of inversion in the spinel structure, with increasing Al^{3+} at the tetrahedral site and Ni^{2+} at the octahedral site. The resulting tetrahedral and octahedral splitting energies cause the change in the spectral absorption (T^* from 25 to 28 for $0.3<x<0.7$). Tinctorial strength at 1085°C is T*~60 for $NiAl_2O_4$ and T*~35 for Ni-willemite [330,331]. Anyway, the presence of nickel can involve safety problems related to its toxicity.

A further class of turquoise pigments derives from the ancient Egyptian blue, i.e. **cuprorivaite** $BaCuSi_4O_{10}$, where Cu^{2+} occurs at a 5-fold coordinated site [334,335]. Barium can be replaced by Ca leading to a darkening of the color [336]. However, once in glaze, it takes a green shade (Fig. 20).

Recently, a different blue chromophore was pointed out: Mn^{3+} in 6-fold coordination in the **$YInO_3$ perovskite** [337,338]. The incorporation of Mn^{3+} at the trigonal bipyramidal site of In^{3+} leads to an ultramarine blue color, given by d–d transitions (E′→A′). The blue hue is darkened by an increase of Mn content (Mn/Y molar ratio $5<x<20$). Colour is strongly influenced by glaze composition and firing temperature, fading away around 900°C in both B-containing glazes and plumbic frits [337]. This behavior severely restricts the end use to very low temperature applications. In any case, the industrial use is hindered by the prohibitive cost of indium and yttrium.

A blue colorant based on the **Y_2O_3-AlO_3-CoO** system was prepared by both solid-state reaction and mechanosynthesis [339]. The result is always multiphasic: YAP perovskite occurs admixed with spinel, YAG, YAM and yttria, in variable amounts depending on calcination temperature. The coloring performance is substantially related to the fraction of $CoAl_2O_4$ present in the mixture.

Amongst new **blue nanopigments**, the Al_2O_3/TiO_2 nanocomposite [340] and the spinel-like phase $Li_{1.33}Ti_{1.66}O_4$ [341] were both prepared by sol–gel methods. The former is doped by Co to obtain a blue colorant usable in DD technology. The color becomes more intense with the increase of Co^{2+} content, but is affected by the calcination temperature, with shift from blue to blue-green, thus limiting the pigment usage at LT and IT application [340]. The latter shows a bright turquoise color, attributed to Ti^{3+}-Ti^{4+} intervalence charge transfer, and a thermal stability up to 1000°C [341].

5.6. Black and gray colorants

In ceramics, black and gray are evaluated on a different basis with respect to other colors. Instead of a good tinctorial strength, the target is to have the lowest values of brightness and chroma. Therefore, the performance of black and gray colorants is assessed in the L*-C* diagram and not in the a*-b* plane.

There is a couple of universal black pigments that are industrially utilized in all the decoration technologies. In addition, few others are in use for BO or LT-IT applications (Fig. 23). In digital decoration, the black color is not used systematically, even if it is known its fundamental role to control the image quality in quadrichromy.

Colorant	Formula	Color	Application – Technology (see Fig. 1)									
			LT		IT		HT-VHT		BO		DD	
Spinel (*Nichromite*)	$(Ni,Fe)(Cr,Fe)_2O_4$ $(Ni,Co,Mn)(Cr,Fe)_2O_4$	black BLACK 30	■		■		■		⊙		■	
Spinel (*Cochromite*)	$(Co,Fe)(Cr,Fe)_2O_4$ $Co(Cr,Fe)_2O_4$	black BLACK 27-29	■		■		■		⊙		■	
Eskolaite-Hematite	$(Cr,Fe)_2O_3$	black not filed	⊙		□	1	□	1	■		⊘	1
Spinel (*Cuprospinel*)	$CuCr_2O_4$	black BLACK 28	⊙		⊘	1	⊘	1	⊘	1	⊘	1
Spinel (*Jacobsite*)	$(Mn,Fe)(Mn,Fe)_2O_4$	black BLACK 26	⊙		⊙		⊘	1	⊙		⊘	1 4
Perovskite	$LaCoO_3$	black not filed	⊘	1	⊘	1	⊘	1	⊘	1	⊘	1
Ru soluble salt	Ru-organometallic	black not filed	⊘	1 4	⊘	1 4	⊘	1 4	■		⊙	
Cassiterite	$(Sn,Sb)O_2$	gray BLACK 23	■		■		■		⊘	1 3	⊘	4
Co-Sn Spinel	Co_2SnO_4	gray BLUE 81	■		⊙		⊙		⊘	3	⊘	4
Bunsenite	(Ni,Co)O	gray BLACK 25	⊙		⊙		⊙		⊘	2	⊘	2 4
Rutile	$(Ti,V,Sb)O_2$	gray BLACK 24	■		□	1	⊘	1	⊘	1	⊘	1
Corundum	$Al_2O_3[MoO_x]$	gray not filed	⊘	3	⊘	1	⊘	1	⊘	3	⊘	4
Pd soluble salt	Pd-organometallic	gray not filed	⊘	1 4	⊘	1 4	⊘	1 4	⊙		⊘	1 4

Fig. 23. Technological properties of industrial black to gray ceramic pigments and dyes. Symbols: widely used (■); limited use (⊙); no longer in use (□); not entered in use (⊘). Unsuitable because of: technological behavior (1), health hazard (2), cost (3), color saturation and purity (4).

Among the best black colorants are **complex spinel compositions, based on cochromite** – also containing Fe and Mn – that are widely utilized in all decoration technologies, including inkjet printing, but rarely in bodies. A deep black color is achieved by the many optical bands due to multiple cations (Co^{2+}, Mn^{2+}, Mn^{3+}, Fe^{3+}, Cr^{3+} and sometimes Fe^{2+}, V^{3+}, Cu^{2+}) partitioned between the tetrahedral and octahedral sites [342-346]. The stability of these pigments is excellent, but in zinc-rich glazes, where they tend to

assume a brownish nuance. A variant of the previous pigment is another **complex spinel based on nichromite**, used in every decoration technology as well, even though specifically addressed to withstand in Zn-rich environments. The larger affinity between the Jahn-Teller inactive Zn^{2+} (d^{10}) and Co^{2+} (d^{7}) ions compared to the Jahn-Teller active Ni^{2+} (d^{8}) ion in chromite spinel, where the strong preference on Cr^{3+} in octahedron prevents Ni^{2+} to be displaced from fourfold to sixfold coordination, provides a possible explanation of the less attitude for Zn to diffuse into nichromite than cochromite lattice. It should be noted that, similar to cochromite, nichromite compositions usually encompass other ions, namely Ni-Fe-Mn-Cr, and occasionally Co-Cu-V and further elements. The complex interchange between these transition metal ions based on their different affinities related to their specific *d* orbitals configurations is likely to play a not fully clarified role on explanation of the above observation. The tinctorial strength is the best among black colorants [15,347-351]. Interestingly, nichromite pigments are characterized by C* on average lower than cochromite, even though L* values are fully comparable (Fig. 24). Further black spinels (e.g., binary Ni-Fe and Fe-Co or ternary Ni-Fe-Cr) exhibit higher L* values with respect to complex nichromite-cochromite formulations, but C* analogous to cochromite-based mixtures. At variance, the addition of Mg gives rise to dark gray pigments.

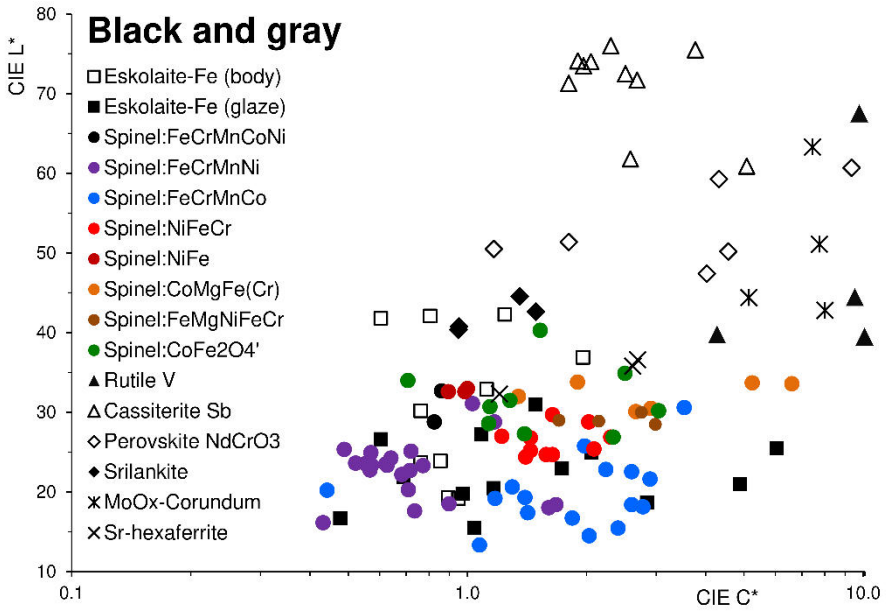

Fig. 24. Black and gray colors in glaze, plotted on the L*-C* plane (CIE-L*a*b*).

Another black pigment is **jacobsite**, i.e. a different solid solution of manganese and iron, which occur in multiple valences in both crystal sites of spinel [2], with respect to the brown variant in section 5.3. It is stable in LT-IT and BO applications, where is used because cheaper than complex black spinels, but unsuitable for porcelain stoneware glazes or digital decoration. A peculiar black pigment is **cuprospinel**, an antimagnet based on $CuCr_2O_4$ with limited doping from other metals [352]. It is stable just in LT and utilized when magnetic properties are needed.

Eskolaite-hematite is a well-known pigment that represents the reference black colorant for porcelain stoneware bodies [353,354]. Its stability in glazes and glassy coatings is limited, especially in presence of Zn, Ca, Ni, and Sn [37,355,356]. As the Cr_2O_3-Fe_2O_3 solid solution is complete, the pigment synthesis is

easy over a wide range of compositions [357], which can give rise to reddish or greenish nuances, depending on the Cr:Fe ratio [358].

Ruthenium organometallics are the dye present in penetrating soluble salts to achieve a black color [103].

No universal gray colorant is able to satisfy all the different requirements of ceramic decoration (Fig. 23). Some pigments are used in traditional techniques (LT, IT, HT) but not in mass-stone or digital decoration, along with technological reasons, because in these applications the gray color is easy to be reproduced dosing properly a black colorant.

Cassiterite SnO_2 doped with Sb is an appreciated gray pigment, available in various shades depending on co-doping with Mn, Ti and Si [37,359,360]. It is a well-known semiconductor: the color stems from electronic transitions due to additional energy levels in the band linked to Sb^{3+} ions. Its electrical conductivity was exploited for special applications, as anti-electrostatic glazes [361,362]. The main limit to its use is the high cost of tin oxide.

Bunsenite encapsulated in zircon was a popular gray pigment, rather stable in all applications but DD. Various shades can be obtained, depending on the Co:Ni ratio and co-doping by Al, Fe, Mn, and Zn [37]. A strong limitation is the toxicity and carcinogenicity of NiO, which likely discouraged the registration in the REACH. In addition, the risk of Ni^{2+} leaching to glazes and bodies, if encapsulation is broken, prevented any use by inkjet printing, which requires micronized pigments.

Cobalt stannate is a gray pigment, with more or less accentuated greenish-blue shades, based on the inverse spinel Co_2SnO_4 (or sometimes a Co-doped cassiterite). Color derives from Co^{2+} at both tetrahedral and octahedral sites, giving rise to blue and pink colors, respectively, and a complex outcome of this mix with a blue prevalence. At variance of cochromite, it is not stable in HT applications [37] and not suited for DD. Its use in LT technology is contrasted by the high cost related to the large percentage of cobalt oxide.

Palladium organometallics are sometimes used to get gray shades by means of penetrating soluble salts [103].

Rutile doped with V and a proper counterion (generally Sb or Nb) is a well-known gray pigment that can show different tones, from bluish to reddish as a function of co-doping [181,182,363]. Its stability is ensured only in LT applications.

Black colorants never entered in use encompass perovskite **$LaCoO_3$**, which applications are limited to LT-IT. Its dark colour is given by crystal field, intevalence and Co-O charge transfer transitions ensured by different oxidation states of cobalt (Co^{2+} and Co^{3+}). The substitution of La with Ca allows reducing the pigment cost without importantly changes is L*, a* and b* parameters [364].

Sr-hexaferrite, $SrFe_{12}O_{19}$, in principle considered for its magnetic properties, was investigated (as BO and HT) in porcelain stoneware bodies. The addition of Co, Mn, Ni or Fe improved the light absorbance at lower wavenumbers, but resulted always in polyphasic products, containg also hematite and/or magnetite [365]. The color in fired bodies and glazes is a dark gray (L*~35 and C*~2.7) with greenish shades (Fig. 24).

Great interest has been devoted in the latest years to carbon-based pigments, instead heavy metals based ones, in order to reduce toxicity. The target is **carbon encapsulated in zircon**, composed of two insoluble structures: a carbon core and a transparent zircon coating to prevent pigment oxidation [366-370]. Soft-wet chemical routes were used to realize encapsulation, either by covering the carbonous particles or by direct in-situ carbon formation. In-situ carbon provided by carbon-containing precursors favors a homogeneous encapsulation. Many variables must be controlled, among which C/Zr molar ratio, layer thickness and deposition order of zircon precursors, and calcination schedule strongly affect the quality of pigments. A

deep black can be obtained (down to L*~14) even though most literature data are in the 21<L*<42 range [370]. A particle size reduction brought about an undesired increase of L* that depends on synthesis parameters, which affect the final cover and pigment dimension. Correctly encapsulated pigments present an excellent color saturation (L*~34 and C*~0.9 at 900°C) in LT glazes [368].

An interesting candidate is **Al_2O_3-MoO_x**, a chemi-adsorbed pigment with a gray color and turquoise nuances (Fig. 22). Its peculiarity consists in clusters of molybdenum oxides that adhere on the corundum surface, where they are incorporated during calcination [371]. For this reason, high temperature annealing can cause a molybdenum volatilisation. Different valences (Mo^{4+}, Mo^{5+}, Mo^{6+}) contribute to a different extent to the final color, even if is the predominant Mo^{5+} the main responsible of the characteristic bluish gray. It displays a rather saturated color (60<T*<65 at 1200°C) in both HT and BO applications (Fig. 24).

5.7. White colorants

Opacifiers are extensively employed in all ceramic applications (Fig. 25) to get matt and semi matt glazes [2,372] as well as engobes [373] or white and “super white” porcelain stoneware bodies [37,374]. In contrast, the use of white inks is marginal in digital decoration [10]. White pigments have the basic role to mask the color of substrates by enhancing the light scattering [375]. For this purpose, a strict control on the amount, particle size and shape of white pigment is crucial [376,377] along with proper optical properties (see section 3.3). The final appearance may be dull to bright white, with a variable degree of translucency, and determined surface attributes (matt, semi matt, satin, translucent, etc). The color is usually evaluated by the CIE L* parameter (combined with a* and b* values as low as possible) or by the Kubelka-Munk formalism [39,378]. Opacifiers often fulfil additional functions, as damping the chemical attack to other pigments by saturation of the glaze (e.g., Zr^{4+} to improve the stability of Zr-colorants, see section 3.4). In other cases, white pigments are utilized to impart specific characteristics, like scratch resistance or anti-slip ability of ceramic surfaces [379].

Zirconium silicate, obtained by fine milling of natural zircon sands, is the most popular opacifier in all decoration techniques [380-382]. Its success stems from outstanding chemical stability in most ceramic matrices [383-387] and excellent optical properties (almost no light absorption in the visible spectrum, see Figure 7, joined to high refractive indices, Table 2). No significant interaction is known for $ZrSiO_4$ with other pigments [37]. In addition, it is able to improve the stability of Zr-bearing colorants, and rutile pigments as well (Table 5). The main limitation is a certain radioactivity [388] due to small amounts of U and Th in natural zircons (usually 50-100 $mg \cdot kg^{-1}$ each).

Baddeleyite is seldom utilized as opacifier in glazes, because it has good optical properties, but some disadvantages with respect to zirconium silicate [389]. ZrO_2 cannot be employed in mass-stone (zirconia reacts with silica to form zircon) or in digital inks (since they are micronized by zirconia microspheres, the milling yield is too low). In addition, more baddeleyite pigment is required to get the same whiteness, in force of its specific weight higher than zircon. Baddeleyite has a level of radioactivity analogous to zircon [388].

Pigment, Dye, Effect	Formula	Color	Application – Technology (see Fig. 1)									
			LT		IT		HT-VHT		BO		DD	
Zircon	$ZrSiO_4$	white not filed	⊙		■		■		■		■	
Cassiterite	SnO_2	white WHITE 15	■		□	3	⊘	3	⊘	3	⊘	3
Corundum	Al_2O_3	white,effect not filed	⊘	4	⊙		⊙		⊙		⊙	
Baddeleyite	ZrO_2	white,effect WHITE 12	⊙		⊙		⊙		⊘	1	⊘	1
Zr soluble salt	Zr-organometallic	white,effect not filed	⊘	1 4	⊘	1 4	⊘	1 4	⊙		⊙	
Rutile	TiO_2	white WHITE 6	⊙		⊘	1	⊘	1	□	3	⊘	1
Spinel	$MgAl_2O_4$	white not filed	⊘	4	⊘	4	⊘	4	⊘	3	⊘	4
Cerianite	CeO_2	effect(white) not filed	⊙		⊙		■		⊘	3	⊙	
Fe phosphates	$Fe_2Fe(P_2O_7)_2$ $NaFe_3(PO_4)_3$	metallic luster	■		■		□	1	⊘	1	⊘	1
Scheelite	$CaWO_4$	metallic luster	■		■		⊙		⊘	1	⊘	1
Hematite	Fe_2O_3	aventurine	⊙		■		■		⊘	1	⊘	1
Shcherbinaite	V_2O_5	sink effect	■		■		■		⊘	1	■	
Clinobisvanite	$BiVO_4$	sink effect YELLOW 184	■		■		■		⊘	1	■	
Mica (*coated by metal oxide*)	$KAl_3Si_3O_4(OH)_2$ @TiO_2 or Fe_2O_3	pearlescent luster	■		⊘	1	⊘	1	⊙		⊘	1
Titania slag	Ti-rich slag	speckle effect	⊙		⊘	1	⊘	1	⊙		⊘	1 4

Fig. 25. Technological properties of industrial white pigments (opacifiers) and some ceramic effects. Symbols: widely used (■); limited use (⊙); no longer in use (□); not entered in use (⊘). Unsuitable because of: technological behavior (1), health hazard (2), cost (3), color saturation and purity (4).

Cassiterite is a historical opacifier, widely used in ancient glazes [390,391]. SnO_2 exhibits the best optical characteristics for a white pigment: high refractive indices and negligible light absorbance in the visible range (Fig. 7). It has a good stability, ensured by its low solubility in ceramic glazes [392] and can be used to enhance the chemical resistance of tin-bearing pigments (malayaite, cassiterite doped with Cr, Sb or V). However, the occurrence of Sn^{4+} in the glaze is detrimental for eskolaite (green and black) and many spinel pigments [37]. Cassiterite is no longer used today, mainly because of its high cost (approximately 5 times that of zircon sand).

Corundum, although a common ingredient in ceramic frits, is seldom used as opacifier in glazes [393-395] but more frequently in engobes and "super white" bodies [37,374,396]. Its behavior is generally satisfactory in the various decoration techniques, and alumina is able to improve the chemical stability of many pigments (Table 5). However, the performance of α-Al_2O_3 as white pigment is lesser than other opacifiers in force of the low refractive indices (Table 2).

Zirconium, Cerium and Zinc organometallics provide the "white" color to the palette of soluble salts [103]. Although seldom employed in BO applications, their role has been revitalized by the chance to be used as white effect [397] or as primer in digital decoration.

Spinel $MgAl_2O_4$ is a white pigment proposed for glazes [398,399] where it never entered in use due to its low refractive index (Table 2). Nevertheless, it attracted the industrial interest for white-firing bodies, especially in times of zircon shortage [396]. Gahnite is a common component of Zn-rich glazes, as $ZnAl_2O_4$ and solid

solutions with $MgAl_2O_4$. However, it usually occurs as a crystalline phase formed during firing by reaction of Zn and Al present in frits and raw glazes. The direct use of gahnite as white pigment is not carried out in the industrial practice, even though proposed in the literature [400,401].

Rutile and **cerianite** – although employed by the ceramic industry in the past [402-404] – have nowadays a limited use as opacifier in glazes, despite their very high refractive indices [405]. The main limitation is their unsatisfactory color purity, due to absorption of some violet-blue wavelengths that results in yellowish nuances (Fig. 7). In some glaze compositions, both titania and ceria undergo a rapid crystal growth, incompatible with the opacifier function [406,407]. This tendency is otherwise exploited to get peculiar aesthetic effects, as described in the following section.

There are some opacifiers that found just a limited use in the industrial production. Andalusite, wollastonite, and diopside are sporadically added as white pigments to glazes or porcelain stoneware bodies [29,408-410]. Glass-ceramic frits (e.g., precipitating baghdadite, $Ca_3ZrSi_2O_9$) or even zincite are sometimes utilized in "super white" batches [411,412]. Sapphirine, $Mg_6Al_4Si_4O_{20}$, was proposed as opacifier in glazes [413].

5.8. Ceramic effects

The ceramic effects are used to impart peculiar optical, textural and functional properties to ceramic surfaces. Although utilized occasionally in LT, IT and HT applications, they have turned into a fundamental integration of quadrichromy (or hexachromy) in digital decoration. Recently, the pigment industry spent a considerable effort to search for new effects and develop proper suspensions for inkjet printing. This advancement is not mirrored in the scientific literature, where only few contributions deal with ceramic effects.

Account must be taken there is no classification of ceramic effects and no general agreement on criteria and terminology for their description. Therefore, the range of attributes that can be part of ceramic effects is rather wide, especially in the field of surface functionalization of ceramics. In the present review, we consider only the effects commonly utilized in ceramic manufacturing or candidates developed at least to the the industrial level (see some examples in Fig. 25).

The **gloss** or **matt** appearance, as bestowed on ceramic surfaces by inkjet decoration, is achieved by micronized transparent glasses or opacified glazes. These materials are formulated according to the conventional glaze technology, conveniently modified to account for the consequence of their small particle size. In fact, the firing behavior of micronized glazes is substantially changed in the kinetics of "melting", densification and crystallization, if any [414]. It is not disclosed which crystalline phases form in digital inks, among the ones known in ceramic glazes [28,415]. Further effects may be used to realize specific optical appearances (e.g., satin, transluscent) by tuning opportunely the amount and features of crystalline compounds and bubbles dispersed in the glaze [28,416]. In particular, translucency can be obtained by using BAS frits ($BaO\text{-}Al_2O_3\text{-}SiO_2$) that precipitate celsian, $BaAl_2Si_2O_8$ [411].

A classical way to realize a bas-relief pattern on the glaze surface is by a **sink** effect. It is achieved by applying low melting point compounds, typically based on V and Bi. The quintessential sink is vanadium pentoxide, but the incoming restrictions about V_2O_5 (connected with its toxicity and carcinogenity) have recently moved the industrial interest to bismuth vanadate, a well-known yellow colorant [417-420]. However, the color is lost on melting, leaving just the desired sink.

Lustre effects are pursued since antiquity [421] and for long time fulfilled by noble metal nanoparticles: Au, Pt, Ag, Cu [422-426]. Such applications are nowadays limited to third fire decoration of fine tableware. The metallic appearance on ceramic tiles is typically reproduced by surface precipitation of iron phosphate

crystals in appropriate glazes [427]. However, this lustre is difficult to be realized by DD and is characterized by a poor chemical and tribological resistance. Therefore, to overcome these limitations, new solutions were developed in recent years, based on cerianite CeO_2 [428], tenorite CuO [429], scheelite $CaWO_4$ [430], powellite $CaMoO_4$ [416] or even stainless steel and a NiCoCrAlY alloy [431]. Gold lustre can be simulated in LT (third fire) also using pearlescent pigments, like TiO_2-coated mica [432].

The **glittering** effect is since long time known in ceramic decoration and often referred to as *aventurine* [433]. The mechanism behind shimmering glazes was disclosed, consisting of tiny crystal inclusions preferencially oriented in a translucent matrix [434,435]. By this way, light reflection depends on the incident angle, giving rise to a form of goniochromatism [436]. Industrially, the aventurine effect in glazes is imparted through precipitation of hematite in properly designed glazes [435-439].

The creation of a casual **speckle** effect, now easily reproduced by digital decoration graphics, was easily obtained by applying on the glaze colored refractory minerals (e.g., chromite) or man-made colored grains, like titania slag [440].

Phosphorescent glazes have been realized for ceramic tiles by introducing a phosphor, like Eu^{2+}-doped $SrAl_2O_4$ [441-443]. The main challenge is twice: i) having a sufficiently long afterglow of a proper color, and ii) preserving the phosphor during firing from the chemical attack of glaze. Since efficient phosphors have a limited thermal stability, satisfactory solutions were developed for LT or at most IT firings, best as thrid fire applications.

Cool pigments are characterized by a high solar reflectance (300-2500 nm) combined with a high thermal emissivity (4000-40000 nm). They are employed to get solar-reflective surfaces, which represent an effective countermeasure to the Urban Heat Island effect [444]. To be suitable for ceramic applications, such pigments must fulfil all requirements listed at sections 3 and 4. For this reason, the attention has been initially focused on current industrial colorants [444-447]. Recently, new cool pigments were proposed, including: yellow chromium-doped scheelite [205]; cyan cobalt-doped celsian, magenta chromium-doped armalcolite, yellow nickel-geikielite, green $CrNdO_3$ perovskite [447]; iron and tungsten co-doped lanthanum cerium oxide [448]; red-orange Tb-Fe and Pr-Fe co-doped pyrochlore $Y_2Zr_2O_7$ [155,449].

The performance improvement of ceramic products attracted a remarkable industrial interest in the last decade. It has been primarily pursued by surface functionalization through application of functional films or addition of the active compounds to glazes and glassy coatings. Three are the main industrial achievements, amongst the many proposals: **scratch resistant surfaces** have been developed adding soluble salts providing zirconium [396] or titanium and silver [450]; or alternatively nanoparticles of aluminium and zirconium oxides [451]. **Self-cleaning surfaces** have been realized by exploiting the photocatalytic effect of titania nanoparticles [452,453]. Attempts to achieve photocatalytic surfaces in the usual manufacturing conditions were unsuccessful, because of the anatase to rutile transition and concurrent crystal growth during firing at high temperatures [454,455]. Thus, photocatalytic tiles are currently produced by a second fire at low temperature [454,456]. New pigments have been proposed in order to improve both the photocatalytic efficiency and activity under visible light irradiation: they consist of anatase doped with N [457], Nb [458], W [459], rare earths and transition metals [460] or composites of titania and silica [461] and silver [450,462-464]. **Antibacterial activity** has been basically pursued through the application of silver compounds on ceramic surfaces. The challenge is to have enough Ag^+ ions available in the long run, but both silver oxidation and incorporation into the glass network of glazes must be prevented. For this purpose, various composites were proposed: Ag-silica [465], Ag-ZnO [466], Ag-nepheline [467] or Ag with calcium

phosphate [468] as well as titania-coated silver nanoparticles [462-464]. However, the direct application of a thin film containing a sufficiently heat-resistant silver compound is at present preferred by the ceramic industry: e.g., Ag_2WO_4 [469], even though the best compromise of cost and performance was achieved with Nasicon-type solid solutions, like $(Na,Ag)Zr_2(PO_4)_3$ [470].

6. Lines of future research

The advent of digital decoration not only has revolutionized how pigments and dyes are manufactured and applied onto ceramic surfaces, but also the manner by which colorants are designed, formulated, and tested. Technological innovation brought about a groundbreaking change, both conceptual and practical, in the way colorant manufacturers conceive and carry out research and development activities.

From the conceptual point of view, the design of ceramic colorants underwent a paradigm shift, with emphasis moving to inks and related matters. This circumstance saw unexpected issues to stand out, such as the behavior of pigments during micronization or the interactions of colorants with organic carriers and additives, among others. At the same time, well-known aspects of decoration technology had to be reappraised at the light of the new characteristics of digital pigments and dyes. For instance, the relationship between color saturation and particle size of pigments, or the increased reactivity of micronized colorants in touch with glazes and glassy coatings. These questions have been magnified by the task to understand phenomena occurring at the scale of the ink drop, with all complications stemming from techniques used for color reproduction (quadrichromy typically plots four different ink drops on the same 64x64 µm target, with 400 dpi of native resolution).

In practice, the R&D laboratory was totally revamped, as new machinery and instrumentations are necessary to faithfully reproduce the industrial processes at the lab or pilot scale. This entails both ink-making (high-energy ball mill for micronization) and decoration (inkjet plotter to print test charts). Not to mention all techniques for ink characterization (including submicronic particle size, viscosity, surface tension) and measurement of the colorimetric coordinates on test charts. At the end of the day, the industry-academia distance increased a lot: before the digital decoration would take place, it was simple – in any ceramic laboratory – to simulate the manufacturing cycle of pigments and dyes. This because all the operations (solid-state synthesis in refractory crucibles, successive washing and milling, application by screen printing, spraying or pouring on ceramic substrates) could be run practically at the same scale of the industrial processes.

Notwithstanding the global diffusion of digital decoration in the ceramic tile industry (and its spreading through other ceramic and glass fields) not every technological question found a fully satisfactory answer yet. Further R&D efforts are necessary to overcome specific technological challenges of inkjet printing of pigments, dyes and effects. Hereafter, the main technological challenges still on the table are shortly reviewed, along with the evergreen issue of the search for new colorants. It is not an exhaustive list, but a summary of hot topics that can represent lines of future research. They pertain to the three pillars aimed at improving: the process efficiency, the performance of colorants, and the environmental sustainability.

Improving the efficiency of the ink-making process, from the colorant viewpoint, means essentially a better control on the micronization step. This task requires a deeper comprehension on the behavior of pigments and glasses during comminution, e.g. which mechanisms are active during high-energy milling in industrial conditions. Key points seem to be: i) the degree of pigment amorphization that is likely the cause of the loss of color saturation in digital inks; ii) the occurrence of plastic deformation and particle agglomeration

phenomena during milling of vitreous materials, which is probably behind the current high energy consumption and very low efficiency to get submicronic glazes.

The performance of digital colorants can be improved by various routes, even though R&D investments are now hindered by the low price of digital inks. Two main strategies can be envisaged to enhance the colorant stability in ceramic matrices: i) shielding the pigment from the chemical attack of glaze, or ii) weakening the chemical aggressiveness of glaze against the pigment. The shield option primarily consists in a protective coating applied on a high-performance pigment: the challenge is to go beyond current encapsulation techniques in order to have a proper core-shell structure with the particle size imposed by inkjet printing. The option to damp the glaze aggressiveness needs to understand in depth the mechanisms of decomposition which pigments undergo during firing. This is the only way to improve the dual approach followed in DD, now entirely empirical. On one hand, the pigment dissolution is minimized by an inert glass (the "protective coating") or a primer (able to "saturate" the glaze in some ingredients of the pigment) applied respectively after and prior inkjet decoration. On the other hand, undesired color shades, due to a given transition metal ion incorporated in the glaze after pigment leaching, are counterbalanced through another cation (absorbing further visible wavelengths) intentionally released to the glaze by a reformulation of the ink composition.

Reducing the impact of digital decoration on the Environment and Human health is a constant concern pursued by ink-makers and colorant manufacturers through a set of actions on well-defined aspects of pigment manufacturing and application. Sustainability implies also research to ban or minimize the use of toxic ingredients and mitigate the risks all along the chain from colorant synthesis to end use. New questions recently arose and need investigation to prevent possible problems. For instance, any chemical interaction of pigments with the organic compounds constituting the digital ink, particularly during the very early stage of firing, might catalyze the formation of undesired byproducts released to the flue gases.

Finally, the *search for new colorants* should be better focused on the actual (and foreseeable) needs of the ceramic industry. First of all, a complete technological characterization of candidate ceramic colorants is recommended, especially to include the most popular applications (DD with firing temperatures always above 1000°C and commonly close to 1200°C). The industrial interest seems now polarized by new effects and new functionalities (e.g., cool pigments). Looking at present-day color palette, new pigments and dyes should approach the chromatic coordinates of industrial cyan, magenta, yellow and black colorants. Another issue is to prevent problems in the access to colorant raw materials, e.g. by shortage and/or increasing price of some commodities. Considering that DD currently rests on a restricted variety of colorants, suitable alternatives should be actively searched, especially for cobalt (cyan and black inks) and praseodymium (yellow ink) which are likely to turn into critical raw materials in the future.

It must be clear that the lines of research illustrated above have been envisaged from a strictly technological point of view. Therefore, this industry-oriented perspective cannot cover all the possible subjects of investigation on ceramic dyes and pigments. First and foremost, basic research is crucial to provide that solid scientific background for any industrial development, particularly in a manufacturing sector – like ceramic colorants production is – still massively relying on an empirical approach. From this standpoint, investigating basic properties and synthesis processes is essential to improve the knowledge base necessary to understand in depth many facts occurring in the industrial production and ceramic application of pigments, dyes and effects. For instance, relating optical properties with crystal chemistry and structure turns fundamental to an efficacious pigment design. On the other hand, disclosing single and mutual effects of different parameters in the synthesis process is the key to improve industrial-scale operations. Last, but not

least, it comes modelling, as a pressing request from colorant-makers to predict and design both physical or chemical features (e.g., optical properties) and behavior during synthesis or ceramic applications of pigments, dyes and effects.

References

[1] Bell, B. T. (1993). Ceramic colorants. Journal of the Society of Dyers and Colourists, 109(3), 101-105.

[2] Dondi, M., & Eppler, R. A. (2000). Ceramic colorants. Ullmann's Encyclopedia of Industrial Chemistry, 1-18.

[3] Dondi, M., Raimondo, M., & Zanelli, C. (2014). Clays and bodies for ceramic tiles: Reappraisal and technological classification. Applied Clay Science, 96, 91-109.

[4] Enrique, J. E., Amorós, J. L., & Moreno, A. (1996). Evolution of ceramic tile glazes. International Ceramics Journal, 20-26.

[5] Sánchez, E., García-Ten, J., Sanz, V., & Moreno, A. (2010). Porcelain tile: almost 30 years of steady scientific-technological evolution. Ceramics International, 36(3), 831-845.

[6] Nassetti, G., & Palmonari, C. (1997). Decoration of porcelain stoneware tiles. Ceram. Acta, 9(5), 15-21.

[7] Gardini, D., Dondi, M., Costa, A.L., Matteucci, F., Blosi, M., Galassi, C., Baldi, G. & Cinotti, E. (2008). Nano-sized ceramic inks for drop-on-demand ink-jet printing in quadrichromy. Journal of nanoscience and nanotechnology, 8(4), 1979-1988.

[8] Hutchings, I. (2010). Ink-jet printing for the decoration of ceramic tiles: technology and opportunities. Proc. XI World Congress on the Quality of Ceramic Tiles, Qualicer 2010, 16 p., Castellon (Spain).

[9] Solana Sanz, V. (2014). Inkjet printing technology for ceramic tile decoration. Proceedings XIII World Congress on the Quality of Ceramic Tiles, Qualicer 2014, 15 p., Castellon (Spain).

[10] Dondi, M., Blosi, M., Gardini, D., & Zanelli, C. (2012). Ceramic pigments for digital decoration inks: an overview. Ceramic Forum International, 89(8-9), E59-E64.

[11] Gardini, D., Blosi, M., Zanelli, C., & Dondi, M. (2015). Ceramic ink-jet printing for digital decoration: physical constraints for ink design. Journal of Nanoscience and Nanotechnology, 15(5), 3552-3561.

[12] Williams, E. S., Panko, J., & Paustenbach, D. J. (2009). The European Union's REACH regulation: a review of its history and requirements. Critical Reviews in Toxicology, 39(7), 553-575.

[13] Applegate, J. S. (2008). Synthesizing TSCA and REACH: practical principles for chemical regulation reform. Ecology LQ, 35, 721.

[14] Gualtieri, A. F., Mazzucato, E., Venturelli, P., Viani, A., Zannini, P., & Petras, L. (1999). Determination of nickel (II) oxide in ceramic pigments by in situ X-ray diffraction quantitative analysis. Journal of the American Ceramic Society, 82(9), 2566-2568.

[15] Calbo, J., Sorlí, S., Llusar, M., Tena, M. A., & Monrós, G. (2004). Minimisation of toxicity in nickel ferrite black pigment. British Ceramic Transactions, 103(1), 3-9.

[16] Eppler, R. A. (1987). Selecting ceramic pigments. Am. Ceram. Soc. Bull., 66(11) 1600-1604.

[17] Ardit M., Cruciani G., Dondi M., Zanelli C. (2016). Pigments based on perovskites. In: Perovskites and related mixed oxides: concepts and applications, V.I. Parvulescu, S. Kaliaguine, P. Granger, and W. Prellier (eds.), chapter 12, 259-288, Wiley-VCH Verlag GmbH & Co.

[18] Eppler, D. R., & Eppler, R. A. (1997). The relative stability of ceramic pigments. Ceramic Engineering and Science Proceedings, 18(2), 139-149.

[19] Eppler, R. A., & Eppler, D. R. (1994). Which colors can and cannot be produced in ceramic glazes? Ceramic Engineering and Science Proceedings, 15, 281-288.

[20] Murdock, S. H., Wise, T. D., & Eppler, R. A. (1990). Predicting the color of a ceramic glaze. American Ceramic Society Bulletin, 69(2), 228-30.

[21] Westland, S. (2003). Review of the CIE system of colorimetry and its use in dentistry. Journal of Esthetic and Restorative Dentistry, 15, S5-S12.

[22] Schanda, J., Ed. (2007). Colorimetry: understanding the CIE system. John Wiley & Sons, p. 453.

[23] Glaze stains – Body stains. Esmalglass-Itaca. https://www.esmalglass-itaca.com/en/products-and-solutions/colors (last access: March 19, 2020).

[24] Nassau, K. (2001). The fifteen causes of colour. John Wiley & Sons, New York, p. 481.

[25] Lever, A. P. (1984). Inorganic electronic spectroscopy. Elsevier, Amsterdam-New York, p. 863.

[26] Burns, R. G., & Burns, R. G. (1993). Mineralogical applications of crystal field theory. Cambridge University Press, Cambridge, p. 551.

[27] Henderson, B., & Imbusch, G. F. (2006). Optical spectroscopy of inorganic solids. Oxford University Press, Oxford, p. 662.

[28] Eppler, R. A., & Eppler, D. R. (2000). Glazes and glass coatings. American Ceramic Society.

[29] Casasola, R., Rincón, J. M., & Romero, M. (2012). Glass-ceramic glazes for ceramic tiles: a review. Journal of Materials Science, 47(2), 553-582.

[30] Katz, M., Gebhart, T., & Carty, W. (2003). The reevaluation of the unity molecular formula limits for glazes. Ceramic Engineering and Science Proceedings, 24(2), 13-24.

[31] Henderson, C. M. B., Charnock, J. M., & Plant, D. A. (2007). Cation occupancies in Mg, Co, Ni, Zn, Al ferrite spinels: a multi-element EXAFS study. Journal of Physics: Condensed Matter, 19(7), 076214.

[32] Malavergne, V., Guyot, F., Wang, Y., & Martinez, I. (1997). Partitioning of nickel, cobalt and manganese between silicate perovskite and periclase: a test of crystal field theory at high pressure. Earth and planetary science letters, 146(3-4), 499-509.

[33] Linton, J., Navrotsky, A., & Fei, Y. (1998). The thermodynamics of ordered perovskites on the $CaTiO_3$-$FeTiO_3$ Join. Physics and Chemistry of Minerals, 25(8), 591-596.
[34] Štemprok, M. (1990). Solubility of tin, tungsten and molybdenum oxides in felsic magmas. Mineralium Deposita, 25(3), 205-212.
[35] Dickinson Jr, J. E., & Hess, P. C. (1982). Zircon saturation in lunar basalts and granites. Earth and Planetary Science Letters, 57(2), 336-344.
[36] Ryerson, F. J., & Watson, E. B. (1987). Rutile saturation in magmas: implications for Ti-Nb-Ta depletion in island-arc basalts. Earth and Planetary Science Letters, 86(2-4), 225-239.
[37] Italian Ceramic Society (2003). Colour, Pigments and Colouring in Ceramics. SALA, Modena.
[38] Murdock, S. H., Wise, T. D., & Eppler, R. A. (1989). The effect of pigment particle size on glaze color. Ceramic Engineering and Science Proceedings, 9, 55-64.
[39] Schabbach, L. M., Bondioli, F., Ferrari, A. M., Manfredini, T., Petter, C. O., & Fredel, M. C. (2008). Color in ceramic glazes: Analysis of pigment and opacifier grain size distribution effect by spectrophotometer. Journal of the European Ceramic Society, 28(9), 1777-1781.
[40] Güngor, G.L., Kara, A., Blosi, M., Gardini, D., Guarini, G., Zanelli, C., Dondi, M. (2015). Micronizing ceramic pigments for inkjet printing: Part I. Grindability and particle size distribution. Ceramics International, 41, 6498-6506.
[41] Zanelli, C., Güngor, G.L., Kara, A., Blosi, M., Gardini, D., Guarini, G., Dondi, M. (2015). Micronizing ceramic pigments for inkjet printing: Part II. Effect on phase composition and color. Ceramics International, 41, 6507-6517
[42] Wang Y. & Forssberg E. 2007. Enhancement of energy efficiency for mechanical production of fine and ultra-fine particles in comminution. China Particuol., 5, 193-201.
[43] Holdich, R.G. (2002). Fundamentals of Particle Technology. Midland Information Technology and Publishing.
[44] Hukki, R.T. (1962). Proposal for a Solomonic settlement between the theories of Von Rittinger, Kick, and Bond. AIME Transactions, 223, 403-408.
[45] Walker W.H., Lewis W.K., McAdams W.H., Gilliland E.R. (1937). Principles of Chemical Engineering. McGraw-Hill, New York.
[46] Voller V.R. (1983). A note on energi-size reduction relationships in comminution. Powder Technology, 36, 281-286.
[47] Tanaka T. (1966). Comminution laws. I&EC Process Design and Development, 5, 353-358.
[48] Yüngevis H. & Ozel E. (2013). Effect of the milling process on the properties of $CoFe_2O_4$ pigment. Ceramics International, 39, 5503-5511.
[49] Guo D., Yang Q., Chen P., Chu Y., Zhang Y., Rao P. (2018). The influence of micronization on the properties of Pr-$ZrSiO_4$ pigment. Dyes and Pigments, 153, 74-83.
[50] Wang Y., Wang Q., Chang Q., Hu S., Wang X., Yang K. (2018). Effect of particle size on the blue chromate pigment $CoAl_2O_4$. Journal of Ceramic Science and Technology, 9, 43-46.
[51] Liu H., Wang Q., Chang Q., Wang C., Wang Y., Wang Y., Zhang X. (2019). Relationship between the colour and particle size of the ultrafine V-$ZrSiO_4$ and Pr-$ZrSiO_4$ pigments and their mixture. Materials Research Express, 6, 075214: 1-12.
[52] Ardit M., Cruciani G., Di Benedetto F., Sorace L., Dondi M. (2018). New spectroscopic and diffraction data to solve the vanadium-doped zircon pigment conundrum. Journal of the European Ceramic Society, 38, 5234-5245.
[53] Richet P. & Gillet P. (1997). Pressure-induced amorphization of minerals: a review. European Journal of Mineralogy, 9, 907-933.
[54] Anderson D. L. (1989). Theory of the Earth. Blackwell Scientific Publications, Oxford, 367 p.
[55] Angel R. J. (2000). Equations of State. In "High-Temperature and High-Pressure Crystal Chemistry", Hazen R. M. & Downs R. T. eds., Reviews in Mineralogy and Geochemistry, 41, 35-59.
[56] Finger, L. W. & Hazen, R. M. (1978). Crystal structure and compression of ruby to 46 kbar. Journal of Applied Physics, 49, 5823-5826.
[57] d'Amour, H., Schiferl, D., Denner, W., Schulz, H., & Holzapfel, W. B. (1978). High-pressure single-crystal structure determinations for ruby up to 90 kbar using an automatic diffractometer. Journal of Applied Physics, 49, 4411-4416.
[58] Richet, P., Xu, J.-A., & Mao, H.-K. (1988). Quasi-hydrostatic compression of ruby to 500 kbar. Physics and Chemistry of Minerals, 16, 207-211.
[59] Kim-Zajonz, J., Werner, S., & Schulz, H. (1999). High-pressure single crystal X-ray diffraction study on ruby up to 31 GPa. Zeitschrift für Kristallographie, 214, 331-336.
[60] Holland, T. J. B., & Powell, R. (2011). An improved and extended internally consistent thermodynamic dataset for phases of petrological interest, involving a new equation of state for solids. Journal of Metamorphic Geology, 29, 333-383.
[61] Catti, M., & Pavese, A. (1998). Equation of state of α-Al_2O_3 (Corundum) from Quasi-Harmonic atomistic simulations. Acta Crystallographica B, 54, 741-749.
[62] Goto, T., Anderson, O. L., Ohno, I., & Yamamoto, S., (1989). Elastic constants of corundum up to 1825 K. Journal of Geophysical Research, 94, 7588-7602.
[63] Pavese, A. (2002). Pressure-volume-temperature equation of state: a comparative study based on numerical simulation. Physics and Chemistry of Minerals, 29, 43-51.
[64] Özkan, H., Cartz, L., & Jamieson, J. C. (1974). Elastic constants of non-metamict zirconium silicate. Journal of Applied Physics, 45, 556-562.
[65] Özkan, H., & Jamieson, J. C. (1978). Pressure dependence of the elastic constants of non-metamict zircon. Physics and Chemistry of Minerals, 2, 215-224.

[66] Hazen, R. M., & Finger, L. W. (1979). Crystal structure and compressibility of zircon at high pressure. American Mineralogist, 64, 196-201.

[67] Ríos, S., & Boffa-Ballaran, T. (2003). Microstructure of radiation-damaged zircon under pressure. Journal of Applied Crystallography, 36, 1006-1012.

[68] Özkan, H. (2008). Correlations of the temperature and pressure dependencies of the elastic constants of zircon. Journal of the European Ceramic Society, 28, 3091-3095.

[69] Manghnani, M. H. (1969). Elastic constants of single-crystal rutile under pressures to 7.5 kilobars. Journal of Geophysical Research, 74, 4317-4328.

[70] Ming, L.-C., & Manghnani, M. H. (1979). Isothermal compression of TiO_2 (rutile) under hydrostatic pressure to 106 kbar. Journal of Geophysical Research, 84, 4777-4779.

[71] Hazen, R. M., & Finger, L. W. (1981). Bulk moduli and high-pressure crystal structures of rutile-type compounds. Journal of Physics and Chemistry of Solids, 42, 143-151.

[72] Mo, S.-D., & Ching, W. Y. (1995). Electronic and optical properties of three phases of titanum dioxide: rutile, anatase, and brookite. Physical Review B, 51, 13023-13032.

[73] Staun Olsen, J., Gerward, L., & Jiang, J. Z. (1999). On the rutile/α-PbO_2-type phase boundary of TiO_2. Journal of Physics and Chemistry of Solids, 60, 229-233.

[74] Staun Olsen, J., Gerward, L., & Jiang, J. Z. (2002). High-pressure behaviour of nano titanium dioxide. High Pressure Research, 22, 385-389.

[75] Haines, J., & Léger, J. M. (1997). X-ray diffraction study of the phase transitions and structural evolution of tin dioxide at high pressure: Relationships between structure types and implications for other rutile-type dioxides. Physical Review B, 55, 11144-11154.

[76] Liebermann, R. C. (1973). Elastic properties of polycrystalline SnO_2 and GeO_2: Comparison with stishovite and rutile data. Physics of the Earth and Planetary Interiors, 7, 461-465.

[77] Chang, E., & Graham, E. K. (1975). The elastic constants of cassiterite SnO2 and their pressure and temperature dependence. Journal of Geophysical Research, 80, 2595-2599.

[78] Ross, N. L., Zhao, J., & Angel, R. J., (2004). High-pressure single-crystal X-ray diffraction study of YAlO3 perovskite. Journal of Solid State Chemistry, 177, 1276-1284.

[79] Ross, N. L. (1996). Distortion of $GdFeO_3$-type perovskites with pressure: A study of $YAlO_3$ to 5 GPa. Phase Transitions, 58, 27-41.

[80] Wu, X., Qin, S., & Wu, Z. (2006). Generalized gradient approximation calculations of the pressure-induced phase transition of $YAlO_3$ perovskite. Journal of Physics: Condensed Matter, 18, 3907-3916.

[81] Li, Z., Fisher, E. S., Liu, J. Z., & Nevitt M. V. (1991). Single-crystal elastic constants of Co-Al and Co-Fe spinels. Journal of Materials Science, 26, 2621-2624.

[82] Akbudaka, S., Kushwahab, A. K., Uğurc, G., Uğurc, Ş., & Yaşar Ocak, H. (2018). Structural, electronic, elastic, optical and vibrational properties of MAl_2O_4 (M = Co and Mn) aluminate spinels. Ceramics International, 44, 310-316.

[83] Blasco, J., Subías, G., García, J., Popescu, C., & Cuartero, V. (2015). High-pressure transformation in the cobalt spinel ferrites. Journal of Solid State Chemistry, 221, 173-177.

[84] Levy, D., Diella, V., Pavese, A, Dapiaggi, M., & Sani, A. (2005). P-V equation of State, thermal expansion, and P-T stability of synthetic ($ZnCr_2O_4$ spinel). American Mineralogist, 90, 1157-1162.

[85] Zhang, Y., Liu, X., Xiong, Z., & Zhang, Z. (2016). Compressional behavior of $MgCr_2O_4$ spinel from first-principles simulation. Science China Earth Sciences, 59, 989-996.

[86] Liu, Y., Xing, J., Lia, Y., Tan, J., Sun, L., & Yan, J. (2016). Mechanical properties and anisotropy of thermal conductivity of $Fe_{3-x}Cr_xO_4$ (x = 0-3). Journal of Materials Research, 31, 3805-3813.

[87] Angel, R. J., Kunz, M., Miletich, R., Woodland, A. B., Koch, M., & Xirouchakis, D. (1999). High-pressure phase transition in $CaTiOSiO_4$ titanite. Phase Transitions, 68, 533-543.

[88] Rath, S., Kunz, M., & Miletich, R. (2003). Pressure-induced phase transition in malayaite, $CaSnOSiO_4$. American Mineralogist, 88, 293-300.

[89] Akdemir, S., Ozel, E., & Suvaci, E. (2011). Solubility of blue $CoAl_2O_4$ ceramic pigments in water and diethylene glycol media. Ceramics International, 37(3), 863-870.

[90] Ferrari, G., & Zannini, P. (2016). Thermal behavior of vehicles and digital inks for inkjet decoration of ceramic tiles. Thermochimica Acta, 639, 41-46.

[91] Ferrari, G., & Zannini, P. (2017). VOCs monitoring of new materials for ceramic tiles decoration: GC–MS analysis of emissions from common vehicles and inkjet inks during firing in laboratory. Boletín de la Sociedad Española de Cerámica y Vidrio, 56(5), 226-236.

[92] Escardino, A., Mestre, S., Feliu, C., Jodar, P., & Díaz, L. (2002). Stability of (Cr)CaO.SnO_2.SiO_2 pink pigment in ceramic frits. British Ceramic Transactions, 101(5), 213-220.

[93] Harisanov, V., Pavlov, R. S., Marinova, I. T., Kozhukharov, V., & Carda, J. B. (2003). Influence of crystallinity on chromatic parameters of enamels coloured with malayaite pink pigments. Journal of the European Ceramic Society, 23(3), 429-435.

[94] Cruciani G., Dondi M., Stoyanova T., Matteucci F., Carda J., Costa A.L., Malayaite ceramic pigments: a combined optical spectroscopy and neutron/X-ray diffraction study. Materials Research Bulletin, 44 (2009) 1778-1785.

[95] Lopez-Navarrete, E., Caballero, A., Orera, V. M., Lázaro, F. J., & Ocaña, M. (2003). Oxidation state and localization of chromium ions in Cr-doped cassiterite and Cr-doped malayaite. Acta Materialia, 51(8), 2371-2381.

[96] D[95oménech, A., Torres, F. J., Ruiz de Sola, E., & Alarcón, J. (2006). Electrochemical detection of high oxidation states of chromium (IV and V) in chromium-doped cassiterite and tin-sphene ceramic pigmenting systems. European Journal of Inorganic Chemistry, 2006(3), 638-648.

[97] Cordoncillo, E., Del Rio, F., Carda, J., Llusar, M., & Escribano, P. (1998). Influence of some mineralizers in the synthesis of sphene-pink pigments. Journal of the European Ceramic Society, 18(8), 1115-1120.

[98] Lee, H. S., & Lee, B. H. (2008). Colouring effect of malayaite formation and synthesis sphene-pink pigment. Journal of the Korean Ceramic Society, 45(3), 172.
[99] Lee, H. S., Park, J. S., & Lee, B. H. (2009). Synthesis of sphene-pink pigment under various firing conditions. Journal of the Korean Ceramic Society, 46(6), 615-620.
[100] Cavalcante P.M.T., Dondi M., Guarini G., Raimondo M., Baldi G., Colour performance of ceramic nano-pigments. Dyes and Pigments, 80 (2009) 226-232.
[101] Lambertson, R. H., Lacy, C. A., Gillespie, S. D., Leopold, M. C., & Coppage, R. H. (2017). Gold nanoparticle colorants as traditional ceramic glaze alternatives. Journal of the American Ceramic Society, 100(9), 3943-3951.
[102] Colomban, P. (2009). The use of metal nanoparticles to produce yellow, red and iridescent colour, from bronze age to present times in lustre pottery and glass: solid state chemistry, spectroscopy and nanostructure. Journal of Nano Research, 8, 109-132.
[103] Vignali, G. (2003). Soluble salts: organometallic complexes for colouring and decoration of porcelain gres tiles. In: "Colour, Pigments and Colouring in Ceramics", chapter 10, pp. 163-182, Italian Ceramic Society and SALA, Modena, Italy.
[104] Mestre, S., Palacios, M. D., & Agut, P. (2012). Synthesis of a red pigment from gold nanoparticles. Boletin de la Sociedad Española de Ceramica y Vidrio, 51(2), 75-82.
[105] Saket, S., Rasouli, S., Arabic, A. M., & Sani, M. F. (2016). A novel approach to the synthesis of a wide range of ink jet printer pigment from yellow to magenta for tiles via gold nanoparticles. Journal of Ceramic Processing Research, 17(3), 246-252.
[106] Blosi M., Gatti F., Albonetti S., Baldi G., Dondi M., Au-Ag nanoparticles as red pigment in ceramic inks. Dyes and Pigments, 94 (2012) 355-362.
[107] Mestre, S., Chiva, C., Palacios, M. D., & Amorós, J. L. (2012). Development of a yellow ceramic pigment based on silver nanoparticles. Journal of the European Ceramic Society, 32(11), 2825-2830.
[108] López-Navarrete, E., González-Elipe, A. R., & Ocana, M. (2003). Non-conventional synthesis of Cr-doped SnO_2 pigments. Ceramics international, 29(4), 385-392.
[109] Julián, B., Beltrán, H., Cordoncillo, E., Escribano, P., Folgado, J. V., Vallet-Regí, M., & Real, R. P. D. (2002). A study of the method of synthesis and chromatic properties of the Cr-SnO_2 pigment. European Journal of Inorganic Chemistry, 2002(10), 2694-2700.
[110] Tena, M. A., Meseguer, S., Gargori, C., Forés, A., Badenes, J. A., & Monrós, G. (2007). Study of Cr-SnO_2 ceramic pigment and of Ti/Sn ratio on formation and coloration of these materials. Journal of the European Ceramic Society, 27(1), 215-221.
[111] Trojan, J., Luxová, J., & Šulcová, P. (2018). The effect of transition metals and rare-earth metals admixtures on the pigmentary properties of the cassiterite pigments. Scientific papers of the University of Pardubice. Series A, Faculty of Chemical Technology. 24/2018.
[112] Liu, H. F., Dai, W. B., Wang, H., Zeng, L. K., & Wang, Y. M. (2015). Study on the preparation of the $CdS_xSe_{1-x}@ZrSiO_4$ red ceramic pigments and its properties. Journal of Sol-Gel Science and Technology, 75(1), 198-205.
[113] Zhang, Y., Zeng, D., Rao, P., Cao, A., & Wu, J. (2008). Hydrothermal synthesis of cadmium sulfoselenide inclusion pigment. Journal of Sol-Gel Science and Technology, 48(3), 289-293.
[114] Zannini, P. (2019). Degradation due to milling of Cd, Se, Pr and Sn based pigments for ceramic inks. XVI Conference of the European Ceramic Society, Torino, Italy.
[115] Berry, F. J., Eadon, D., Holloway, J., & Smart, L. E. (1999). Iron-doped zircon: the mechanism of formation. Journal of Materials Science, 34(15), 3631-3638.
[116] Llusar, M., Badenes, J. A., Calbo, J., Tena, M. A., & Monros, G. (2000). Environmental and colour optimisation of mineraliser addition in synthesis of iron zircon ceramic pigment. British Ceramic Transactions, 99(1), 14-22.
[117] Ardizzone, S., Binaghi, L., Cappelletti, G., Fermo, P., & Gilardoni, S. (2002). Iron doped zirconium silicate prepared by a sol–gel procedure. The effect of the reaction conditions on the structure, morphology and optical properties of the powders. Physical Chemistry Chemical Physics, 4(22), 5683-5689.
[118] Cappelletti, G., Ardizzone, S., Fermo, P., & Gilardoni, S. (2005). The influence of iron content on the promotion of the zircon structure and the optical properties of pink coral pigments. Journal of the European Ceramic Society, 25(6), 911-917.
[119] Chu, H. L., Wang, C. L., Hwang, W. S., Lee, K. C., Zhou, X., & Wang, M. C. (2014). Kinetics of phase transformation and optical property of pink coral zirconia powders. Journal of Alloys and Compounds, 601, 307-318.
[120] Zumaquero, E., Orts, M. J., Sanz, V., & Mestre, S. (2017). Iron zircon pigment synthesis: Proposal of a mixing index for the raw materials mixtures. Boletín de la Sociedad Española de Cerámica y Vidrio, 56(4), 177-185.
[121] Wang, Y., Wang, Q., Chang, Q., Wang, Y., Zhao, Y., Wang, X., & Wang, Y. (2019). Chromatic study on the coloration mechanism of iron zircon pigment. Materials Chemistry and Physics, 121740.
[122] Sempio, A., & Gualtieri, A. (2002). Mineralogy of the "Grès de Thiviers" (Northern Aquitaine, France). Periodico di Mineralogia, 71(1), 65-84.
[123] Gualtieri, A. (2003). Different applications of "Grès de Thiviers", a red pigment for traditional ceramics. Bulletin of European Ceramic Society, 1, 14-18.
[124] Bondioli, F., Ferrari, A. M., Leonelli, C., & Manfredini, T. (1998). Syntheses of Fe_2O_3/silica red inorganic inclusion pigments for ceramic applications. Materials Research Bulletin, 33(5), 723-729.
[125] Hosseini-Zori, M., Bondioli, F., Manfredini, T., & Taheri-Nassaj, E. (2008). Effect of synthesis parameters on a hematite–silica red pigment obtained using a coprecipitation route. Dyes and Pigments, 77(1), 53-58.
[126] Hosseini-Zori, M., Taheri-Nassaj, E., & Mirhabibi, A. R. (2008). Effective factors on synthesis of the hematite–silica red inclusion pigment. Ceramics International, 34(3), 491-496.
[127] Zhang, Y., Rao, P., Lü, M., Zeng, D., & Wu, J. (2009). Synthesis and color evolution of silica-coated hematite nanoparticles. Journal of the American Ceramic Society, 92(8), 1877-1880.

[128] Costa A.L., Zama I., Matteucci F., Dondi M., Albonetti S., Baldi G., Heterocoagulation-spray drying process for the inclusion of ceramic pigments. Journal of the European Ceramic Society 28 (2008) 169–176.
[129] Spinelli, A., Oliveira, A. P. N., Soledade, L. E. B., Paskocimas, C. A., Longo, E., Souza, A. G., Chicariano, C. A. & Flores, J. A. (2005). Propiedades ópticas del pigmento α-Fe_2O_3/SiO_2. Boletín de la Sociedad Española de Cerámica y Vidrio, 44(4), 223-227.
[130] Chen, S., Cheng, M., Lang, Y., Tian, C., Wei, H., & Wang, C. A. (2019). Preparation and characterization of monodispersed spherical $Fe_2O_3@SiO_2$ reddish pigments with core–shell structure. Journal of Advanced Ceramics, 8(1), 39-46.
[131] Baldi, G., Dolen, N., Barzanti, A., & Faso, V. (2004). Synthesis of a new class of red pigments based on perovskite-type lattice $A_xB_{2-xy}Cr_yO_3$ with 0.90<x<1, 0.05<y<0.12, A=Y, Lanthanides, B=Al for use in body stain and high temperature glazes. Key Engineering Materials, 264, 1545-1548.
[132] Marinova, Y., Hohemberger, J. M., Cordoncillo, E., Escribano, P., & Carda, J. B. (2003). Study of solid solutions, with perovskite structure, for application in the field of the ceramic pigments. Journal of the European Ceramic Society, 23(2), 213-220.
[133] Cruciani, G., Ardit, M., Dondi, M., Matteucci, F., Blosi, M., Dalconi, M. C., & Albonetti, S. (2009). Structural relaxation around Cr^{3+} in $YAlO_3$–$YCrO_3$ perovskites from electron absorption spectra. The Journal of Physical Chemistry A, 113(49), 13772-13778.
[134] Stobierska, E., Lis, J., Bućko, M. M., & Gubernat, A. (2006). Ceramic pigments with perovskite structure. Advances in Science and Technology, 45, 276-280.
[135] Shirpour, M., Sani, M. F., & Mirhabibi, A. (2007). Synthesis and study of a new class of red pigments based on perovskite YAlO3 structure. Ceramics International, 33(8), 1427-1433.
[136] Shin, K. H., & Lee, B. H. (2008). Synthesis of Cr-doped Y_2O_3-Al_2O_3 red pigments and their application. Journal of the Korean Ceramic Society, 45(8), 453.
[137] Matteucci F., Lepri Neto C., Dondi M., Cruciani G., Baldi G., Boschi A.O., Colour development of red perovskite pigment $Y(Al,Cr)O_3$ in various ceramic applications. Advances in Applied Ceramics, 105 [2] (2006) 99-106.
[138] Kato, M., & Takahashi, M. (2001). Synthesis of Cr-doped $NdAlO_3$-Al_2O_3 reddish pink pigment. Journal of Materials Science Letters, 20(5), 413-414.
[139] Shin, K. H., & Lee, B. H. (2009). Synthesis and Characterization of (Cr,Fe)-doped Y_2O_3-Al_2O_3 Red Pigments. Journal of the Korean Ceramic Society, 46(4), 350-356.
[140] Ianoş, R., Lazău, R., Băbuță, R., Muntean, E., Moacă, E. A., & Păcurariu, C. (2018). Solution combustion synthesis: a straightforward route for the preparation of chromium-doped lanthanum aluminate, $LaAl_{1-x}Cr_xO_3$, pink red pigments. Dyes and Pigments, 155, 218-224.
[141] Martos, M., Martínez, M., Cordoncillo, E., & Escribano, P. (2007). Towards more ecological ceramic pigments: Study of the influence of glass composition on the colour stability of a pink chromium-doped ceramic pigment. Journal of the European Ceramic Society, 27(16), 4561-4567.
[142] Bondioli, F., Ferrari, A. M., Leonelli, C., Manfredini, T., Linati, L., & Mustarelli, P. (2000). Reaction mechanism in alumina/chromia (Al_2O_3–Cr_2O_3) solid solutions obtained by coprecipitation. Journal of the American Ceramic Society, 83(8), 2036-2040.
[143] López-Navarrete, E., Caballero, A., González-Elipe, A. R., & Ocana, M. (2004). Chemical state and distribution of Mn ions in Mn-doped α-Al_2O_3 solid solutions prepared in the absence and the presence of fluxes. Journal of the European Ceramic Society, 24(10-11), 3057-3062.
[144] Lopez-Navarrete, E., & Ocana, M. (2004). Aerosol-derived Mn-doped Al_2O_3 pink pigments prepared in the absence of fluxes. Dyes and Pigments, 61(3), 279-286.
[145] Ricceri, R., Ardizzone, S., Baldi, G., & Matteazzi, P. (2002). Ceramic pigments obtained by sol-gel techniques and by mechanochemical insertion of color centers in Al_2O_3 host matrix. Journal of the European Ceramic Society, 22(5), 629-637.
[146] Maslennikova, G. N. (2001). Pigments of the spinel type. Glass and ceramics, 58(5-6), 216-220.
[147] Prim, S. R., Garcia, A., Galindo, R., Cerro, S., Llusar, M., Folgueras, M. V., & Monros, G. (2013). Pink ceramic pigments based on chromium doped $M(Al_{2-x}Cr_x)O_4$, M= Mg, Zn, normal spinel. Ceramics International, 39(6), 6981-6989.
[148] Fernández-Osorio, A., Pineda-Villanueva, E., & Chávez-Fernández, J. (2012). Synthesis of nanosized $(Zn_{1-x}Co_x)Al_2O_4$ spinels: new pink ceramic pigments. Materials Research Bulletin, 47(2), 445-452.
[149] Zhang, T., Huang, J., Yan, J., Pu, Z., Yin, X., & Wang, Y. (2019). The structural evolution and optical properties of $Mg_{1-x}Zn_xAl_{1.8}Cr_{0.2}O_4$ pink ceramic pigments. Ceramics International, 45, 16848-16854.
[150] Pavlov, R. S., Castelló, J. B. C., Marzá, V. B., & Hohembergerger, J. M. (2002). New red-shade ceramic pigments based on $Y_2Sn_{2-x}Cr_xO_{7-\delta}$ pyrochlore solid solutions. Journal of the American Ceramic Society, 85(5), 1197-1202.
[151] López-Navarrete, E., Orera, V. M., Lázaro, F. J., Carda, J. B., & Ocaña, M. (2004). Preparation through aerosols of cr-doped $Y_2Sn_2O_7$ (Pyrochlore) red-shade pigments and determination of the Cr oxidation state. Journal of the American Ceramic Society, 87(11), 2108-2113.
[152] Matteucci F., Cruciani G., Dondi M., Baldi G., Barzanti A. (2007). Crystal structural and optical properties of Cr-doped $Y_2Ti_2O_7$ and $Y_2Sn_2O_7$ pyrochlores. Acta Materialia, 55, 2229-2238.
[153] Martos, M., Julián-López, B., Cordoncillo, E., & Escribano, P. (2008). Structural and spectroscopic study of a novel erbium titanate pink pigment prepared by sol–gel methodology. Journal of Physical Chemistry B, 112(8), 2319-2325.
[154] Martos, M., Julián-López, B., Cordoncillo, E., & Escribano, P. (2009). Structural and spectroscopic study of a new pink chromium-free $Er_2(Ti,Zr)_2O_7$ ceramic pigment. Journal of the American Ceramic Society, 92(12), 2987-2992.

[155] Jovaní, M., Fortuño-Morte, M., Beltrán-Mir, H., & Cordoncillo, E. (2018). Environmental-friendly red-orange ceramic pigment based on Pr and Fe co-doped $Y_2Zr_2O_7$. Journal of the European Ceramic Society, 38(4), 2210-2217.

[156] Lyubenova, T. S., Carda, J. B., & Ocaña, M. (2009). Synthesis by pyrolysis of aerosols and ceramic application of Cr-doped $CaYAlO_4$ red–orange pigments. Journal of the European Ceramic Society, 29(11), 2193-2198.

[157] Thieme, C., & Rüssel, C. (2014). Temperature resistant red and purple ceramic pigments based on the solid solution series $BaZn_{2-x}Ni_xSi_2O_7$ and $BaMg_{2-x}Ni_xSi_2O_7$. Dyes and Pigments, 111, 75-80.

[158] Thieme, C., Waurischk, T., Lin, C., & Rüssel, C. (2016). Lilac ceramic pigments based on $Ba_{0.5}Sr_{0.5}Zn_{2-x}Ni_xSi_2O_7$ solid solutions. Ceramics International, 42(11), 13035-13040.

[159] Llusar, M., García, A., Gargori, C., Galindo, R., Badenes, J. A., & Monrós, G. (2012). Synthesis of diphosphate $Mn_{2-x}Mg_xP_2O_7$ solid solutions with thortveitite structure: New pink ceramic dyes for the colouration of ceramic glazes. Journal of the European Ceramic Society, 32(4), 765-776.

[160] Gu, X. Y., Luo, W. Q., & Chen, Y. X. (2010). Study on Co-$KZr_2(PO_4)_3$-type crystalline purple ceramic pigments. Applied Mechanics and Materials, 34, 790-794.

[161] Hunault, M., Robert, J. L., Newville, M., Galoisy, L., & Calas, G. (2014). Spectroscopic properties of five-coordinated Co^{2+} in phosphates. Spectrochimica Acta Part A: Molecular and Biomolecular Spectroscopy, 117, 406-412.

[162] Badenes, J. A., Vicent, J. B., Llusar, M., Tena, M. A., & Monros, G. (2002). The nature of Pr-$ZrSiO_4$ yellow ceramic pigment. Journal of Materials Science, 37(7), 1413-1420.

[163] Kar, J. K., Stevens, R., & Bowen, C. R. (2005). Processing and characterisation of Pr–zircon pigment powder. Advances in Applied Ceramics, 104(5), 233-238.

[164] Del Nero, G., Cappelletti, G., Ardizzone, S., Fermo, P., & Gilardoni, S. (2004). Yellow Pr-zircon pigments: The role of praseodymium and of the mineralizer. Journal of the European Ceramic Society, 24(14), 3603-3611.

[165] Kar, J. K., Stevens, R., & Bowen, C. R. (2004). Novel terbium-zircon yellow pigment. Journal of materials science, 39(18), 5755-5763.

[166] Kar, J. K., Stevens, R., & Bowen, C. R. (2007). Effect of cerium oxide on colour hue of praseodymium–zircon yellow pigment. Advances in Applied Ceramics, 106(4), 175-179.

[167] Guo, D., Xie, M., Ma, N., Yang, Q., Luo, Z., Chu, Y., & Rao, P. (2019). Synthesis and characterization of (Pr, Ce)-$ZrSiO_4$ ceramic pigments: The properties of the pigments and the effect of Ce. Journal of the American Ceramic Society, 102(5), 2619-2628.

[168] Bondioli, F., Corradi, A. B., Ferrari, A. M., Manfredini, T., & Baldi, G. (2000). Environmental scanning electron microscopy (ESEM) investigation of the reaction mechanism in praseodymium-doped zircon. Journal of the American Ceramic Society, 83(6), 1518-1520.

[169] Montoya, N., & Alarcón, J. (2012). Microstructural Evolution from Praseodymium-Containing Zircon Gels to Pr-ZrSiO4 Solid Solutions. Journal of the American Ceramic Society, 95(4), 1255-1260.

[170] Ocaña, M., Caballero, A., González-Elipe, A. R., Tartaj, P., Serna, C. J., & Merino, R. I. (1999). The effects of the NaF flux on the oxidation state and localisation of praseodymium in Pr-doped zircon pigments. Journal of the European Ceramic Society, 19(5), 641-648.

[171] Hill, K., Lehman, R., & Swiler, D. (2000). Effects of selected processing variables on color formation in praseodymium-doped zircon pigments. Journal of the American Ceramic Society, 83(9), 2177-2182.

[172] Pyon, K. R., & Lee, B. H. (2009). The influence of firing conditions on the color properties of Pr-$ZrSiO_4$ pigments synthesized using rice husk ash. Journal of the Korean Ceramic Society, 46(4), 397-404.

[173] Ren, F., Ishida, S., & Takeuchi, N. (1993). Color and vanadium valency in V-doped ZrO_2. Journal of the American Ceramic Society, 76(7), 1825-1831.

[174] Monrós, G., García, A., Sorlí, S., Benet, P., & Tena, M. A. (2003). Quantum sized chromophores in vanadium ceramic pigments. Materials Science Forum, 426, 2423-2427.

[175] Alarcón, J. (2001). Synthesis and characterization of vanadium-containing ZrO_2 solid solutions pigmenting system from gels. Journal of materials science, 36(5), 1189-1195.

[176] Torres, F. J., Amigó, J. M., & Alarcón, J. (2003). X-ray powder diffraction study of monoclinic V^{4+}-ZrO_2 solid solutions obtained from gels. Journal of Solid State Chemistry, 173(1), 40-44.

[177] Calatayud, J. M., & Alarcón, J. (2017). V-containing ZrO_2 inorganic yellow nano-pigments prepared by hydrothermal approach. Dyes and Pigments, 146, 178-188.

[178] Dondi M., Matteucci F., Zama I., Cruciani G., High-performance yellow ceramic pigments $Zr(Ti_{1-x-y}Sn_{x-y}V_yM_y)O_4$ (M = Al, In, Y): crystal structure, colouring mechanism and technological properties. Materials Research Bulletin, 42 (2007) 64-79.

[179] Lei, B., Qin, W., Kang, G., Peng, C., & Wu, J. (2015). Modeling and evaluation for encapsulation efficiency of zircon-based heteromorphic encapsulation pigments. Dyes and Pigments, 112, 245-254.

[180] Joo, I. D., Hwang, D. H., Lee, H. S., Park, J. S., & Lee, B. H. (2009). Synthesis of SnO_2-TiO_2-V_2O_5 System Yellow Pigment. Journal of the Korean Ceramic Society, 46(6), 639-642.

[181] Matteucci F., Cruciani G., Dondi M., Raimondo M., The Role of Counterions (Mo, Nb, Sb, W) in Cr-, Mn-, Ni- and V-doped Rutile Ceramic Pigments. Part 1. Crystal Structure and Phase Transformations. Ceramics International, 32 (2006) 385-392.

[182] Dondi M., Cruciani G., Guarini G., Matteucci F., Raimondo M., The Role of Counterions (Mo, Nb, Sb, W) in Cr-, Mn-, Ni- and V-doped Rutile Ceramic Pigments. Part 2. Colour and Technological Properties. Ceramics International, 32 (2006) 393-405.

[183] Sorlí, S., Tena, M. A., Badenes, J. A., Calbo, J., Llusar, M., & Monrós, G. (2004). Structure and color of $Ni_xA_{1-3x}B_{2x}O_2$ (A= Ti, Sn; B= Sb, Nb) solid solutions. Journal of the European Ceramic Society, 24(8), 2425-2432.

[184] Martos, M., Julián, B., Dehouli, H., Gourier, D., Cordoncillo, E., & Escribano, P. (2007). Synthesis and characterization of $Ti_{1-2x}Nb_xNi_xO_{2-x/2}$ solid solutions. Journal of Solid State Chemistry, 180(2), 679-687.

[185] Maloney, J. (2009). Titanate pigments: colored rutile, priderite, and pseudobrookite structured pigments. In: High Performance Pigments, pp. 53-73, Wiley-VCH Verlag GmbH & Co., Weinheim, Germany.

[186] Carter, M. L., & Withers, R. L. (2005). A universally applicable composite modulated structure approach to ordered $Ba_xM_yTi_{8-y}O_{16}$ hollandite-type solid solutions. Journal of Solid State Chemistry, 178(6), 1903-1914.

[187] Siggel, A., & Jansen, M. (1990). $ZrSn_{0,5}Ti_{0,5}O_4$ als Wirtsstruktur für keramische Farbkörper Strukturuntersuchungen an ZrTiO4 und $ZrSn_{0,5}Ti_{0,5}O_4$. Zeitschrift für anorganische und allgemeine Chemie, 582(1), 93-102.

[188] Dondi M., Matteucci F., Cruciani G., Zirconium titanate ceramic pigments: Crystal structure, spectroscopy and technological properties. Journal of Solid State Chemistry, 179 (2006) 233-246.

[189] Tena, M. A., Monrós, G., Carda, J., Cordoncillo, E., Escribano, P., & Alarcón, J. (1994). Synthesis of CrxTi1−2xNbxO2 O 2 0≤ x≤ 0.5 rutile solid solutions from alkoxides. Journal of Materials Science, 29(14), 3817-3821.

[190] Tena, M. A., Llusar, M., Badenes, J. A., Vicente, M., & Monrós, G. (2000). Influence of precursors on formation of TiO_2–$CrTaO_4$ rutile solid solutions. British Ceramic Transactions, 99(5), 219-224.

[191] Tena, M. A., Escribano, P., Monrós, G., Carda, J., & Alarcón, J. (1992). Influence of niobate structures on the formation of rutile solid solutions [$M^{III}NbO_4$-1bTiO_2, where M^{III} = Al, Fe, Cr]. Materials Research Bulletin, 27(11), 1301-1308.

[192] Gargori, C., Cerro, S., Galindo, R., & Monrós, G. (2010). In situ synthesis of orange rutile ceramic pigments by non-conventional methods. Ceramics International, 36(1), 23-31.

[193] Večeřa, J., Dohnalová, Ž., Mikulášek, P., & Šulcová, P. (2014). The influence of concentration of doping elements on anatase–rutile transformation at the synthesis of rutile pigments $(Ti,Cr,Nb)O_2$ and their pigmentary properties. Journal of Thermal Analysis and Calorimetry, 116(2), 547-555.

[194] Dik, J., Tichelaar, F., Goubitz, K., Peschar, R., & Schenk, H. (2002). 19th Century Naples yellow re-examined. Zeitschrift für Kunsttechnol. Konserv., 16, 291-306.

[195] Matteucci F., Cruciani G., Dondi M., Gasparotto G., Tobaldi D.M., Crystal structure, optical properties and colouring performance of karrooite $MgTi_2O_5$ ceramic pigments. Journal of Solid State Chemistry, 180 (2007) 3196-3210.

[196] Llusar, M., García, E., García, M. T., Gargori, C., Badenes, J. A., & Monrós, G. (2015). Synthesis, stability and coloring properties of yellow–orange pigments based on Ni-doped karrooite $(Ni,Mg)Ti_2O_5$. Journal of the European Ceramic Society, 35(1), 357-376.

[197] Kim, G. & Lee, B.-H. (2011). Synthesis and characterization of V_2O-doped karrooite brown pigments. Journal of the Korean Ceramic Society, 48(4), 303-306.

[198] Adolfová, L., Dohnalová, Ž., & Šulcová, P. (2013). New inorganic pigments based on $SrSnO_3$ doped by V_2O_5. Journal of thermal analysis and calorimetry, 113(1), 161-167.

[199] Adolfová, L., Dohnalová, Ž., Šulcová, P., & Matušková, M. (2014). Ceramic pigments based on doped strontium stannates. Journal of Thermal Analysis and Calorimetry, 116(2), 709-714.

[200] Luňáková, P., Trojan, M., Luxová, J., & Trojan, J. (2013). $BaSn_{1-x}Tb_xO_3$: A new yellow pigment based on a perovskite structure. Dyes and Pigments, 96(1), 264-268.

[201] Ishida, S., Ren, F., & Takeuchi, N. (1993). New yellow ceramic pigment based on codoping pyrochlore-type $Y_2Ti_2O_7$ with V^{5+} and Ca^{2+}. Journal of the American Ceramic Society, 76(10), 2644-2648.

[202] Gargori, C., Galindo, R., Cerro, S., García, A., Llusar, M., & Monrós, G. (2010). Synthesis of a new $Ca_xY_{2-x}VxSn2-_xO_7$ yellow pigment. Physics Procedia, 8, 84-87.

[203] Pailhé, N., Gaudon, M., & Demourgues, A. (2009). (Ca^{2+}, V^{5+}) co-doped $Y_2Ti_2O_7$ yellow pigment. Materials Research Bulletin, 44(8), 1771-1777.

[204] Šulcová, P., Fukalová, P., Válek, L., & Trojan, M. (2009). Study of ceramic pigments based on $Dy_2Sn_{2-x}V_xO_7$. Scientific papers of the University of Pardubice. Series A, Faculty of Chemical Technology. 14 (2008).

[205] Cerro, S., Llusar, M., Gargori, C., & Monrós, G. (2019). Cool and photocatalytic yellow ceramic pigments; from lead-tin to Cr doped scheelite pigments. Ceramics International, 45(4), 4613-4625.

[206] Stránská, L., Šulcová, P., & Mouchová, J. (2012). Study of ceramic pigments based on $Er_2Ce_{2-x}Mo_xO_7$. Journal of thermal Analysis and Calorimetry, 109(2), 643-648.

[207] Llusar, M., García, E., García, M. T., Esteve, V., Gargori, C., & Monrós, G. (2015). Synthesis and coloring performance of Ni-geikielite $(Ni,Mg)TiO_3$ yellow pigments: Effect of temperature, Ni-doping and synthesis method. Journal of the European Ceramic Society, 35(13), 3721-3734.

[208] He, X., Wang, F., Liu, H., Li, J., & Niu, L. (2017). Synthesis and coloration of highly dispersed $NiTiO_3$@TiO_2 yellow pigments with core-shell structure. Journal of the European Ceramic Society, 37(8), 2965-2972.

[209] Galindo, R., Gargori, C., Fas, N., Llusar, M., & Monrós, G. (2015). New chromium doped powellite (Cr–$CaMoO_4$) yellow ceramic pigment. Ceramics International, 41(5), 6364-6372.

[210] De la Luz, V., Prades, M., Beltrán, H., & Cordoncillo, E. (2013). Environmental-friendly yellow pigment based on Tb and M (M = Ca or Ba) co-doped Y_2O_3. Journal of the European Ceramic Society, 33(15-16), 3359-3368.

[211] Milao, T. M., Oliveira, J. F. A., Araújo, V. D., & Bernardi, M. I. B. (2010). $Zn_{0.97}M_{0.03}O$ (M = Co, Fe, and V) pigments: thermal, structural, and optical characterization. Journal of thermal analysis and calorimetry, 103(3), 873-877.

[212] Silvestri, S., Kubaski, E. T., Sequinel, T., Pianaro, S. A., Varela, J. A., & Tebcherani, S. M. (2013). Optical properties of the MoO_3-TiO_2 particulate system and its use as a ceramic pigment. Particulate Science and Technology, 31(5), 466-473.

[213] Šulcová, P., Trojan, M., & Šolc, Z. (1998). Cerium dioxide fluorite type pigments. Dyes and Pigments, 37(1), 65-70.

[214] Llusar, M., Vitásková, L., Šulcová, P., Tena, M. A., Badenes, J. A., & Monrós, G. (2010). Red ceramic pigments of terbium-doped ceria prepared through classical and non-conventional coprecipitation routes. Journal of the European Ceramic Society, 30(1), 37-52.

[215] Topuz, H., Ozel, E., & Turan, S. (2004). Synthesis of the CeO_2 Based Pigments by Using Enriched Rare-earth Oxides Located at Eskişehir Kızılcaören Region. Key Engineering Materials, 264, 1553-1556.
[216] Bondioli, F., Ferrari, A. M., Leonelli, C., Siligardi, C., Hart, N. A., & Evans, N. G. (2001). The application of microwaves in the synthesis of $Ce_{0.9}Pr_{0.1}O_2$ nanostructured powders. Journal of Materials Chemistry, 11(10), 2620-2624.
[217] Ocaña, M. (2002). Preparation and properties of uniform praseodymium-doped ceria colloidal particles. Colloid and Polymer Science, 280(3), 274-281.
[218] Masó, N., Beltrán, H., Muñoz, R., Julián, B., Carda, J. B., Escribano, P., & Cordoncillo, E. (2003). Optimization of praseodymium-doped cerium pigment synthesis temperature. Journal of the American Ceramic Society, 86(3), 425-430.
[219] Bondioli, F., Manfredini, T., Siligardi, C., & Ferrari, A. M. (2005). New glass–ceramic inclusion pigment. Journal of the American Ceramic Society, 88(4), 1070-1071.
[220] Bae, B., Tamura, S., & Imanaka, N. (2016). Novel environmentally friendly inorganic yellow pigments based on gehlenite-type structure. Ceramics International, 42(13), 15104-15106.
[221] Bondioli, F., Ferrari, A. M., Leonelli, C., & Manfredini, T. (1997). Chromite as a pigment for fast-fired porcelain tiles. Ceramic Engineering and Science Proceedings, 18, 44-58.
[222] Ozel, E., Kucuk, I., & Turan, S. (2002). Synthesis of an iron-chromium ceramic pigment by using limonite and chromite mixtures. Key Engineering Ceramics, 206, 1827-1830.
[223] Aly, M. H., Ismael, I. S., & Bondioli, F. (2010). Synthesis of coloured ceramic pigments by using chromite and manganese ores mixtures. Cerâmica, 56(338), 156-161.
[224] Xavier, C. S., Candeia, R. A., Bernardi, M. I. B., Lima, S. J. G., Longo, E., Paskocimas, C. A., & Santos, I. M. (2007). Effect of the modifier ion on the properties of $MgFe_2O_4$ and $ZnFe_2O_4$ pigments. Journal of Thermal Analysis and Calorimetry, 87(3), 709-713.
[225] Dohnalová, Ž., Šulcová, P., & Trojan, M. (2009). Effect of Er^{3+} substitution on the quality of Mg-Fe spinel pigments. Dyes and Pigments, 80(1), 22-25.
[226] Gurbuz, N., Coskun, E., & Ozel, E. (2010). Production of Ni and Co-gahnite pigments using ZnO powder produced from metal slags. Journal of Ceramic Processing Research, 11(2), 184-190.
[227] Souza, S. C., Souza, M. A. F., Lima, S. J. G., Cassia-Santos, M. R., Fernandes Jr, V. J., Soledade, L. E. B., & Santos, I. M. (2005). The effects of Co, Ni and Mn on the thermal processing of Zn_2TiO_4 pigments. Journal of Thermal Analysis and Calorimetry, 79(2), 455-459.
[228] Bernardin, A. M. (2008). Diffusion of Cr–Fe–Al–Zn pigment in a zirconia glaze. Dyes and Pigments, 79(1), 54-58.
[229] Naghibzadeh, S., Faghihi-Sani, M. A., & Baghshahi, S. (2013). Synthesis of beige pigment on the basis of (Fe, Zn, Cr, Al) spinel. International Journal of Engineering and Advanced Technology, 2(3), 606-609.
[230] Caki, M., Karasu, B., & Kaya, G. Use of iron and zinc oxide based pigments in stoneware glazes. In: J.G.Heinrich and C. Aneziris (eds.), Proc. 10th ECerS Conf., Göller Verlag, Baden-Baden, 2007, 1784-1787.
[231] Andreozzi, G. B., Baldi, G., Bernardini, G. P., Di Benedetto, F., & Romanelli, M. (2004). ^{57}Fe Mössbauer and electronic spectroscopy study on a new synthetic hercynite-based pigment. Journal of the European Ceramic Society, 24(5), 821-824.
[232] Vieira, F. T. G., Melo, D. S., de Lima, S. J. G., Longo, E., Paskocimas, C. A., Júnior, W. S., de Souza, A. G. & dos Santos, I. M. G. (2009). The influence of temperature on the color of TiO_2:Cr pigments. Materials Research Bulletin, 44(5), 1086-1092.
[233] Turan, S., Inceefe, Y., & Ozel, E. (2004). Production and characterisation of pigments produced using grinding waste from cast iron foundry. Key Engineering Materials, 264, 2473-2476.
[234] Ozel, E., Unluturk, G., & Turan, S. (2006). Production of brown pigments for porcelain insulator applications. Journal of the European Ceramic Society, 26(4-5), 735-740.
[235] Katsuki, H., & Komarneni, S. (2003). Role of α-Fe_2O_3 Morphology on the Color of Red Pigment for Porcelain. Journal of the American Ceramic Society, 86(1), 183-185.
[236] Opuchovicn, O., Kareiva, A. (2015). Historical hematite pigment: Synthesis by an aqueous sol-gel method, characterization and application for the colouration of ceramic glazes. Ceramics International 41, 4504-4513.
[237] Rodrigues Fiuza, T. E., Marcelino Borges, J. F., Marimon da Cunha, J. B., Masetto Antunes, S. R., Chaves de Andrade, A. V., Celso Antunes, A., Ferreira de Souza, E. C. (2018). Iron-based inorganic pigments from residue: Preparation and application in ceramic, polymer, and paint. Dyes and Pigments 148, 319-328.
[238] Dondi M., Matteucci F., Cruciani G., Gasparotto G., Tobaldi D.M., Pseudobrookite ceramic pigments: crystal structural, optical and technological properties. Solid State Sciences, 9 (2007) 362-369.
[239] Mesíková, Ž., Šulcová, P., & Trojan, M. (2006). Yellow pigments based on Fe_2TiO_5 and TiO_2. Journal of Thermal Analysis and Calorimetry, 83(3), 561-563.
[240] Gargori, C., Cerro, S., Galindo, R., García, A., Llusar, M., & Monrós, G. (2012). Iron and chromium doped perovskite (CaMO3 M= Ti, Zr) ceramic pigments, effect of mineralizer. Ceramics International, 38(6), 4453-4460.
[241] García, A., Galindo, R., Gargori, C., Cerro, S., Llusar, M., & Monrós, G. (2013). Ceramic pigments based on chromium doped alkaline earth titanates. Ceramics International, 39(4), 4125-4132.
[242] Hajjaji, W., Zanelli, C., Seabraa, M.P., Dondi, M., Labrinchaa, J.A. (2011). Cr-doped perovskite and rutile pigments derived from industrial by-products. Chemical Engineering Journal 171, 1178– 1184.
[243] Zou, J., Zhang, T., & He, X. (2019). Dark brown Cr doped $CaTiO_3$ pigments with high NIR reflectance. Materials Letters, 248, 173-176.
[244] Gargori, C., Cerro, S., Galindo, R., García, A., Llusar, M., Badenes, J., & Monrós, G. (2011). New vanadium doped calcium titanate ceramic pigment. Ceramics International, 37(8), 3665-3670.
[245] Ianoş, R., & Lazău, R. (2014). Chromium-doped calcium zirconate–A potential red shade pigment: Preparation, characterization and testing. Dyes and Pigments, 105, 152-156.

[246] Ianoş, R., Muntean, E., Lazău, R., Băbuță, R., Moacă, E. A., Păcurariu, C., & Hulka, I. (2018). One-step synthesis of near-infrared reflective brown pigments based on iron-doped lanthanum aluminate, $LaAl_{1-x}Fe_xO_3$. Dyes and Pigments, 152, 105-111.

[247] Kar, J. K., Stevens, R., & Bowen, C. R. (2008). Processing and characterisation of various mixed oxide and perovskite-based pigments for high temperature ceramic colouring application. Journal of Alloys and Compounds, 461(1-2), 77-84.

[248] Dohnalová, Ž., Šulcová, P., & Trojan, M. (2008). Synthesis and characterization of $LnFeO_3$ pigments. Journal of Thermal Analysis and Calorimetry, 91(2), 559-563.

[249] Liu, L., Han, A., Ye, M., & Zhao, M. (2015). Synthesis and characterization of Al^{3+} doped $LaFeO_3$ compounds: a novel inorganic pigments with high near-infrared reflectance. Solar Energy Materials and Solar Cells, 132, 377-384.

[250] Galindo, R., Llusar, M., Tena, M. A., Monrós, G., & Badenes, J. A. (2007). New pink ceramic pigment based on chromium (IV)-doped lutetium gallium garnet. Journal of the European Ceramic Society, 27(1), 199-205.

[251] Monrós, G., Pinto, H., Badenes, J., Llusar, M., & Tena, M. A. (2005). Chromium (IV) stabilisation in new ceramic matrices by coprecipitation method: application as ceramic pigments. Zeitschrift für anorganische und allgemeine Chemie, 631(11), 2131-2135.

[252] Stoyanova Lyubenova T., Matteucci F., Costa A.L. Dondi, M., Carda J., Ceramic pigments with sphene structure obtained by both spray- and freeze-drying techniques. Powder Technology, 193 (2009) 1-5.

[253] Stoyanova Lyubenova T., Matteucci F., Costa A.L., Dondi M., Ocaña M., Carda J., Synthesis of Cr-Doped CaTiSiO5 pigments by spray drying. Materials Research Bulletin, 44 (2009) 918–924

[254] Lyubenova, T. S., Ocaña, M., & Carda, J. (2008). Brown ceramic pigments based on chromium (III)-doped titanite obtained by spray pyrolysis. Dyes and pigments, 79(3), 265-269.

[255] Candeia, R. A., Souza, M. A. F., Bernardi, M. I. B., Maestrelli, S. C., Santos, I. M. G., Souza, A. G., & Longo, E. (2007). Monoferrite $BaFe_2O_4$ applied as ceramic pigment. Ceramics International, 33(4), 521-525.

[256] Candeia, R. A., Souza, M. A. F., Bernardi, M. I. B., Maestrelli, S. C., Santos, I. M. G., Souza, A. G., & Longo, E. (2006). $MgFe_2O_4$ pigment obtained at low temperature. Materials Research Bulletin, 41(1), 183-190.

[257] Candeia, R. A., Bernardi, M. I. B., Longo, E., Santos, I. M. G., & Souza, A. G. (2004). Synthesis and characterization of spinel pigment $CaFe_2O_4$ obtained by the polymeric precursor method. Materials Letters, 58(5), 569-572.

[258] Dohnalová, Ž., Šulcová, P., & Trojan, M. (2010). Synthesis and colour properties of pigments based on terbium-dopped Mg_2SnO_4. Journal of thermal analysis and calorimetry, 101(3), 973-978.

[259] Gouveia, D. S., Soledade, L. E. B., Paskocimas, C. A., Longo, E., Souza, A. G., & Santos, I. M. G. (2006). Color and structural analysis of $Co_xZn_{7-x}Sb_2O_{12}$ pigments. Materials Research Bulletin, 41(11), 2049-2056.

[260] Medina, E. A., Li, J., & Subramanian, M. A. (2017). Colored oxides with hibonite structure II: structural and optical properties of $CaAl_{12}O_{19}$-type pigments with chromophores based on Fe, Mn, Cr and Cu. Progress in Solid State Chemistry, 45, 9-29.

[261] Gargori, C., Cerro, S., Fas, N., Llusar, M., & Monrós, G. (2018). Ceramization of heavy metals in $(Ba_{1-x}M_x)$ $Al_2Si_2O_8$ celsian solid solutions and recycling as pigments. Materials Letters, 221, 187-191.

[262] Zhang, Q., Yang, Q., Sun, Y., & Wang, H. (2018). Low temperature synthesis of a new yellowish brown ceramic pigment based on $FeNbO_4$@$ZrSiO_4$. Ceramics International, 44(11), 12621-12626.

[263] Roth, R. S., & Waring, J. L. (1964). Ixiolite and other polymorphic types of $FeNbO_4$. American Mineralogist, 49(3-4), 242-246.

[264] Kumari, L. S., George, G., Rao, P. P., & Reddy, M. L. P. (2008). The synthesis and characterization of environmentally benign praseodymium-doped $TiCeO_4$ pigments. Dyes and Pigments, 77(2), 427-431.

[265] Dondi M., Stoyanova Lyubenova T., Carda J., Ocaña M., M-doped Al_2TiO_5 (M=Cr,Mn,Co) solid solutions and their use as ceramic pigments. Journal of the American Ceramic Society, 92 [9] (2009) 1972-1980.

[266] Badenes, J. A., Llusar, M., Tena, M. A., Calbo, J., & Monros, G. (2002). Praseodymium-doped cubic Ca–ZrO_2 ceramic stain. Journal of the European Ceramic Society, 22(12), 1981-1990.

[267] Tena, M. A. (2012). Characterization of MgxM2–xP2O7 (M= Cu and Ni) solid solutions. Journal of the European Ceramic Society, 32(2), 389-397.

[268] Tena, M. A., Mendoza, R., García, J. R., & García-Granda, S. (2017). Structural characterization and colour of $Ni_3V_xP_{2-x}O_8$ ($0 \leq x \leq 2$) and $Ni_2V_yP_{2-y}O_7$ ($0 \leq y \leq 2$) materials. Results in physics, 7, 1095-1105.

[269] Tena, M. A., Mendoza, R., Martínez, D., Trobajo, C., García, J. R., & García-Granda, S. (2019). Beige materials for the ceramic industry: $Al_xV_yFe_{1-x}P_{1-y}O_4$ ($0.0 \leq x \leq 0.3$, $0.0 \leq y \leq 0.1$) solid solutions. Ceramics International, 45(7), 8271-8278.

[270] Tena, M. Á., Mendoza, R., Trobajo, C., García, J. R., & García-Granda, S. (2019). $Co_2P_2O_7$–$Ni_2P_2O_7$ solid solutions: Structural characterization and color. Journal of the American Ceramic Society, 102(6), 3695-3704.

[271] Liang, S. T., Zhang, H. L., Luo, M. T., Luo, K. J., Li, P., Xu, H. B., & Zhang, Y. (2014). Colour performance investigation of a Cr_2O_3 green pigment prepared via the thermal decomposition of CrOOH. Ceramics International, 40(3), 4367-4373.

[272] Li, P., Xu, H. B., Zheng, S. L., Zhang, Y., Li, Z. H., & Bai, Y. L. (2008). A green process to prepare chromic oxide green pigment. Environmental science & technology, 42(19), 7231-7235.

[273] Carda, J., Monros, G., Escribano, P., & Alarcon, J. (1989). Synthesis of uvarovite garnet. Journal of the American Ceramic Society, 72(1), 160-162.

[274] Carda, J., Monrós, G., Tena, M. A., Marti, M. C., Cordoncillo, E., & Escribano, P. (1992). Profundizacíon en el estudio de la síntesis y microcaracterización del pigmento verde victoria ($Ca_3Cr_2Si_3O_{12}$) de aplicación en la industria cerámica. Boletín de la Sociedad Española de Cerámica y Vidrio, 31(1), 19-31.

[275] Llusar, M., Vicent, J. B., Tena, M. A., Badenes, J., Escribano, P., & Monrós, G. (1997). Environmental optimization of green Victoria ceramic pigment by sol-gel methods. Key Engineering Materials, 132, 2236-2239.

[276] Llusar, M., Monros, G., Tena MÁ, Vicent, J. B., & Badenes, J. A. (1999). Effect of synthesis methods and aging on synthesis of uvarovite garnet by ceramic and sol-gel processes. British Ceramic Transactions, 98(3), 113-121.

[277] Verger, L., Dargaud, O., Rousse, G., Cotte, M., & Cormier, L. (2017). The stability of gahnite doped with chromium pigments in glazes from the French manufacture of Sèvres. Journal of the American Ceramic Society, 100(1), 86-95.

[278] Catalan, L., Contreras, G., Ramos, F., Bedoya, D., Vicente, M., & Monros, G. (2000). Structural modification of cobalt chromite by doping with Mg^{2+} and Zn^{2+} ions and their effect on colour in glassy matrices. Proc. VI World Congress on the Quality of Ceramic Tiles, Qualicer 2000, Vol. 3, Castellon (Spain).

[279] Gilabert, J., Palacios, M.D., Sanz, V., Mestre, S. (2018). Effects of composition and furnace temperature on $(Ni,Co)(Cr,Al)_2O_4$ pigments synthesized by solution combustion route. Int J Appl Ceram Technol.,15, 179-190.

[280] Wang, Y., Wang, Q., Chang, Q., Hu, S., Wang, X., & Yang, K. (2018). Effect of particle size on the blue chromate pigment $CoAl_2O_4$. Journal of Ceramic Science and Technology, 9(1), 43-46.

[281] Esteves, D., Hajjaji, W., Seabra, M. P., & Labrincha, J. A. (2010). Use of industrial wastes in the formulation of olivine green pigments. Journal of the European Ceramic Society, 30(15), 3079-3085.

[282] El Hadri, M., Ahamdane, H., & Raghni, M. E. I. (2015). Sol gel synthesis of forsterite, M-doped forsterite (M= Ni,Co) solid solutions and their use as ceramic pigments. Journal of the European Ceramic Society, 35(2), 765-777.

[283] Pavlov, R. S., Marzá, V. B., & Carda, J. B. (2002). Electronic absorption spectroscopy and colour of chromium-doped solids. Journal of Materials Chemistry, 12(9), 2825-2832.

[284] Ardit M., Cruciani G., Dondi M., Matteucci F., Ti-Ca-Al-doped $YCrO_3$ pigments: an XRD and UV-vis-NIR investigation. Materials Research Bulletin, 44 (2009) 666-673

[285] Kim, Y. J., & Lee, B. H. (2011). Synthesis of tialite ceramic pigments and coloring in glazes. Korean Journal of Materials Research, 21(8), 450-455.

[286] Kim, Y. J., & Lee, B. H. (2011). Cr-doped Tialite Pigments. Korean Journal of Materials Research, 21(9), 515-519.

[287] Llusar, M., Bermejo, T., Primo, J. E., Gargori, C., Esteve, V., & Monrós, G. (2017). Karrooite green pigments doped with Co and Zn: Synthesis, color properties and stability in ceramic glazes. Ceramics International, 43(12), 9133-9144.

[288] Gaudon, M., Toulemonde, O., & Demourgues, A. (2007). Green coloration of Co-doped ZnO explained from structural refinement and bond considerations. Inorganic chemistry, 46(26), 10996-11002.

[289] Ekambaram, S. (2005). Combustion synthesis and characterization of new class of ZnO-based ceramic pigments. Journal of Alloys and Compounds, 390(1-2), L4-L6.

[290] Zhou, N., She , S., Zhang, Y. , Li, S., Xu, S., Luan, J. (2020). Coprecipitation synthesis of a green Co-doped wurtzite structure high near-infrared reflective pigments using ammonia as precipitant, Journal of Alloys and Compounds, 820, 153183.

[291] Fernandez, F., Colon, C., Duran, A., Barajas, R., d'Ors, A., Becerril, M., Llopisc, J., Pajec, S.E., Saez-Puche, R. & Julian, I. (1998). The Y2BaCuO5 oxide as green pigment in ceramics. Journal of Alloys and Compounds, 275, 750-753.

[292] Kar, J. K., Stevens, R., & Bowen, C. R. (2008). Rare-earth cuprates for ceramic colouring application—An investigation. Journal of Alloys and Compounds, 455(1-2), 121-129.

[293] Ocana, M., González-Elipe, A. R., Andrés-Vergés, M., Tartaj, P., Serna, C. J., & Orera, V. M. (1998). Preparation by hydrolysis of aerosols and colour properties of Cr-doped and Co-doped zircon powders. Journal of the European Ceramic Society, 18(7), 821-830.

[294] Trojan, M. (1990). Synthesis of a blue-green pigment from the mineral zircon. Ceramics international, 16(5), 295-299.

[295] Trojan, M. (1990). Synthesis of blue-violet and brown-green zirconium silicate pigments from zircon mineral. Dyes and Pigments, 13(4), 311-323.

[296] Ke, S., Wang, Y., & Pan, Z. (2014). Synthesis of $Nd_2Si_2O_7$ ceramic pigment with LiCl as a mineralizer and its color property. Dyes and Pigments, 108, 98-105.

[297] Gayo, G. X., Troncoso, F., & Lavat, A. E. (2014). Application of $LnCrTeO_6$ oxides as new ceramic pigments of the type “green chromium”. Ceramics International, 40(1), 611-617.

[298] Galindo Llorach, R., Gargori García, C., Llusar, M., García López, A., Badenes March, J. A., & Monrós Tomás, G. (2011). Ecopigmentos cerámicos verdes y amarillos de $Pr_2Mo_2O_9$ dopados con calcio obtenidos en presencia de mineralizadores y por coprecipitación química. Boletín de la Sociedad Española de Cerámica y Vidrio, 50, 5, 219-224.

[299] Luxová, J., Těšitelová, K., Podzemná, V., Šulcová, P., Bosacka, M., Błońska-Tabero, A., & Filipek, E. (2019). Components of the $Co_3Cr_4(PO_4)_6$-$Cr(PO_3)_3$ system and the compound $CoCr_2(P_2O_7)_2$ as new ceramic pigments. Materials Chemistry and Physics, 121763.

[300] Hashimoto, H., Sayo, K., Asoh, H., Fujii, T., Takano, M., & Masuno, A. (2019). Bright greenish-yellow pigments based on $Sc_{2-x}Fe_xO_3$ solid solutions with bixbyite structure. Materials Research Bulletin, 109, 190-194.

[301] Dondi M., Ardit M., Cruciani G., Zanelli C., Tetrahedrally coordinated Co^{2+} in oxides and silicates: Effect of local environment on optical properties. American Mineralogist, 99 (2014) 1736-1745.

[302] Keppler, H., & Bagdassarov, N. (1999). The speciation of Ni and Co in silicate melts from optical absorption spectra to 1500°C. Chemical Geology, 158(1-2), 105-115.

[303] Llusar, M., Forés, A., Badenes, J. A., Calbo, J., Tena, M. A., & Monrós, G. (2001). Colour analysis of some cobalt-based blue pigments. Journal of the European Ceramic Society, 21(8), 1121-1130.

[304] El Hadri, M., Ahamdane, H., & Raghni, M. E. I. (2017). Effect of sol–gel method on colour properties of the classical cobalt olivine (Co_2SiO_4) ceramic pigment. Bulletin of Materials Science, 40(2), 375-382.

[305] Meseguer, S., Tena, M. A., Gargori, C., Badenes, J. A., Llusar, M., & Monrós, G. (2007). Structure and colour of cobalt ceramic pigments from phosphates. Ceramics international, 33(5), 843-849.

[306] Meseguer, S., Tena, M. A., Gargori, C., Galindo, R., Badenes, J. A., Llusar, M., & Monrós, G. (2008). Development of blue ceramic dyes from cobalt phosphates. Ceramics International, 34(6), 1431-1438.

[307] Llusar, M., Zielinska, A., Tena, M. A., Badenes, J. A., & Monrós, G. (2010). Blue-violet ceramic pigments based on Co and $MgCo_{2-x}Mg_xP_2O_7$ diphosphates. Journal of the European Ceramic Society, 30(9), 1887-1896.

[308] Llusar, M., Badenes, J. A., García, A., Gargori, C., Galindo, R., & Monrós, G. (2011). Solid solutions of mixed metal $Mn_{3-x}Mg_xFe_4(PO_4)_6$ orthophosphates: Colouring performance within a double-firing ceramic glaze. Ceramics International, 37(2), 493-504.

[309] Ardit, M., Cruciani, G., & Dondi, M. (2012). Structural relaxation in tetrahedrally coordinated Co^{2+} along the gahnite-Co-aluminate spinel solid solution. American Mineralogist, 97(8-9), 1394-1401.

[310] Tang, Y., Wu, C., Song, Y., Zheng, Y., & Zhao, K. (2018). Effects of colouration mechanism and stability of $CoAl_2O_4$ ceramic pigments sintered on substrates. Ceramics International, 44(1), 1019-1025.

[311] Mesíková, Ž., Šulcová, P., & Trojan, M. (2006). Preparation and practical application of spinel pigment $Co_{0.46}Zn_{0.55}(Ti_{0.064},Cr_{0.91})_2O_4$. Journal of thermal Analysis and Calorimetry, 84(3), 733-736.

[312] He, X., Wang, F., Liu, H., Niu, L., & Wang, X. (2018). Synthesis and color properties of the TiO_2@$CoAl_2O_4$ blue pigments with low cobalt content applied in ceramic glaze. Journal of the American Ceramic Society, 101(6), 2578-2588.

[313] Wang, Q., Wang, Y., Liu, K., Liu, J., Wang, C., Wang, Y., & Chang, Q. (2020). Synthesis and characterization of high-performance spherical urchin-like $CoAl_2O_4$ pigment prepared via microemulsion-hydrothermal-precipitation method. Advanced Powder Technology. https://doi.org/10.1016/j.apt.2019.12.041

[314] Forés, A., Llusar, M., Badenes, J. A., Calbo, J., Tena, M. A., & Monrós, G. (2000). Cobalt minimisation in willemite ($Co_xZn_{2-x}SiO_4$) ceramic pigments. Green Chemistry, 2(3), 93-100.

[315] Pozas, R., Orera, V. M., & Ocana, M. (2005). Hydrothermal synthesis of Co-doped willemite powders with controlled particle size and shape. Journal of the European Ceramic Society, 25(13), 3165-3172.

[316] Ozel E., Yurdakul H., Turan S., Ardit M., Cruciani G., Dondi M. (2010). Co-doped willemite ceramic pigments: Technological behaviour, crystal structure and optical properties. Journal of the European Ceramic Society, 30, 3319-3329.

[317] Dondi M., Ardit M., Cruciani G., Sorace L., Di Benedetto F., New spectroscopic and diffraction data to solve the vanadium-doped zircon pigment conundrum. Journal of the European Ceramic Society, 38 (2018) 5234-5245.

[318] Monrós, G., Carda, J., Tena, M. A., Escribano, P., Sales, M., & Alarcón, J. (1993). Different kinds of solid solutions in the V_2O_5-$ZrSiO_4$-NaF system by sol-gel processes and their characterization. Journal of the European Ceramic Society, 11(1), 77-86.

[319] Ardizzone, S., Cappelletti, G., Fermo, P., Oliva, C., Scavini, M., & Scime, F. (2005). Structural and spectroscopic investigations of blue, vanadium-doped $ZrSiO_4$ pigments prepared by a sol-gel route. The Journal of Physical Chemistry B, 109(47), 22112-22119.

[320] Caselli, C., Lusvardi, G., Malavasi, G., Menabue, L., & Miselli, P. (2007). Multitechnique approach to V–$ZrSiO_4$ pigment characterization and synthesis optimization. Journal of the European Ceramic Society, 27(2-3), 1743-1750.

[321] Schabbach, L. M., Bondioli, F., Ferrari, A. M., Manfredini, T., Petter, C. O., & Fredel, M. C. (2007). Influence of firing temperature on the color developed by a $(Zr,V)SiO_4$ pigmented opaque ceramic glaze. Journal of the European ceramic society, 27(1), 179-184.

[322] Dondi M., Zanelli C., Ardit M., Cruciani G., Co-doped hardystonite, $Ca_2(Zn,Co)Si_2O_7$, a new blue ceramic pigment. Journal of the American Ceramic Society, 94 (2011) 1025-1030.

[323] Mantovani L., Tribaudino M., Dondi M., Zanelli C., Synthesis and color performance of $CaCoSi_2O_6$ pyroxene, a new ceramic colorant. Dyes and Pigments, 120 (2015) 118-125.

[324] Gori C., Mantovani L., Tribaudino M., Zanelli C., Dondi, M., Colour of $Ca(Co_xMg_{1-x})Si_2O_6$ pyroxenes and their technological behaviour as ceramic colorants. Ceramics International, 44 (2018) 12745-12753.

[325] Leite, A., Costa, G., Hajjaji, W., Ribeiro, M. J., Seabra, M. P., & Labrincha, J. A. (2009). Blue cobalt doped-hibonite pigments prepared from industrial sludges: Formulation and characterization. Dyes and Pigments, 81(3), 211-217.

[326] Hajjaji, W., Seabra, M. P., & Labrincha, J. A. (2009). Recycling of solid wastes in the synthesis of Co-bearing calcium hexaluminate pigment. Dyes and Pigments, 83(3), 385-390.

[327] Costa G., Ribeiro M.J., Labrincha J.A., Dondi M., Matteucci F., Cruciani G., Ni-doped hibonite ($CaAl_{12}O_{19}$): a new turquoise blue ceramic pigment. Journal of the European Ceramic Society, 29 (2009) 2671-2678.

[328] Li, J., Medina, E. A., Stalick, J. K., Sleight, A. W., & Subramanian, M. A. (2016). Colored oxides with hibonite structure: a potential route to non-cobalt blue pigments. Progress in Solid State Chemistry, 44(4), 107-122.

[329] Ardit M., Borcănescu S., Cruciani G., Dondi M., Lazău I., Păcurariu C., Zanelli C., Ni-Ti co-doped hibonite ceramic pigments by combustion synthesis: crystal structure and optical properties. Journal of the American Ceramic Society, 99 (2016) 1749-1760.

[330] Gaudon, M., Robertson, L. C., Lataste, E., Duttine, M., Ménétrier, M., & Demourgues, A. (2014). Cobalt and nickel aluminate spinels: blue and cyan pigments. Ceramics International, 40(4), 5201-5207.

[331] Forés, A., & Llusar, M. (2001). Alternative turquoise blue pigments for glazes. American Ceramic Society Bulletin, 80(5), 47-52.

[332] Lavat, A. E., & Gayo, G. X. (2014). In situ formation of coloured M(II)–doped Zn_2SiO_4–willemite in ceramic glazes (M = Mn, Co, Ni, Cu). Ceramics International, 40(8), 11947-11955.

[333] Yan, J., Huang, J., Zhang, T., Tian, H., Yu, J., Zhang, L., & Zhang, Y. (2019). Investigation of the microstructure, cation distribution and optical properties of nanoscale $Ni_xMg_{1-x}Al_2O_4$ spinel pigments. Ceramics International, 45(11), 14073-14083.

[334] Kendrick, E., Kirk, C. J., & Dann, S. E. (2007). Structure and colour properties in the Egyptian Blue Family, $M_{1-x}M'_xCuSi_4O_{10}$, as a function of M, M′ where M,M′ = Ca, Sr and Ba. Dyes and Pigments, 73(1), 13-18.

[335] Zhang, C., Zhang, N., Wang, X., & Zhang, L. (2018). Novel preparation of an ancient ceramic pigment $BaCuSi_4O_{10}$ and its performance investigation. Materials Research Bulletin, 101, 334-339.

[336] Kusumoto, K. (2018). Synthesis of Co-free inorganic blue pigments based on turquoise blue glaze. Journal of the Ceramic Society of Japan, 126(5), 408-411.

[337] Ocaña, M., Espinós, J. P., & Carda, J. B. (2011). Synthesis, through pyrolysis of aerosols, of $YIn_{1-x}Mn_xO_3$ blue pigments and their efficiency for colouring glazes. Dyes and Pigments, 91(3), 501-507.

[338] Li, J., & Subramanian, M. A. (2019). Inorganic pigments with transition metal chromophores at trigonal bipyramidal coordination: Y(In,Mn)O_3 blues and beyond. Journal of Solid State Chemistry, 272, 9-20.

[339] Dohnalová, Ž., Šulcová, P., & Gorodylova, N. (2014). Study of ceramic pigments based on cobalt doped Y_2O_3-Al_2O_3 system. Journal of Thermal Analysis and Calorimetry, 116(2), 647-654.

[340] Hafez, H. S., & El-Fadaly, E. (2012). Synthesis, characterization and color performance of novel Co^{2+}-doped alumina/titania nanoceramic pigments. Spectrochimica Acta Part A: Molecular and Biomolecular Spectroscopy, 95, 8-14.

[341] Fernández-Osorio, A., Jiménez-Segura, M. P., Vázquez-Olmos, A., & Sato-Berru, R. (2011). Turquoise blue nanocrystalline pigment based on $Li_{1.33}Ti_{1.66}O_4$: Synthesis and characterization. Ceramics International, 37(5), 1465-1471.

[342] Dondi M., Zanelli C., Ardit M., Cruciani G., Mantovani L., Tribaudino M., Andreozzi G.B., Ni-free, black ceramic pigments based on Co-Cr-Fe-Mn spinels: a reappraisal of crystal structure, optical properties and technological behaviour. Ceramics International, 39 (2013) 9533-9547.

[343] Shin, K. H., & Lee, B. H. (2007). Synthesis of Fe_2O_3–CoO–Cr_2O_3–MnO_2 pigments and coloring in glazes. Journal of the Korean Ceramic Society, 44(10), 554-561.

[344] Lee, K. H., Myung, M. S., & Lee, B. H. (2007). Development of black color spinel pigment for high temperature. Journal of the Korean Ceramic Society, 44(5), 160.

[345] Tanisan, B., & Turan, S. (2011). Black ceramic pigments for porcelain tile bodies produced with chromite ores and iron oxide waste. Journal of Ceramic Processing Research, 12(4), 462-467.

[346] Kim, J. H., Lee, S. H., Suh, M. C., & Lee, B. H. (2007). Synthesis of cobalt oxide free black color spinel pigment. Journal of the Korean Ceramic Society, 44(11), 639-644.

[347] Eliziário, S. A., de Andrade, J. M., Lima, S. J., Paskocimas, C. A., Soledade, L. E., Hammer, P., Longo, E., Souza, A.G., & Santos, I. M. (2011). Black and green pigments based on chromium–cobalt spinels. Materials Chemistry and Physics, 129(1-2), 619-624.

[348] Calbo, J., Tena, M., Monrós, G., Llusar, M., Galindo, R., & Badenes, J. A. (2005). Flux agent effect on nickel ferrite black pigment. American Ceramic Society Bulletin, 84(12), 9201-9206.

[349] Costa, G., Della, V. P., Ribeiro, M. J., Oliveira, A. P. N., Monrós, G., & Labrincha, J. A. (2008). Synthesis of black ceramic pigments from secondary raw materials. Dyes and Pigments, 77(1), 137-144.

[350] Gargori, C., Prim, S. R., Llusar, M., Folgueras, M. V., & Monrós, G. (2018). Recycling of Cr/Ni/Cu plating wastes as black ceramic pigments. Materials Letters, 218, 341-345.

[351] Lee, K. H., Lee, Y. S., Park, J. S., & Lee, B. H. (2008). Preparation and characterization of black zirconia ceramics by black color spinel pigment. Journal of the Korean Ceramic Society, 45(4), 214.

[352] Ye, M. Q., Han, A. J., Chu, Z. S., Che, J. F., & Wang, C. (2013). Synthesis and characterization of Mn-doped copper chromite black pigments. Advanced Materials Research, 602, 71-75.

[353] Mestre, S., Gómez-Tena, M. P., Gazulla, M. F., & Gozalbo, A. (2013). Interaction of the chromium–iron black pigment with porcelanised stoneware. Ceramics International, 39(7), 7453-7459.

[354] De la Torre, Á. G., Aranda, M. A., León-Reina, L., & Pérez, J. (2011). Ceramic pigments and the European REACH legislation: black Fe_2O_3–Cr_2O_3, a case study. International Journal of Applied Ceramic Technology, 8(4), 905-910.

[355] Ozel, E., & Turan, S. (2003). Production and characterisation of iron-chromium pigments and their interactions with transparent glazes. Journal of the European Ceramic Society, 23(12), 2097-2104.

[356] Yurdakul, H., Turan, S., & Ozel, E. (2011). The mechanism for the colour change of iron chromium black pigments in glazes through transmission electron microscopy techniques. Dyes and Pigments, 91(2), 126-133.

[357] Escardino, A., Mestre, S., Barba, A., Beltrán, V., & Blasco, A. (2000). Synthesis mechanism of an iron–chromium ceramic pigment. Journal of the American Ceramic Society, 83(1), 29-32.

[358] Escardino, A., Mestre, S., Barba, A., Monzo, M., Blasco, A., & Beltran, V. (2003). Colorimetric study of black $(Fe,Cr)_2O_3$ pigment synthesis reaction: relation between chromatic coordinates and synthesis conditions. British Ceramic Transactions, 102(6), 247-250.

[359] Tena, M. A., Sorlí, S., Llusar, M., Badenes, J. A., Forés, A., & Monrós, G. (2005). Study of Sb-doped SnO_2 gray ceramic pigment with cassiterite structure. Zeitschrift für anorganische und allgemeine Chemie, 631(11), 2188-2191.

[360] Bernardi, M., Leite, E., Longo, E., Conceição, M., & Souza, A. (2004). Development of SnO_2/Sb-based ceramic pigments. Journal of Thermal Analysis and Calorimetry, 75(2), 481-486.

[361] Carceller, J.V., Jovaní, M.A., Nebot, A., Soler, A., Carda, J.B., Gómez, J.J., Garcia, G. (1998). Study of electrical conductivity in ceramic floor tiles. Development of an antielectrostatic vitrifiable glaze. Proc. V World Congress on the Quality of Ceramic Tiles, Qualicer98, Castellón, Spain.

[362] Wang, Y., Wu, J., & Zhou, J. (2007). Antistatic ceramic tiles modified by Sb-doped SnO_2. Key Engeneering Materials, 280-283, 279-280.

[363] Tena, M. A., Mestre, A., García, A., Sorlí, S., & Monrós, G. (2003). Synthesis of gray ceramic pigments with rutile structure from alkoxides. Journal of sol-gel science and technology, 26(1-3), 813-816.

[364] Melo, D., Vieira, F. T. G., Costa, T. C. C., Soledade, L. E. B., Paskocimas, C. A., Melo, D. M. A., Longo, E., Marinho, E.P., Souza, A.G. & Santos, I. M. G. (2013). Lanthanum cobaltite black pigments with perovskite structure. Dyes and Pigments, 98(3), 459-463.

[365] Hajjaji W., Pullar R.C., Zanelli C., Seabra M.P., Dondi M., Labrincha J.A., Compositional and chromatic properties of strontium hexaferrite as pigment for ceramic bodies and alternative synthesis from wiredrawing sludge. Dyes and Pigments, 96 (2013) 659-664.

[366] Peng, C., Zhang, C., Lv, M., & Wu, J. (2013). Preparation of silica encapsulated carbon black with high thermal stability. Ceramics International, 39(6), 7247-7253.

[367] Chang, Q., Wang, X., Wang, Y., Bao, Q., Zhou, J. E., & Zhu, Q. (2014). Encapsulated carbon black prepared by sol–gel-spraying: A new black ceramic pigment. Journal of the European Ceramic Society, 34(13), 3151-3157.

[368] Tang, H., Hu, Q., Jiang, F., Jiang, W., Liu, J., Chen, T., & Luo, W. (2019). Size control of C@$ZrSiO_4$ pigments via soft mechano-chemistry assisted non-aqueous sol-gel method and their application in ceramic glaze. Ceramics International, 45(8), 10756-10764.

[369] Tang, H., Hu, Q., Jiang, W, Liu, J, Feng, G., Chen, T, Tan, G, Zhang, X, Miao, L., Facile non-aqueous synthesis of high color rendering C@$ZrSiO_4$ encapsulation pigment with carbon-containing precursors as in-situ carbon sources, Ceramic International 44 820189 16498-16506.

[370] Chen, S., Fu, S., Lang, Y., Tian, C., Wei, H., & Wang, C. A. (2020). Submicronic spherical inclusion black pigment by double-shell reaction sintering. Journal of the American Ceramic Society, 103(3), 1520-1526.

[371] Dondi M., Matteucci F., Baldi G., Barzanti A., Cruciani G., Zama I., Bianchi C.L., Gray-blue Al_2O_3-MoO_x ceramic pigments: crystal structure, colouring mechanism and technological performance. Dyes & Pigments, 76 (2008) 179-186.

[372] Levitskii, I. A., & Mazura, N. V. (2005). Opacified glazes produced by high-temperature firing for sanitary ceramicware. Glass and Ceramics, 62(7-8), 215-218.

[373] Moreno, A., Bou, E., Cabrera, M. J., & Quereda, P. (1998). Zirconium silicate opacification mechanism in ceramic engobes. Proc. XI World Congress on the Quality of Ceramic Tiles, Qualicer98, Castellon (Spain).

[374] Cavalcante, P. T., Dondi, M., Ercolani, G., Guarini, G., Melandri, C., Raimondo, M., & e Almendra, E. R. (2004). The influence of microstructure on the performance of white porcelain stoneware. Ceramics International, 30(6), 953-963.

[375] Thiele, E. S., & French, R. H. (1998). Light-scattering properties of representative, morphological rutile titania particles studied using a finite-element method. Journal of the American Ceramic Society, 81(3), 469-479.

[376] Snyders, E., Potgieter, J. H., & Nel, J. T. (2005). The upgrading of an inferior grade zircon to superior opacifier for sanitary ware and glazes. Journal of the Southern African Institute of Mining and Metallurgy, 105(7), 459-463.

[377] Wang, S., Peng, C., Huang, Z., Zhou, J., Lü, M., & Wu, J. (2014). Clustering of zircon in raw glaze and its influence on optical properties of opaque glaze. Journal of the European Ceramic Society, 34(2), 541-547.

[378] Schabbach, L. M., Bondioli, F., & Fredel, M. C. (2011). Colouring of opaque ceramic glaze with zircon pigments: formulation with simplified Kubelka–Munk model. Journal of the European Ceramic Society, 31(5), 659-664.

[379] Sarjahani, R., Sheikhattar, M., Javadpour, S., & Hashemi, B. (2016). The effect of opacifiers on surface roughness of ceramic glazes. Iranian Journal of Materials Science and Engineering, 13(1), 37-42.

[380] Jacobs, C. W. F., & Baldwin, W. J. (1954). Effects of zirconium-type opacifiers on properties of glazes. Journal of the American Ceramic Society, 37(6), 258-266.

[381] Bhushan, B., Das, B., & Sen, S. (1966). Zircon opacifiers: Their preparation and performance in glazes. Transactions of the Indian Ceramic Society, 25(1), 97-106.

[382] Castilone, R. J., Sriram, D., Carty, W. M., & Snyder, R. L. (1999). Crystallization of zircon in stoneware glazes. Journal of the American Ceramic Society, 82(10), 2819-2824.

[383] Blonski, R. (1993). The effect of zircon dissolution and reprecipitation on the color development of glazes. Ceramic Engineering Science Proceedings, 14(1-2) 176-189.

[384] Earl, D. A., & Clark, D. E. (2000). Effects of glass frit oxides on crystallization and zircon pigment dissolution in whiteware coatings. Journal of the American Ceramic Society, 83(9), 2170-2176.

[385] Assifaoui, A., Atmani, W., Daoudi, A., Moussa, R., & Blanchart, P. (2003). Grain growth of zircon pigment in tile glaze. British Ceramic Transactions, 102(2), 57-60.

[386] Wang, S., Peng, C., Xiao, H., & Wu, J. (2015). Microstructural evolution and crystallization mechanism of zircon from frit glaze. Journal of the European Ceramic Society, 35(9), 2671-2678.

[387] Atkinson, I., Smith, M. E., & Zaharescu, M. (2012). Examining correlations between composition, structure and properties in zircon-containing raw glazes. Ceramics International, 38(3), 1827-1833.

[388] Bruzzi, L., Baroni, M., Mazzotti, G., Mele, R., & Righi, S. (2000). Radioactivity in raw materials and end products in the Italian ceramics industry. Journal of Environmental Radioactivity, 47(2), 171-181.

[389] Atkinson, I., Teoreanu, I., Mocioiu, O. C., Smith, M. E., & Zaharescu, M. (2010). Structure property relations in multicomponent oxide systems with additions of TiO_2 and ZrO_2 for glaze applications. Journal of Non-Crystalline Solids, 356(44-49), 2437-2443.

[390] Tite, M., Pradell, T., & Shortland, A. (2008). Discovery, production and use of tin-based opacifiers in glasses, enamels and glazes from the late iron age onwards: A reassessment. Archaeometry, 50(1), 67-84.

[391] Matin, M. (2019). Tin-based opacifiers in archaeological glass and ceramic glazes: a review and new perspectives. Archaeological and Anthropological Sciences, 11(4), 1155-1167.

[392] Atkinson, I., Teoreanu, I., & Zaharescu, M. (2008). Correlation among composition properties of SnO_2 opacified glazes. UPB Sci Bull Ser B, 70(3), 11-22.

[393] Bou, E., Moreno, A., Escardino, A., & Gozalbo, A. (2007). Microstructural study of opaque glazes obtained from frits of the system: SiO_2-Al_2O_3-B_2O_3-(P_2O_5)-CaO-K_2O-TiO_2. Journal of the European Ceramic Society, 27(2-3), 1791-1796.

[394] Yildiz, B., Ozturk, Z., & Kara, A. (2015). Effects of alumina and white fused alumina addition on transparent wall and floor tile glazes. Acta Physica Polonica A, 4(127), 1090-1093.

[395] Ozturk, Z. B., Yıldız, B., & Kara, A. (2019). Effects of alumina and white fused alumina addition on technological properties of transparent floor tile glazes. Journal of Thermal Analysis and Calorimetry, 1-7.
[396] Tucci, A., Esposito, L., Malmusi, L., & Rambaldi, E. (2007). New body mixes for porcelain stoneware tiles with improved mechanical characteristics. Journal of the European Ceramic Society, 27(2-3), 1875-1881.
[397] Bondioli, F., Manfredini, T., Giorgi, M., & Vignali, G. (2010). Functionalization of ceramic tile surface by soluble salts addition: Part I. Journal of the European Ceramic Society, 30(1), 11-16.
[398] Cai, J., Lv, M., Guan, K., Sun, Q., Peng, C., Wu, J., & Liu, Y. (2018). Development of spinel opaque glazes for ceramic tiles. Journal of the European Ceramic Society, 38(1), 297-302.
[399] Nebot-Diaz, I., Sanchez-Muñoz, L., Bakali, J., & Carda, J. B. (1999). Spinel glass-ceramics glaze for porcelain stoneware. Br. Ceram. Proc., 60, 91-92.
[400] Gajek, M., Partyka, J., Leśniak, M., Rapacz-Kmita, A., & Wójcik, Ł. (2018). Gahnite white colour glazes in ZnO–R_2O–RO–Al_2O_3–SiO_2 system. Ceramics International, 44(13), 15845-15850.
[401] Cai, J., Lu, M., Guan, K., Li, W., He, F., Chen, P., & Wu, J. (2018). Effect of ZnO/MgO ratio on the crystallization and optical properties of spinel opaque glazes. Journal of the American Ceramic Society, 101(4), 1754-1764.
[402] Vincenzini, P., Biffi, G., & Ortelli, G. (1975). TiO_2 as an opacifier of ceramic glazes firing in the range 900-1000°C. Ceramurgia, 5(1), 3-12.
[403] Tellier, C. (1979). Opacification of glazes for sanitary ware by titanium dioxide and zinc oxide. Bull. Soc. Fr. Ceram., 125, p. 21.
[404] Bobkova, N. M., Boloban, L. V., & Gailevich, S. A. (1997). Phase formation in titanium glazes. Glass and ceramics, 54(1-2), 17-19.
[405] Teixeira, S., & Bernardin, A. M. (2009). Development of TiO_2 white glazes for ceramic tiles. Dyes and Pigments, 80(3), 292-296.
[406] Xia, Y. F., Huang, Z. H., Yuan, J. Z., Wang, L. J., & Xie, J. H. (2010). Preparation of rutile crystalline glaze. In Advanced Materials Research, 105, 778-781.
[407] Pekkan, K. (2015). The thermal and microstructural behavior of a R_2O–RO–(ZnO)–Al_2O_3–(TiO_2)–SiO_2 based macro-crystalline raw glaze system. Ceramics International, 41(6), 7881-7889.
[408] Safi, M., Khalili, N., & Arabi, M. (2012). Effect of various opacifiers on color parameters and gloss of glazed tiles. Journal of Color Science and Technology, 5, 261-253.
[409] Montazerian, M., Javadi, S., & Shahriyari, M. (2014). An investigation into the replacement of zircon with fluorspar, andalusite and wollastonite as whitening agent of the body. Proc. XIII World Congress on the Quality of Ceramic Tiles, Qualicer2014, p. 7, Castellon, Spain.
[410] Tarhan, M. (2019). Whiteness improvement of porcelain tiles incorporated with anorthite and diopside phases. Journal of Thermal Analysis and Calorimetry, 138(2), 929-936.
[411] Zanelli, C., Baldi, G., Dondi, M., Ercolani, G., Guarini, G., & Raimondo, M. (2008). Glass–ceramic frits for porcelain stoneware bodies: Effects on sintering, phase composition and technological properties. Ceramics International, 34(3), 455-465.
[412] Siligardi, C., Miselli, P., Lusvarghi, L., & Reginelli, M. (2011). Influence of CaO–ZrO_2–Al_2O_3–SiO_2 glass-ceramic frits on the technological properties of porcelain stoneware bodies. Ceramics International, 37(6), 1851-1858.
[413] Li, R., Lv, M., Cai, J., Guan, K., He, F., Li, W., & Wu, J. (2018). Development of sapphirine opaque glazes for ceramic tiles. Journal of the European Ceramic Society, 38(16), 5632-5636.
[414] Nieves, L. J. J., Lot, A. V., Melchiades, F. G., & Boschi, A. O. (2020). Digital decoration for ceramic tiles: The effect of glazes particle size distribution on the inkjet decoration. Boletín de la Sociedad Española de Cerámica y Vidrio, 59(1), 44-48.
[415] Dakhai, S., Orlova, L. A., & Mikhailenko, N. Y. (1999). Types and compositions of crystalline glazes. Glass and Ceramics, 56(5-6), 177-180.
[416] Sorlí, S., Tena, M. A., Mestre, A., Llusar, M., & Monrós, G. (2004). Effect of the major devitrifying phase on ceramic glaze microstructure and mechanical properties. Proceedings of VIII World Congress on Ceramic Tile Quality, Qualicer 2004, 99-110, Castellon, Spain.
[417] Tücks, A., & Beck, H. P. (2005). The photochromic effect of bismuth vanadate pigments. Part I: Synthesis, characterization and lightfastness of pigment coatings. Journal of Solid State Chemistry, 178(4), 1145-1156.
[418] Sameera, S. F., Rao, P. P., Kumari, L. S., & Koshy, P. (2009). New Scheelite-based Environmentally Friendly Yellow Pigments:(BiV)x(CaW)1–xO4. Chemistry Letters, 38(11), 1088-1089.
[419] Masui, T., Honda, T., & Imanaka, N. (2013). Novel and environmentally friendly (Bi,Ca,Zn)VO_4 yellow pigments. Dyes and Pigments, 99(3), 636-641.
[420] Dolić, S. D., Jovanović, D. J., Štrbac, D., Far, L. Đ., & Dramićanin, M. D. (2018). Improved coloristic properties and high NIR reflectance of environment-friendly yellow pigments based on bismuth vanadate. Ceramics International, 44(18), 22731-22737.
[421] Sciau, P., Noé, L., & Colomban, P. (2016). Metal nanoparticles in contemporary potters' master pieces: Lustre and red "pigeon blood" potteries as models to understand the ancient pottery. Ceramics International, 42(14), 15349-15357.
[422] Wynn, N. (1959). Platinum in the decoration of ceramic wares. Platinum Metals Review, 3(2), 60-65.
[423] Dvornichenko, I. N., & Matsenko, S. V. (2000). Production of iron-containing crystalline glazes. Glass and Ceramics, 57(1-2), 67-68.
[424] Bobin, O., Schvoerer, M., Miane, J. L., & Fabre, J. F. (2003). Coloured metallic shine associated to lustre decoration of glazed ceramics: a theoretical analysis of the optical properties. Journal of Non-Crystalline Solids, 332(1-3), 28-34.
[425] Fredrickx, P., Helary, D., Schryvers, D., & Darque-Ceretti, E. (2004). A TEM study of nanoparticles in lustre glazes. Applied Physics A, 79(2), 283-288.
[426] Pekkan, K., Başkırkan, H., & Çakı, M. (2018). Development of gold-bronze metallic glazes in a clay-based system for stoneware bodies. Ceramics International, 44(5), 4789-4794.

[427] Pekkan, K., Taşçı, E., & Uz, V. (2015). Production of metallic glazes and their industrial applications. Journal of The Australian Ceramic Society, 51(1), 110-115.
[428] Siligardi, C., Montecchi, M., Montorsi, M., & Pasquali, L. (2010). Ceria-containing frit for luster in modern ceramic glaze. journal of the american ceramic society, 93(9), 2545-2550.
[429] Siligardi, C., Montecchi, M., Montorsi, M., & Pasquali, L. (2009). Lead free Cu-containing frit for modern metallic glaze. Journal of the American Ceramic Society, 92(11), 2784-2790.
[430] Gualtieri, A. F., Canovi, L., Viani, A., Bertocchi, P., Corradini, C., Gualtieri, M. L., & Berthier, S. (2013). Mechanism of lustre formation in scheelite-based glazes. Journal of the European Ceramic Society, 33(11), 2055-2064.
[431] Siligardi, C., Tagliaferri, L., Lusvarghi, L., Bolelli, G., & Venturelli, D. (2014). Preparation of innovative metallic composite glazes for porcelainized stoneware tiles. Ceramics International, 40(1), 1821-1828.
[432] Tenorio Cavalcante P.M., Dondi M., Guarini G., Barros F.M., da Luz A.B., Ceramic application of mica titania pearlescent pigments. Dyes and Pigments, 74 (2007) 1-8.
[433] Parmelee, C. W., & Lathrop, J. S. (1924). Aventurine glazes. Journal of the American Ceramic Society, 7(7), 567-574.
[434] Levitskii, I. A. (2001). Mechanism of phase formation in aventurine glaze. Glass and Ceramics, 58(5-6), 223-226.
[435] Gozalbo, A., Orts, M. J., Mestre, S., Gómez, P., Agut, P., Lucas, F., & Blanco, C. (2006). Ceramic glazes with aventurine effect. Proceedings of IX World Congress on Ceramic Tile Quality, Qualicer 2006, 189-202, Castellon, Spain.
[436] Eliseev, S. Y., Rodtsevich, S. P., & Dostanko, E. V. (2000). Enamel with the aventurine effect. Glass and Ceramics, 57(3-4), 140-142.
[437] Casan, E., Lleo, E., Palomares, F., Rodriguez, V., Marti, V., Seores, J., & Cabrera, M. J. (2010). Goniochromatism study on metallized effects of aventurine enamels. Boletin de la Sociedad Espanola de Ceramica y Vidrio, 49(3), 142-146.
[438] Păcurariu, C., Lazău, R. I., Lazău, I., Tiţa, D., & Dumitrel, A. (2011). Non-isothermal crystallization kinetics of some aventurine decorative glaze. Journal of thermal Analysis and Calorimetry, 105(2), 435-441.
[439] Lazău, I., Borcănescu, S., Păcurariu, C., & Vancea, C. (2013). Kinetic study of the non-isothermal crystallization process of hematite in ceramic glazes obtained from CRT wastes. Journal of Thermal Analysis and Calorimetry, 112(1), 345-351.
[440] Dondi, M., Cruciani, G., Balboni, E., Guarini, G., & Zanelli, C. (2008). Titania slag as a ceramic pigment. Dyes and Pigments, 77(3), 608-613.
[441] Soares, F. D. S., & Valerio, M. E. G. (2017). Laser sintering of doped strontium aluminate via modified sol-gel for use as a ceramic pigment. Cerâmica, 63(365), 90-98.
[442] Kaya, S. Y., Karasu, B., & Karacaoğlu, E. (2009). General review of application of phosphorescence pigments in ceramic industry. Proceedings of SERES, 9, 608-616.
[443] Karacaoğlu, E., & Karasu, B. (2013). The effects of re-firing process under oxidizing atmosphere and temperatures on the properties of strontium aluminate phosphors. Materials Research Bulletin, 48(10), 3702-3706.
[444] Ferrari, C., Muscio, A., Siligardi, C., & Manfredini, T. (2015). Design of a cool color glaze for solar reflective tile application. Ceramics International, 41(9), 11106-11116.
[445] Ferrari, C., Muscio, A., & Siligardi, C. (2016). Development of a solar-reflective ceramic tile ready for industrialization. Procedia Engineering, 169, 400-407.
[446] Schabbach, L. M., Marinoski, D. L., Güths, S., Bernardin, A. M., & Fredel, M. C. (2018). Pigmented glazed ceramic roof tiles in Brazil: Thermal and optical properties related to solar reflectance index. Solar Energy, 159, 113-124.
[447] Gargori, G., Cerro, L., Fas, A., Llusar, V., & Monrós, T. (2017). Study of the photocatalytic activity and cool characteristics of a novel palette of pigments. Boletin de la Sociedad Espanola de Ceramica y Vidrio, 56(4), 166-176.
[448] Chen, J., Xiao, Y., Huang, B., & Sun, X. (2018). Sustainable cool pigments based on iron and tungsten co-doped lanthanum cerium oxide with high NIR reflectance for energy saving. Dyes and Pigments, 154, 1-7.
[449] Jovaní, M., Sanz, A., Beltrán-Mir, H., & Cordoncillo, E. (2016). New red-shade environmental-friendly multifunctional pigment based on Tb and Fe doped $Y_2Zr_2O_7$ for ceramic applications and cool roof coatings. Dyes and Pigments, 133, 33-40.
[450] Bondioli, F., Dinelli, M., Giovanardi, R., & Giorgi, M. (2010). Functionalization of ceramic tile surface by soluble salts addition: Part II. Titanium and silver addition. Journal of the European Ceramic Society, 30(9), 1873-1878.
[451] Rambaldi, E., Tucci, A., Esposito, L., Naldi, D., & Timellini, G. (2010). Nano-oxides to improve the surface properties of ceramic tiles. Boletín de la Sociedad Española de Cerámica y Vidrio, 49(4), 253-258.
[452] Shimohigoshi, M., & Saeki, Y. (2005). Development of photocatalyst tile and commercial production. In PRO 41: International RILEM Symposium on Environment-Conscious Materials and Systems for Sustainable Development, 41, p. 35.
[453] Tobaldi, D. M., Tucci, A., Camera-Roda, G., Baldi, G., & Esposito, L. (2008). Photocatalytic activity for exposed building materials. Journal of the European Ceramic Society, 28(14), 2645-2652.
[454] da Silva, A. L., Dondi, M., Raimondo, M., & Hotza, D. (2018). Photocatalytic ceramic tiles: Challenges and technological solutions. Journal of the European Ceramic Society, 38(4), 1002-1017.
[455] Tezza, V. B., Scarpato, M., Oliveira, L. F. S., & Bernardin, A. M. (2015). Effect of firing temperature on the photocatalytic activity of anatase ceramic glazes. Powder Technology, 276, 60-65.
[456] Raimondo, M., Guarini, G., Zanelli, C., Marani, F., Fossa, L., & Dondi, M. (2012). Printing nano TiO_2 on large-sized building materials: Technologies, surface modifications and functional behaviour. Ceramics International, 38(6), 4685-4693.

[457] Vaiano, V., Sarno, G., Ciambelli, P., & Sannino, D. (2014). Functionalization of ceramic tiles with N-doped TiO_2 and their photocatalytic function under UV or visible light irradiation. Journal of Advanced Oxidation Technologies, 17(2), 193-201.

[458] da Silva, A. L., Dondi, M., & Hotza, D. (2017). Self-cleaning ceramic tiles coated with Nb_2O_5-doped-TiO_2 nanoparticles. Ceramics International, 43(15), 11986-11991.

[459] Vaiano, V., Sarno, G., Sannino, D., & Ciambelli, P. (2014). Photocatalytic and antistain properties of ceramic tiles functionalized with tungsten-doped TiO2. Chemical Engineering Transactions, 39, 499-504.

[460] Tobaldi, D. M., Škapin, A. S., Pullar, R. C., Seabra, M. P., & Labrincha, J. A. (2013). Titanium dioxide modified with transition metals and rare earth elements: phase composition, optical properties, and photocatalytic activity. Ceramics International, 39(3), 2619-2629.

[461] Sciancalepore, C., & Bondioli, F. (2015). Durability of SiO_2–TiO_2 photocatalytic coatings on ceramic tiles. International Journal of Applied Ceramic Technology, 12(3), 679-684.

[462] Machida, M., Norimoto, K., & Kimura, T. (2005). Antibacterial activity of photocatalytic titanium dioxide thin films with photodeposited silver on the surface of sanitary ware. Journal of the American Ceramic society, 88(1), 95-100.

[463] de Niederhausern, S., Bondi, M., & Bondioli, F. (2013). Self-cleaning and antibacteric ceramic tile surface. International Journal of Applied Ceramic Technology, 10(6), 949-956.

[464] Gurbuz, M., Atay, B., & Dogan, A. (2015). Synthesis of high-temperature-stable TiO_2 and its application on Ag^+-activated ceramic tile. International Journal of Applied Ceramic Technology, 12(2), 426-436.

[465] Baheiraei, N., Moztarzadeh, F., & Hedayati, M. (2012). Preparation and antibacterial activity of Ag/SiO_2 thin film on glazed ceramic tiles by sol–gel method. Ceramics international, 38(4), 2921-2925.

[466] Zhang, Q., Xu, L. S., & Guo, X. (2017). Improvement of mechanical properties, microscopic structures, and antibacterial activity by Ag/ZnO nanocomposite powder for glaze-decorated ceramic. Journal of Advanced Ceramics, 6(3), 269-278.

[467] Ghafari-Nazari, A., Moztarzadeh, F., Rabiee, S. M., Rajabloo, T., Mozafari, M., & Tayebi, L. (2012). Antibacterial activity of silver photodeposited nepheline thin film coatings. Ceramics International, 38(7), 5445-5451.

[468] Uzgur, E., Bayrakci, F., Koparal, S., & Dogan, A. (2004). Applications of calcium phosphate based antibacterial ceramics on sanitary and tile wares. Key Engineering Materials, 264, 1573-1576.

[469] Wang, Q. P., Guo, X. X., Wu, W. H., & Liu, S. X. (2011). Preparation of fine Ag_2WO_4 antibacterial powders and its application in the sanitary ceramics. Advanced Materials Research, 284, 1321-1325.

[470] Anantharamulu, N., Rao, K. K., Rambabu, G., Kumar, B. V., Radha, V., & Vithal, M. (2011). A wide-ranging review on Nasicon type materials. Journal of Materials Science, 46(9), 2821-2837.

National Research Council of Italy
istec Institute of Science and Technology for Ceramics

Faenza, May 3, 2020

Declaration of interests

☒ On behalf of all the authors, I declare that we have no known competing financial interests or personal relationships that could have appeared to influence the work reported in this paper.

☐The authors declare the following financial interests/personal relationships which may be considered as potential competing interests:

Michele Dondi

Michele Dondi

V.A.T. 02118311006
C.F. 80054330586
Via Granarolo, 64 – 48018 FAENZA (RA) - Italy
Phone: +39 0546 699711-Fax +39 0546 46381
e-mail: istec@istec.cnr.it
PEC: istec@pec.cnr.it